Aalborg Universitet

AALBORG UNIVERSITY
DENMARK

System Level Performance Analysis of Advanced Antenna Concepts in WCDMA

Ramiro-Moreno, Juan

Publication date:
2008

Document Version
Publisher's PDF, also known as Version of record

[Link to publication from Aalborg University](#)

System Level Performance Analysis of Advanced Antenna Concepts in WCDMA

Ph.D. Thesis
by
Juan Ramiro Moreno

July 2003

Main supervisor:
Research professor Dr. Preben E. Mogensen, Aalborg Univesity

Co-supervisor:
Dr. Klaus I. Pedersen, Nokia Networks R&D, Aalborg

Department of Communication Technology
Institute of Electronic Systems, Aalborg University
Niels Jernes Vej 12, DK-9220 Aalborg Øst, Denmark

Ph.D. Thesis

System Level Performance Analysis of Advanced Antenna Concepts in WCDMA

Department of Communication Technology
Institute of Electronic Systems
Aalborg University
Niels Jernes Vej 12, DK-9220 Aalborg Øst, Denmark

Abstract

The Universal Mobile Telecommunications System (UMTS) has already started to be deployed in many countries. After some time, the traffic volume in these networks is expected to further push the demand for spectral efficient solutions in order to increase the capacity offered by the radio access systems. Among these solutions, advanced antenna concepts are considered to be an attractive technology because they can provide outstanding capacity and/or coverage gains by means of increased protection against fast fading, thermal noise and multiple access interference.

Most studies on antenna arrays (AAs) conducted so far have been oriented to link level investigations. However, less attention has been paid to the system level implications associated with the deployment of this technology. In this study, the capacity gain from beamforming AAs and transmit and/or receive (Tx/Rx) diversity techniques in UMTS is assessed at system level, with special emphasis on radio resource management considerations.

In order to support the use of beamforming AAs at the Node-B, conventional power based admission control (AC) criteria are extended to a directional power based AC algorithm. This algorithm captures the available capacity gain from spatial filtering while maintaining the network stability in both up and downlink (DL), regardless of the spatial distribution of the interference. Uplink simulations with four-element AAs show a capacity gain of approximately 200% for power controlled dedicated channels (DCHs). In DL, the capacity gain is around 150% for the case without channelisation code restrictions. However, when one scrambling code per cell is used, channelisation code shortage is a serious limitation. Different factors resulting in higher channelisation code shortage, such as low time dispersion, low link activity factor or large soft handover (SHO) overhead, are investigated. To solve this problem, a solution is analysed, where the cell is split into spatially isolated scrambling code regions. With four-element AAs, this solution has a marginal penalty of 4−8% due to the lack of orthogonality between signals with different scrambling codes.

The next step is to analyse the use of dual antenna Rake (2Rake) receivers at the UE. The analysis is conducted for circuit switched DL connections over power controlled DCHs. The achievable capacity gain and the potential channelisation code shortage are analysed for different power delay profiles, block error rate (BLER) targets and SHO configurations. For example, in Pedestrian A, with a BLER target of 10%, no SHO and no channelisation code restrictions, the capacity gain is 167%. However, channelisation code shortage decreases the achievable capacity with 36%. The dependency of the capacity gain upon the penetration rate of the UEs with 2Rake receivers is analysed theoretically and simulation results verify the outcome of such study. In addition, the radio resource management implications of having 2Rake receivers implemented at the UE are discussed.

As a third step, the High Speed Downlink Packet Access (HSPDA) concept of UMTS is considered. In HSDPA, fast packet scheduling (PS) is feasible, so that the system can track the instantaneous variations of the channel quality of all the UEs and therefore provide multi-user diversity. This diversity mechanism, together with other sources of diversity embedded in HSDPA, affects the capability of the system to benefit from Tx/Rx diversity techniques. The HSDPA cell capacity with different Tx/Rx diversity techniques is assessed under three PS algorithms: Round Robin (RR), Proportional Fair (PF) and Fair Throughput (FT). The benefit is measured in terms of HSDPA cell capacity gain and/or increased coverage. For example, in Pedestrian A at 3 kmph, the HSDPA cell capacity gain from closed loop transmit diversity at the Node-B combined with 2Rake at the UE equals 201%, 123% and 38% for FT, RR and PF, respectively. However, for RR under the same conditions, the average throughput gain for UEs with G=-4 dB is 320%, which involves a coverage gain. The impact of both the UE speed and the frequency selectivity of the radio channel on the HSDPA cell capacity are also addressed.

Dansk Resumé

Translation: Michael Støttrup and Lars Nielsen

Opsætningen af telefonsystemet Universal Mobile Telecommunications System (UMTS) er allerede startet i mange lande. Det forventes, at trafikvolumen i disse netværk efter et stykke tid vil øge behovet for tekniske løsninger, der giver højere spektral effektivitet for at forøge kapaciteten af radio-adgangsnetværket. Blandt de mulige tekniske løsninger anses advancerede antenneteknikker som interessante, fordi de giver en fremragende kapacitets- og/eller dækningsforbedring. Forbedringen kommer ved at reducere virkningerne fra fast fading, termisk støj og multiple access-interferens.

De fleste studier af antenna arrays (AAs) hidtil har fokuseret på linkniveau-analyse. Derfor har der været mindre fokus på hvordan denne teknologi klarer sig på systemniveau. Dette studie præsenterer resultater for kapacitetsforøgelse på systemniveau ved anvendelse af beamforming AAs og teknikker til udnyttelse af sende/modtage-diversitet i UMTS. Specielt er der fokuseret på betragtninger omkring radioresource-styring.

For at understøtte beamforming AAs i Node-B er det konventionelle sendestyrke-baserede adgangs-kriterium blevet udvidet til en retningsbestemt sendestyrke-baseret adgangskontrol-algoritme. Denne algoritme giver en kapacitets forøgelse, ved at udnytte rumlig filtrering samtidig med at den bibeholder netværksstabilitet i både uplink og downlink, uanset fordelingen af rumlig inteferens. Simuleringer i uplink med AAs med fire antenneelementer viser en kapacitetsforøgelse på ca. 200% for sendestyrke-kontrollerede dedikerede kanaler (DCHs). I downlink,er kapacitetsforøgelsen ca. 150% når begrænsninger i antallet af kanal-koder ikke tages i betragtning. Når der anvendes en forvrængningskode pr celle, viser det sig at mangel på kanal-koder er en alvorlig begrænsning. Flere ting der bidrager til større mangel på kanal-koder undersøges, såsom lav tids-dispersion, lav unyttelsesgrad af de enkelte links og stort overhead til soft handover. For at løse problemet med begrænsning i antal kanal-koder foreslås en løsning, hvor en celle indeles i regioner med rumligt isolerede forvrængningskoder. Den praktiske løsning med AAs med fire elementer giver en minimal reduktion i kapaciteten på 4-8% på grund af lav ortogonalitet mellem signaler med forskellige forvrængningskoder.

Næste skridt er at analysere dual Rake (2Rake)-modtagere i mobilterminalen. Denne analyse laves for circuit switched downlink-forbindelser på sendestyrke-kontrollerede DCHs. Den opnåelige kapacitetsforøgelse og den potentielle mangel på kanal-koder bliver analyseret for forskellige forsinkelsesprofiler, tilsigtede block error rate (BLER) og soft handover-konfigurationer. F.eks. giver Pedestrian A, med BLER 10%, ingen soft handover og ingen begrænsninger på antallet af kanal-koder en kapacitetsforøgelse på 167%. Men, kanal-kode-begrænsninger reducerer den opnåelige kapacitetsforøgelse til 36%. Kapacitetsforøgelsens afhængighed af udbredelsen af terminaler med 2Rake-modtagere analyseres teoretisk, og simuleringsresultater bliver brugt til at kontrollere rigtigheden af analysen. Derudover diskuteres hvordan 2Rake-modtagere i terminalen påvirker kravene til radioresource-styring.

Det tredje skridt er at analysere High Speed Downlink Packet Access (HSDPA)-konceptet i UMTS. HSDPA udnytter at packet scheduling kan fortages så hurtigt, at det er muligt at følge de øjeblikkelige variationer i kanal-kvaliteten for alle terminaler, og derved opnås multibruger-diversitet. Denne mekanisme, sammen med andre diversitetskilder i HSDPA, påvirker systemets mulighed for at udnytte sende/modtage-diversitet.

Kapaciteten af HSDPA–celler ved forskellige sende/modtage-diversitetsteknikker bestemmes for tre forskellige packet scheduling-algoritmer: Round Robin, Proportional Fair og Fair Throughput. Forbedringen bliver målt som forøgelse i HSDPA cellekapacitet og/eller forøget celledækning. F.eks. for Pedestrian A ved 3km/t, closed loop sende-diversitet i Node-B kombineret med en 2Rake modtager i terminalen giver HSDPA en cellekapacitetsforøgelse på 201%, 123% og 38% for henholdsvis FT, RR og PF. Den samme opsætning giver for RR og en terminal med G=-4dB en 320% kapacitetsforøgelse, hvilket medfører en dækningsforøgelse. HSDPA cellekapacitetens afhængighed af terminalens hastighed og frekvensvalg af radio-kanalen bliver også diskuteret.

Preface and acknowledgement

Table of contents

Table of contents

Abbreviations

Abbreviations

AA	Antenna Array
AC	Admission Control
ACK	Acknowledge
AICH	Acquisition Indication Channel
AS	Azimuth Spread
AVI	Actual Value Interface
BCH	Broadcast channel
BEP	Block Error Probability
BLER	Block Error Rate
BPSK	Binary Phase Shift Keying
CD/CA-ICH	Collision Detection/Channel Assignment Indicator Channel
CDF	Cumulative Distribution Function
CDMA	Code Division Multiple Access
CLPC	Closed Loop Power Control
CLTD	Closed Loop Transmit Diversity
CPCH	Common Packet Channel
CPICH	Common Pilot Channel
CQI	Channel Quality Indicator
CS	Circuit Switched
CSICH	CPCH Status Indication Channel
DCH	Dedicated Channel
DL	Downlink
DoA	Direction of Arrival
DPCCH	Dedicated Physical Control Channel
DPCH	Dedicated Physical Channel
DPDCH	Dedicated Physical Data Channel
DPIE	Directional Power Increase Estimator
DS	Direct Sequence
DSCH	Downlink Shared Channel
DTX	Discontinuous Transmission
FACH	Forward Access Channel
FBI	Feedback Information

FDD	Frequency Division Duplex
FER	Frame Erasure Rate
FT	Fair Throughput
GSM	Global System for Mobile communications
H-ARQ	Hybrid Automatic Repeat reQuest
HC	Handover Control
HSDPA	High Speed Downlink Packet Access
HS-DPCCH	High Speed Dedicated Physical Control Channel
HS-DSCH	High Speed Downlink Shared Channel
HS-PDSCH	High Speed Physical Downlink Shared Channel
HS-SCCH	High Speed Shared Control Channel
LA	Link Adaptation
LC	Load Control
MCS	Modulation and Coding Scheme
MIMO	Multiple-Input-Multiple-Output
MRC	Maximal Ratio Combining
NACK	Negative Acknowledgement
NR	Noise Rise
NRT	Non-Real Time
OLPC	Outer Loop Power Control
OLTD	Open Loop Transmit Diversity
PAS	Power Azimuth Spectrum
PC	Power Control
PCCPCH	Primary Common Control Physical Channel
PCH	Paging Channel
PCPCH	Physical Common Packet Channel
P-CPICH	Primary Common Pilot Channel
PDP	Power Delay Profile
PDS	Power Delay Spectrum
PDSCH	Physical Downlink Shared Channel
PF	Proportional Fair
PICH	Paging Indication Channel
PIE	Power Increase Estimator
PRACH	Physical Random Access Channel
PS	Packet Scheduling

QAM	Quadrature Amplitude Modulation
QoS	Quality of Service
QPSK	Quadrature Phase Shift Keying
RACH	Random Access Channel
RLC	Radio Link Control
RM	Resource Manager
RNC	Radio Network Controller
RR	Round Robin
RRC	Radio Resource Control
RRM	Radio Resource Management
Rx	Receive
SAW	Stop And Wait
SCCPCH	Secondary Common Control Physical Channel
SCH	Synchronisation Channel
S-CPICH	Secondary Common Pilot Channel
SF	Spreading Factor
SHO	Soft Handover
SHOO	Soft Handover Overhead
SINR	Signal-to-Interference-plus-Noise Ratio
TDD	Time Division Duplex
TSTD	Time Switch Transmit Diversity
TTI	Transmission Time Interval
Tx	Transmit
Tx/Rx	Transmit and/or Receive
UE	User Equipment
UL	Uplink
UMTS	Universal Mobile Telecommunications System
UTRA	Universal Terrestrial Radio Access
WCDMA	Wideband Code Division Multiple Access
3GPP	3rd Generation Partnership Project

Chapter 1

Introduction

1.1 Preliminaries

Third generation cellular systems are tailored to support a large variety of bit rates and services, while the current second generation systems were mainly designed for voice and low data rate services. Introduction of services that require high data rates pushes the demand for solutions that increase the capacity of these systems.

In order to increase the capacity of cellular systems, there are two main paths that can be followed. On one hand, the capacity can be increased by adding more sites, applying deeper sectorisation or using more carriers. Though increasing the site density of the network has a positive effect on the system capacity [1]-[2], it involves an obvious extra deployment cost. Applying deeper sectorisation also involves extra cost, mainly due to the deployment of more equipment, although it does not require further site acquisitions, which may be difficult and expensive. Moreover, adding extra carriers can also have serious financial implications, due to the potentially large licensing costs.

Another way to increase the capacity in cellular networks is to apply techniques that increase the spectral efficiency of the system. On one hand, advanced base-band multi-user detection techniques can be used. The optimal multi-user detector was derived by Verdú [3] but, unfortunately, this detector is too complex for practical systems. Therefore, over the last years, a lot of research has been done in order to find sub-optimal multi-user detectors whose implementation is more feasible. The different multi-user detection techniques can be

classified into two main groups: linear detectors and subtractive interference cancellation detectors. Linear detectors ([4], [5]) apply a linear transformation to the soft output of the conventional detector in order to reduce the multiple access interference seen by each user. Subtractive interference cancellation detectors generate estimates of the interference and subtract it out of the received signals. They can be classified into successive [6] and parallel [7] interference cancellation detectors.

In general, multi-user detection techniques involve extra complexity in the receiver, and many times the nature of many of the proposed algorithms makes it impossible to use them for the downlink (DL) case, due to the fact that the system does not provide the receiver with all the necessary pieces of information. However, in the uplink (UL) case, all the needed information can be obtained, which makes these techniques feasible.

Another possibility to increase the spectral efficiency of the system is the application of adaptive antenna arrays (AAs) [8], which are considered to be an attractive technology because they can provide capacity and/or coverage gains in both UL and DL by means of increased protection against fast fading, thermal noise and multiple access interference.

The use of AAs also involves extra complexity in the system, i.e. extra antennas, extra cabling, extra amplifiers and extra management complexity at the base station, as well as serious implementation challenges at the terminal side. Moreover, the performance enhancement that can be provided by AAs is not attractive for all environments. For example, in the case of conventional beam steering towards the average direction of arrival of each UE, the performance gain is expected to be low when the azimuth spread of the radio channel at the base station is high. Additionally, the deployment of AAs (if clearly visible as a set of antennas) at the sites could be perceived by the population as an increase in the radiated signal power, which the subsequent increase of the public health concerns that have been already raised during the recent years about the potential effects of cellular radio networks. Among others, these issues could be one reason why adaptive AAs have not been massively deployed so far.

Regarding the question about whether it is better to use deeper sectorisation or adaptive AAs with conventional beam steering, it has to be pointed out that adaptive AAs can be used to perform deeper sectorisation if desired, offering more flexibility in the system configuration. This possibility is discussed and analysed in [9], where the different alternatives are assessed. The result of this study suggests that the deployment adaptive AAs within one cell offers better performance than the option in which deeper sectorisation is conducted.

Compared with the deployment of extra sites, the use of adaptive AAs (in an environment where their performance is attractive) should be less expensive, due to the fact that no extra sites have to be acquired. In addition, adaptive AAs can be used for capacity or coverage enhancement. Thus, in the initial roll-out phase, adaptive AAs can be used for coverage enhancement so that the number of necessary sites is reduced. Later, when the traffic demand starts to grow, more sites can be installed and adaptive AAs can start to be exploited for capacity enhancement rather than for increasing the coverage range.

This Ph.D. thesis is focussed on the system level performance of adaptive AAs as a capacity enhancing technique. In this context, the expression *adaptive AAs* includes both beamforming and diversity techniques, which can be used for either signal transmission or reception. As already seen, there is a practical cost associated to the use of this technology.

However, this practical cost is not going to be considered throughout the research, which is only focused on the system level performance gain that can be obtained from the deployment of this technology.

As already stated, adaptive AAs can increase the capacity of mobile cellular systems significantly. Indeed, the implementation of antenna arrays (AAs) at the base station has proven to yield a significant capacity gain in both time division multiple access (TDMA) [10]-[11] systems and code division multiple access (CDMA) systems [12]-[13]. During the last two decades a lot of work has been published on derivation of various base-band algorithms for AAs [14]-[17], comparison of different AA topologies, and link level performance evaluation of various AA schemes. However, little attention has been given to network aspects of AAs in wideband CDMA (WCDMA) systems. As an example, AAs influence on radio resource management algorithms (RRM) such as admission control [18]-[19], power control [20]-[21], congestion control, and handover control needs further attention in order to answer the following questions: What is the capacity gain that can be achieved with adaptive AAs? How is it affected by the RRM configuration? And, what are the limitations that the system imposes on the capacity gain?

The chapter is organised as follows. Since the Universal Mobile Telecommunications System (UMTS) is taken as a case study for this Ph.D. thesis, a short description of this system is given in Section 1.2. The different assessment methodologies available for the analysis of cellular systems are described in Section 1.3. The objectives of this Ph.D. study are formulated in Section 1.4. An outline of the thesis report is given in Section 1.5. Section 1.6 provides a list of the publications produced during the Ph.D. study.

1.2 UMTS overview

Among the available third generation systems, the scope of this Ph.D. thesis is narrowed down to the WCDMA system that has been standardised in the 3rd Generation Partnership Project (3GPP) [24], which is a joint project of the standardisation bodies from Europe, Japan, Korea, the USA and China. The WCDMA system standardised by 3GPP is called Universal Terrestrial Radio Access (UTRA), and has two modalities: Frequency Division Duplex (FDD) and Time Division Duplex (TDD). For this Ph.D. thesis, the UTRA FDD system is considered as a case study. For simplicity, in the rest of the thesis this system will be referred to as UMTS [1].

This section is a short description of the basic architecture and features of UMTS (meaning UTRA FDD). The description is in line with the specifications of Release'99 and the most relevant upgrades for Release 5 with High Speed Downlink Packet Access (HSDPA). Note that this description is not meant to be exhaustive, but to provide the reader with an insight into the system that is enough to understand the system specific issues that arise throughout the rest of the thesis.

1.2.1 System architecture and radio resource management

The UMTS system architecture is sketched in Figure 1.1, which shows the logical network elements, the names of the different interfaces and the manner in which the radio resource management (RRM) algorithms are distributed among the network elements. In UMTS terminology, the term Node-B refers to what is usually called base station, while the

term user equipment (UE) refers to the terminal. In the sequel, the UMTS terminology presented here will be used.

The Radio Network Controller (RNC) owns and controls the radio resources in its domain (the set of Node-Bs connected to it), and it takes care of the following RRM algorithms: uplink (UL) outer loop power control (OLPC), handover control (HC), packet scheduling (PS), admission control (AC), load control (LC) and resource manager (RM). When a UE is connected to the UMTS network (i.e., when it is not in idle mode [1]), its identity is known by its serving RNC[1]. Moreover, the RNC interacts with the core network and also terminates the Radio Resource Control (RRC) protocol that defines the messages and procedures between the UE and the UMTS network. In fact, most of the control signalling between the UE and the network is based on RRC messages, which carry all parameters to set up, modify and release connections. For example, all the measurements reports and commands related to UE mobility across the network are conveyed by means of RRC signalling. For more details, see some practical examples of the use of RRC messages in Section 4.3.4.

The Node-B converts the data flow between the Iub and the Uu interfaces [1], and it is responsible for fast UL closed loop power control (CLPC) and fast LC. Furthermore, the UE is responsible for fast downlink (DL) CLPC and DL OLPC. As shown in Figure 1.1, a UE can be connected to several Node-Bs via soft handover (SHO), no matter which RNC each Node-B is connected to. Furthermore, RRM algorithms can be classified into cell specific and connection specific. The connection specific RRM algorithms are: UL/DL OLPC, UL/DL CLPC and HC. The rest of them are cell specific.
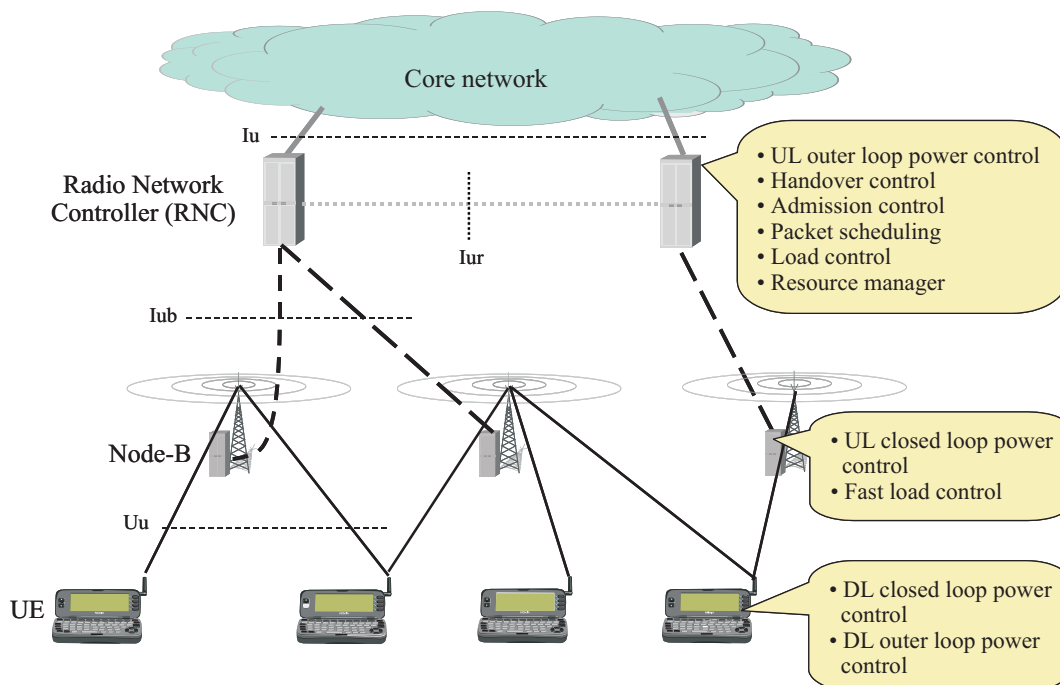
Figure 1.1: UMTS system architecture.

---

[1] For simplicity, the possibility of having a UE connected to several RNCs is not considered in this preliminary discussion. Thus, further clarification of concepts such as *serving* and *drift* RNC is not required. For further information in this respect, see [1].

In the following, the working principles of the main RRM algorithms are described [1], [25]:

Fast closed loop power control (CLPC) is responsible for controlling the transmit power at each link via a closed loop feedback scheme, in order to fulfil the SINR target in all the links while minimising the total amount of transmitted power. In UL, such algorithm is essential in order to overcome the so-called near far effect [22], and its use in DL increases the capacity [26].

Outer loop power control (OLPC) adjusts the SINR target for CLPC in order to maintain the quality of the communication in terms of frame erasure rate (FER) at the desired level.

Handover control (HC) is needed in order to provide mobility across the network, supporting robust transitions between cells. HC decides the set of Node-Bs the UE should be connected to. Such decision can be based on coverage and/or load reasons, and is normally aided by pilot quality measurements conducted at the UE. In UMTS, a UE can be connected to several Node-Bs at the same time via SHO, which provides macro and micro diversity protection and guarantees a smooth transition between cells.

Admission control (AC) is responsible for controlling the load of the system so that the available capacity can be exploited without compromising the system stability. Before admitting a new UE or modifying the connection of an already admitted UE, AC checks whether these actions will sacrifice the planned coverage area or the quality of the existing connections. When a new UE is admitted or an existing connection is modified, AC is also in charge of setting the parameters for the new connection, e.g. the initial DL transmission power.

Packet scheduling (PS) is the algorithm in charge of coordinating the resource allocation for non-real time (NRT) traffic. The quality of service (QoS) requirements of the different UEs must be fulfilled while making an efficient use of scarce resources, so that the system capacity is maximised under the given constraints.

Resource manager (RM) is the name of the algorithm that coordinates the distribution of the code resources among the different UEs in an efficient manner.

Load control (LC) makes sure that the system is not overloaded, so that stability is not compromised. Basically, when an overload situation occurs, LC must bring the load back to the targeted levels. In order to do so, the possible actions are: inter-frequency or inter-system handover for some UEs, quality decrease for some connections, throughput decrease for packet traffic and controlled dropping of low priority UEs. These actions are taken at the RNC. However, other related actions can be taken at the Node-B by means of the so-called fast LC algorithm.

1.2.2 Transport channels and their mapping to the physical layer

The data generated at higher layers is carried over the air with transport channels, which are mapped to different physical channels. The physical layer is required to support variable bit rate transport channels in order to offer bandwidth-on-demand services, and to be able to multiplex several services to one connection [1].

In Release'99, there are two types of transport channels: dedicated transport channels and common transport channels [27]. The only dedicated transport channel is the dedicated channel (DCH). There are six types of common transport channels: broadcast channel (BCH), forward access channel (FACH), paging channel (PCH), random access channel (RACH), UL common packet channel (CPCH) and downlink shared channel (DSCH). Further explanations for each channel can be found in [1], and detailed information about how these channels are mapped onto the physical layer is given in [27] and illustrated in Figure 1.2. In order to understand the rest of the thesis, only the DCH needs further explanation.

Transport channels   Physical channels

Transport channels	Physical channels
BCH	Primary common control physical channel (PCCPCH)
FACH	Secondary common control physical channel (SCCPCH)
PCH	
RACH	Physical random access channel (PRACH)
DCH	Dedicated physical data channel (DPDCH)
	Dedicated physical control channel (DPCCH)
DSCH	Physical downlink shared channel (PDSCH)
CPCH	Physical common packet channel (PCPCH)
	Synchronisation channel (SCH)
	Common pilot channel (CPICH)
	Acquisition indication channel (AICH)
	Paging indication channel (PICH)
	CPCH status indication channel (CSICH)
	Collision detection/Channel assignment indicator channel (CD/CA-ICH)

Figure 1.2: Mapping of transport channels onto physical channels (Release'99) [27].

One DCH is exclusively allocated to one UE. The DCH conveys all the information intended for that UE coming from higher layers, including data for the actual service. It can be used for both UL and DL, and supports CLPC with one power update per slot[2], multi-code operation, bit rate variations with one frame resolution, SHO and the use of AAs. With spreading factor (SF) 4 and three parallel multi-codes, a DL DCH can carry approximately 2.8 Mbps when the coding rate equals ½ [27]. The same approximate bit rate can be obtained for the UL with SF 4, three parallel multi-codes and a coding rate of ½.

All Release'99 transport channels are terminated at the RNC. Thus, retransmissions for packet data are controlled by the Radio Link Control (RLC) functionality at the RNC.

---

[2] The slot duration is 0.667 ms, and the radio frame duration is 10 ms, i.e. 15 slots [27].

1.2.3 Physical layer and air interface

UMTS uses WCDMA as a multiple access technique. WCDMA is a direct-sequence (DS) CDMA technique in which the information bits are spread over a wide bandwidth by multiplying them with the quasi-random bits (chips) of the CDMA spreading code [1]. In order to support very high variability of the bit rates, the use of a variable SF and multi-code connections is supported. The basic principles of CDMA are described in [28] and [29].

The chip rate is $3.84 \cdot 10^6$ chips per second, with a carrier bandwidth of 5 MHz. The large bandwidth allows the support of high user data rates, and opens for exploitation of multipath diversity. Separate 5 MHz frequency bands are used for UL and DL.

In DL, signals transmitted at the same cell are separated by means of synchronised orthogonal codes (referred to as channelisation codes) extracted from an orthogonal variable spreading factor (OVSF) code tree [30], which is derived from the set of Walsh codes. Since orthogonal codes do not have white noise properties, the total transmitted signal at each cell is scrambled by a pseudo noise (PN) sequence that is referred to as scrambling code. The scrambling codes are complex-valued, and are obtained by I-Q multiplexing a Gold code and a delayed replica of the same Gold code. According to the UMTS specifications, only one OVSF code tree per scrambling code is available [31], which imposes a hard limit on the cell capacity that can be achieved with one single scrambling code per cell. In radio channels with no time dispersion, signals transmitted under the same scrambling code are fully orthogonal. However, this orthogonality is partly destroyed in time dispersive radio channels, and the part of the interference that is not orthogonal is just attenuated with the processing gain when despreading the desired signal [32]. The processing gain is defined as the ratio between the chip rate and the bit rate. Note that the DL DCH is mapped onto a dedicated physical data channel (DPDCH) and a dedicated physical control channel (DPCCH) (as shown in Figure 1.2), which are time multiplexed forming a DL dedicated physical channel (DPCH) [27], as shown in Figure 1.3.
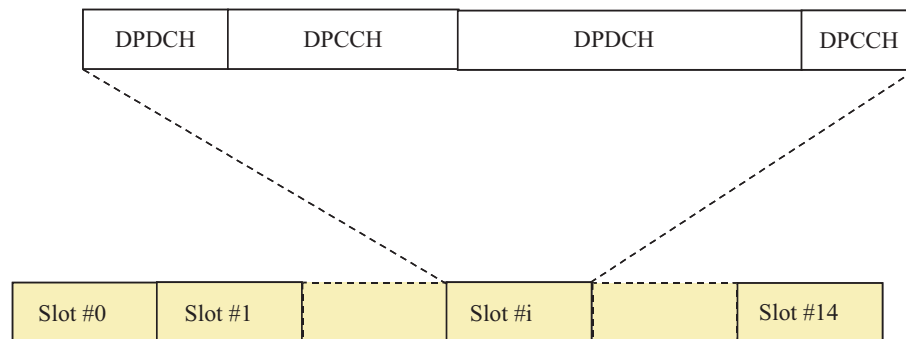
Figure 1.3: Time multiplexing of a DPDCH and a DPCCH in order to form a DL DPCH [27].

Figure 1.4 illustrates how several DL DPCHs are transmitted under the same scrambling code at the Node-B. The modulation scheme for the DL DPCH is quadrature phase shift keying (QPSK).
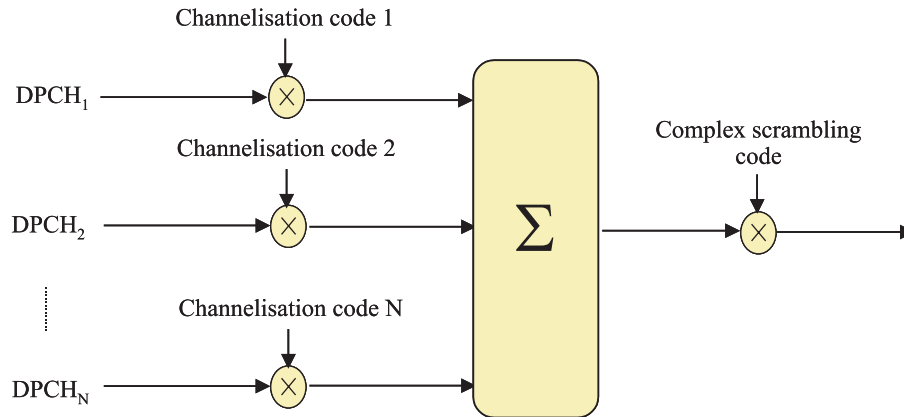
Figure 1.4: Transmission of several DPCHs under one scrambling code at the Node-B [31].

In UL, a scrambling code per UE is used. Channelisation codes are used to separate different channels that are transmitted by a certain UE at the same time. Signals transmitted from different UEs use different scrambling codes. Thus, when despreading the signal from one UE, the noise and the signals coming from other UEs are attenuated with the processing gain. In UL, a DCH is mapped onto a DPCCH and one or more (up to six) DPDCHs, which are I-Q/code multiplexed (see Figure 1.5 and Figure 1.6). The modulation scheme for the UL DPDCH and the UL DPCCH is binary phase shift keying (BPSK).
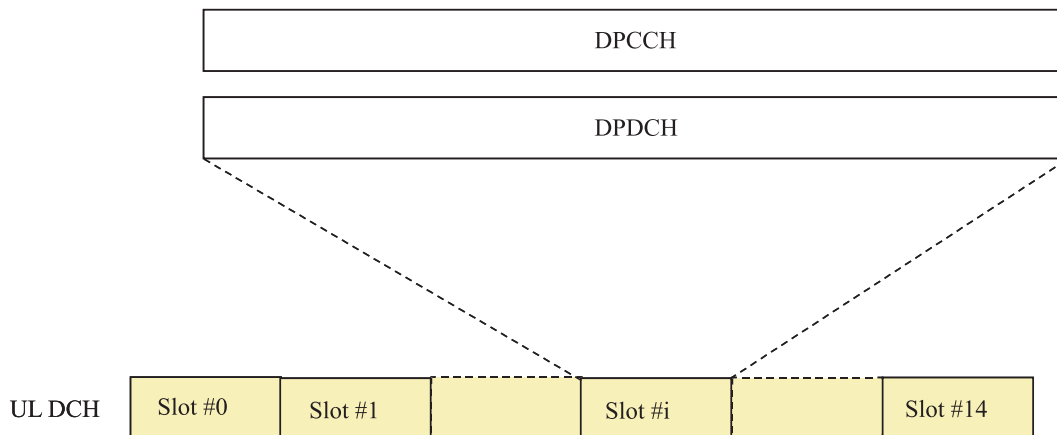
Figure 1.5: UL DCH structure [27].
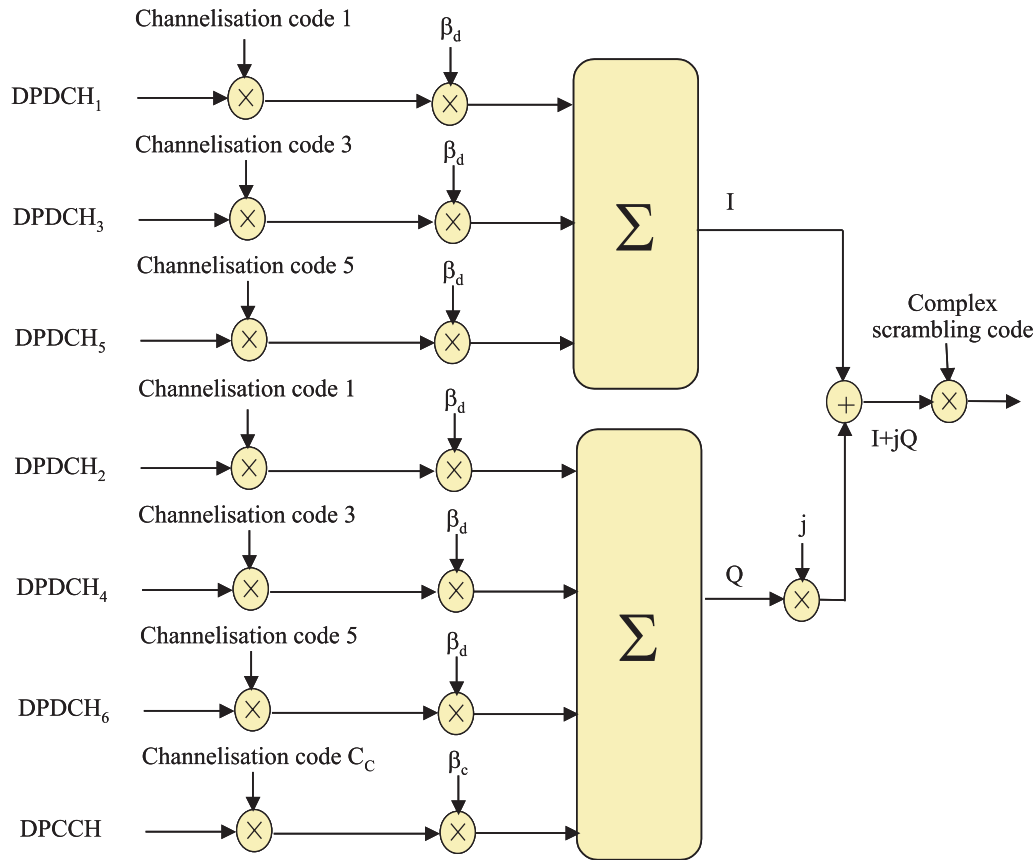
Figure 1.6: I-Q/code multiplexing of a DPCCH and several DPDCHs at the UE [31].

1.2.4 The HSDPA concept

In HSDPA, a new transport channel called the high speed downlink shared channel (HS-DSCH) is introduced in order to achieve higher data rates. The HS-DSCH can be time and/or code multiplexed between the UEs[3] in a cell, and is transmitted with fixed SF. All the UEs with access to the HS-DSCH have an associated DL DPCH. The HS-DSCH is mapped onto one or several high speed physical downlink shared channels (HS-PDSCHs), which can use QPSK or 16QAM (quadrature amplitude modulation). Note for comparison that the DPCH can only use QPSK for DL transmission. Moreover, two other physical channels are included to facilitate the HSDPA operation: (i) the high speed shared control channel (HS-SCCH), which carries the key information necessary for HS-DSCH demodulation; and (ii) the UL high speed dedicated physical control channel (HS-DPCCH), which carries the ACK/NACK (acknowledge/negative acknowledgement) messages and the channel quality indicator (CQI) feedback from the UE to the Node-B.

Given certain transmit power for the HS-DSCH, the bit rate is adapted to the state of the radio channel by varying the modulation and coding scheme (MCS) and the number of used HS-PDSCHs accordingly to the channel quality estimates fed back from the UE. This

---

[3] In this Ph.D. thesis, no code multiplexion of several UEs on the HS-DSCH is considered. Thus, only scenarios in which the HS-DSCH is time multiplexed are studied.

adaptive variation of the transmission parameters is referred to as link adaptation (LA), and can be done every 2 ms (i.e. three slots), which is the duration of the radio frame, also referred to as Transmission Time Interval (TTI). The channel quality estimates for the LA algorithm can be obtained from the CLPC commands for the associated DL DPCH, the ACK/NACK ratio or the CQI sent by the UEs through the UL HS-DPCCH [33]. Note that fast power control is not allowed on the HS-PDSCHs.

A fast physical layer retransmission scheme with chase combining or incremental redundancy (Hybrid Automatic Repeat reQuest, H-ARQ) is specified, which provides time diversity and facilitates faster retransmissions than in Release'99, where this process is handled by the RLC functionality at the RNC. In addition, the PS functionality is also moved from the RNC to the Node-B, which enables the possibility to consider the fast variations of the radio channel in the scheduling decisions, which can be made on a TTI basis. The operational principle of HSDPA is illustrated in Figure 1.7, and Table 1.1 provides a summary of the key properties of DCH and HS-DSCH [1], [34].

Channel quality feedback (CQI, Ack/Nack, CLPC commands)

Data

UE1

Channel quality feedback (CQI, Ack/Nack, CLPC commands)

Data

UE2

• Constant transmit power

• Adaptive modulation & coding

• Fast packet scheduling

• Fast layer 1 retransmissions (HARQ)

Fast scheduling is done directly in Node-B based on feedback information from the UE and knowledge of current traffic state.
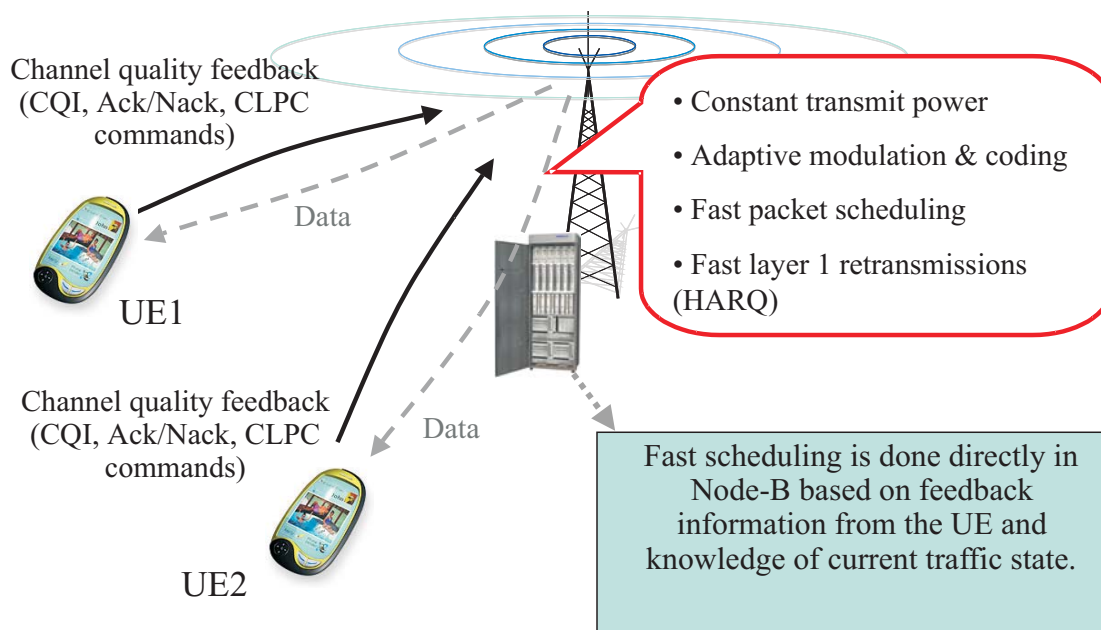
Figure 1.7: HSDPA operational principle.

1.3 Assessment methodology

As shown in Figure 1.8, there are several approaches to evaluate the performance of cellular systems. Each of them has advantages and disadvantages. Typically, simple theoretical studies involve low cost, and can give a reasonable approximation by using simple mathematical models. However, more detailed studies are problematic due to the high complexity of UMTS.

Table 1.1: Comparison of the different channel types [1], [34].

	HS-DSCH	DL DCH	UL DCH
SF	Fixed, 16	Variable (512-4)	Variable (256-4)
Modulation	QPSK/16QAM	QPSK	BPSK
Power control	Fixed /slow power setting	Fast with 1500 Hz	Fast with 1500 Hz
H-ARQ	Fast Layer 1 retransmissions	At RLC level	At RLC level
Interleaving period	2 ms	10-80 ms	10-80 ms
Radio frame length	2 ms	10 ms	10 ms
Channel coding schemes	Turbo coding	Turbo or convolutional coding	Turbo or convolutional coding
SHO	No	Yes	Yes
Release including it	Release 5	Release'99	Release'99
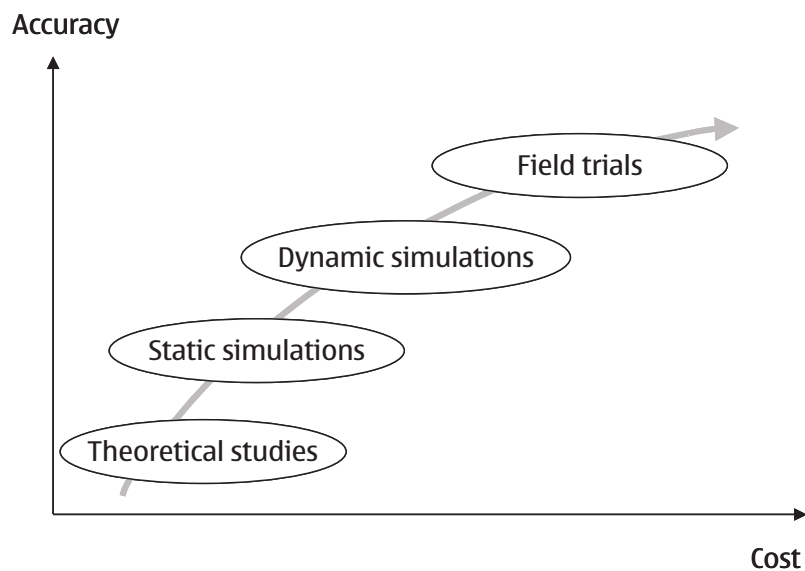
Figure 1.8: Assessment strategies for the analysis of cellular networks.

Another possibility is to use computer simulations of cellular networks, which allows the introduction of more realistic models and even specific algorithms for a more detailed study. Computer simulations can be static or dynamic. In static simulations, the time

dimension is not included, and results are obtained by extracting statistics of a sufficiently large set of snapshots of the system (Monte Carlo approach). Dynamic simulations include the time dimension, and are useful to analyse mechanisms that cannot be understood without considering the time dimension. Examples of such mechanisms are some RRM algorithms, such as CLPC or PS, which cannot be assessed under a static approach. In addition, there is also a so-called semi static approach, in which only one time dependent process is observed, while the rest of the mechanisms affecting the system performance are treated as in static simulations.

The third option is to conduct field tests in a trial or operational network. For a given network with a specific configuration, this approach yields the most accurate results. However, at the early stage of the development process, an operational network may not be available, and the deployment of a trial network is associated with high cost. Moreover, the results tend to be network specific (depending on the network configuration and environment) and may therefore differ from network to network.

In this Ph.D. thesis, most of the results are obtained by semi static and dynamic system level simulations, which are sometimes accompanied by theoretical discussions to provide a further insight into the involved phenomena. In general, this Ph.D. thesis includes modelling, system performance analysis and RRM algorithmic design of UMTS networks.

1.4 Objectives

The overall objective in this Ph.D. thesis is to evaluate the system performance of adaptive AAs as a capacity enhancing technique in a WCDMA terrestrial cellular system, with special emphasis on RRM considerations. Although the investigations are particularised for UMTS as a case study, the main trends and conclusions are general findings, which are valid for other cellular systems using CDMA.

One of the objectives is to assess the capacity gain provided by beamforming AAs at the Node-B. First, RRM algorithms that can automatically capture the available capacity gain while still maintaining the system stability must be investigated. Based on these algorithms, the actual capacity gain is determined for both UL and DL. In DL, it is of paramount importance to quantify the effect of the potential channelisation code limitations that may appear when only one scrambling code per cell is used. The UMTS specifications offer a solution to overcome this problem, in which the cell is divided into several scrambling code regions. The capacity gain that can be achieved with this solution is a key result, since it will be used in order to dimension the number of simultaneous scrambling codes that a Node-B with beamforming AAs should support.

The second objective is to evaluate the capacity gain that can be achieved when dual antenna Rake receivers with maximal ratio combining (MRC) are deployed at the UE. In this case, code blocking is also expected to be a potential problem, whose impact on the achievable capacity gain is going to be investigated as a function of the propagation conditions, the penetration of dual antenna UEs and the RRM configuration.

The third step is to assess the capacity gain that can be obtained when the traffic is carried over HSDPA and transmit and/or receive (Tx/Rx) diversity techniques are deployed. In HSDPA, some PS algorithms can provide multi-user diversity due to the fact that the fast

variations of the radio channels can be considered for the scheduling decisions. Evaluating the interaction between the multi-user diversity and antenna diversity techniques is of special interest, since the combination of several sources of diversity is known to provide diminishing returns.

It is important to emphasise that the study is conducted at system level, although it is based on previous link level studies conducted elsewhere. In this respect, it is not considered to be enough to extrapolate the results and conclusions from link level studies, since there are mechanisms, like e.g. the effect of some RRM algorithms on the system performance, that can only be fully understood by conducting a system level evaluation.

1.5 Outline of the thesis

This Ph.D. thesis is organised as follows:

Chapter 2 is an overview of the different AA techniques that are applicable in UMTS. Guidelines for the scope of application of each technique are given, together with some indications of their expected performance. The chapter addresses conventional beamforming at the Node-B, open and closed loop transmit diversity at the Node-B, and receive antenna diversity at both the Node-B and the UE. At the end, a discussion is presented on the combination of the described AA techniques at both the Node-B and the UE so that multiple-input-multiple-output (MIMO) operation can be enabled in UMTS.

Chapter 3 presents an analysis of the different UL AC algorithms that have been proposed in the open literature. Among them, a power based AC algorithm is selected and extended to the case with beamforming AAs at the Node-B. As a result, a directional power based UL AC algorithm is formulated. This algorithm is shown to automatically capture the available capacity gain of beamforming AAs while still maintaining the system stability, regardless of the spatial distribution of the interference. The study is conducted for power controlled DCHs, and has been carried out with a semi static network simulation tool built by the author in order to test the performance of the proposed scheme.

Chapter 4 describes the DL capacity gain of beamforming AAs at the Node-B. While maintaining the system stability by means of a directional power based DL AC algorithm, the achieved system capacity with power controlled DCHs is such that channelisation code shortage occurs. Based on the spatial filtering capabilities of beamforming AAs, a solution to overcome this problem with a low performance penalty is evaluated. For this chapter, a much more complete and complex dynamic network simulation platform has been used in order to obtain the results. When this study was started, this platform was under development in Nokia, the company sponsoring the project, and the author designed and added the support for beamforming AAs at the Node-B. Such support was included for both UL and DL, though extensive simulation studies have only been conducted for the DL case.

Chapter 5 deals with the DL capacity gain that is obtained when deploying dual antenna Rake receivers with MRC at the UE. Due to the large capacity gain achieved with power controlled DCHs, potential channelisation code shortage is identified as a serious limitation. The impact of the power delay profile of the radio channel on the capacity gain is studied, together with the influence of the SHO configuration and the QoS requirements. A simple theoretical model that relates the capacity gain to the penetration rate of dual antenna

UEs is presented in order to validate the trends observed in simulations. In order to obtain the results included in this chapter, the author has utilised the same dynamic simulation platform that was used in Chapter 4. For this purpose, the author designed and added the support for multiple antenna Rake receivers at the UE in the aforementioned simulation tool.

Chapter 6 shifts the focus of the study towards HSDPA. The capacity gain from deploying open and closed loop transmit diversity, and/or antenna receive diversity at the UEs is evaluated under different PS algorithms. In this case, the interaction between the antenna diversity and the multi-user diversity made available by fast quality based PS is of paramount importance. The results included in this chapter have been obtained with a dynamic HSDPA network simulator that was entirely developed by the author.

Chapter 7 summarises the thesis report and highlights the main conclusions of each chapter.

The reader of this Ph.D. thesis is expected to have a basic knowledge about system level aspects of UMTS and radio propagation. In principle, the different chapters can be read independently, although there are some cross-references between chapters. Citations are given by a number in square brackets, referring to a section placed at the end of the thesis, which contains the corresponding references. All the abbreviations are introduced in each chapter, and a list summarising the meaning of all of them is included at the beginning of the thesis.

1.6 Publications

The following articles have been published during the Ph.D. study:

- J. Ramiro-Moreno, K.I. Pedersen, P.E. Mogensen, "Directional power based admission control for WCDMA systems using antenna arrays", *IEEE Proc. 53rd Vehicular Technology Conference,* Vol. 1, pp. 53-57, May 2001.

- J. Ramiro-Moreno, K.I. Pedersen, P.E. Mogensen, "Network performance of WCDMA base stations deploying smart antennas", *Proceedings of the WPMC-01,* Vol. 2, pp. 1027-1032, September 2001.

- J. Ramiro-Moreno, K.I. Pedersen, P.E. Mogensen, "Radio resource management for WCDMA networks supporting dual antenna terminals", *IEEE Proc. 55th Vehicular Technology Conference,* Vol. 2, pp. 694-698, May 2002.

- J. Ramiro-Moreno, K.I. Pedersen, P.E. Mogensen, "Network performance of transmit and receive antenna diversity in HSDPA under different packet scheduling strategies", *IEEE Proc. 57th Vehicular Technology Conference,* Vol. 2, pp. 1454-1458, April 2003.

- J. Ramiro-Moreno, K.I. Pedersen, P.E. Mogensen, "Capacity gain of beamforming techniques in a WCDMA system under channelization code constraints", accepted for publication in the *IEEE Transactions on Wireless Communications*, May 2003.

In addition, the following articles were co-authored during the Ph.D. study:

- L. Schumacher, L. Berger and J. Ramiro-Moreno, "Recent advances in propagation characterisation and multiple antenna processing in the 3GPP framework", *Proceedings of XXVIIth URSI General Assembly, Maastricht, The Netherlands*, August 2002, Session C2.

- L. Berger, L. Schumacher, J. Ramiro-Moreno, P. Ameigeiras, T. E. Kolding and P.E. Mogensen, "Interaction of transmit diversity and proportional fair scheduling", *IEEE Proc. 57th IEEE Vehicular Technology Conference,* Vol. 4, pp. 2423-2427, April 2003.

- K.I. Pedersen, P.E. Mogensen and J. Ramiro-Moreno, "Application and performance of downlink beamforming techniques in UMTS", *IEEE Communications Magazine*, Vol. 44, Issue 10, pp. 134-143, October 2003.

Chapter 2

Adaptive antennas in UMTS

2.1 Introduction

Adaptive antenna arrays (AAs) are considered to be one of the attractive technologies that can be used to increase the spectral efficiency of the Universal Mobile Telecommunications System (UMTS). As reported in [8], AAs can be used to offer increased protection against fading, thermal noise and/or co-channel (multiple access) interference, i.e. the three major capacity limiting factors that arise as high speed data services are introduced. In this respect, it must be stressed that the comment about the increased protection against thermal noise only applies to cases with multiple antennas at the receiver.[4]

Conventionally, AAs can be operated in one of two distinct modes: (i) Diversity mode or (ii) Beamforming mode. Beamforming techniques create narrow beams towards each user equipment (UE), in such a way that the multiple access interference is reduced by means of spatial filtering [17] and potential suppression of interfering signals. The spatial filtering of the interference is only efficient when the azimuth spread (AS) is low, and therefore this is the scope of application of these techniques [35].

---

[4] The use of several antennas for signal reception can provide an increased protection against thermal noise. However, as will be seen later, using multiple antennas for transmit diversity (e.g. space time transmit diversity) does not offer any extra protection against thermal noise, and the effect of thermal noise on the signal quality becomes actually more severe, since it contributes to poorer channel estimation for each diversity branch.

Diversity techniques rely on the statistical independence between the AA elements and reduce the likelihood of deep fades [36]. When they are used for reception, or in conjunction with a priori knowledge of the radio channel at the transmitter [37], they are additionally able to provide an average signal-to-interference-plus noise ratio (SINR) gain. When the AS of the radio channel is large, low correlation between the antenna elements can be achieved without excessive antenna separation [35], which makes the use of diversity techniques feasible. Low correlation between antenna elements can be also obtained by using polarisation diversity.

In this chapter, the different AA techniques that are allowed in the Release 5 of the UMTS specifications are described. The new proposals currently under discussion in the 3rd Generation Partnership Project (3GPP) (see e.g. [38]) are excluded, since their performance is not assessed in this Ph.D. thesis.

The possibility of deploying AAs at both the Node-B and the UE is also discussed in this chapter, as a manner to enable multiple-input-multiple-output (MIMO) operation in UMTS. Note that the combination of AA techniques already allowed in UMTS opens for the use of MIMO systems that aim at improving the SINR of a certain link conveying a single data stream, without conducting spatial multiplexing of parallel data streams. This approach is often referred to as diversity MIMO. There are also proposals in the open literature to utilise the MIMO systems so that several parallel spatial multiplexed data streams are transmitted between two transceivers equipped with AAs [39], leading to the so-called information MIMO approach. Some of these proposals are being currently discussed within 3GPP [38].

The chapter is organised as follows. Section 2.2 describes different manners in which AAs can be used at the Node-B in UMTS. Note that such description is based on the Rake receiver with maximal ratio combining (MRC) of the Rake finger outputs as a basic structure for dealing with multipath propagation environments. In Section 2.3, a similar discussion is shown for the case where multiple antennas are implemented at the UE side. The deployment of AAs at both the transmitter and the receiver in order to enable MIMO operation in UMTS is addressed in Section 2.4. Concluding remarks are given in Section 2.5.

2.2 Antenna arrays at the Node-B

2.2.1 Uplink case − signal reception with AAs

Figure 2.1 depicts a general Rake receiver with M antenna elements deployed for uplink (UL) signal reception at the Node-B. It is assumed that an independent antenna combining operation is conducted for each Rake finger, followed by MRC of the N Rake finger outputs. In this section, different options for the antenna combining are discussed. Since the AA is operated at the receiver side, it is possible to estimate the radio channel and the spatial covariance matrix of the interference, which opens for the use of advanced combining schemes that make use of all this information. As will be seen, the receiver structure can be simplified for some of the described options for antenna combining.

2.2.1.1 Optimum combining

The weights that maximise the SINR of the received signal were derived by Wiener [14], and constitute a solution that is very often referred to as optimum combining. This

combining scheme fully exploits the information of the spatial covariance matrix of the interference, and provides *M*-1 degrees of freedom that can be used for diversity reception or interference suppression. When the number of mutually interfering UEs in the system (*K*) does not exceed *M*, optimum combining for the reception of the signal of one UE is capable to null out the signals from all the interfering (*K*-1) UEs, and still use the remaining *M-K* degrees of freedom to provide increased diversity protection [40].
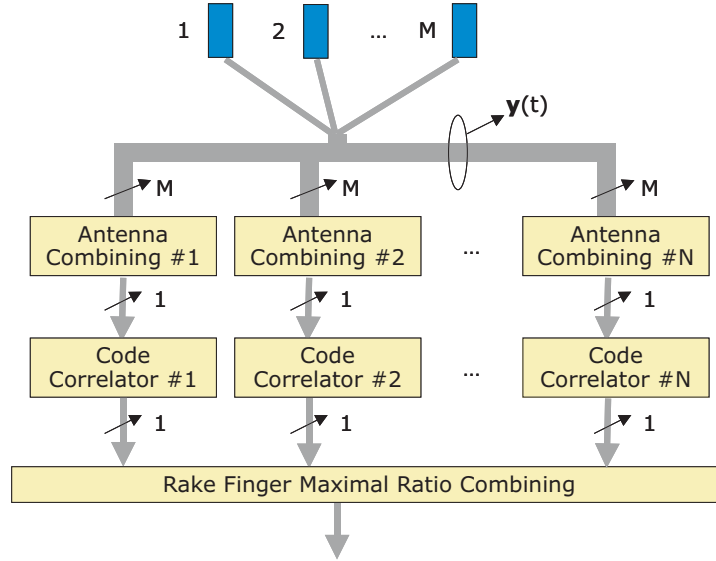
Figure 2.1: General Rake receiver with multiple antennas.

2.2.1.2 Maximal ratio combining

When the spatial distribution of the interference is white, optimum combining converges to the well-known MRC scheme [15], which is less complex to implement. In order to perform MRC of the signals at several branches, the following weight has to be used for each one of them:

$$w_i = \frac{\alpha_i^*}{I_i},$$

(2.1)

where α_i is the complex value of the radio channel affecting the desired signal at branch *#i*, and I_i the power of the interference received at that branch. After that, the weighted signals at all the branches are summed. As can be seen, MRC involves co-phasing and amplitude weighted sum of the received signals at the different branches. When all the AA elements are uncorrelated, the resulting SINR after ideal MRC of all the fingers at all the antennas can be written as [36]:

$$SINR = \sum_{m=1}^{M} \sum_{n=1}^{N} SINR_{n,m}$$

(2.2)

where $SINR_{n,m}$ is the SINR at the nth finger of the mth antenna. Note that it has been assumed that there are sufficient Rake fingers to track all the resolvable multipath components in the

power delay profile (PDP). For MRC, the structure shown at Figure 2.1 can be changed for another one in which N Rake fingers are directly connected each antenna. At the output, MRC of the $M \cdot N$ Rake fingers yields the same result as the one shown in (2.2).

When the branch power ratio between the antenna elements equals zero dB and channel estimation is ideal, MRC provides an average SINR gain that equals M. In addition, the diversity order of the system is increased with a factor of M. However, as many other diversity techniques, the diversity gain of MRC is of diminishing returns if other sources of diversity, such as soft handover (SHO) or frequency selective channels are available.

However, with power controlled channels, the achieved SINR gain from receive diversity makes the UE transmit less power. As a consequence, the received signal energy at each diversity branch is lower than in the case of single antenna reception, which results in poorer channel estimation and makes the overall gain from receive diversity be lower than the one described for ideal channel estimation.

Measurement and simulation campaigns for UL MRC with M=4 are described in [41] for power controlled dedicated channels (DCHs). In that work, the capacity gain due to migration from M=2 to M=4 is reported to equal 2.7 dB for Vehicular A [42] at both 3 and 50 kmph for a block error rate (BLER) target of 10%. For Pedestrian A [42], the capacity gain due to migration from M=2 to M=4 equals 3.3 dB at 3 kmph and 3.6 dB at 50 kmph. In this Ph.D. thesis, the system level performance of AAs with MRC at the Node-B for UL signal reception is not studied.

2.2.1.3 Conventional beamforming

When the AS of the radio channel at the Node-B is low, another alternative is to use conventional beamforming (CBF) [17]. In short, the CBF concept consists of pointing a narrow beam towards the desired UE, so that the power transmitted by UEs at other azimuth locations is suppressed. This spatial filtering of the interference, which facilitates a capacity increase, is illustrated in Figure 2.2.
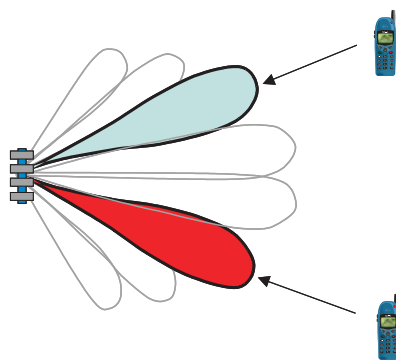
Figure 2.2: Spatial filtering of the interference.

In [15], extensive link level studies are conducted for a scheme in which a different beam is generated for each multipath component, i.e. for each Rake finger. That scheme works exactly as MRC for the special case with AS=0°. In addition, it also allows diversity gain by tracking the short-term variations of the direction of arrival (DoA) of the different

multipath components at the expense of higher receiver complexity [43]. This diversity gain, also known as Jitter diversity, depends on the update rate of the steering direction of the beams.

For this study, the considered CBF technique is the one in which a single beam is generated towards the average DoA of the UE, which is defined as the azimuth direction at which a pointed beam captures the maximum desired energy. Thus, only a single antenna combining operation is needed for the whole set of Rake fingers, which reduces the receiver complexity and allows simpler and more robust operation. In addition, only estimation of the average DoA of the UE is needed, instead of the *M* complex parameters per Rake finger that have to be estimated for optimum combining. The block diagram for CBF is depicted in Figure 2.3, which includes MRC of the output of the different Rake fingers. The solution with a single beam per UE is only attractive if the azimuth direction of most of the impinging paths at different delays fall within the beamwidth of the AA, i.e. if the AS at the Node-B is low compared with the beamwidth of the synthesised beams.
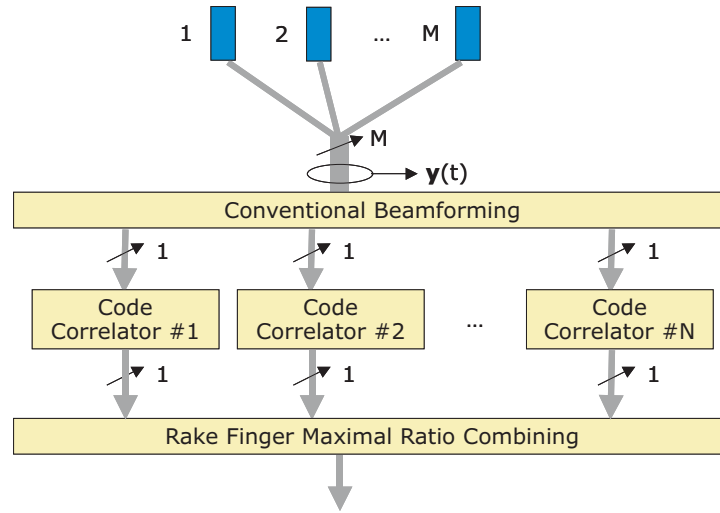
Figure 2.3: Rake receiver with CBF synthesising a single beam per UE.

For this scheme, the combining weights are selected so that the radiation pattern is focused at the DoA of the desired UE:

$$\mathbf{w}(\phi_{Avg}) = \left[w_1(\phi_{Avg}), w_2(\phi_{Avg}), ..., w_M(\phi_{Avg}) \right]^T, \tag{2.3}$$

where w_m is the combining weight at the mth element of the AA, which is calculated as

$$w_m(\phi_{Avg}) = \frac{1}{\sqrt{M}} \exp\left[-j(m-1)\pi \sin(\phi_{Avg}) \right], \tag{2.4}$$

where ϕ_{Avg} is the average DoA of the desired UE (defined relative to the broadside direction of the AA) and *j* is the imaginary unit. Note that (2.4) is written for a uniform linear AA with half-a-wavelength spacing between the antenna elements. As can be seen, a constant phase rotation is applied to consecutive antenna elements before combining and no amplitude weighting is conducted.

In order to illustrate the spatial filtering gain from CBF, which is an allowed AA technique for all the UL channels in UMTS, the radiation patterns that are created for the different UEs depending on their DoA are analysed in the following. The amplitude antenna gain of the AA at ϕ_2 when a beam is pointed at ϕ_1 can be expressed by

$$G(\phi_1;\phi_2) = \mathbf{w}^H(\phi_1)\,\mathbf{c}(\phi_2), \qquad (2.5)$$

where $[]^H$ denotes Hermitian transposition, $\mathbf{w}(\phi)$ is defined in (2.3), and $\mathbf{c}(\phi)$ represents the array steering vector, which yields

$$\mathbf{c}(\phi) = [c_1(\phi), c_2(\phi), ..., c_M(\phi)]^T, \qquad (2.6)$$

with

$$c_m(\phi) = f(\phi)\exp[-j(m-1)\pi\sin(\phi)], \qquad (2.7)$$

where $f(\phi)$ is the complex radiation pattern of the antenna elements. The effective power radiation pattern of the directional beam is influenced by the radio channel's azimuth dispersion seen at the Node-B, so the effective power antenna gain at ϕ_2 when a directional beam is pointed at ϕ_1 equals [35]

$$W(\phi_1;\phi_2) = \oint |G(\phi_1;\varphi)|^2\, p_A(\varphi - \phi_2)d\varphi, \qquad (2.8)$$

where $p_A(\phi)$ is the power azimuth spectrum (PAS) of the radio channel at the Node-B. Field measurements have shown that the PAS can be approximated with a Laplacian function for typical urban environments, with a local average AS of 5°–10° [44]. Alternative models for the PAS are discussed in [45] and [46], among others. However, the actual shape of the PAS does not have a strong influence on the effective power antenna gain in (2.8), provided that the AS at the Node-B is smaller than the beamwidth of the directional beams. For this study, the radiation pattern of the antenna elements is given by

$$f(\phi) = \begin{cases} \sqrt{\beta}\cos^{1.4}(\phi) \ for \ \phi \in [-90°,90°] \\ \sqrt{\beta/R} \ otherwise \end{cases}, \qquad (2.9)$$

where β is the broadside antenna gain, and R is the front-to-back ratio. In this case, $\beta = 18$ dBi and $R = -33.8$ dB. This radiation pattern is selected in order to provide a coverage area corresponding to a hexagonal cell [47].

Figure 2.4 shows the effective radiation pattern of a set of directional beams that have been generated with a uniform linear AA of four antenna elements. This plot has been obtained for an AS of 5° and six beams pointing at $\phi = [-50°, -25°, -8°, 8°, 25°, 50°]$. For comparison, a sector beam covering the whole cell is also depicted. The radiation pattern for the sector beam is assumed to equal that of the antenna elements of the AA, although it is also generated by the AA. As in the case of the directional beams, the effective power radiation pattern of the sector beam is affected by the PAS of the radio channel and equals

$$S(\phi) = \oint |f(\varphi)|^2\, p_A(\varphi - \phi)d\varphi \qquad (2.10)$$
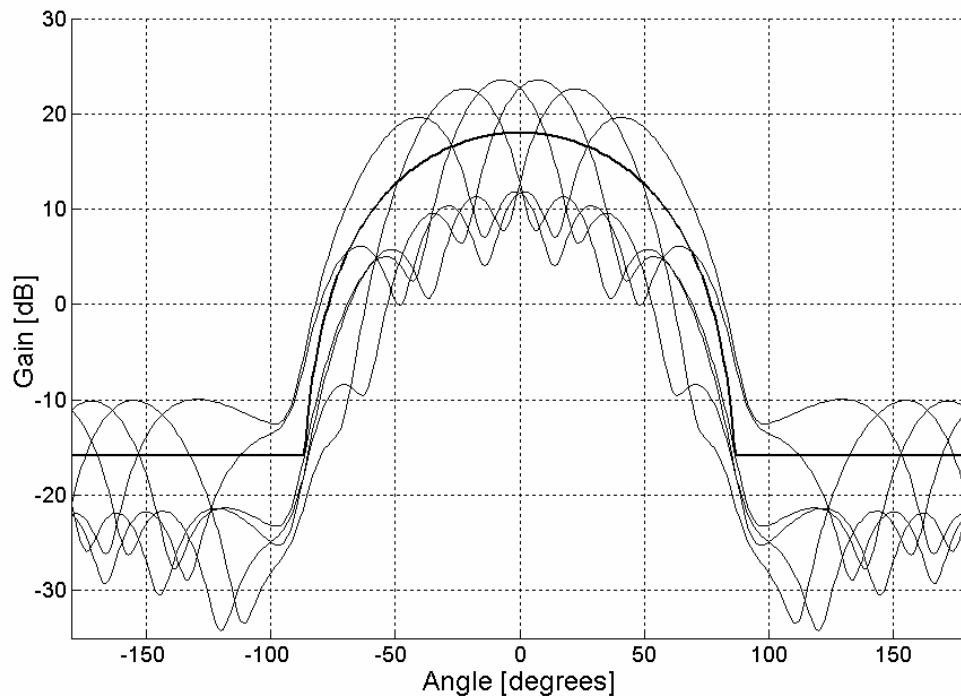
Figure 2.4: Effective power radiation patterns of the generated beams. AS = 5°. *M* = 4.

As can be seen, the generated directional beams are much narrower than the sector beam, which facilitates the spatial filtering of the interference. Moreover, their gain is larger since the radiation pattern is concentrated only in one direction. As a simple approximation, the ratio between the gain of one directional beam at its steering direction and the gain of the sector beam at the same azimuth direction can be written as

$$\frac{W(\phi;\phi)}{S(\phi)} \cong M \tag{2.11}$$

However, when the AS at the Node-B is large, the capability to perform spatial filtering of the interference is degraded, due to the fact that the beams become effectively wider. In order to illustrate this, let us consider the UL of a two-UE scenario where both UEs are received with equally strong power. If the AA is able to point a beam at the exact DoA of the desired UE, the carrier-to-interference ratio (C/I) between the desired UE located at ϕ_1 and the interfering UE located at ϕ_2 is thus expressed as [35]

$$\frac{C}{I} = \frac{W(\phi_1;\phi_1)}{W(\phi_1;\phi_2)} \tag{2.12}$$

Figure 2.5 plots the C/I as a function of the azimuth separation between the two UEs for *M*=4 and several values of the AS. For this analysis, it has been assumed that ϕ_1=0°. As can be seen, large AS degrades the spatial filtering capability of the AA, measured in this simple model as the achieved C/I. For example, in order to achieve a C/I of 9 dB, the necessary azimuth separation is 21° when AS=1°, while it is 34° when AS=15°. The reason is that, due to azimuth dispersion, the effective power radiation pattern of the synthesised beams becomes

wider (see (2.8)). As suggested in [48], the actual capacity gain that can be achieved is strongly related to the beamwidth reduction i.e., the ratio between the sector antenna's beamwidth and that of the synthesised narrow directional beams. For example, the results in [48] when AAs are implemented in a cell with circular coverage area indicate that a beamwidth reduction of 3 corresponds to a capacity gain of 170% approximately.
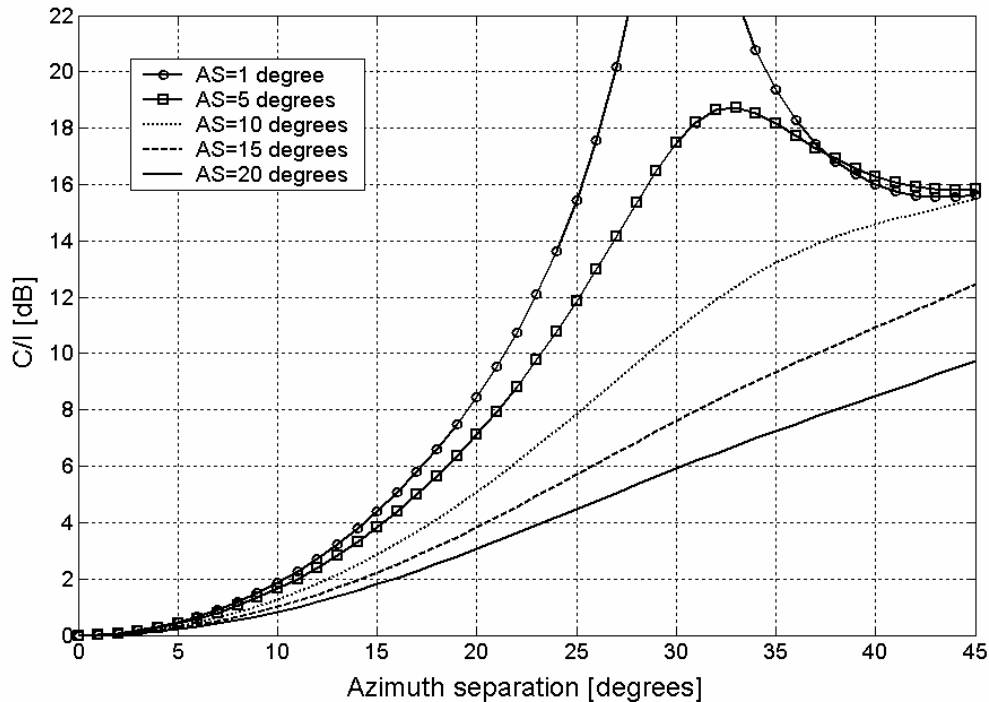
Figure 2.5: C/I versus azimuth separation when using 4 antenna elements.

2.2.2 Downlink case – signal transmission with AAs

The AA processing techniques described for UL can also be used for the downlink (DL) case. However, due to frequency division duplex (FDD) operation, the Node-B cannot estimate the DL radio channel. As a consequence, the AA has to be operated either blindly or based on limited radio channel information that is fed back by the UEs.

As in the UL case, beamforming is advisable when the azimuth dispersion is low, and diversity techniques are suitable when low correlation between the antenna elements can be achieved. Furthermore, transmit diversity techniques can be classified into two main groups: (i) the ones not requiring any feedback information from the UEs about the instantaneous radio channel state (open loop transmit diversity techniques) [49], and (ii) the ones requiring this type of feedback information (closed loop transmit diversity techniques) [50], [51].

2.2.2.1 Conventional beamforming

The average steering direction for DL beamforming towards a UE can be estimated based on the UL average DoA [52]. Besides complexity issues, the Node-B's lack of DL channel knowledge is the reason why multi-beam combining approaches are excluded from

the following considerations. Instead, the same single beam CBF technique as described for the UL case can be deployed to enable DL spatial interference filtering.

Even though CBF is used in UMTS, a sector beam providing coverage for the entire cell has to be deployed in order to transmit all the common channels that have to be broadcasted to all the UEs in the cell. One of the channels that have to be transmitted on the sector beam is the primary common pilot channel (P-CPICH), which is used for handover measurements by the UEs, etc. [1]. In addition, a number of directional beams can be synthesised with AAs in order to carry the signals that do not have to be transmitted to the entire cell. Note that the phase reference of the P-CPICH is not valid for reception of signals transmitted under the synthesised directional beams, since the pilot signal used for phase reference has to be transmitted under the same radiation pattern as the desired signal.

In UMTS, it is mandatory for the UEs to support phase reference using a P-CPICH, a secondary common pilot channel (S-CPICH) or dedicated pilot symbols for demodulation of DPCHs. However, since the P-CPICH cannot be used for phase reference when applying beamforming, in that case the UE is informed via higher layer protocols to use dedicated pilot symbols (transmitted on the dedicated physical channels) or one S-CPICH for this purpose.

Let us now distinguish two manners to apply beamforming within one logical cell. On one hand, the generation of beams towards the DoA of each specific UE can be conducted, which will be called in this context "user specific beamforming". On the other hand, another possibility is to synthesise only a finite set of beams at the Node-B, and serve each UE with the most suitable beam. With this option, which will be called in this context "fixed beamforming", many UEs may receive signals transmitted under the same beam.

Due to the use of beamforming, phase estimation is only possible based on S-CPICH or dedicated pilot symbols. In the case of "fixed beamforming", either dedicated pilots or an S-CPICH can be used for pilot reference. In this study, the option in which a unique S-CPICH is permanently broadcasted on each beam for phase reference is selected for further discussion, and in the sequel it will be simply referred to as "fixed beamforming". In the case of "user specific beamforming", the transmission of an S-CPICH per beam is in principle allowed. However, it is not considered to be efficient, since the number of synthesised beams could be very large and the transmission of an S-CPICH per beam would imply a very large pilot power overhead. Therefore, the case of "user specific beamforming" with phase estimation based on dedicated pilot symbols is also selected for further discussion in this study, and in the sequel it will be simply referred to as "user specific beamforming".

The solution with "fixed beamforming" suffers from an additional S-CPICH pilot overhead compared with the configuration with "user specific beamforming". On the other hand, "user specific beamforming" does in general result in higher SINR requirements for the UEs due to poorer channel estimation (phase reference) from using dedicated pilot symbols compared with S-CPICH. The potential loss of using "fixed beamforming" is furthermore contributed by the finite set of steering directions, which may be mapped into an equivalent steering error compared with the scenario with infinite resolution in steering directions. A comparison of the two beamforming modes in [13] concludes that the two schemes offer comparable gains in an interference limited network when the traffic is carried by DCHs. Furthermore, the support of "user specific beamforming" is not mandatory for UEs receiving the high speed shared control channel (HS-SCCH) and the high speed physical downlink shared channel (HS-PDSCH), since phase reference estimation for these channels is only mandatory using the P-CPICH and S-CPICH. Notice that both the HS-PDSCH and the

HS-SCCH belong to the high speed downlink packet access (HSDPA) concept, introduced as a part of the Release 5 of UMTS [1].

In this study, "fixed beamforming" is the selected CBF technique for performance evaluation, since it can be used for both HSDPA and DCHs. In a mixed scenario where some traffic classes are carried by HSDPA and others are carried on DCHs, it is preferred to use "fixed beamforming" for the traffic conveyed on DCHs, since this is the selected option for HSDPA and the associated pilot overhead is going to be experienced anyway. Details about which channels, according to the specifications [27], allow beamforming are given in Table 2.1. In those cases in which beamforming is allowed, information is also provided about whether they can use S-CPICH or dedicated pilots for phase reference.

Table 2.1: Possibilities to conduct CBF on DL channels in a cell [27].

Transport Channels	Physical Channels	CBF allowed	S-CPICH for phase reference allowed	Dedicated pilots for phase reference allowed
Dedicated channel (DCH)	Dedicated physical channel (DPCH)	Yes	Yes	Yes
Downlink shared Channel (DSCH)	Physical downlink shared channel (PDSCH)	Yes [1]	Yes	Yes
High speed downlink shared channel (HS-DSCH)	High speed physical downlink shared channel (HS-PDSCH)	Yes [2]	Yes	Optional
Broadcast channel (BCH)	Primary common control physical channel (P-CCPCH)	No	--	--
Forward access channel (FACH) Paging channel (PCH)	Secondary common control channel (S-CCPCH)	No	--	--
-	Synchronisation channel (SCH)	No	--	--
-	Acquisition indicator channel (AICH)	No	--	--
-	High speed shared control channel (HS-SCCH)	Yes	Yes	Optional
-	Paging indicator channel (PICH)	No	--	--
-	Primary common pilot channel (P-CPICH)	No	--	--
-	Secondary common pilot channel (S-CPICH)	Yes	Yes	No

[1] Assuming that the associated DPCH is transmitted under the same beam as the PDSCH.
[2] Assuming that the HS-SCCH and the associated DPCH are transmitted under the same beam.

Signals towards different UEs in the same cell are typically transmitted under the same primary scrambling code, and separated by means of orthogonal channelisation codes, selected from a channelisation code tree [1]. The number of available channelisation codes is limited, corresponding to an equivalent maximum DL capacity of approximately 2 Mbps when the traffic is carried by DCHs with a coding rate of 1/3. In order to exceed that capacity, a new scrambling code has to be enabled, which allows the use of a new instance of the channelisation code tree. The penalty of introducing multiple scrambling codes in the same cell is a poorer equivalent DL orthogonality factor [53], since only signals transmitted under the same scrambling code are orthogonal, while signals under different scrambling codes are non-orthogonal. However, the loss due to poorer orthogonality can be reduced in the case of beamforming by splitting the cell into multiple scrambling code regions, so that a new instance of the channelisation code tree is available for each utilised scrambling code. In this case, the spatial isolation between beams using different scrambling codes helps compensate for the lack of code orthogonality.

According to the UMTS specifications, there are channels, like e.g. the P-CPICH, that must be transmitted under the primary scrambling code [27]. Thus, the sector beam is transmitted under the cell's primary scrambling code, while the directional beams can be transmitted either under the cell's primary scrambling code or under any of the 15 different secondary scrambling codes associated with the cell's primary scrambling code [31]. Figure 2.6 shows an example with the mapping of channels onto a grid of six directional beams plus one sector beam.

Directional Beams:

• DPCH

• PDSCH

• S-CPICH

• HS-SCCH

• HS-PDSCH

—— Primary Scrambling Code

- - - - Secondary Scrambling Code

Sector Beam:

• P-CPICH

• P-CCPCH

• SCH

• AICH

• PICH

• etc.

x M

Number of antenna elements

Node-B with AA
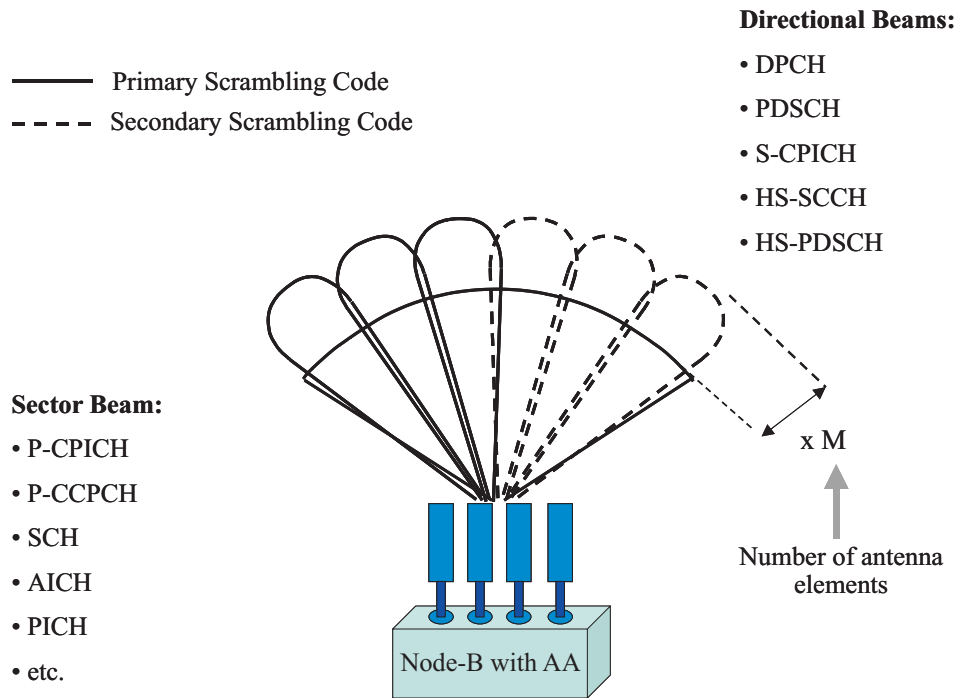
Figure 2.6: Mapping of physical channels onto a grid of fixed beams for the case of _M_ = 4. Six directional beams and a sector beam are synthesised.

As in the UL case, the capacity gain from CBF is based on the spatial filtering of the interference. Therefore, it is also strongly related to the beamwidth reduction, i.e. the ratio between the sector antenna's beamwidth and that of the synthesised narrow directional beams. Furthermore, there are other DL specific phenomena that do not occur in the UL case. For example, the pilot overhead from the S-CPICH is expected to affect the achieved capacity gain. On the other hand, the aforementioned potential channelisation code shortage is also of interest, as well as the impact of the described cell splitting strategy on the achieved capacity gain.

2.2.2.2 Open loop transmit diversity

In UMTS there are two different open loop transmit diversity techniques: time switched transmit diversity (TSTD) and space time transmit diversity (STTD).

TSTD [27] uses two antennas, and the transmission is alternated from one antenna to another on a slot basis (note that the slot duration is 0.667 ms). The use of TSTD is only allowed for the broadcast primary and secondary synchronisation channels (SCH). Support for this technique is optional for the network and mandatory for the UE [27].

The standard procedure for STTD [27], which is optional for the network and mandatory for the UE, is a slightly modified version of the dual antenna space time block coding scheme proposed by Alamouti [49]. Symbol pairs [s_1 s_2] are encoded and transmitted during two consecutive symbol intervals as depicted in Figure 2.7. Notice that the system is still transmitting two symbols during two symbol periods, and works under the assumption that the radio channel remains constant during that time.
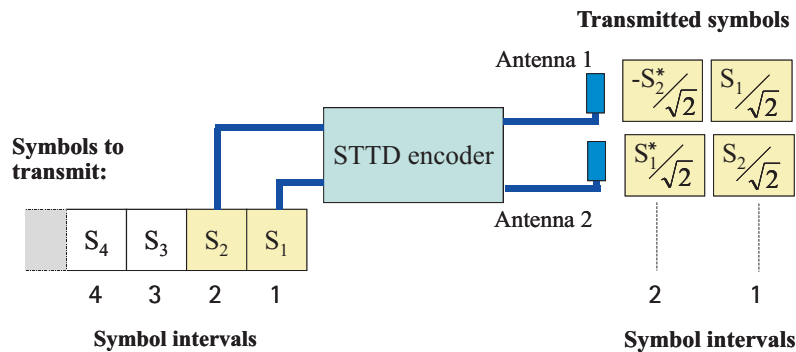
Figure 2.7: Alamouti STTD encoding scheme.

As it can be seen, the transmitted symbols are normalised in such a way that half of the power is transmitted on each antenna. Thus, the fact that two transmit antennas are deployed does not imply that the symbols are transmitted with twice as much power compared with the single transmit antenna case. Details for signal reception with one or more antennas are given in [49].

This scheme does not provide any average SINR improvement. However, the diversity order of the system is doubled when the branch power ratio between antenna elements equals zero dB, which reduces the probability of deep fades. At the same time, the probability of experiencing constructive fades with very large signal strength is also reduced, i.e. the tails of

the fading depth distribution become shorter on both sides. This can be seen in Figure 2.8, which shows the cumulative distribution function (CDF) of the fading depth of the radio channel for single antenna transmission and STTD in a Pedestrian A environment. The fading depth of the radio channel is defined as the normalised signal strength after Rake combining and STTD decoding.
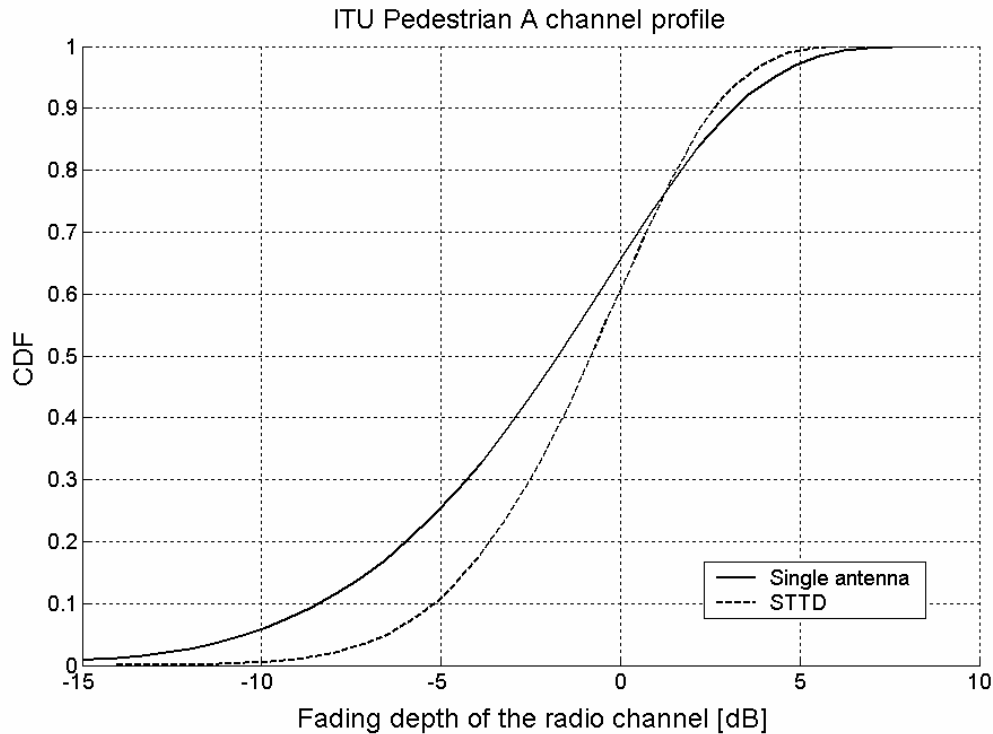
Figure 2.8: CDF of the fading depth of the radio channel for single antenna transmission and STTD. ITU Pedestrian A channel profile.

Two pilot signals are required for phase reference. Therefore, the common pilot channel (CPICH) has to be transmitted from both antennas with the same channelisation and scrambling code. However, the pre-defined bit sequence of the CPICH is different for each antenna (see [27]). Note that both the P-CPICH and the S-CPICH can be used as phase reference to detect a DL physical channel using STTD. If none of these channels can be used as a phase reference, it is not possible to use STTD.

When using STTD, the transmission power is split into two diversity branches. As a consequence, the channel estimates for the signals coming from each one of the diversity branches are jeopardised, which makes the benefits from STTD be lower than predicted for the case of ideal channel estimation.

Capacity gain results for STTD with power controlled DCHs can be found in [54], where a capacity gain of up to 40% is reported for scenarios with almost no diversity of any other kind. For scenarios with multipath diversity, the capacity gain is reported to fall below 10%. Other results from the open literature are more optimistic. See e.g. [37], where a capacity gain between 40% and 100% is reported, depending on the UE speed. In general, as other sources of diversity are introduced in the system, the capacity gain from deploying

STTD is reduced. This is typically the case when SHO is enabled. If under some conditions the deployment of STTD with power controlled DCHs leads to a situation in which channelisation code shortage becomes a serious limitation, it is not straightforward to find a solution to overcome this problem. Note that this was possible in the CBF case due to the spatial filtering properties of AAs with CBF, which make it possible to spatially isolate regions with different scrambling codes.

2.2.2.3 Closed loop transmit diversity

In cases where instantaneous DL channel information can be made available to the Node-B via UL signalling, closed loop transmit diversity (CLTD) presents an attractive alternative to open loop techniques. The transmitter/receiver structure for CLTD is shown in Figure 2.9.
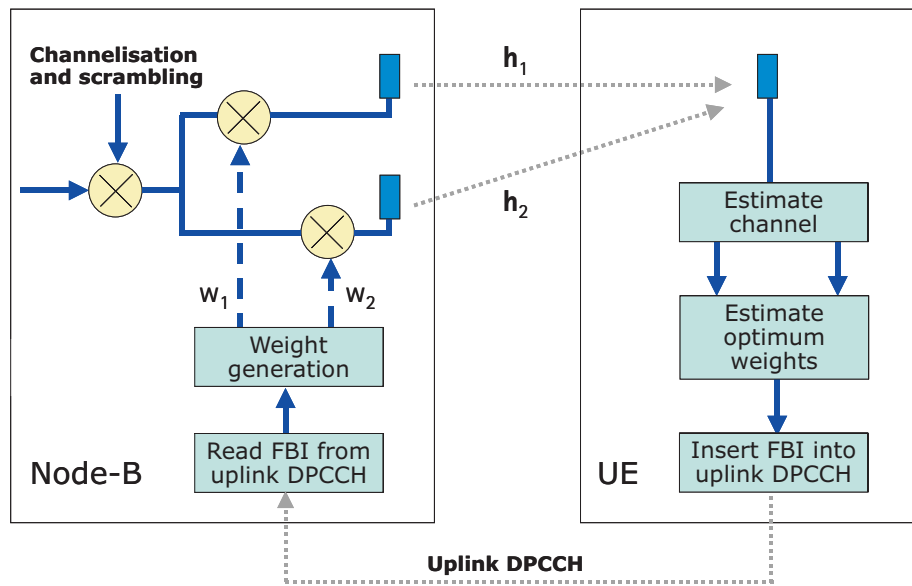
Figure 2.9: Transmitter/Receiver structure for CLTD.

The complex wideband signal is fed to the transmit antennas, weighted by a complex factor per antenna. The weight factors are determined at the UE, which estimates the channel coefficients from the pilot signals sent from the antennas at the Node-B. With these channel estimates, the UE can select the best weights from a restricted set, so that the normalised received signal power

$$P = \mathbf{w}^H \mathbf{H}^H \mathbf{H} \mathbf{w} \tag{2.13}$$

is maximised [33], [50]. In (2.13), $\mathbf{H} = [\mathbf{h}_1 \ \mathbf{h}_2]$ is the channel matrix containing the estimated channel impulse responses, represented as $\mathbf{h}_n = [\alpha_{n1} \ \alpha_{n2} \dots \alpha_{nL}]^T$, and α_{nl} refers to the complex channel coefficient of the lth multipath component at antenna #n. Moreover, $\mathbf{w} = [w_1 \ w_2]^T$ is the applied vector of coefficients. Notice that only one coefficient is available for each transmit antenna. Thus, there are not enough degrees of freedom to fully adapt to the wideband nature of the radio channel.

If the set of coefficients could be selected without constraints, this solution would be equivalent to antenna MRC at the receiver in the narrowband case. However, even in the narrowband case, the set of possible weights is limited due to restrictions in the UL bandwidth for signalling.

The weights are fed back using the feedback information (FBI) word in the UL dedicated physical control channel (DPCCH), carrying up to 2 bits per slot [27]. The 2 bits carry the same information, which means that the redundancy can be used to improve the SINR of the FBI word at the receiver. Therefore, the information rate for the feedback of the weights is only 1 bit per slot.

If the set of possible weights were large, the feedback would take several slots, which would increase the feedback delay, resulting in poor performance in a fast varying channel. Therefore, the choice of the weight quantisation is a trade-off between accuracy and update rate. For that reason, two modes of operation are supported.

Mode 1: Mode 1 is designed for a fast varying channel. The weights are updated every slot, but the total number of weights to choose from per slot is only 2. The feedback information gives the absolute phase difference between the diversity antennas: for even slot numbers, the phase is either 0° or 180°, and for odd slot numbers, the phase difference is either 90° or 270°. Both antennas transmit with the same power. The Node-B bases its transmit weight adjustment on an average of the information included in the current and previous weight feedback bit, resulting in a phase resolution of 90°. The phase of the first antenna is always zero.

Mode 2: Mode 2 is designed for a more slowly varying channel. The total number of weights to choose from is increased to 16, which means that the transmission of a full weight takes four slots. In order to respond faster to the changing channel conditions, mode 2 uses progressive updating of the weights. This means that the antenna weights are slowly sent over several slots in such a way that the first bit carries a coarse description of the weight, which is later fine-tuned by the last sent bits. The phase difference between the diversity antennas can be set in steps of 45°, and the power difference can be either +6dB or -6dB. The phase of the first antenna is always zero.

The sets of allowed weights for each mode are summarised in Table 2.2.

Table 2.2: Sets of allowed weights for CLTD.

CLTD mode	Antenna 1	Antenna 2
1	$w_1 = \dfrac{1}{\sqrt{2}}$	$w_2 = \dfrac{1}{\sqrt{2}} \cdot e^{j\phi}, \phi \in \left[45°,\ 135°,\ 225°,\ 315°\right]$
2	$w_1 \in \left[\sqrt{0.2}, \sqrt{0.8}\right]$	$w_2 = \sqrt{1 - w_1{}^2} \cdot e^{j\phi}$ $\phi \in \left[\begin{array}{l}45°,\ 90°,\ 135°,\ 180°,... \\ ...\ 225°,\ 270°,\ 315°,\ 360°\end{array}\right]$

When the UE is in SHO, the weights can be selected so that the normalised received signal power

$$P = \mathbf{w}^H \left(\mathbf{H}_1{}^H \mathbf{H}_1 + \mathbf{H}_2{}^H \mathbf{H}_2 + ... \right) \mathbf{w} \qquad (2.14)$$

is maximised [33]. In (2.14), $\mathbf{H}_i$ denotes the estimated channel matrix for the ith branch of the active set of SHO. The reason why only one set of weighting coefficients is selected for all the branches is that there is only one UL command that can be fed back by the UE.

For phase reference, both common and dedicated pilots are transmitted on both diversity antennas. The common pilots are transmitted with constant phase and power, while the dedicated pilots are transmitted with the same weight coefficients as the dedicated data signal. The common pilots on the two antennas have different orthogonal patterns in order to enable separate channel estimation for each diversity branch in the receiver.

For all CLTD modes, phase rotation is only applied for the dedicated signals transmitted on the second antenna, whereas no phase rotation is applied on the first antenna. Therefore, the common pilot can always be used for channel estimation for the first antenna.

For the second antenna, the common and dedicated channels may have different phases due to the transmitter weighting. If the UL feedback channel were error free, the applied weights would always correspond to the requested ones, and then the phase reference could be estimated based on the common channel and the last requested weights. Unfortunately, the UL feedback channel is not error free, which means that in case of feedback error this estimation of phase reference is biased, resulting in a potential reception error. In order to mitigate this problem, antenna verification can be performed [33]. This means that the dedicated and common pilots are compared to decide which weights were most probably used at the transmitter, which allows channel estimation based on the common pilot and the weights applied at the transmitter. Antenna verification is only feasible in mode 1, since the large number of possible weights in mode 2 drastically reduces the probability of being able to estimate the most probably utilised weights.

In the uncorrelated narrowband case with a branch power ratio of zero dB, ideal CLTD with infinite resolution in the weight quantisation and no feedback delays would yield the same performance enhancement as dual antenna MRC at the UE, i.e. a 3 dB average SINR gain and a two-fold diversity order increase. In reality, the performance of CLTD is degraded due to the following already mentioned impairments: (i) feedback delays, (ii) errors in the feedback channel, (iii) quantisation of the weights, (iv) lack of degrees of freedom to adapt the transmission to a radio channel with time dispersion, and (v) imperfections in the channel estimates for calculating the optimum set of weights.

Moreover, as in the STTD case, the transmit power at the Node-B is split into two branches, which degrades the channel estimates for the signals coming from each one of the diversity branches. As a consequence, the benefits from CLTD is lower than predicted for the case of ideal channel estimation

The performance gain associated with CLTD is obtained at the expense of some UL bandwidth reservation for weight feedback, and the extra complexity at the UE for supporting the weight calculations.

Capacity gain results for CLTD with power controlled DCHs are presented in [55]. For example, in single path channels, the capacity gain of mode 1 is reported to be 195% at 3 kmph, while it reduces to 68% at 50 kmph, due to the impact of feedback delays. For radio channels with time dispersion, the reported capacity gains for mode 1 are significantly lower: 50% at 3 kmph and 28% at 50 kmph. A theoretical analysis of the impact of frequency selectivity and feedback delay can be found in [56] and [57]. If under some conditions the deployment of CLTD with power controlled DCHs leads to a situation in which channelisation code shortage becomes a serious limitation, it is not straightforward to find a solution to overcome this problem. Note that this was possible in the CBF case due to the spatial filtering properties of AAs with CBF, which make it possible to spatially isolate regions with different scrambling codes.

For further releases of UMTS, several alternatives are under discussion in order to extend the CLTD scheme to more than two antennas. For further details, see [58]. Moreover, there are also proposals to use selection transmit diversity for HSDPA [59]. With this closed loop scheme, the best antenna is selected for transmission based on the instantaneous channel quality experienced from each antenna.

Table 2.3 shows a summary of the main characteristics of the transmit diversity techniques that have been presented in this section. In addition, Table 2.4 summarises the applicability of TSTD, STTD and CLTD in UMTS [27].

Table 2.3: Transmit diversity techniques in UMTS.

	Open loop		Closed loop
	STTD	**TSTD**	**Mode 1 & 2**
Average combining gain	No	No	Yes
Channel randomisation	No	Yes	No
Possible to broadcast	Yes	Yes	No
Vulnerable to feedback delays	No	No	Yes
Vulnerable to feedback errors	No	No	Yes

2.3 Multiple antennas at the UE

The use of CBF at the UE is discarded for this study, due to the fact that it is not considered to be an attractive solution for UL nor for DL. The reasons for this decision are explained in the following. First, the number of antenna elements that can be implemented at the UE is rather limited due to practical restrictions related to power consumption, size [60] and antenna isolation, which reduces the spatial filtering gain significantly. Second, the experienced AS of the radio channel at the UE side is usually high due to the low antenna height and the subsequent proximity of local scatters (see [61], among others), which has been shown to degrade the gain from spatial filtering. Third, the UE is very likely to change the orientation of the AA in a relatively fast manner, which makes the beamforming management

more difficult. Fourth, the impact of the human body affects the radiation pattern of each antenna element in a different way, which makes it more difficult to synthesise narrow beams towards the desired azimuth direction.

Table 2.4: Applicability of TSTD, STTD and CLTD in UMTS.

Transport Channels	Physical Channels	TSTD	STTD	CLTD
Dedicated channel (DCH)	Dedicated physical channel (DPCH)	No	Yes	Yes
Downlink shared channel (DSCH)	Physical downlink shared channel (PDSCH)	No	Yes	Yes
High speed downlink shared channel (HS-DSCH)	High speed physical downlink shared channel (HS-PDSCH)	No	Yes	Yes
Broadcast channel (BCH)	Primary common control physical channel (P-CCPCH)	No	Yes	No
Forward access channel (FACH) Paging channel (PCH)	Secondary common control channel (S-CCPCH)	No	Yes	No
-	Synchronisation channel (SCH)	Yes	No	No
-	Acquisition indicator channel (AICH)	No	Yes	No
-	High speed shared control channel (HS-SCCH)	No	Yes	Yes
-	Paging indicator channel (PICH)	No	Yes	No
-	Primary common pilot channel (P-CPICH)	No	Yes	No
-	Secondary common pilot channel (S-CPICH)	No	Yes	No

Regarding transmit diversity techniques, no scheme has been standardised for UL transmission in UMTS. Therefore, in this study, the use of multiple antennas at the UE is restricted to DL signal reception.

The use of antenna MRC at the UE is convenient, since the correlation between the antenna elements is usually low [61]. As stated before, there are limitations regarding the

number of antennas that can be implemented at the UE. Due to these limitations, the maximum number of antennas at the UE for this study is assumed to be two. The basic mechanisms behind MRC were already explained in Section 2.2.1.2, including the degradation of the channel estimates for power controlled channels, due to the fact that the signal quality on each diversity branch is lower because the other end (in this case, the Node-B) lowers the transmit power as a consequence of the MRC gain. In DL, this is only true if channel estimation is done based on dedicated pilots. If it is done based on common pilots and these do not alter their transmit power, the quality of the channel estimate at each diversity branch remains the same.

Link level studies for power controlled DCHs dealing with dual antenna Rake receivers at the UE with MRC between the antennas are available in [62] and [63]. In the DL of UMTS, the link level improvement from the deployment of such receivers has been reported to range between 3 dB and 4.5 dB for a block error rate (BLER) target of 10%, depending on the frequency selectivity of the radio channel [63]. More advanced dual antenna receivers with linear minimum mean-square error chip level equalisers are described in [64], and their link level improvement over dual antenna Rake receivers with MRC in Vehicular A is reported to be up to 8−9 dB for UEs very close to the serving Node-B [63]. However, their performance is more modest when the UE is far for the serving Node-B and other cell interference is not negligible.

If under some conditions the deployment of multiple antennas at the UE with power controlled DCHs leads to a situation in which channelisation code shortage becomes a serious limitation, it is not straightforward to find a solution to overcome this problem. Note that this was possible in the CBF case due to the spatial filtering properties of AAs with CBF, which make it possible to spatially isolate regions with different scrambling codes.

2.4 MIMO systems

The combination of the described AA techniques at both the Node-B and the UE opens for the use of MIMO systems that improve the SINR of a certain link conveying a single data stream, without conducting spatial multiplexing of parallel data streams. This approach is often referred to as diversity MIMO. There are also proposals to utilise the MIMO systems so that several parallel spatial multiplexed data streams are transmitted between two transceivers equipped with AAs [39]. This approach is called information MIMO, which is considered to be out of the scope of this thesis.

The different options for diversity MIMO in UMTS are discussed in the sequel. As already stated, UMTS does not support transmit diversity at the UE side and, in addition, the use of CBF at the UE has been disregarded earlier in this chapter. Thus, since AAs at the UE are only considered for signal reception, this MIMO discussion is limited to the DL case. The following combinations for diversity MIMO in UMTS are commented:

- STTD at the Node-B and dual antenna MRC at the UE.

- CLTD at the Node-B and dual antenna MRC at the UE.

In addition, another MIMO configuration is possible in UMTS: the combination of CBF at the Node-B and dual antenna MRC at the UE. This solution cannot be defined as diversity

MIMO, since no diversity technique is used at the transmitter. However, since multiple antennas are involved at both the transmitter and the receiver, it is worth mentioning it when describing the MIMO configurations in UMTS.

2.4.1 STTD at the Node-B and dual antenna MRC at the UE

The joint deployment of STTD at the Node-B and dual antenna MRC at the UE is not expected to show a significantly superior performance compared with the case where single antenna transmission is used at the Node-B and dual antenna MRC is deployed at the UE. This is explained by the fact that dual antenna MRC at the UE already provides diversity and average SINR gain. In this case, the increased diversity order due to STTD only provides diminishing returns. This solution is not evaluated in this Ph.D. thesis.

If under some conditions the joint deployment of STTD at the Node-B and dual antenna MRC at the UE with power controlled DCHs leads to a situation in which channelisation code shortage becomes a serious limitation, it is not straightforward to find a solution to overcome this problem. Note that this was possible in the CBF case due to the spatial filtering properties of AAs with CBF, which make it possible to spatially isolate regions with different scrambling codes.

2.4.2 CLTD at the Node-B and dual antenna MRC at the UE

The comments given in Section 2.4.1 regarding the diversity gain from the combination of STTD at the Node-B and dual antenna MRC at the UE are also valid here. However, in the case of CLTD, there is also an average SINR gain that can be added to the one provided by dual antenna MRC. In the case of UEs with antenna diversity, one of the possible options is to select the weights for CLTD so that the total received signal power is maximised. In order to derive an expression for the total received signal power, let us assume the simple model shown in Figure 2.10, where the feedback link is not represented for the sake of simplicity.
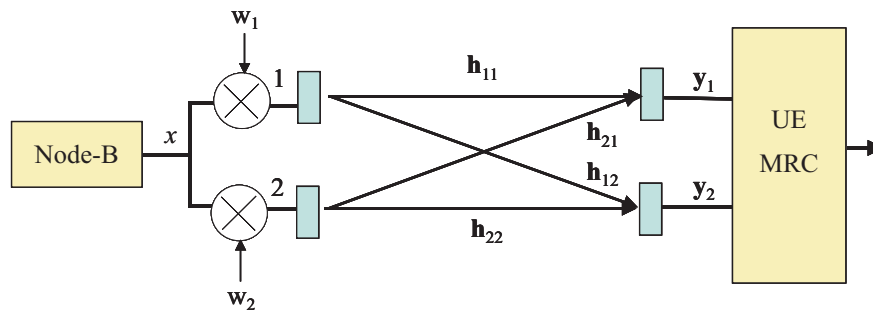
Figure 2.10: Signal model for CLTD with dual antenna MRC at the UE.

For compact notation, the applied weights can be expressed as $\mathbf{w} = [w_1 \ w_2]^T$, and $\mathbf{h}_{tr}$ denotes the impulse response of the radio channel between the tth transmit antenna and the rth receive antenna, represented as $\mathbf{h}_{tr} = [\alpha_{tr1} \ \alpha_{tr2} \ ... \ \alpha_{trL}]^T$, where α_{trl} refers to the complex channel coefficient of the lth multipath component of the channel between the tth transmit antenna and the rth receive antenna. The number of multipath components is denoted by L. The channel matrix describing the two radio channels that end at the rth receive antenna is given by $\mathbf{H}^r = [\mathbf{h}_{1r} \ \mathbf{h}_{2r}]$, and $\mathbf{y}_r = [y_{r1} \ y_{r2} \ ... \ y_{rL}]$ is the received signal vector at the rth antenna

before MRC, where y_{rl} is the output of the lth Rake finger connected to the rth antenna. Given this signal model, $\mathbf{y}_r$ can be written as

$$\mathbf{y}_r = \mathbf{w}^T \mathbf{H^r}^T x , \qquad (2.15)$$

where x is the complex amplitude of the data signal. Assuming that $\|x\|^2=1$, the target is to find the set of allowed weights maximising the total received signal power, which is given by

$$P = \sum_{r=1}^{2} \|\mathbf{y}_r\|^2 = \sum_{r=1}^{2} \mathbf{w}^H \mathbf{H^r}^H \mathbf{H^r} \mathbf{w} \qquad (2.16)$$

A similar analysis proposing the maximisation of the total received signal power can be found in [66], and this is the approach that will be adopted throughout this Ph.D. thesis. However, instead of maximising the total received signal power, another option is to maximise the total SINR. In order to do so, the set of weights maximising the following expression must be found

$$SINR_{Norm} = \sum_{r=1}^{2} \sum_{l=1}^{L} \frac{|w_1 \alpha_{1rl} + w_2 \alpha_{2rl}|^2}{P_{Total,r} - P_{Own,r,l}} , \qquad (2.17)$$

where $SINR_{Norm}$ is the SINR normalised with the processing gain and the power of the desired signal (attenuated by both the corresponding deterministic path loss and shadow fading), $P_{Total,r}$ is the total wideband received power at the rth antenna and $P_{Own,r,l}$ is the wideband received power of the signals that were transmitted under the same scrambling code as the desired signal and arrive at the rth receive antenna through the lth multipath.

If under some conditions the joint deployment of CLTD at the Node-B and dual antenna MRC at the UE with power controlled DCHs leads to a situation in which channelisation code shortage becomes a serious limitation, it is not straightforward to find a solution to overcome this problem. Note that this was possible in the CBF case due to the spatial filtering properties of AAs with CBF, which make it possible to spatially isolate regions with different scrambling codes.

2.4.3 CBF at the Node-B and dual antenna MRC at the UE

The use of CBF at the Node-B and dual antenna MRC at the UE are compatible. In practice, the system will enjoy the spatial filtering gain from CBF and the already described benefits from dual antenna MRC. The combination of both techniques makes the potential channelisation code shortage problem even more severe, but the possibility of the Node-B to allocate the scrambling codes on a beam basis opens for a solution to this problem. Probably, this solution requires the use of more scrambling codes than in the case of CBF at the Node-B with single antenna reception at the UE. As a consequence, the overall capacity gain is expected to be slightly below the multiplication of the capacity gains provided by both techniques separately. This solution is not evaluated in this Ph.D. thesis.

2.5 Concluding remarks

Throughout this chapter, an overview of the different adaptive antenna schemes that can be used in UMTS has been presented, and an overview diagram of the analysed techniques is shown in Figure 2.11.
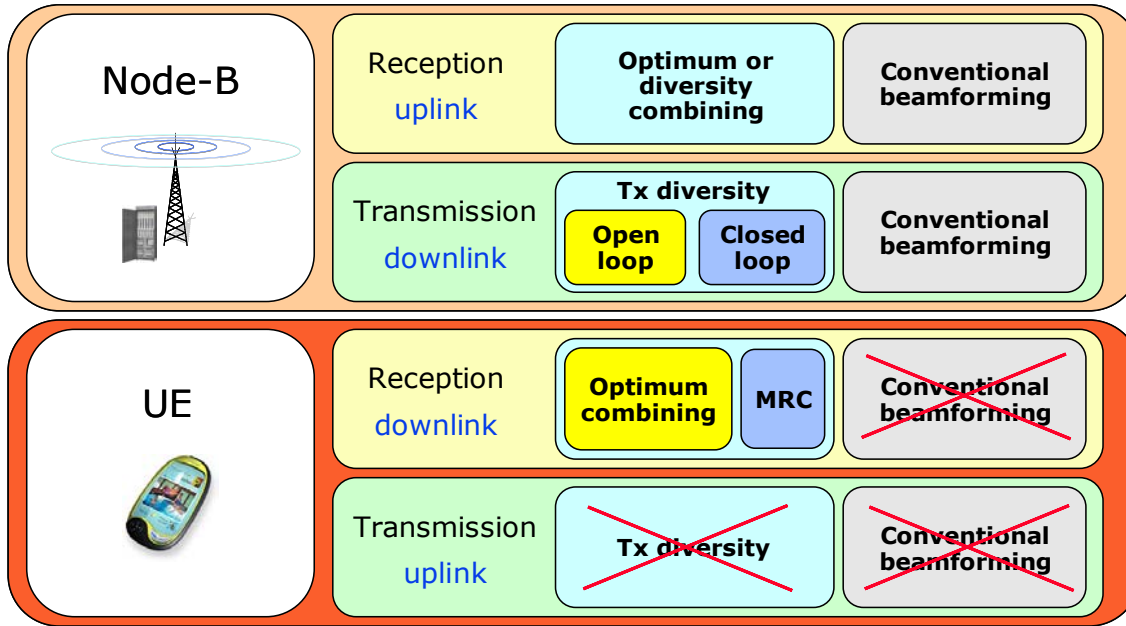
Figure 2.11: Adaptive antenna concepts addressed in this chapter.

As a general rule for the use of the AAs, it has been shown that, when the AS is low, CBF yields a reasonable spatial filtering gain and can be used for both transmission and reception. The actual capacity gain that can be achieved is strongly related to the ratio between the sector antenna's beamwidth and that of the synthesised narrow directional beams [48]. In this Ph.D. thesis, the UL and DL capacity gain with beamforming AAs at the Node-B will be assessed for power controlled DCHs under different traffic and propagation conditions, and the impact of the radio resource management configuration on the achieved capacity gain is of special interest. The use of CBF at the UE has been discarded in this study due to practical reasons.

On the other hand, when the antenna elements are uncorrelated, which typically happens when the AS is large or when different polarisations are exploited, the use of antenna transmit diversity techniques has a clear potential. UMTS allows the use of antenna transmit diversity only for the DL, and there are two possibilities: open loop and closed loop transmit diversity. Both offer extra diversity protection in terms of deep fade mitigation, but the latter also offers an average SINR gain at the expense of the need for feedback information from the UE, which makes the system more sensitive towards the UE speed. These techniques have been already studied with power controlled DCHs at system level (see [37], [54] and [55]). In this Ph.D. thesis, their capacity and coverage gain will be evaluated for HSDPA under different packet scheduling algorithms.

The use of antenna diversity at the reception is possible in UMTS for both UL and DL. In general, receive diversity techniques do not only provide extra diversity protection, but also an average SINR gain. In this chapter, some previous studies showing very promising link level performance improvements when deploying several antennas for signal reception have been cited. In this Ph.D. thesis, the benefits from dual antenna MRC at the UE will be assessed at system level for the case with power controlled DCHs, and for HSDPA under different packet scheduling algorithms.

For DL, different ways to combine the described transmission and reception techniques have been discussed as a manner to enable MIMO operation in UMTS. In this Ph.D. thesis, the system level performance of CLTD at the Node-B in conjunction with dual antenna MRC at the UE will be investigated for HSDPA under different packet scheduling strategies.

Chapter 3

Uplink capacity gain with beamforming AAs at the Node-B

3.1 Introduction

The objective in this chapter is to assess the capacity gain that can be achieved in the uplink (UL) of the Universal Mobile Telecommunications System (UMTS) when antenna arrays (AAs) with conventional beamforming (CBF) are deployed at the Node-B. Specific details regarding the utilised beamforming technique are explained in Section 2.2.1.3 of Chapter 2, and no further descriptions are given here in this respect.

In order to investigate the capacity gain when AAs with CBF are deployed, admission control (AC) is the key radio resource management (RRM) algorithm to look into, since it is in charge of controlling the load of the system. Therefore, it is of paramount importance to study the different UL AC algorithms for conventional sector antennas available in the open literature. From previous studies, it is well-known that power is a robust integral measure of the network load for wideband code division multiple access (WCDMA) systems, supporting both speech and variable bit rate data users (see [67], [68] and [69]). In general, power based AC algorithms are attractive as they offer trade-offs between capacity and coverage, while taking advantage of the soft capacity offered by WCDMA systems [1]. After presenting an

overview of the different alternatives for UL AC with conventional sector antennas, the manner to extend the power based AC algorithms to the case where AAs with CBF are deployed at the Node-B is discussed. As a result, a directional power based UL AC algorithm is proposed and tested by means of semi static system simulations.

The study is conducted for power controlled dedicated channels (DCHs), and the chapter is organised as follows. An overview of the different available UL AC algorithms is presented in Section 3.2. In Section 3.3 the selected power based AC algorithm is generalised to the case where AAs with CBF are used, leading to the formulation of the directional power based UL AC algorithm. The system model to be used in the sequel is described in Section 3.4. The directional power increase estimator (DPIE), which is a mathematical tool needed in the AC algorithm, is derived in Section 3.5. The utilised simulation set-up is described in Section 3.6. In Section 3.7, the simulation results are analysed, and Section 3.8 gives the concluding remarks.

3.2 Uplink cell load and AC algorithms

When using power control (PC), the power transmitted by the UEs at each link is varied according to the per-slot[5] measured signal-to-interference-plus-noise ratio (SINR) at the Node-B. By this mean, the system can react to the variations of the radio channel and the extra interference caused by the admission of new UEs. The objective of PC is to minimise the sum of the powers transmitted by the different UEs in the network, i.e. to achieve at set of transmit powers that fulfils the following condition

$$\min\left\{\sum_{all\ UEs} P_i\right\}, \tag{3.1}$$

subject to the two following constraints:

$$\rho_i \geq \rho_{i,target} \ \forall i \tag{3.2}$$

and

$$P_i \leq P_{i,max} \ \forall i, \tag{3.3}$$

where P_i is the transmit power at UE #i, ρ_i is the energy-per-bit to noise ratio (E_b/N_0) of UE #i, $\rho_{i,target}$ is the E_b/N_0 target of UE #i, and $P_{i,max}$ is the maximum power that can be transmitted by UE #i.

According to the simple model presented in [1] and [70], the E_b/N_0 for UE #i can be described in the following way:

$$\rho_i = \frac{G_i P_i h_i}{P_N + \sum_{\substack{all\ k \\ k \neq i}} P_k h_k}, \tag{3.4}$$

---

[5] Note that the slot duration is 0.667 ms.

where P_N is the thermal noise power, G_i is the processing gain of UE #i and h_k is the path gain between UE #k and the Node-B at the cell in which UE #i is served.

Every time a new UE is admitted into the network, it behaves as an extra source of interference that degrades the E_b/N_0 of the rest of the UEs. As a consequence, the UEs increase their transmit power in order to maintain their E_b/N_0 target. When the system is not very highly loaded, the PC process converges to a stable situation where a feasible solution can be found for the joint optimisation problem described by (3.1), (3.2) and (3.3). However, when the load of the system is too high, no feasible solution exists for that problem, and the UEs cannot increase their transmit power to maintain their E_b/N_0 target because their maximum transmit power has been reached. At this point, the system becomes instable and calls start to be dropped, as the E_b/N_0 requirements are not fulfilled.

An analytical expression for the total wideband received power at the Node-B (P_{Total}) at a certain cell #c can be written

$$P_{Total} = P_N + \sum_{all\ k} P_k h_k \tag{3.5}$$

Thus (3.4) can be rewritten as

$$\rho_i = \frac{G_i P_i h_i}{P_{Total} - P_i h_i}, \tag{3.6}$$

which can be transformed into

$$P_i h_i = \frac{1}{1 + \dfrac{G_i}{\rho_i}} P_{Total} \tag{3.7}$$

Therefore, (3.5) can be written as

$$P_{Total} = P_N + P_{Total} \sum_{all\ k} \frac{1}{1 + \dfrac{G_k}{\rho_k}} \tag{3.8}$$

Now, the ratio between the other cell and the own cell interference (denoted by i in the sequel) is defined as

$$i = \frac{P_{Other}}{P_{Own}}, \tag{3.9}$$

where P_{Own} is the own cell interference, which comes from the UEs being served by the cell under evaluation. Similarly, P_{Other} is the other cell interference, which comes from the rest of the UEs in the system. Making use of this definition, the following expression can be written

$$P_{Total} = P_N + (1+i)P_{Total} \sum_{k \in \mathbf{C}} \frac{1}{1+\dfrac{G_k}{\rho_k}} , \qquad (3.10)$$

where $\mathbf{C}$ is the set of indexes identifying the UEs being served at cell #c. For simplicity, this expression can be written as

$$P_{Total} = P_N + P_{Total}(1+i)\eta , \qquad (3.11)$$

where η is the own cell load factor of cell #c, defined as [1]

$$\eta = \sum_{k \in \mathbf{C}} \frac{1}{1+\dfrac{G_k}{\rho_k}} , \qquad (3.12)$$

Thus, it is straightforward to write the following expression for P_{Total} in a given cell as a function of η

$$P_{Total} = \frac{P_N}{1-(1+i)\,\eta} \qquad (3.13)$$

In (3.13), it can be seen that the total wideband received power at the Node-B is directly proportional to P_N. As will be seen later, this is the reason why all the power thresholds in UL power based AC are defined relative to P_N. Based on (3.5) and (3.13), it can be seen that if P_N is doubled the rest of the received power at the Node-B is also doubled.

Figure 3.1 shows the value of P_{Total} as a function of the own cell load factor for several values of i. For this plot, which is referred to as the load curve, $P_N = -102.9$ dBm. From Figure 3.1, it is straightforward to conclude that the capacity of one cell is strongly affected by the load of the surrounding cells. If the surrounded cells are low loaded, less interference is transmitted into the cell, resulting in lower P_{Total} for the same own cell load factor and, therefore, in a capacity increase. This mechanism is defined as soft capacity [1], and it implies that one cell can borrow its neighbouring cells' capacity when they are not fully exploiting it.

Notice the non-linearity of the load curve depicted in Figure 3.1, which indicates that it is not desirable to operate the system at a very large own cell load factor. The reason is that the slope of the load curve becomes too large when the own cell load factor is too high, and a very low benefit (in terms of capacity) is obtained at the expense of a large increase of P_{Total}, with the subsequent increased risk of instability.

AC is the algorithm in charge of preventing the system from entering an instable situation. In order to do so, AC has to block all the connection requests that are estimated to lead the system into an instable situation. Thus, the consequence from deploying AC is a certain (intentional) increase of the call blocking probability, which is the price to be paid for a substantial decrease of the call dropping probability.
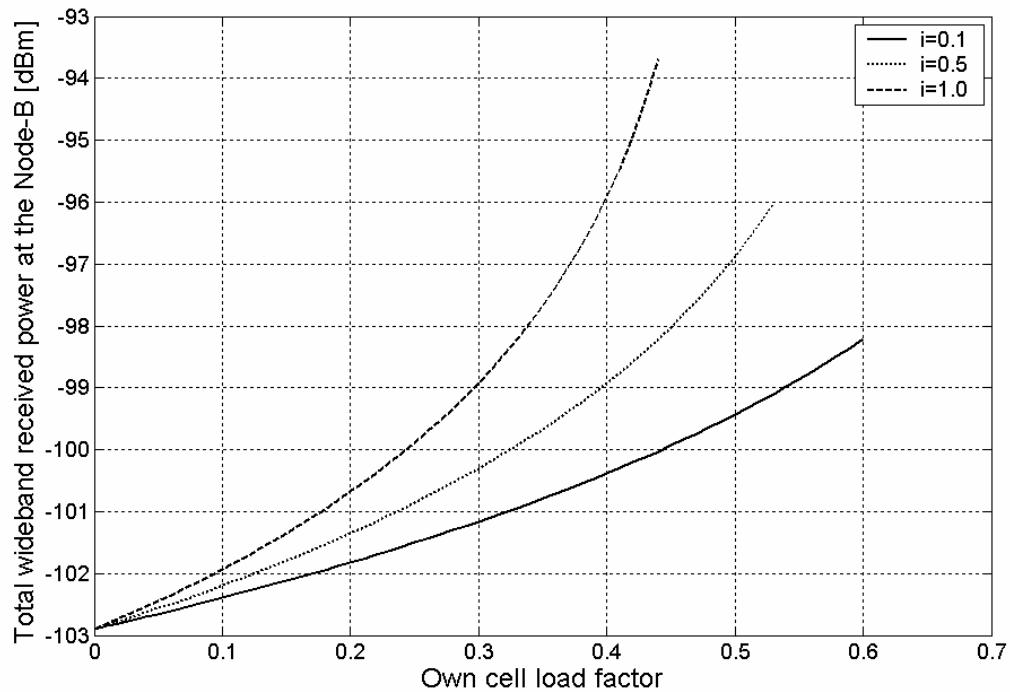
Figure 3.1: Total wideband received power at the Node-B vs. own cell load factor when the thermal noise power equals -102.9 dBm.

In [71], the AC techniques are classified into throughput and power based. In throughput based AC techniques, the throughput that can be delivered by the system is determined according to some dimensioning calculations, assuming some conditions in the system. In power based AC techniques, the AC decisions are based on periodic power measurements of the system.

Throughput based AC techniques have several drawbacks. First, the dimensioning is done for some propagation conditions and it is not valid in other situations. In addition, it is very difficult for them to take into account the soft capacity gain that can be obtained if the load in the system is not homogeneous. As can be seen in Figure 3.1, the own cell load factor (which can be expressed in terms of throughput if the service profile is known) at which the system is likely to become instable strongly depends on the value of *i*. Such techniques are studied in [72], among others, and [73] discusses further enhancements in order to make the system tolerant to the load variations due to bursty packet traffic.

Power based AC techniques have several advantages. First, the different propagation conditions are automatically included in the measured power values. Furthermore, the potential soft capacity gain is also indirectly included in the measurements, since low loaded surrounding cells result in a better power situation, i.e. in less received power at the cell under consideration. However, they have also practical drawbacks. First, they rely on measured power values, which are subject to measurement inaccuracies. Second, they require the specification of thresholds that are used in order to guarantee the system stability while still exploiting the available capacity; in practice, the specification of such thresholds is not

straightforward. These techniques have been widely studied in the literature (see [68]-[69] and [74]-[78]).

For UL, two subtypes of power based AC techniques have been proposed. Previous works reported in [67], [69] and [74]-[78] propose the use of P_{Total} as a load measure of the cell. Others [79]-[81] present an AC algorithm based on the SINR of the UEs, which has to be maintained after the admission of any potential new UE. There are also works that combine both techniques [82]. In [82], P_{Total} is considered as a measure of the system load. However, as has been shown in (3.13), P_{Total} is directly proportional to P_N. Therefore, the AC condition is expressed in terms of Noise Rise (NR), which is defined as [78], [82]

$$NR = \frac{P_{Total}}{P_N},$$ (3.14)

With this AC algorithm, a UE is admitted in a given cell of the system (referred to as the target cell) if the following condition is estimated to remain true after the admission

$$NR < NR_{Target},$$ (3.15)

where NR_{Target} is a pre-defined threshold. Its specification is not straightforward and constitutes a trade-off between system stability and system capacity. A very conservative (low) value of NR_{Target} improves the system stability at the expense of wasting system capacity.

In order to estimate the value of the NR in the target cell after the admission of the new UE, a power increase estimator (PIE) is needed. The PIE proposed in [82] offers an estimate of the NR in the target cell when the new UE has been admitted and PC has converged to a feasible solution where the E_b/N_0 requirements of all the UEs are fulfilled. Thus, if an outage situation is predicted to occur, i.e., if it is not possible to fulfil all the E_b/N_0 requirements (even with no transmit power constraints at the UEs), it will be noticed when using the PIE, since the result will indicate that the system has gone into an outage situation. Therefore, although this AC algorithm uses P_{Total} as a measure of the cell load, it is also SINR based, since the involved power increase estimation checks whether the SINR of all the UEs can be fulfilled.

When using P_{Total} (or the NR) as a measure of the cell load, the AC criterion can be formulated in two ways. On one hand, it is possible to state that the average NR should not exceed a threshold, which also requires an averaging window to be specified. On the other hand, it is also possible use a statistical approach, which imposes that the probability of the instantaneous P_{Total} exceeding a certain threshold should be kept below a certain value. The latter concept is further explained in [69].

Single cell AC algorithms only use the information of the target cell in order to carry out the power increase estimation. However, it is also possible to use the load information of the neighbouring cells in order to avoid excessive dropping in non-homogenous load scenarios, leading to the so-called multi cell AC algorithms, which are studied for the UL case in [80]-[81] and [83]-[84]. By taking into account the load information of the surrounding cells, less conservative values for NR_{Target} can be utilised because the risk of instability under non-homogeneous load conditions is lower. As a consequence, a capacity increase can be achieved at the expense of requiring information of several cells in order to run the AC

algorithm. For example, in [84] the capacity gain due to the use of a multi cell AC algorithm is reported to be 34% for a network with non-homogeneous load conditions.

Very few studies have dealt with UL AC for WCDMA systems with AAs. For example, in [19], a SINR based UL AC algorithm was formulated for the case of AAs with optimum combining by using the correlation matrix of the total received signals and noise at the Node-B. For the study described in this chapter, power based AC algorithms using the NR as a measure of the cell load are considered to be attractive because they offer trade-offs between capacity and coverage, while automatically taking advantage of the soft capacity gain offered by WCDMA systems [82]. In Section 3.3, their generalisation to the case with beamforming AAs at the Node-B will be further discussed in order to define an algorithm that is capable to capture the potential capacity gain that is made available when the deploying AAs.

3.3 Directional power based AC

When using AAs with CBF, the potential capacity gain that can be achieved is based on spatial filtering of the interference. Figure 3.2 shows a possible scenario, where the UEs are uniformly distributed in the azimuth domain. Since a narrow beam is pointed to UE #1, the signal received from that UE is not strongly interfered by the signals transmitted from UEs at different azimuth locations, with the subsequent capacity increase. The synthesised beams have a certain beamwidth, which limits the spatial filtering gain. When the UEs are uniformly distributed in the azimuth domain, the available capacity gain (compared with the case with sector antennas) can be directly related to the beamwidth reduction ratio between the directional antenna beams and the sector beam [48].
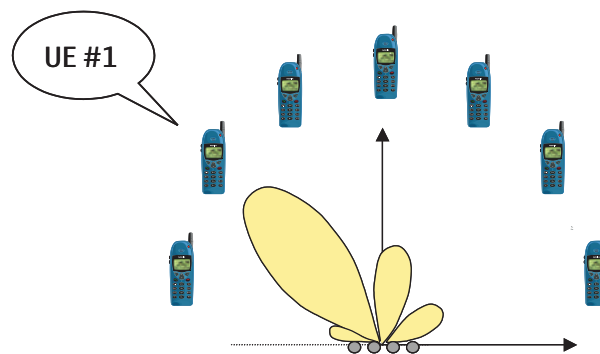
Figure 3.2: Spatial filtering of the interference when it is uniformly distributed in the azimuth domain.

However, other scenarios are also possible. Figure 3.3 illustrates the case where all the UEs are located in azimuth directions that are very close to each other, and cannot be resolved by the synthesised beams. Under these circumstances, the spatial filtering capacity gain converges to zero.
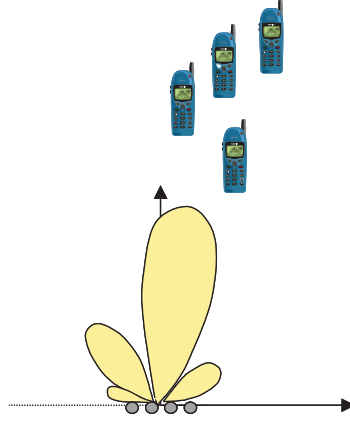
Figure 3.3: Spatial filtering of the interference when all the UEs are positioned at the same azimuth direction.

Thus, the capacity gain is very sensitive to the spatial distribution of the interference. Maximum capacity gain is achieved when the interference is spatially white[6], while the obtainable gain is reduced when the spatial distribution of the interference becomes more directional. Consequently, it is important that the AC algorithm conveniently captures this mechanism in order to exploit the capacity gain while still maintaining system stability under all possible conditions. This is especially important for systems with mixed speech and high bit rate data users, where the spatial distribution of the interference is likely to deviate from the spatially white assumption; such assumption is only valid for WCDMA systems supporting a large number of uniformly distributed low bit rate users [85].

In order to be able to capture the capacity gain from AAs without jeopardising the system stability, the power based AC algorithm taking the NR as a measure of the cell load is extended so that the spatial interference distribution is automatically taken into account. Thus, the AC condition can be written as

$$NR(\phi) < NR_{Target} \quad \forall \phi \in \mathbf{S}, \tag{3.16}$$

where $\mathbf{S}$ is the set of azimuth directions in the cell covered by the AA, and

$$NR(\phi) = \frac{P(\phi)}{P_N}, \tag{3.17}$$

where $NR(\phi)$ is the directional NR, and $P(\phi)$ is the average total wideband received power at the Node-B when pointing a beam at the azimuth direction ϕ. Note that ϕ is measured relative to the broadside direction of the AA. Similarly to the case with conventional sector antennas, a DPIE is needed to estimate $NR(\phi)$ after the admission of the new UE.

When evaluating the capacity gain, both the system with conventional sector antennas and the one with AAs will be compared for the same value of NR_{Target}. Ideally, the NR_{Target}

---

[6] This statement is considered to be valid under the following assumptions: (i) sufficiently large number of UEs, (ii) UEs uniformly distributed in the azimuth domain, (iii) same kind of traffic for all the UEs, (iv) same E_b/N_0 requirements for all the UEs, and (v) same shape for the radiation patterns of the beams pointed at the different azimuth directions.

should be designed so that the system does not become instable in terms of not being able to find a feasible solution for PC.

Note that the AC condition in (3.16) captures the effect of the spatial interference distribution. To illustrate this, let us consider a single cell case where all UEs are located at the same azimuth direction (ϕ_{All}). For simplicity, it is assumed that all the UEs have the same bit rate and required E_b/N_0. Since the spatial filtering gain converges to zero, the value of $NR(\phi_{All})$ for a given number of UEs equals the NR that would be experienced if the Node-B had a sector antenna. In this case, NR_{Target} is reached with the same number of UEs for both antenna configurations, which means that the AC algorithm has successfully detected that AAs with CBF do not provide any capacity gain in this case.

On the other hand, when all the UEs are uniformly distributed in the azimuth domain, the signal transmitted by one UE has a small interfering impact for UEs positioned at different azimuth directions. Thus, the required received signal power from each UE at the Node-B is lower than in the previous case. As a consequence, the NR at all the azimuth directions is lower and the AC algorithm can admit more UEs until NR_{Target} is reached, hereby capturing that the uniform spatial distribution of the interference allows for extra capacity in the system due to the spatial filtering gain. The extra capacity depends on the degree of isolation between UEs positioned at different azimuth locations. This isolation depends directly on the effective beamwidth, which is a function of the number of antennas in the AA and the azimuth spread (AS) of the radio channel (see Section 2.2.1.3 in Chapter 2).

3.4 System model

All the UEs are power controlled so that the specified E_b/N_0 (ρ) is maintained at the Node-B. The use of AAs with CBF is allowed at the Node-B, and PC is implemented in a distributed manner, in such a way that it is independent from the CBF operations. Thus, schemes that conduct joint optimisation of beamforming and PC [20] are not considered here.

Signals transmitted from the UEs are affected by deterministic path loss and shadow fading before arriving at the Node-B. Since the AC algorithm under evaluation is based on average power values, fast fading is not modelled.

Even though fast fading is not modelled, an iterative PC scheme is needed in order to calculate the transmitted and received powers when the system reaches a state of equilibrium after the admission of a new UE, which causes an increase of the interference levels and therefore makes the UEs adjust their transmitted power in order to keep their specified signal quality requirements.

As already stated, the average total wideband received power at the Node-B when pointing a beam at the azimuth direction ϕ is denoted by $P(\phi)$. This value refers to the state of the system before the admission of the new UE. The value of this power after the admission of the new UE is denoted by $P_{New}(\phi)$, and the estimation of $P_{New}(\phi)$ given by the DPIE is called $P_{New\_Est}(\phi)$. The average power received from the new admitted UE when the beam is pointed at ϕ is denoted by $P^{UE}(\phi)$.

In addition, it is also important to define the notation for the required E_b/N_0 of the new UE (ρ_{UE}), its processing gain (G_{UE}) and its direction of arrival –DoA– (ϕ_{UE}). The power antenna gain (including the effect of the azimuth dispersion in the radio channel, as described in Chapter 2) at ϕ_2 when pointing a beam at ϕ_1 is denoted by $W(\phi_1; \phi_2)$.

Moreover, the threshold for AC given in (3.16) is rewritten in the following manner

$$NR_{Target} = NR_{Th} - \Delta_{Offset},$$
(3.18)

which is illustrated in Figure 3.4. Note that the operation in (3.18) is done in dB.
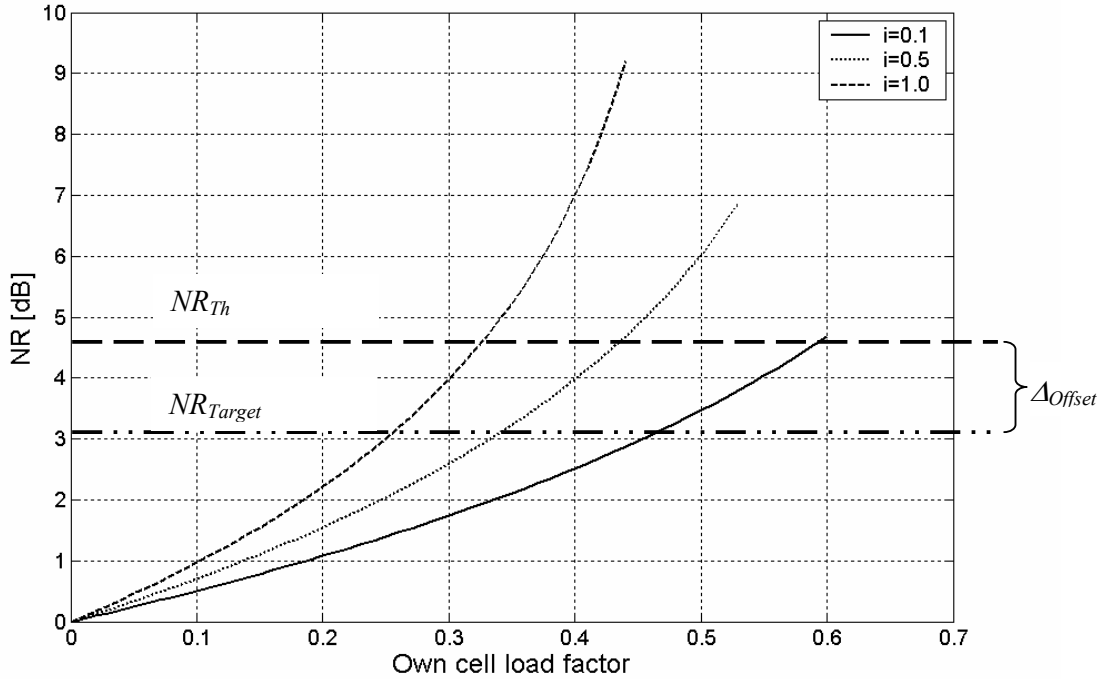
Figure 3.4: Definition of thresholds for UL AC.

In the system model presented here, AC tries to keep the NR of the system at all ϕ below NR_{Target}. An overload situation is defined to occur when the NR exceeds NR_{Th} for some ϕ. The offset area between the two aforementioned thresholds (Δ_{Offset}) is often referred to as the *marginal load* area, where the system starts taking the necessary load preventive measures.

When a UE is estimated not to drive the cell load above N_{Target} for any ϕ, it is admitted into the system. In order to quantify the consequences of the estimation errors of the DPIE, two types of error are defined [86]:

- A Type 1 error is registered if the NR after the admission of the new UE exceeds N_{Th} for some ϕ. In this case, an overload situation is defined to occur.

- A Type 2 error is made when a UE is erroneously denied access to the system, i.e. when the AC rejects the connection request of a UE that would not have caused any overload situation.

3.5 Derivation of the DPIE

The DPIE yields an estimation of what the directional NR of the cell would be if the UE requesting access were admitted into the system. In order to conduct such estimation, the DPIE is based on the following input: $P(\phi)$, P_N, ρ_{UE}, G_{UE}, ϕ_{UE} and the value of $W(\phi_1; \phi_2)$ for all $(\phi_1; \phi_2)$.

The DPIE is conducted in the following steps:

- First, $P_{New}(\phi_{UE})$ is estimated, i.e. $P_{New\_Est}(\phi_{UE})$ is calculated. The procedure to estimate this magnitude will be described after describing the whole estimation sequence. For the moment, let us assume that this estimate is available.

- Then, $P_{New\_Est}(\phi_{UE})$ is expressed in the following way:

$$P_{New\_Est}(\phi_{UE}) = \chi(\phi_{UE}; \phi_{UE})P(\phi_{UE}) + P^{UE}(\phi_{UE}),$$ (3.19)

which means that $P_{New\_Est}(\phi_{UE})$ is contributed by two terms: the power coming from the new UE, and an amplified version of the total received power before the admission of the new UE. Such amplification models the fact that the already existing UEs have to increase their transmit power as a consequence of the interference created by the new UE.

- In the model in (3.19), $\chi(\phi_{UE}; \phi_{UE})$ and $P^{UE}(\phi_{UE})$ are still unknown. In order to calculate them, the expression describing ρ_{UE} is used to relate $P_{New\_Est}(\phi_{UE})$ and $P^{UE}(\phi_{UE})$:

$$\rho_{UE} = \frac{G_{UE}P^{UE}(\phi_{UE})}{P_{New\_Est}(\phi_{UE}) - P^{UE}(\phi_{UE})},$$ (3.20)

which can be written as

$$P^{UE}(\phi_{UE}) = \frac{1}{1 + \dfrac{G_{UE}}{\rho_{UE}}} P_{New\_Est}(\phi_{UE})$$ (3.21)

Then, by combining (3.19) and (3.21):

$$\chi(\phi_{UE};\phi_{UE}) = \left(1 - \cfrac{1}{1 + \cfrac{G_{UE}}{\rho_{UE}}}\right) \frac{P_{New\_Est}(\phi_{UE})}{P(\phi_{UE})} \qquad (3.22)$$

Thus, if the estimate $P_{New\_Est}(\phi_{UE})$ can be obtained, all the terms in (3.19) can be obtained by using the specified input information and combining (3.19) with (3.22).

- The next step is to generalise (3.19) so that the gain factors that amplify $P(\phi)$ and the impact of $P^{UE}(\phi_{UE})$ are projected into the other azimuth directions:

$$P_{New\_Est}(\phi) = \chi(\phi;\phi_{UE})P(\phi) + P^{UE}(\phi_{UE})\gamma(\phi;\phi_{UE}), \qquad (3.23)$$

where

$$\gamma(\phi;\phi_{UE}) = \frac{W(\phi;\phi_{UE})}{W(\phi_{UE};\phi_{UE})} \qquad (3.24)$$

and

$$\chi(\phi;\phi_{UE}) = (\chi(\phi_{UE};\phi_{UE}) - 1)\gamma(\phi;\phi_{UE}) + 1 \qquad (3.25)$$

As can be seen, $\gamma(\phi;\phi_{UE})$ models the normalised antenna gain for a signal coming from ϕ_{UE} when the beam is pointed at ϕ. Of course, the gain is normalised with $W(\phi_{UE};\phi_{UE})$ because this is the antenna gain affecting all the reference magnitudes in (3.19). Moreover, when projecting the factor that models the amplification of the signal coming from the already existing UEs, the factor $\gamma(\phi;\phi_{UE})$ is only applied to that part of $\chi(\phi_{UE};\phi_{UE})$ exceeding one, since this is the only part that really models a power increase, rather than the persistence of the already existing power level.

At this point, the problem is reduced to finding an closed expression for $P_{New\_Est}(\phi_{UE})$. In order to do so, a discrete-time dynamic PC process is emulated at $\phi = \phi_{UE}$ by a set of recursive equations that model how all the power magnitudes in the system evolve when a new UE is admitted. Since the goal is to calculate average power values, no fast fading is considered in this model. The starting point is balanced situation in which all the UEs satisfy their E_b/N_0 requirements. Then, the new UE enters the system and, from that moment, the evolution in the power received at the Node-B is emulated in order to find the stable situation in which all the E_b/N_0 requirements are fulfilled. After the emulated system has converged, it is assumed that the transmitted power of all the UEs and, therefore, the received power at the Node-B have reached a steady state situation.

In order to model the discrete-time process that describes how the power magnitudes in the system evolve when a new UE is added, the following two discrete-time variables are defined:

- $y[n]$ is the value of $P_{New\_Est}(\phi_{UE})$ at the discrete-time instant n. Since the new UE is added to the system at $n=0$, $y[-1]=P(\phi_{UE})$.

- $x[n]$ is the total power (at instant n) that the Node-B receives from all the UEs that were already present in the system before the admission of the new UE, including the thermal noise. In order to maintain the required E_b/N_0, the power transmitted by these UEs grows when a new UE is added, and therefore $x[n]$ also grows with n. However, it is important to make clear that this variable never includes the power that the Node-B receives from the new UE. It is straightforward to write that $x[0]=P\ (\phi_{UE})$.

Based on the given definition for these two variables, the only difference between them is that $y[n]$ includes the power coming from the new UE, while this value is excluded from $x[n]$. In (3.21), a relationship is given between the total received power at $\phi=\phi_{UE}$ and the power coming from the new UE. Making use of that equation, it is possible to write

$$y[n] = x[n] + \frac{1}{1+\dfrac{G_{UE}}{\rho_{UE}}} y[n-1],$$
(3.26)

where the second term of the sum corresponds to the power received from the new UE at the Node-B. Notice that, in (3.26), it has been implicitly assumed that, at instant n, the power received from the new UE is adapted to the total received power at the previous instant ($y[n-1]$).

Similarly, a part of $x[n]$ is assumed to evolve in connection with the temporal evolution of $y[n]$. This makes sense, since the growth of the power coming from the UEs that were already in the system is attached to the growth of the total received power at the Node-B. This modelling approach assumes that the variation in that part $x[n]$ occurs as a result of a decision taken by the PC entities of all the UEs at the time instant $n-1$. According to this model, at the time instant $n-1$, the system senses how the total received power has grown since the last instant ($n-2$) and motivates a power increase with the same proportion at time instant n.

Of course, there should be a part of $x[n]$ that does not vary along the PC process. This magnitude is denoted by A. Obviously, the thermal noise power has to be included in A, since it will not increase as a consequence of a higher level of total interference caused by the admission of a new UE. In addition, a certain fraction of the other cell interference at $\phi=\phi_{UE}$ ($P_{Other}(\phi_{UE})$) should be also included, in order to model the partial coupling between the cell under evaluation and the surrounding ones. An expression for A is given in the following:

$$A = P_N + KP_{Other}(\phi_{UE})$$
(3.27)

Based on the aforementioned considerations, the value of $x[n]$ can be written in the following recursive way:

$$x[n] = (x[n-1] - A)\frac{y[n-1]}{y[n-2]} + A$$
(3.28)

Furthermore, this modelling approach is illustrated in Figure 3.5.
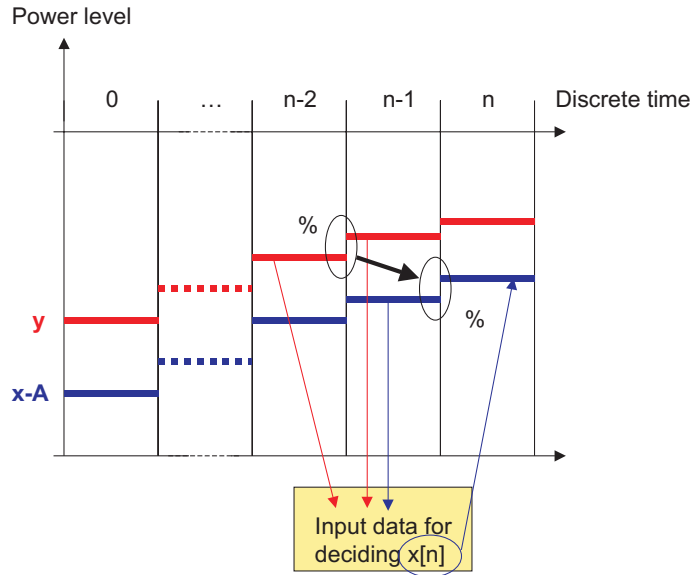
Figure 3.5: Temporal evolution of the variables in the model.

Note that K models the partial coupling between adjacent cells. Simulations have shown the $K=0.5$ is a good value, which has been found by trialling different values and selecting the one for which the estimation error, which will be mathematically defined in Section 3.6, is minimised. Therefore, it has to be noticed that this value of K is only valid for the scenario considered in this study, which will be later summarised in Table 3.1. For different scenarios, the optimal value of K should be found. In practice, this means that a real system should adjust this value on a cell basis by means of, for example, an auto-tuning feature. In addition, it has to be taken into account that for any $K \neq 0$ the system requires an estimate of $P_{Other}(\phi_{UE})$.

In the sequel, for the sake of convenience, let us define L in the following way:

$$L = \frac{1}{1 + \dfrac{G_{UE}}{\rho_{UE}}} \tag{3.29}$$

If (3.26), (3.28) and (3.29) are combined and treated in a recursive way, the next process can be observed:

$$y[n] = (x[n-1] - A) \cdot \frac{y[n-1]}{y[n-2]} + A + L \cdot y[n-1] \tag{3.30}$$

$$y[n] = \left((x[n-2] - A) \cdot \frac{y[n-2]}{y[n-3]} + A - A \right) \cdot \frac{y[n-1]}{y[n-2]} + A + L \cdot y[n-1] \tag{3.31}$$

After n substitutions:

$$y[n] = (x[0] - A) \cdot \frac{y[n-1]}{y[-1]} + A + L \cdot y[n-1] \tag{3.32}$$

Taking into account that $x[0] = y[-1]$, the last equation can be easily written in the following way:

$$y[n] = \left(1 - \frac{A}{x[0]} + L\right) \cdot y[n-1] + A \tag{3.33}$$

In (3.33), it can be seen that, if the PC converges, after a high number of iterations, the final value of the variable y, which represents the outcome of the estimator, follows this expression:

$$y = \lim_{n \to \infty}(y[n]) = A \cdot \sum_{n=0}^{\infty} \left(1 - \frac{A}{x[0]} + L\right)^n = \frac{A}{1 - \left(1 - \frac{A}{x[0]} + L\right)} \tag{3.34}$$

Notice that this expression is only valid if the PC process converges. In case it does not converge, the logical conclusion would be that the power scenario is such that an outage situation has occurred. This intuitive conclusion is consistent with the convergence condition that is derived from the stability analysis of the given model. This stability condition states that there is a stable finite solution for the PC process if the following equation is satisfied:

$$1 - \frac{A}{x[0]} + L < 1 \tag{3.35}$$

By combining (3.27), (3.29) and (3.35), this condition can be written in the following manner:

$$\frac{P(\phi_{UE})}{P_N + KP_{Other}(\phi_{UE})} < 1 + \frac{G_{UE}}{\rho_{UE}} \tag{3.36}$$

By analysing (3.36) for $K=0$, it can be concluded that when a new UE with a certain bit rate requests access to the system, there is a maximum value for the total received power from the already admitted UEs divided into the thermal noise power (NR) that can be tolerated in order to be able to fulfil the quality requirements demanded for all the UEs in the system. Therefore, in the practical utilisation of this DPIE, a negative output value should be interpreted as a predicted outage situation. Notice that this mentioned outage situation is not defined in terms of planned thresholds that are exceeded, but in terms of lack of capability to fulfil the E_b/N_0 requirements of all the connected UEs.

Notice that, the higher the bit rate of the new UE is, the lower the maximum tolerable NR becomes. This trend is easily explainable: if a UE with higher bit rate is intended to be admitted without outage, the maximum tolerable value for the previous load in the system has to be lower than in the case of admitting a lower bit rate UE.

Given that the proposed system is stable, the estimated value of $P_{New}(\phi_{UE})$ equals

$$P_{New\_Est}(\phi_{UE}) = \cfrac{P_N + KP_{Other}(\phi_{UE})}{1 - \left(1 - \cfrac{P_N + KP_{Other}(\phi_{UE})}{P(\phi_{UE})} + \cfrac{1}{1 + \cfrac{G_{UE}}{\rho_{UE}}}\right)} \tag{3.37}$$

Hence, $\chi(\phi_{New}; \phi_{New})$ can be extracted from (3.22). Moreover, $P^{UE}(\phi_{UE})$ can be easily calculated by using (3.21). After this, it is enough just to use (3.23), (3.24) and (3.25) in order to calculate the predicted total received power for all the values of ϕ. Based on this result, it is straightforward to calculate the directional NR by using (3.17).

3.6 Simulation set-up and performance metrics

A semi static UMTS simulator has been built in order to test the performance of the proposed UL AC algorithm. The fact that the simulator is semi static means that the UE locations are not changed along the simulation time. However, the dynamic process in which the system is progressively loaded until UEs start to be rejected is simulated. UEs are connected to the Node-B towards which they exhibit the lowest path loss, and soft handover is not modelled. In this context, the path loss is contributed by the basic deterministic propagation loss due to distance, the shadow fading and the angle specific antenna gain. The simulated network layout is one depicted in Figure 3.6, where all the Node-Bs have the possibility to deploy beamforming AAs.
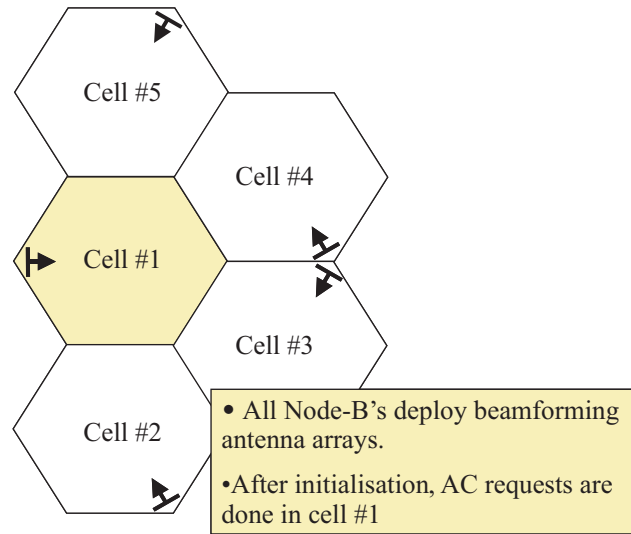
Figure 3.6: Network layout.

The statistics for each simulated case are obtained by conducting 10000 Monte Carlo simulations. This number is assumed to be large enough to provide trustable results. The simulation flow for each one of these Monte Carlo simulations (referred to as realisations) is summarised in Figure 3.7.
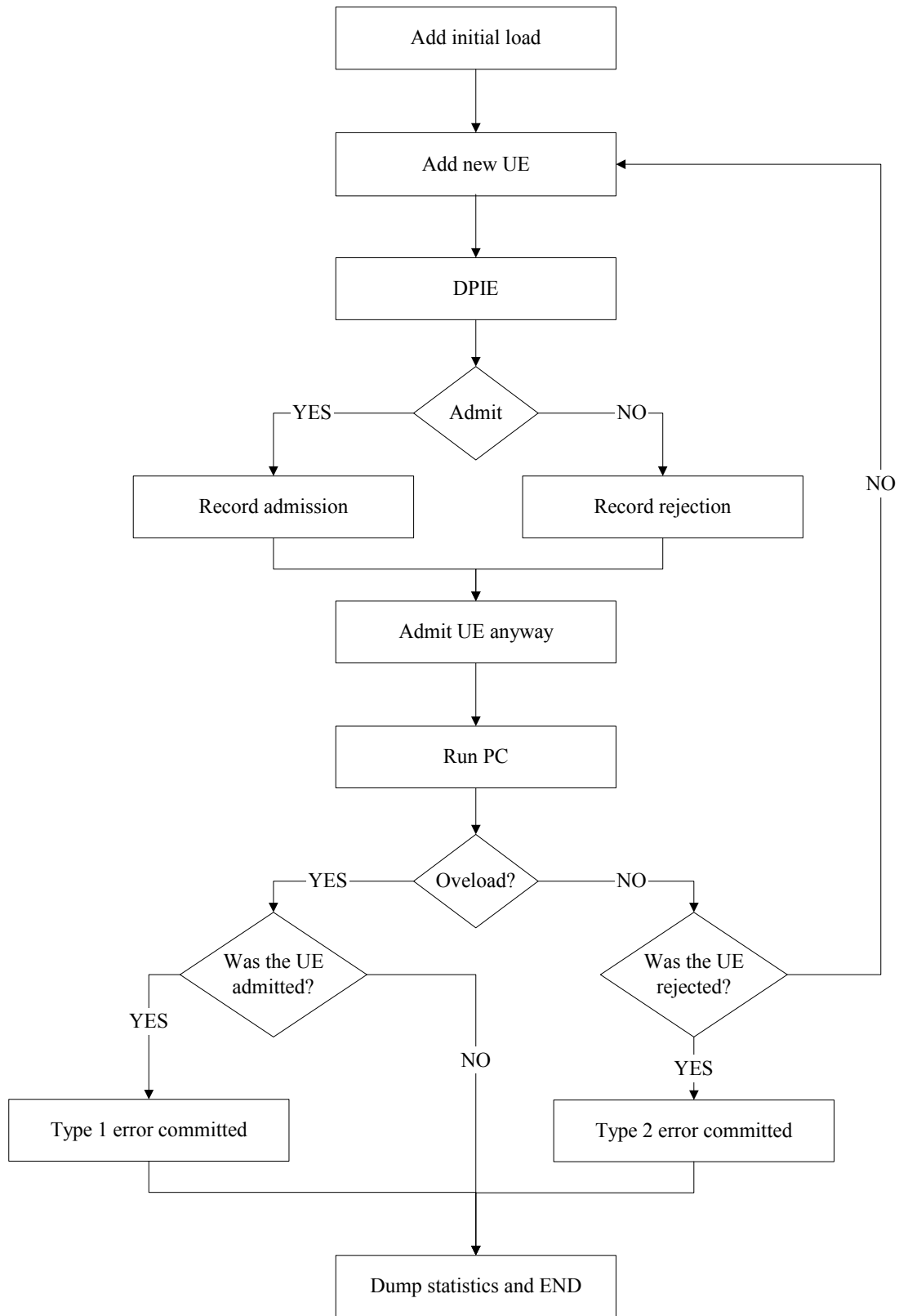
Figure 3.7: Flow chart for one realisation of the simulation process.

When a realisation of the simulation process is started, a certain initial load is added to the system, consisting of a number of UEs that are randomly generated within the five simulated cells. After this, a relatively large number of PC iterations are run in order to stabilise the system so that the E_b/N_0 requirements of all the UEs are fulfilled with the minimum transmitted power. Subsequently, a new UE is generated in such a way that it requests access to cell #1. Note that a UE requests access to cell #1 if this is the cell in which the serving Node-B has the lowest path loss towards that UE. The procedure to generate such UE is iterative, since there are random processes (such as shadow fading) that do not allow the definition the service area of cell #1 just based on geometrical considerations. Instead, the position and the shadow fading statistics of the new UE are generated randomly within an area that is larger than the hexagon marked as cell #1 in Figure 3.6. If the new UE is not generated in a way that it requests access to cell #1, the UE is re-generated iteratively until its propagation and geometry conditions make it request access to cell #1. After a new UE requesting access to cell #1 has been generated, the DPIE is executed in order to see whether the UE should be admitted. If the UE is rejected, the realisation is stopped here, although the rejected UE is admitted before stopping in order to test what would have happened if it had been admitted. If it is not rejected, the system checks whether the new UE makes the NR exceed NR_{Th} for some ϕ. If this threshold is exceeded, an overload event is recorded and the realisation is finished here. If not, the system is identified to remain stable, a new UE requesting access to cell #1 is generated (with the aforementioned iterative process) and the AC procedure is run again. This process is executed iteratively until the system starts rejecting UEs. From each simulation (consisting of 10000 realisations), the following interesting performance figures can be obtained:

- The average cell raw throughput that can be delivered without exceeding the NR_{Th} for any azimuth location.

- The Type 1 error probability.

- The Type 2 error probability.

- The estimation error for the last admission attempt, i.e. the one causing the rejection. This can be measured because the rejected UE is admitted anyway in order to know what would have happened. This error characterises the performance of the DPIE in a high load situation. The estimation error is defined as

$$Error[\%] = \frac{P_{New}(\phi_{Max}) - P_{New\_Est}(\phi_{Max})}{P_{New}(\phi_{Max})}, \tag{3.38}$$

where

$$\phi_{Max} = \arg \max_{\phi} P_{New}(\phi) \tag{3.39}$$

In Table 3.1, a summary of the simulation parameters and models is provided. In addition, a description of the selected simulation cases is given. The system is simulated with both AAs and single antenna reception, in order to be able to quantify the capacity gain that can be expected from the deployment of AAs. Moreover, two traffic cases are analysed. In one of them, higher bit rates are allowed, which is known to yield a more directional spatial distribution of the interference.

Table 3.1: Simulation model and default parameters.

Feature	Chosen option for the simulations
Path loss model	Single slope model with an exponent of –3.5
Shadow fading	Lognormal distributed, with std. of 8.0 dB
Azimuth dispersion model	Laplacian power azimuth spectrum. AS = 5.0°
Site-to-site distance	2.0 km
Chip rate	$3.84 \cdot 10^6$ chips per second
Thermal noise level	-102.9 dBm [1]
Power control	Closed loop with step size of 1.0 dB
Required E_b/N_0	6.0 dB [84]
K parameter for $\Delta P_{OTHER}(\phi_{New})$	0.5
Bit rates	• Traffic case 1: Bit rates =[16, 64, 128, 256] kbps with the following probability vector [0.2, 0.5, 0.2, 0.1] • Traffic case 2: Bit rates =[16, 64] kbps with the following probability vector [0.4, 0.6]
UE antenna	Omni-directional antenna. Gain = 0.0 dB
Beamforming AAs at the Node-B	• Uniform linear AA with half-a-wavelength element spacing • 4 and 8 antenna elements per array. • Amplitude radiation pattern of the antenna elements : $$f(\phi) = \begin{cases} \sqrt{\beta}\cos^{1.4}(\phi) & for \quad \phi \in [-90°, 90°] \\ \sqrt{\beta/R} & otherwise \end{cases}$$ • β = 18 dBi • R = 33.8 dB • Continuous CBF with resolution of 1°
NR_{Th}	6.0 dB [84]
Δ_{Offset}	Spanning from 0.0 to 2.0 dB, with steps of 0.1 dB
Initial load for capacity simulations	• Traffic case 1: 60 UEs in the network for the case with CBF, and 20 UEs in the network for the sector antenna case • Traffic case 2: 116 UEs in the network for the case with CBF, and 39 UEs in the network for the sector antenna case

3.7 Simulation results

Figure 3.8 shows the cell throughput for both AAs with CBF and sector antennas, as a function of Δ_{Offset}. For these simulations, traffic case 1 is selected and the deployment of AAs with CBF yields a capacity gain of 170% for Δ_{Offset} =0 dB, compared with the case where conventional sector antennas are used. For Δ_{Offset} = 2dB, the capacity gain decreases slightly down to 160%.
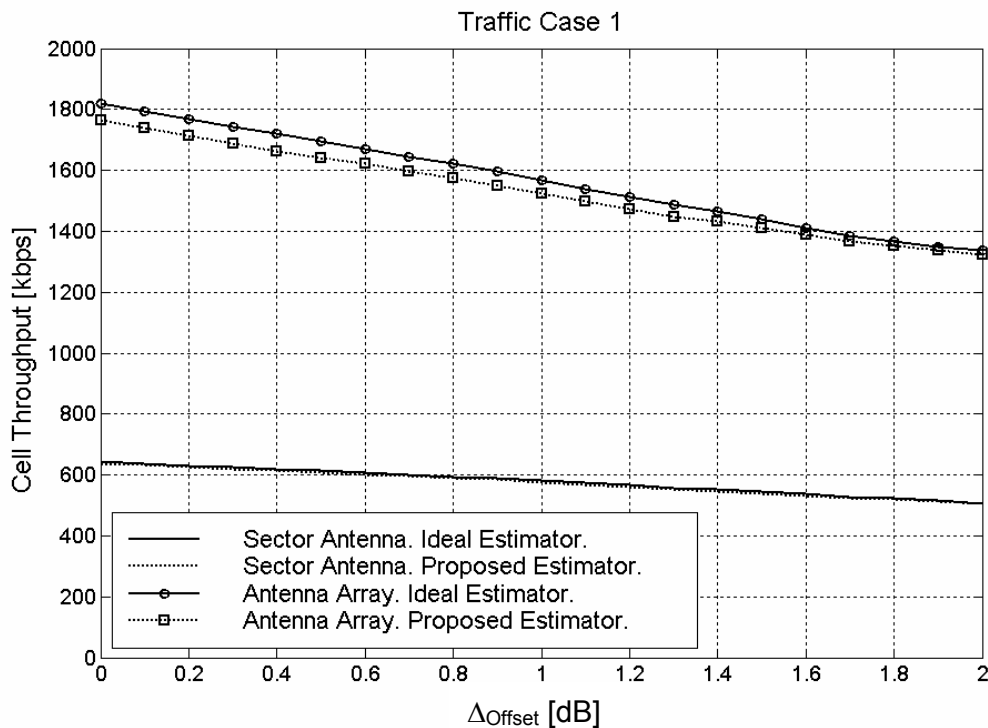
Figure 3.8. Cell throughput vs. Δ_{Offset} for traffic case 1.

The same result is depicted in Figure 3.9 for traffic case 2. Here, larger capacity gain (220% with Δ_{Offset} =0 dB) is obtained from using AAs with CBF. The reason for this higher gain is that the use of traffic case 2 involves lower bit rates, which means that more UEs are admitted in the system, resulting a more uniform spatial distribution of the interference and the subsequent increase of the spatial filtering gain. On the other hand, the higher bit rates allowed in traffic case 1 result in a more directional spatial interference scenario, which prevents AAs with CBF from being able to perform an efficient spatial filtering of the interference. For both sector antennas and AAs with CBF, as the value of Δ_{Offset} grows, the AC algorithm becomes more conservative, resulting in lower cell throughput. Of course, this effect is observed for both traffic cases. In both cases, the cell throughput that an ideal estimator would achieve has also been plot, which shows that the capacity gain captured by the derived estimator is very close to the ideal one.
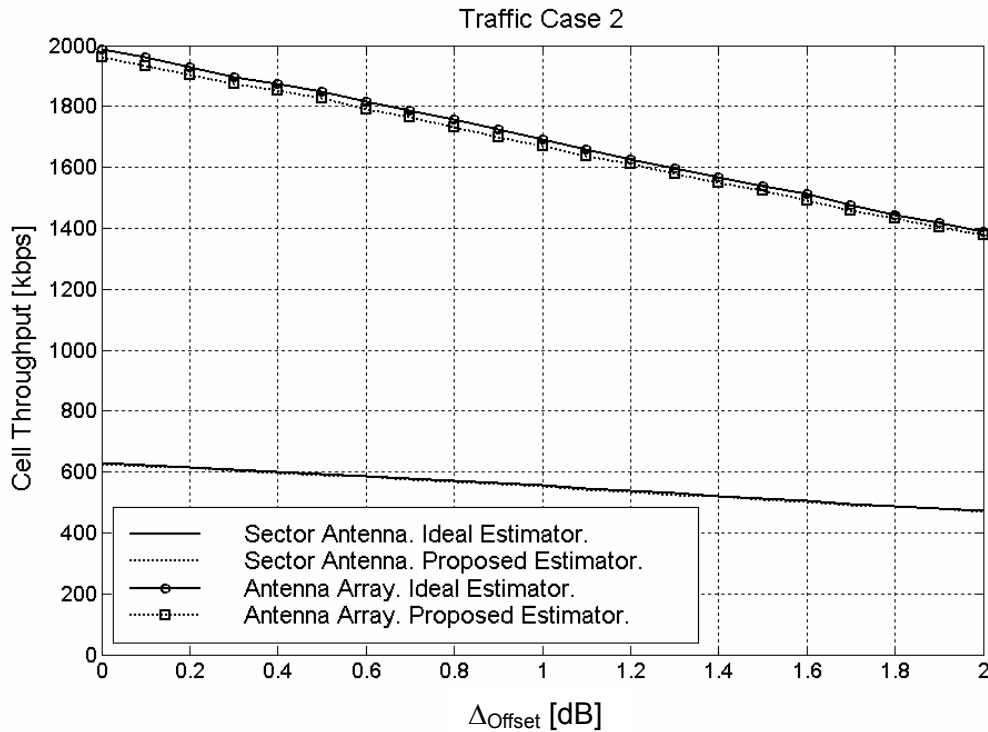
Figure 3.9: Cell throughput vs. $\varDelta_{Offset}$ for traffic case 2.

For the AA configuration used here, the beamwidth reduction ratio between the sector beam and the directional beam (calculated at a 3 dB loss compared with the maximum gain) is approximately 2.8, which gives a rough first order approximation of the capacity gain that equals 180% for a uniform distribution of the interference. As already mentioned, the simulation results show capacity gain figures ranging from 170% to 220%, depending on the traffic distribution. Thus, the simulation results are considered to be within the same order of magnitude as the first order approximation given by the beamwidth reduction ratio.

For comparison, the study presented in [48] shows a similar analysis for the UL of a CDMA system, with a traffic distribution similar to the one given in traffic case 2. The result is that when AAs are implemented in a cell with circular coverage area, a beamwidth reduction of 3 corresponds to a capacity gain between 170% and 200% approximately, depending on the allowed outage. Thus, the figures presented in this study are considered to be within the same order of magnitude as the ones shown in [48].

Figure 3.10 shows the Type 1 and Type 2 error probability as a function of the value of $\varDelta_{Offset}$ for traffic case 1. Due to the given definition of a Type 1 error, it is straightforward to conclude that a higher value of $\varDelta_{Offset}$ implies a more conservative behaviour of the AC algorithm and, therefore, involves a lower Type 1 error probability, which can be interpreted as an improvement in the stability of the system. On the other hand, the more conservative behaviour associated with a higher value of $\varDelta_{Offset}$ causes the rejection of more UEs that would not have driven the system into an overload situation, which can be observed in Figure 3.10 as the Type 2 error probability increases when $\varDelta_{Offset}$ grows. Nonetheless, Type 2 errors are not so harmful and their net effect is already noticed in the capacity loss related to a higher value of $\varDelta_{Offset}$. The same trends are observed for traffic case 2 in Figure 3.11.
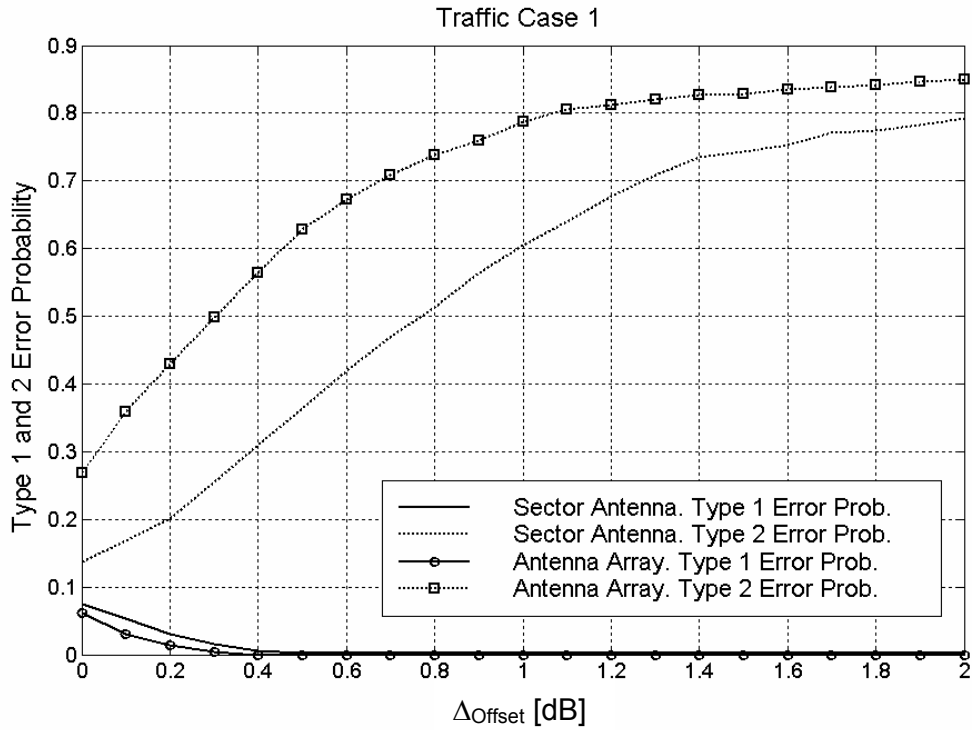
Figure 3.10: Type 1 and 2 error probability vs. Δ_{Offset} for traffic case 1.
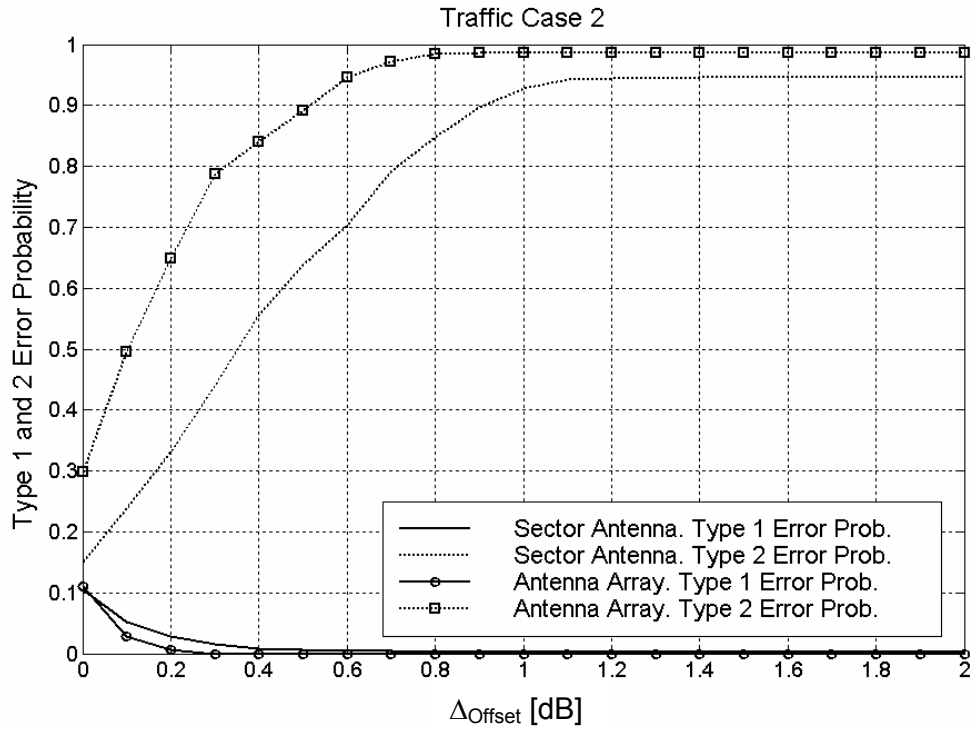
Figure 3.11: Type 1 and 2 error probability vs. Δ_{Offset} for traffic case 2.

As can be seen, for both traffic cases, the Type 1 error probability is kept below 10% for the less conservative settings (Δ_{Offset} = 0 dB) and drops to negligible values for a value for Δ_{Offset} of 0.4 dB.

In addition, it can be observed that the Type 1 error probability is higher for traffic case 1. The reason is that traffic case 1 involves higher bit rates. As a consequence, the NR is increased more drastically when a new UE is added, which is more difficult to be accurately predicted by the DPIE. This is illustrated in Figure 3.12, which shows the cumulative distribution function (CDF) of the estimation error made by the DPIE when the cell is very highly loaded, for both traffic case 1 and 2.
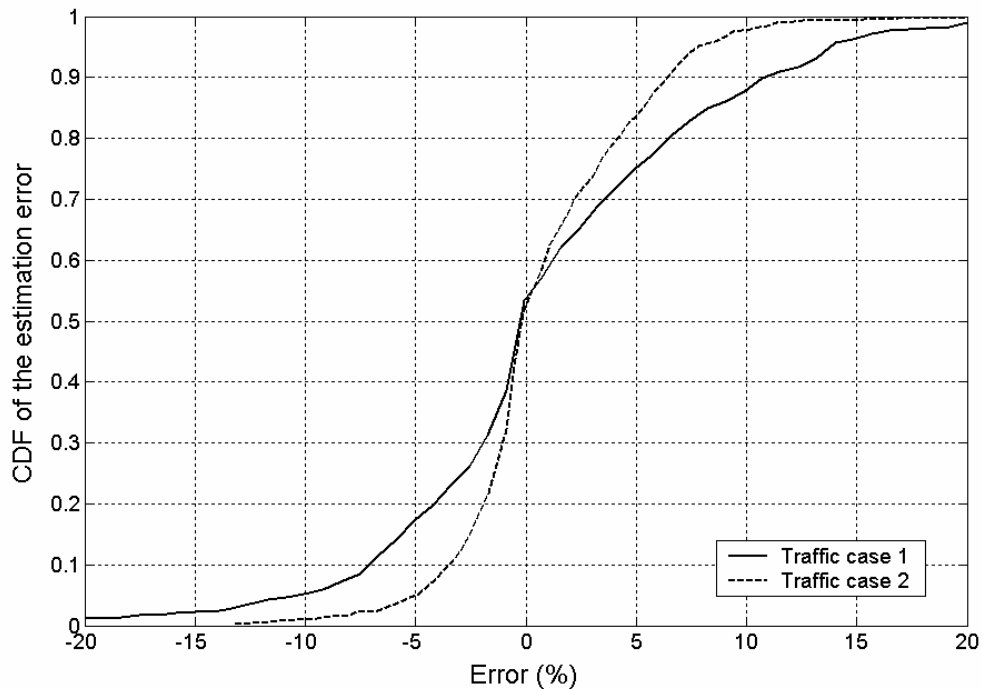
Figure 3.12: CDF of the estimation error for traffic case 1 & 2.

Furthermore, additional simulations with 8 elements in each beamforming AA have been conducted. In this case, a capacity gain of 350% is experienced for traffic case 1 and Δ_{Offset} =0 dB.

3.8 Concluding remarks

In this chapter, a general overview has been given of the different UL AC algorithms proposed in the open literature. Among all the possible choices, UL AC algorithms based on power have been identified to offer an attractive trade-off between capacity and coverage, while automatically taking advantage of the soft capacity gain offered by WCDMA systems.

Generalisation of power based UL AC algorithms to the case where AAs with CBF are deployed at the Node-B has been addressed and, as a conclusion, the convenience of using a

directional power based AC algorithm has been motivated, based on the mechanisms that provide the capacity enhancement by spatial filtering of the interference. In general, the proposed algorithm enjoys the advantages of conventional power based AC algorithms, i.e. adaptation to different propagation environments, automatic exploitation of the soft capacity and suitability for mixed multi rate service profiles. In addition, it captures the available capacity gain by fully adapting the amount of admitted traffic to the spatial distribution of the interference.

The performance of the proposed AC algorithm has been analysed by mean of semi static system simulations, which have shown that the proposed AC algorithm automatically adapts to the available system capacity given by each antenna configuration and traffic distribution. When the offered traffic facilitates a more uniform spatial distribution of the interference, the captured capacity gain is larger (e.g. 220% for traffic case 2 and four antenna elements at the AAs), whereas the capacity gain decreases when higher bit rates are allowed and the interference distribution becomes more directional (e.g., with four antenna elements at the AAs, the capacity gain drops to 170% when traffic case 1 is selected). Moreover, the larger capacity gain facilitated by a higher number of antenna element at the AAs is also automatically detected by the proposed AC algorithm. For example, a capacity gain of 350% is achieved for traffic case 1 and eight antenna elements.

The accuracy of the derived DPIE has been characterised by analysing the statistical behaviour of the estimation error. In addition, the impact of the estimation errors on the AC decisions has been addressed by looking into the Type 1 and Type 2 error probability. In general, the probability of driving the system into overload due to a wrong AC decision (making a Type 1 error) is below 10%, which provides good stability. Moreover, this probability turns negligible when the margin Δ_{Offset} between the AC and the overload threshold is above 0.4 dB.

Note that the reported results have been obtained with a simulation tool that does not consider mobility. In some scenarios, the user mobility can seriously affect the system performance and operation. Let us take an extreme case, in which the UEs are uniformly distributed in the azimuth domain. Under these circumstances, it might be that a new UE is admitted in the system. Then, if after the admission all the UEs change their position and move towards the same azimuth location, the system might become instable. Thus, in a real system, perhaps it would be advisable to include some safety margins in the AC process, in order to account for the possibility that the UE moves to the azimuth locations surrounding the one from which access is being requested. Of course, the deployment of such safety margins has to be designed so that the appropriate trade-off between capacity gain and stability is achieved. In this process, the specific characteristics of the offered traffic in each case have to be considered. The aforementioned analysis about the trade-off between capacity and increased protection against user mobility is therefore regarded as an interesting subject for further study, although an analogue situation will be considered in Chapter 4 for the downlink case, where mobility will be fully included in the study.

Chapter 4

Downlink capacity gain with beamforming AAs at the Node-B

4.1 Preliminaries

The objective of this chapter is to investigate the capacity gain of antenna arrays (AAs) with conventional beamforming (CBF) in the downlink (DL) of the Universal Mobile Telecommunications System (UMTS), devoting special attention to the interrelation between the configuration of the radio resource management (RRM) algorithms and the obtainable spatial filtering gain offered by AAs. As part of this evaluation, the directional power based admission control (AC) algorithm proposed in [87] will be used. For the formulation of this algorithm, conventional power based DL AC algorithms [68], [75], [88] are extended in order to take into account the spatial distribution of the interference, as was done in Chapter 3 for the uplink (UL) case. The capacity gain is determined for different types of services in a network with a combination of cells with AAs and cells with conventional sector antennas. In cells with AAs, a grid of fixed beams is formed, as described in Chapter 2. As reported in [13], this configuration yields a performance that is comparable to the one in which beams can be steered at the exact direction of arrival (DoA) of each user equipment (UE).

In UMTS, signals transmitted within the same cell towards different UEs are separated by means of synchronised orthogonal codes (referred to as channelisation codes) extracted from an orthogonal variable spreading factor (OVSF) tree [30]. The channelisation codes are derived from the set of Walsh codes and there are a finite number of them. Since orthogonal codes do not have white noise properties, the total transmitted signal at each cell is scrambled by a pseudo noise (PN) sequence, referred to as scrambling code [1]. As will be demonstrated in this study, the finite set of available channelisation codes at each cell constitutes a hard capacity limit.

Application of AAs with CBF in a cell provides a capacity gain due to spatial filtering of the interference, which means that more UEs can be supported without reaching the interference limit. This does in many cases result in scenarios where UEs are denied access to the system due to shortage of channelisation codes even though the interference limit is not reached. Potential channelisation code limitations in wideband code division multiple access (WCDMA) systems with single antenna transmission are analysed in [89], and the impact of enabling a secondary scrambling code, with the subsequent availability of a new channelisation code tree, is addressed in [90]. In that work, it can be seen how the uncoordinated co-existence of two scrambling codes in the same cell leads to a drastic performance degradation due to lack of orthogonality between signals with different scrambling codes. However, most of the previous studies of AAs in UMTS have typically ignored the effect of code blocking; see [13] and [87] among others. In this chapter, a method to circumvent this problem (i.e. to minimize code blocking) without seriously jeopardizing the capacity gain will be analysed. In this solution, CBF is used in order to split the cell into several scrambling code regions. Then, different scrambling codes are allocated to each beam or group of beams, and one instance of the channelisation code tree becomes available for each scrambling code region. In this way, mutual interference between signals transmitted with different scrambling codes within the same cell is reduced by the spatial filtering properties of CBF. The aforementioned cell splitting strategy is supported in UMTS, since it is allowed to allocate multiple secondary scrambling codes in a cell (see [27] and [31]).

The capacity reduction due to code blocking mainly depends on the absolute capacity that can be achieved when only interference limitations are taken into account. Moreover, the influence of the activity factor of the connections is also important. Furthermore, the achievable capacity gain when deploying AAs with CBF is affected by other RRM aspects. For example, the use of large soft handover (SHO) margins involves large channelisation code consumption per UE, which contributes to increase the capacity reduction due to code blocking.

This chapter is organised as follows. Section 4.2 introduces the selected directional power based AC algorithm that is used for the case where AAs with CBF are deployed at the Node-B. The simulation set-up that has been selected to evaluate the capacity gain is described in Section 4.3. The obtained simulation results are presented and analysed in Section 4.4, and an extrapolation of these results to the case with bursty packet traffic is discussed in Section 4.5. Finally, concluding remarks are given in Section 4.6.

4.2 Directional power based RRM

When a power based AC algorithm is used in a cell with sector antennas, a UE is admitted if there are enough channelisation code resources and the following condition is

estimated to remain true after the admission

$$P < P_{Target} , \qquad (4.1)$$

where P is the total average wideband transmitted power at the cell and P_{Target} is a pre-defined threshold.

The discussion on the directional power based DL AC algorithm is particularised for the case where a fixed grid of N beams is deployed with a secondary common pilot channel (S-CPICH) per beam for channel estimation, together with a wide sector beam covering the entire cell (see Section 2.2.2.1 in Chapter 2). In order to extend this algorithm to the case where the Node-B is equipped with AAs with a fixed grid of beams, the condition regarding the availability of channelisation code resources remains the same. However, since the capacity gain from CBF is due to spatial filtering of the interference, the spatial distribution of the interference has to be taken into account when formulating the power criterion for AC. According to the algorithm proposed in [87], the directional power based AC criterion yields

$$P(\phi_n) < P_{Target} \quad \forall \quad n \in [1,2,...,N], \qquad (4.2)$$

where ϕ_n is the steering direction of the nth directional beam and $P(\phi_n)$ is the total average normalised transmitted power in that direction. Note that in [91], a similar approach is reported to provide improved system stability, especially when the spatial distribution of the interference is highly directional. The total average normalised transmitted power in each one of the N steering directions can be expressed as [87]

$$\begin{bmatrix} P(\phi_1) \\ P(\phi_2) \\ \vdots \\ P(\phi_n) \end{bmatrix} = \begin{bmatrix} \dfrac{W(\phi_1;\phi_1)}{S(\phi_1)} & \dfrac{W(\phi_2;\phi_1)}{S(\phi_1)} & \cdots & \dfrac{W(\phi_N;\phi_1)}{S(\phi_1)} \\ \dfrac{W(\phi_1;\phi_2)}{S(\phi_2)} & \dfrac{W(\phi_2;\phi_2)}{S(\phi_2)} & \cdots & \dfrac{W(\phi_N;\phi_2)}{S(\phi_2)} \\ \vdots & \vdots & \cdots & \vdots \\ \dfrac{W(\phi_1;\phi_N)}{S(\phi_N)} & \dfrac{W(\phi_2;\phi_N)}{S(\phi_N)} & \cdots & \dfrac{W(\phi_N;\phi_N)}{S(\phi_N)} \end{bmatrix} \begin{bmatrix} P_1 \\ P_2 \\ \vdots \\ P_N \end{bmatrix} + P_{PCICH} , \qquad (4.3)$$

where P_{PCPICH} is the power for the primary common pilot channel (P-CPICH), $W(\phi_1;\phi_2)$ is the effective power antenna gain at ϕ_2 when a directional beam is pointed at ϕ_1, $S(\phi_1)$ is the effective power antenna gain of the sector beam at ϕ_1, and P_n is the average transmitted power allocated to beam #n, which can be expressed as

$$P_n = P_{SCPICH} + P_{USER}^n , \qquad (4.4)$$

where P_{USER}^n is the total average transmit power to all UEs served with beam #n and P_{SCPICH} is the power allocated to the S-CPICH. The beam coupling matrix presented in (4.3) can be pre-computed based on the selected set of steering directions and the radiation pattern of the antenna elements. However, when computing the effective power antenna gains, the power azimuth spectrum (PAS) of the radio channel at the Node-B has to be known. In practice, obtaining an accurate characterisation of the PAS for each cell is a challenging task, and any error in this characterisation is directly mapped into an error when evaluating the power that is transmitted towards each azimuth direction.

Note that the directional power based AC criterion formulated in (4.2) automatically captures the effect of the spatial interference distribution. For M=1 and N=1, the criterion in (4.2) reduces to that in (4.1), for P_{SCPICH}=0. Before a UE is granted access, the transmit power in the N beams should be estimated (assuming that the UE is granted access) and the availability of channelisation codes should be checked, conditioned on the requested bit rate and energy-per-bit to noise ratio (E_b/N_0) requirements. In order to predict how the transmit power at each azimuth direction is going to change when the new UE is admitted, a directional power increase estimator (DPIE) is needed. The DPIE derived in [87] is adopted for this purpose. This DPIE implicitly assumes that all the links (Node-B–UE connections) in the system are power controlled as described in [1], so admission of a new UE also results in higher transmit power to the existing UEs in the systems as they will experience an increased interference level due to the addition of the new UE.

4.3 Simulation set-up and performance metrics

After conducting the simulations in Chapter 3, a decision was made to add extra features to the simulation model in order to make it more realistic. Since the tool used in Chapter 3 was developed in Matlab, an extension of that tool was not considered appropriate, due to the very large simulation time. Therefore, it was decided to change to a completely new simulation platform, which was already under development in Nokia, the company sponsoring this project. Under these new conditions, the author had to get familiar with the much more complex software structure and, in addition, had to design and implement the necessary features for beamforming antenna support that were needed in order to continue with the research work. The beamforming support was developed and thoroughly tested for both UL and DL. This was a very time consuming task and a strategic decision was made to focus the more extensive simulation studies with the new platform on the DL case. The main reason was that the DL case opens for wider studies about beamforming AAs. One clear example is channelisation code shortage, which is not a problem in the UL case.

4.3.1 Basic simulation methodology

A dynamic UMTS simulator is applied for evaluation of the DL capacity gain of AAs. A standard hexagonal grid with three-sector sites and 33 cells is simulated, as pictured in Figure 4.1. For simulations with AAs, these are only deployed in cells #0, #1 and #2. The basic simulation methodology follows that of [92]. The simulator includes dynamic traffic models for UEs, movement of UEs, RRM algorithms such as closed loop power control (CLPC), outer loop power control (OLPC), handover control (HC), and AC. The simulator is operated at slot[7] level, using the so-called actual value interface (AVI) to model the link performance of each Node-B–UE connection [93]. The deterministic path loss between each Node-B and each UE is calculated according to the single-slope model with an exponent of -3.5. Shadow fading is assumed lognormal distributed with an exponentially decaying spatial auto-correlation function in coherence with Gudmundsons model [94]. Multipath fast fading is modelled according to the ITU power delay spectra: Vehicular A and Pedestrian A [42]. The azimuth dispersion at the Node-B is modelled with a Laplacian PAS [35] with an azimuth spread (AS) of 5° in coherence with typical urban macro cell environments. It is furthermore assumed that the average PAS is identical for each multipath delay component in the radio

---

[7] Note that the slot duration is 0.667 ms.

channel so the joint power azimuth-delay spectrum can be expressed as the product of the power delay spectrum (PDS) and the PAS [35]. The latter assumption implies that the shape of the PDS between a Node-B and a UE will be identical for the sector beam and the best narrow directional beam, assuming that the AS is smaller than the beamwidth. At the end of this section, a simplified flowchart of the simulation tool is depicted in order to provide further understanding of the adopted overall simulation strategy. See Figure 4.3, on page 80.
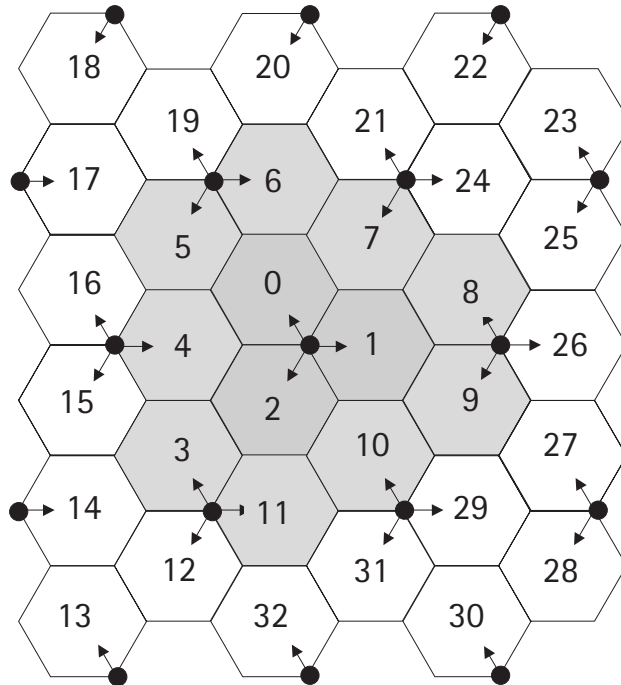
Figure 4.1: Network layout.

4.3.2 Configuration for cells with beamforming AAs

In cells with AAs, a fixed grid of beams with a S-CPICH per beam is used. A sector beam is synthesised for transmission of the common channels, which should be broadcast in the entire cell. For simplicity, it is assumed that the only signal transmitted on the sector beam is the P-CPICH. The coverage area of the P-CPICH implicitly defines the cell area, since the P-CPICH is used for handover measurements by the UEs [1]. A unique secondary common pilot signal (S-CPICH) is transmitted on each directional beam, which can be used for channel estimation purposes at the UEs. Transmission towards a single UE from one cell is assumed to include one directional beam only, selected from a time average UL direction of arrival (DoA) estimate. A typical finding from measurement campaigns is that the time average DoA for the UL and the DL are identical, provided that the averaging period is sufficiently long to average over the fast fading behaviour of the radio channel [52].

The pilot powers (P_{PCPICH} and P_{SCPICH}) are constant, while the link powers to the individual UEs are power controlled, i.e. time-variant. The ratio between the transmit powers of the pilot signals is determined in coherence with the ratio between the gain of the sector beam and the directional beams, i.e.,

$$P_{SCPICH} = \frac{P_{PCPICH}}{M}, \tag{4.5}$$

where *M* is the number of antenna elements in the AA. This relationship is used to provide the same coverage with both the P-CPICH and the S-CPICH. The pilot signals represent a power overhead (i.e. a pilot overhead), which limits the power available for transmission of dedicated physical channels (DPCHs) towards the UEs.

4.3.3 UE performance modelling

All UEs in the network are assumed to use a standard Rake receiver, with Rake finger maximal ratio combining (MRC) [36]. The E_b/N_0 is computed for each Rake finger in every slot interval, followed by MRC to obtain the total E_b/N_0. The effect of using orthogonal channelisation codes is included when computing the E_b/N_0 at each finger, since the time-synchronised orthogonal own cell interference is subtracted from the interference term in the denominator. In the following, an expression for the calculation of the E_b/N_0 at each slot is given

$$\frac{E_b}{N_0} = \sum_{f=1}^{F} \frac{G \cdot P_i g_L(s,i) g_{FF}(s,i,f) W\left(\phi_{beam,beam(i)};\phi_i^s\right)}{\begin{bmatrix} P_N + \\ \sum_{b=1}^{B}\sum_{d=1}^{D(b)}\sum_{l=1}^{L}\left(P_{USER,d}^b + P_{SCPICH}\right)g_L(b,i)g_{FF}(b,i,l)W\left(\phi_{beam,d};\phi_i^b\right) + \\ \sum_{b=1}^{B}\sum_{l=1}^{L} P_{Sector}(b)g_L(b,i)g_{FF}(b,i,l)S\left(\phi_i^b\right) - \\ \sum_{d \in \mathbf{R}(i)}\left(P_{USER,d}^s + P_{SCPICH}\right)g_L(s,i)g_{FF}(s,i,f)W\left(\phi_{beam,d};\phi_i^s\right) - \\ X(i)P_{Sector}(s)g_L(s,i)g_{FF}(s,i,f)S\left(\phi_i^s\right) \end{bmatrix}} \tag{4.6}$$

where the notation given in Table 4.1 is used. Note that this expression assumes that the resulting E_b/N_0 value at the output of the Rake receiver can be computed as the sum of the E_b/N_0 values at the output of the different Rake fingers. This is an approximation that assumes that the noise and interference components at the different Rake fingers are totally uncorrelated, which is not totally true but only a good approximation. For example, in the case of the thermal noise, the same noise sequence is fed as input to all the Rake fingers in the receiver. However, the thermal noise components at the output of the different Rake fingers has been considered to be uncorrelated due to the fact that in each finger the noise sequence is correlated with a differently delayed replica of the spreading sequence, whose autocorrelation is low (but not zero) when the delay does not equal zero. Nonetheless, as will be explained later with more detail, the effect of having partially correlated noised and interference at the Rake fingers is embedded in the AVI, which is based on detailed chip level processing.

It is also important to point out that this expression is for the case where CBF is used at the cell in which the considered UE is served. For the rest of the cells, nothing is assumed and conventional sector antennas can be used, which can be modelled by setting the number of synthesised beams at the corresponding cell to zero. Some of the variables defined in order to write (4.6) are also illustrated in Figure 4.2.

Table 4.1: Notation for the E_b/N_0 calculation.

Symbol	Definition
F	Number of Rake fingers. Perfect MRC between them is assumed
L	Number of multipath components in the considered power delay profile (PDP)
G	Processing gain
P_N	Power for the thermal noise at the UE
B	Number of cells in the network
P_i	Desired signal power transmitted towards UE #i
$P^b_{USER,d}$	Total user signal power transmitted through beam #d at cell #b
$P_{Sector}(b)$	Total power transmitted on the sector beam at cell #b
ϕ^b_i	DoA of UE #i, referred to the broadside direction of the antenna system at cell #b
$\phi_{beam,k}$	Azimuth direction at which beam #k is pointed, referred to the broadside direction of the corresponding AA
$beam(i)$	Beam serving UE #i
$D(b)$	Number of beams synthesised at cell #b
$\mathbf{R}(i)$	Set of beams that belong to the scrambling code region in which UE #i is served
$X(i)$	Variable that equals one if UE #i is served under the primary scrambling code. Otherwise, it equals zero
$g_L(b, i)$	Path gain from the Node-B at cell #b to UE #i, including deterministic path loss and shadow fading. Expressed in terms of power gain for convenience
$g_{FF}(b, i, l)$	Power gain of the fast fading multipath component #l of the link between the Node-B at cell #b and UE #i
s	Cell in which the UE under evaluation is being served

AA at cell #s

$\phi_{beam,beam(i)}$

ϕ_i^s

ϕ_i^k

beam(i)

AA at cell #k

UE #i
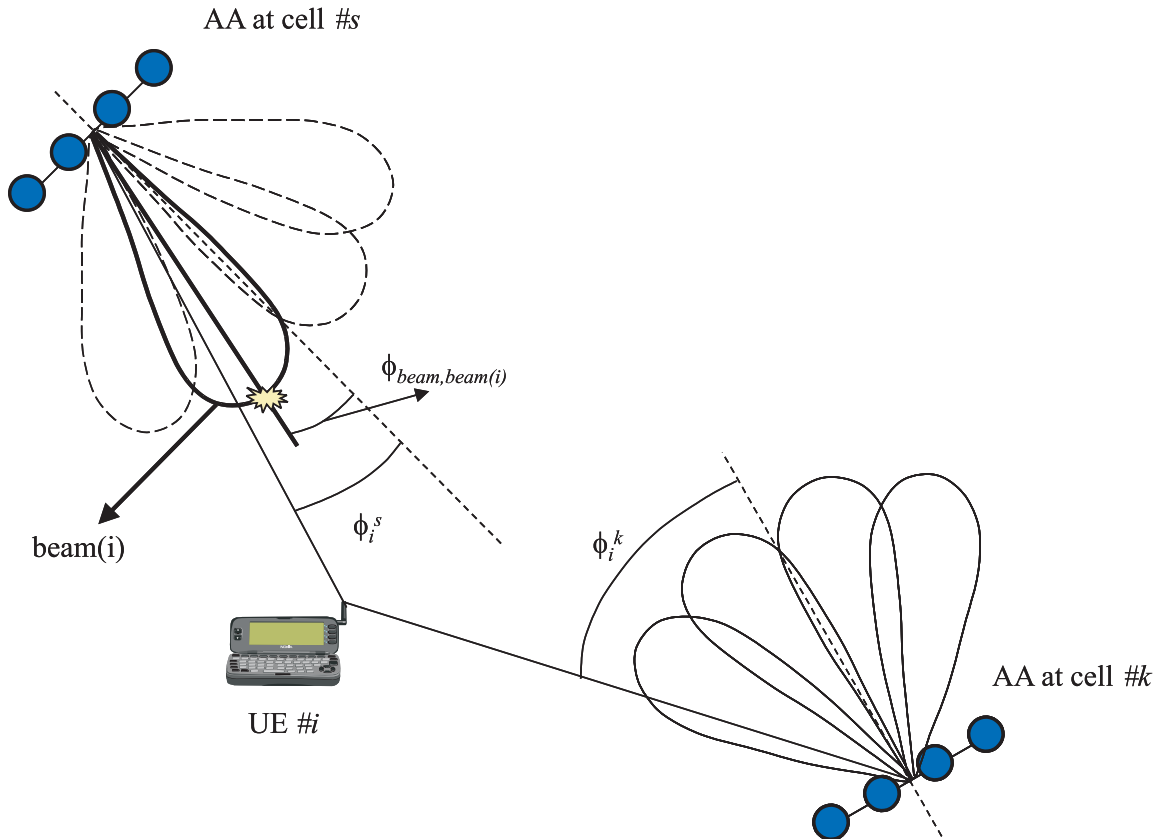
Figure 4.2: Illustration of the notation for the E_b/N_0 calculation.

Regarding the use of CBF, it must me pointed out that the utilised radiation patterns are convolved with the PAS of the radio channel at the Node-B, according to the guidelines provided in Chapter 2. In this manner, the impact of azimuth dispersion on the spatial filtering capabilities of CBF is accounted for in the simulation model. However, the same PDS is assumed for all the connections (served with or without beamforming AAs), which is an approximation. If the AS is zero, this approximation becomes exact. On the other hand, if the AS is extremely large (larger than the beamwidth of the synthesised directional beams), there are some multipath components of the transmitted signals that fall completely out of the radiation pattern of the synthesised beams. Therefore, they should not be included in the PDS that characterises the radio channel between the Node-B and the UE. In the case analysed in this study (AS = 5º), the approximation is considered to be fair for the transmission of the desired signal, since the AS is smaller than the beamwidth of the synthesised beams. However, when modelling the radio channel affecting signals that are transmitted by the interfering beams, the use of the same PDS may become less accurate, since the radiation patterns of the synthesised beams become steeper for those azimuth directions that are not in the surroundings of the one at which the beam has been pointed, which means that the different multipath components are treated very differently by the radiation pattern of the corresponding beam and, therefore, using the same PDS that was used for the desired signal is not fully accurate. Moreover, the fast fading values for the different multipath components of the radio channel between a Node-B and a UE are assumed to be the same for all the beams, which is also an approximation. Nonetheless, these approximations are not expected to affect the results significantly. However, as will be stated in Chapter 7, in order to know the exact impact of these shortcuts, the detailed study of these phenomena including a more thorough

modelling of the coupled space-time characteristics of the radio channel is suggested for further study.

Once a UE has received a number of slots corresponding to one block, the AVI principle is used [93]. Hence, the equivalent block E_b/N_0 is computed as the geometrical average of the E_b/N_0 values per slot in the block. A lookup table (generated from link level simulations) maps the block E_b/N_0 to an equivalent block error probability (BEP). A uniform distributed number ($\chi \in [0; 1]$) is generated and compared with the BEP. If $\chi <$ BEP, the block is labelled as erroneous. Otherwise, it is labelled good.

The utilised AVI tables are obtained from extensive single UE link level Monte Carlo simulations conducted elsewhere, and they represent the BEP versus the geometrically averaged E_b/N_0 per block (e.g. over a 20 ms period for the case of speech traffic) for a certain set of conditions. Different set of AVI tables are obtained for different UE speeds, and the UE speed is not varied within the duration of a single simulation. These simulations are conducted at chip level. The transmitter block includes coding, interleaving, slot formatting, modulation, spreading, scrambling and pulse shaping according to the 3GPP specifications. At the receiver, channel estimation is assumed to be based on the P-CPICH and imperfections in this process are fully modelled. Then, Rake reception with MRC of the different Rake fingers is conducted. In this respect, it must be noticed that delay estimation of the different multipath components is assumed to be perfect. In the end, the receiving chain is completed by the corresponding deinterleaving and decoding operations. It is also relevant to mention that the AVI tables are generated with fast closed loop power control disabled, mainly to include some minor interference and signal fluctuations. In addition, it must be noticed that the geometry factor is not considered as input for the AVI tables, which are generated by simulations in which the interference is modelled as additive white Gaussian noise.

The procedure to generate the AVI tables is detailed in the following. When running the link level simulations, the E_b/N_0 is recorded for each slot period. For each block period, the geometrically averaged E_b/N_0 over the whole block is computed and stored, together with the output of the link level simulator, stating whether the block was successfully decoded or not. After the (long) link level simulation is completed, the intermediate outcome is a long vector with sets of geometrically averaged E_b/N_0 values per block and information about whether the block was successfully decoded. Then, this information is post-processed, by grouping these pieces of information into E_b/N_0 bins of e.g. 0.1 dB. After this, the corresponding BEP per bin is calculated as the ratio between the number of unsuccessfully decoded blocks and the total number of processed blocks. Hence, the AVI table is indeed obtained by post-processing the results of the link level simulations.

As will be more explicitly stated in Table 4.2, different service profiles are considered, which use different link level configurations. Therefore, different sets of AVI tables are generated for different bit rates (8, 64 and 128 kbps), with different spreading factors (128, 32 and 16), different coding schemes (convolutional coding with coding rate ½, and turbo coding with coding rate 1/3) and different interleaving periods (20 ms and 10ms). Moreover, different sets of AVI tables are utilised for the different power delay profiles (PDPs) under study, since the link level performance of the receiver depends on the PDP.

As stated before, the manner in which the E_b/N_0 is calculated assumes uncorrelated noise and interference at the output of the different Rake fingers. Although this is an approximation that is done in system level simulations, the AVI tables assume that the E_b/N_0 is going to be calculated in this manner, and the effect of correlated noise and interference at

the Rake fingers is therefore embedded in the different AVI tables. However, no specific AVI tables are generated for SHO. In this case, ideal MRC between the outputs of the different SHO branches is assumed and the E_b/N_0 values corresponding to each branch are summed. Afterwards, the resulting E_b/N_0 (geometrically averaged over one block) is fed as input to the AVI table.

4.3.4 RRM algorithms

Conventional power based AC is used for cells with conventional sector antennas, while the directional power based AC algorithm is used for cells with AAs as explained in Section 4.2. The parameter P_{Target} is selected to equal 10 W[8], which is a typical parameter setting according to [1] and [2]. Whenever a new UE is generated in the system, it is assumed to request access to the cell towards which the lowest integral average path loss is experienced. In this context, the integral average path loss is formed by the basic deterministic propagation loss due to distance, the shadow fading and the angle specific gain of the sector beam.

When a new UE is admitted into the system, the initial DL transmit power is calculated based on the pilot report sent by that UE to the Radio Network Controller (RNC), which is also used for the AC calculations. In the simulation tool, this pilot report is calculated as

$$\rho_{Pilot} = \frac{P_{PCPICH} \cdot loss}{I},\qquad(4.7)$$

where *loss* is the integral average path loss towards the UE and I is the received interference at the UE. The initial DL transmit power towards the UE must ensure that the initial E_b/N_0 target, ρ_{Target}, is fulfilled:

$$\rho_{Target} \approx \frac{G \cdot P_{Initial} \cdot loss}{I},\qquad(4.8)$$

where $P_{Initial}$ is the initial downlink transmit power towards the UE. Thus, by combining (4.7) and (4.8), the following expression for the initial DL transmit power can be written:

$$P_{Initial} = \frac{P_{PCPICH}}{G} \frac{\rho_{Target}}{\rho_{Pilot}}\qquad(4.9)$$

Note that the value obtained from (4.9) is valid when the new UE is going to be served in a cell with sector antennas. Otherwise, the value given by (4.9) must be divided by M in order to account for the fact that the dedicated signals are going to be transmitted towards the UE with a directional beam whose gain is M times larger than that of the sector beam transmitting the P-CPICH.

The dynamic range for the transmit power towards each UE is 30 dB, and the maximum instantaneous transmit power per link is set to 2 W. With the given simulation set-up, it has been checked that this maximum value of the transmit power per link is reached very seldom.

---

[8] This setting assumes that the maximum transmit power at the Node-B is 20W. Therefore, a power control headroom of 3 dB has been implicitly established.

A resource manager is implemented for each cell to keep track of the available channelisation code resources. Cells with conventional sector antennas are assumed to have only one scrambling code and therefore one channelisation code tree available. Usage of several scrambling codes in cells with conventional sector antennas is not considered. Cells with AAs deploy the number of scrambling codes that is specified for each simulation case, coordinated in such a way that different scrambling code regions are spatially isolated (see e.g. Figure 2.6, on page 27).

SHO decisions are based on the P-CPICH quality measurements at the UEs [1]. A new SHO leg is added to the UE's active set if the ratio between the strongest P-CPICH in the active set and that of the new SHO candidate leg is below a certain threshold, denoted *Wadd*. A SHO leg is removed from the active set if the aforementioned ratio is above a threshold (*Wdrop*) during a certain time-period denoted *Tdrop*. Signals received from the cells in the UEs active set are tracked by separate Rake fingers, and subsequently combined using MRC. Notice that SHO between directional beams within one logical cell is not allowed. The SHO parameter settings listed in Table 4.2 are selected according to the recommendations in [1], [2] and [95].

When a SHO operation is conducted, this is done without considering any detailed layer 3 messaging or signalling delay, and all the involved parts in the system automatically (and with no delay) start operating with the new configuration, i.e. with the UE (or the new SHO branch) being served in the new cell, using the new P-CPICH (or S-CPICH if the target cell is using beamforming) for phase reference and utilising the new scrambling and channelisation codes. This is a simplified model of the real system. In reality the UE should check the handover conditions based on the P-CPICH of the set of monitored cells. Then, when these conditions are fulfilled, the UE sends a handover request to the RNC by means of a Radio Resource Control (RRC) [96] message. After that, the RNC decides whether it is convenient to initiate the handover operation. If the decision is positive, the corresponding RRC message is sent to the UE so that the handover operation occurs[9]. Since these layer 3 procedures have not been explicitly modelled, all the simulation results presented in this chapter ignore the impact of the involved delays. However, this is not considered to be critical at the low simulated speed values (3 kmph, as described in Table 4.2).

Beam switching within the same cell is based on an average UL DoA estimate, extracted from UL power measurements in the *N* different beam directions. The direction with the largest average received power from the UE corresponds to the UL DoA estimate. A directional beam switch is conducted if the average UL received power level in one of the (*N*-1) other beams is *Wbeam* decibels larger than the UL received power of the currently selected beam. Thus, *Wbeam* constitutes a beam selection hysteresis to prevent fast toggling between directional beams due to fast radio propagation variations and DoA estimation errors.

In the employed simulation tool, it has been assumed that the DoA measurements are directly available, i.e. with no delay. Right after the beam switching operation is decided, all the involved parts in the system automatically start to operate with the new configuration, i.e. with the UE being served by the new beam, using the new S-CPICH for phase reference and utilising (if required) the new scrambling and channelisation codes. This is, again, a simplified model of what happens in a WCDMA radio access network. In a real system, the

---

[9] Of course, for this re-configuration to succeed, the Node-B has to be involved in the corresponding operation, so that all the necessary changes are conducted in an ordered manner. This is achieved by means of messages that are sent from the RNC to the Node-B, and by the possibility to use of activation timers [98].

Node-B collects measurements of the signal-to-interference ratio (SIR) for the UE under consideration at different cell portions [97] (which may be considered here as beams). Then, the SIR information regarding the set of cell portions with the highest SIR is reported via the Iub interface to the Radio Network Controller (RNC), which actually takes the beam switching decision when it is considered that the UE is better served by another beam. If this is the case, the beam switching operation is triggered. In order to conduct the beam switching operation, the RNC sends a Radio Resource Control (RRC) physical channel reconfiguration message [96], which tells the UE to change the S-CPICH that is being used for phase reference and, maybe, to start receiving the information on a different scrambling or channelisation code[9]. Of course, this layer 3 messaging procedure involves a certain delay, which is ignored in the simplified model described above. However, the fact that these delays have not been modelled is only expected to make a difference for medium-to-high UE speeds, which is not the case for the presented simulation results (obtained at 3 kmph, as reported in Table 4.2).

A CLPC algorithm is implemented for each radio link connection [22], so the transmit power is adjusted in steps of ±1.0 dB every slot period to obtain a certain E_b/N_o target as described in [1], [2]. The E_b/N_o target is adjusted independently for each UE by an OLPC algorithm so that a predefined block error target is obtained [1], [2].

4.3.5 Offered traffic

UEs are uniformly distributed in each cell. The call arrival rate in cells with AAs is assumed to be larger than that of cells with conventional sector antennas, so cells with AAs are implicitly assumed to cover a hot spot traffic area. All UEs move with a constant speed in a random direction. The position of UEs is updated every slot interval to model the time-variant behaviour of path loss, shadow fading, and fast fading. Speech traffic and two types of circuit switched (CS) data calls are simulated. Speech connections with 8 kbps are assumed to have a block length of 20 ms (30 slots), a rate ½ convolutional encoder, and a voice activity factor of 0.5 [1]. Each speech connection requires a channelisation code with spreading factor (SF) 128. Assuming that channelisation code resources corresponding to a code with SF 32 are reserved for common channels, a maximum of 124 speech calls can be supported within one channelisation code tree [31]. CS calls are assumed to have a block length of 10 ms (15 slots) and a rate 1/3 Turbo encoder [1]. The simulated bit rates are 64 kbps (CS-64) and 128 kbps (CS-128). The required SF for these bit rates is 32 and 16, respectively, which implies that a maximum of 31 CS-64 UEs or 15 CS-128 UEs can be supported within one channelisation code set. Different mapping tables from block E_b/N_0 to BEP are used depending on the traffic type. The call arrival process is modelled with a Poisson process for all traffic types. The call length is assumed to be negative exponentially distributed with a mean length of 30 seconds.

4.3.6 Performance evaluation

When all the Node-Bs in the network have AAs, it is straightforward to compute the achieved capacity gain by taking a network with sector antennas as a reference. However, in cases with a mixture of cells with conventional sector antennas and AAs, the additional system capacity offered by cells with AAs must be computed by taking the coupling between cells into account, due to the soft capacity mechanisms captured by the utilised power based RRM approach [1]. Hence, when AAs are deployed in a subset of the cells in the network, the surrounding cells with conventional sector antennas may also experience a capacity increase.

For example, if code blocking occurs in the cells with AAs (cells #0, #1 and #2), the interference generated by these cells is lower, which decreases the other cell interference at the surrounding cells (cells #3 to #11) and therefore increases their capacity. Since this extra capacity in the surrounding cells is due to the deployment of AAs in cells #0, #1 and #2, this effect is taken into account when evaluating the capacity gain.

First, a simulation campaign with sector antennas in all cells is conducted, and the average cell capacity C_c is computed only for the grey shaded cells (cells #0 to #11) in Figure 4.1 (on page 69). Cells on the border are not included in these capacity calculations in order to avoid any border effects. Subsequently, a simulation campaign with AAs in cells #0, #1 and #2 is run. Then, the average cell capacity C_{AA} is calculated for the grey shaded cells (cells #0 to #11). The total capacity of the whole set of grey shaded cells equals $S{\cdot}C_c$ for the sector antenna case, where S is the number of cells in the grey shaded area (in this case, $S=12$). For the case with AAs, the total capacity of the whole set of grey shaded cells equals $S{\cdot}C_{AA}$.

The process to calculate the capacity gain is based on the idea that all the capacity gain comes from the deployment of AAs in cells #0, #1 and #2. Thus, for the capacity gain calculations, the total capacity of the whole set of grey shaded cells for the case with AAs ($S{\cdot}C_{AA}$) is artificially distributed as follows: (i) all the cells with conventional sector antennas are assumed to have the same capacity as in the case where all the cells in the network had conventional sector antennas, i.e. the total capacity for the whole set of cells with conventional sector antennas (cells #3 to #11) equals $(S{-}B){\cdot}C_c$, where B is the number of cells with AAs (in this case, $B=3$); (ii) the rest of the total capacity for the whole set of grey shaded cells in the case with AAs $(S{\cdot}C_{AA}{-}(S{-}B){\cdot}C_c)$ is equally distributed among the B cells with AAs. Thus, the equivalent capacity for a cell with AAs (when the total capacity has been redistributed so that the surrounding cells have the same capacity as in the case with conventional sector antennas in the whole network) can be expressed as

$$C'_{AA} = \frac{SC_{AA} - (S-B)C_C}{B} \, , \tag{4.10}$$

Thus, the corresponding equivalent capacity gain per cell with AA can be simply expressed as

$$Gain = \frac{C'_{AA}}{C_C} = \frac{S}{B}\left[\frac{C_{AA}}{C_C} - 1\right] + 1, \tag{4.11}$$

To ensure that the capacity gain is not achieved at the expense of a lower quality of service, the block error rate (BLER) statistics of the calls are collected, and the 95% quantile is used as a quality measure.

As already mentioned, simulation campaigns with and without channelisation code restrictions have been conducted. For each cell, the code blocking rate is defined as

$$Code \; blocking \; rate[\%] = \left(1 - \frac{C_{Restricted}}{C_{Unrestricted}}\right){\cdot}100, \tag{4.12}$$

where $C_{Unrestricted}$ is the cell capacity that is achieved when no channelisation code restrictions are considered, and $C_{Restricted}$ is the cell capacity when the channelisation code restrictions are

considered[10]. This measure is taken on a cell basis. The analysis of the code blocking rate is concentrated on the cells with AAs. Due to the fact that all the cells with AAs operate under the same conditions, the average of the code blocking rates of the these cells is taken as the effective code blocking rate for each simulation set-up. Table 4.2 summarises the default simulation parameters.

4.4 Simulation results

In order to quantify whether the number of cells with AAs in the network has an impact on the equivalent capacity gain, two simulations have been conducted. In one of them, all cells in the network implement AAs. In the other, AAs are only deployed in cells #0, #1 and #2 (see Figure 4.1 on page 69). For both scenarios, the equivalent capacity gain is the same for the case with no channelisation code restrictions.

The reason for this is the fact that the simulations were conducted for fully loaded networks and no channelisation code restrictions. Under these circumstances, let us focus on cells #0, #1 and #2. Since the surrounding cells are fully loaded, the interference coming from them is the same for both cases, as the power based AC algorithms are designed so that the transmitted power is the same for both kinds of cell (with or without AAs) when they reach their maximum load. Thus, the other cell interference in cells #0, #1 and #2 is the same for both analysed cases. As a consequence, the achieved capacity in cells #0, #1 and #2 is the same.

Moreover, the amount of interference that cells #0, #1 and #2 generate towards the rest of the network is the same in both cases, and this interference equals the one that would be generated by cells with sector antennas, due to the particularities of the power based AC algorithms (notice that the discussion assumes fully loaded cells and no channelisation code constraints). As a result, the other cells will have the same capacity as cells #0, #1 and #2 when they deploy AAs. However, if they deploy conventional sector antennas, they will have the same capacity as in the case in which all the network is deploying sector antennas, since in both cases they will experience the same amount of other cell interference.

Taking into account the manner in which the capacity gain is computed (see Section 4.3.6), it is straightforward to conclude that the same capacity gain is computed in both cases. In the case in which cells #3 to #11 are equipped with sector antennas, they have been justified to have the same capacity as in the reference case (the one in which sector antennas are deployed in the whole network). Thus, the artificial redistribution of the capacity in the monitored area described in Section 4.3.6 for the partial deployment case, which leaves cells #3 to #11 with the capacity they had in the reference case and attributes all the extra capacity to the cells with AAs, does not have any effect, since the cells #3 to #11 are already having the same capacity as in the reference case. Therefore, in the end, the capacity gain is effectively computed as the ratio between the average measured capacity for one cell with AAs and the average cell capacity in the reference case. Since the average capacity of cells with AAs is the same for both analysed cases, the computed capacity gain is concluded to be the same for both of them.

---

[10] Note that the difference between the two simulations providing input to (4.12) must be only the fact that one is assuming infinite channelisation codes, while the other is taking the channelisation code restrictions into account. Thus, when evaluating the code blocking rate of a scenario with several scrambling code regions per cell with AAs, the simulation with no code restrictions must be also run with several scrambling code regions per cell with AAs, although an infinite number of channelisation codes per scrambling code region is assumed.

Table 4.2: Default parameters for the simulation campaign.

Parameter	Default value
Site-to-site distance	2 km
Std for shadow fading	8 dB
Correlation distance for shadow fading	50 m
Thermal noise power	-97.9 dBm
PDP	Pedestrian A and Vehicular A
Azimuth dispersion	Laplacian distribution. AS = 5°
Step size for CLPC	1 dB
Step size for OLPC	0.3 dB
Max. active set size / Candidate set size	3/8
Wadd / Wdrop for SHO	1/3 dB
Wbeam	1 dB
Tdrop for SHO	200 ms
Update rate for beam selection	100 Hz
P_{PCPICH}	1 W
P_{TARGET}	10 W
Cells with AAs	Cells number 0, 1, and 2
Amplitude radiation pattern of the antenna element (see Chapter 2, page 22)	$f(\phi) = \begin{cases} \sqrt{\beta}\cos^{1.4}(\phi) & for \quad \phi \in [-90°, 90°] \\ \sqrt{\beta/R} & otherwise \end{cases}$
Broadside power gain of the antenna element	β = 18 dBi
Front-to-back ratio of the antenna element	R = 33.8 dB
AA configuration	M = 4 antennas; N = 6 beams M = 6 antennas; N = 8 beams M = 8 antennas; N = 10 beams
Speech	Bit rate = 8 kbps Convolutional coding. Rate = ½ Spreading factor = 128 Interleaving period = 20 ms Discontinuous transmission. Activity factor = 0.5 BLER target = 1%
CS-64	Bit rate = 64 kbps Turbo coding. Rate = 1/3 Spreading factor = 32 Interleaving period = 10 ms BLER target = 10%
CS-128	Bit rate = 128 kbps Turbo coding. Rate = 1/3 Spreading factor = 16 Interleaving period = 10 ms BLER target = 10%
Call arrival process	Poisson distributed
Call duration	Negative exponentially distributed. Average call length = 30 seconds.
UE's speed kmph	3 kmph
Simulation length	300 s

```
                    ┌─────────────────┐
                    │   Initialise    │
                    └─────────────────┘
                             │
                             ▼
  ┌──────────────────────────────────────┐◄──────────────────┐
  │       Update propagation models      │                    │
  └──────────────────────────────────────┘                    │
                             │                                 │
                             ▼                                 │
            ┌──────────────────────────────┐                  │
            │   Interference calculations  │                  │
            └──────────────────────────────┘                  │
                             │                                 │
                             ▼                                 │
            ┌──────────────────────────────┐                  │
            │   Closed loop power control  │                  │
            └──────────────────────────────┘                  │
                             │                                 │
  NO                         ▼                                 │
            ┌──────────────────────────────┐                  │
            │           Move UEs           │                  │
            └──────────────────────────────┘                  │
                             │                                 │
                             ▼                                 │
            ┌──────────────────────────────┐                  │
            │   Dump slot-based statistics │                  │
            └──────────────────────────────┘                  │
                             │                                 │
                             ▼                                 │
                         ╱ End of ╲                            │
                        ╱  block?  ╲                           │ NO
                        ╲          ╱                           │
                         ╲        ╱                            │
                          YES                                  │
                             ▼                                 │
            ┌──────────────────────────────┐                  │
            │          AVI look-up         │                  │
            └──────────────────────────────┘                  │
                             │                                 │
                             ▼                                 │
            ┌──────────────────────────────┐                  │
            │   Generate UEs / Finish calls│                  │
            └──────────────────────────────┘                  │
                             │                                 │
                             ▼                                 │
            ┌──────────────────────────────┐                  │
            │    AC, SHO, beam switching   │                  │
            └──────────────────────────────┘                  │
                             │                                 │
                             ▼                                 │
            ┌──────────────────────────────┐                  │
            │    Dump general statistics   │                  │
            └──────────────────────────────┘                  │
                             │                                 │
                             ▼                                 │
                          ╱ End? ╲──────────────────────────────┘
                          ╲      ╱
                           YES
                             ▼
            ┌──────────────────────────────┐
            │          Finalise            │
            └──────────────────────────────┘
```
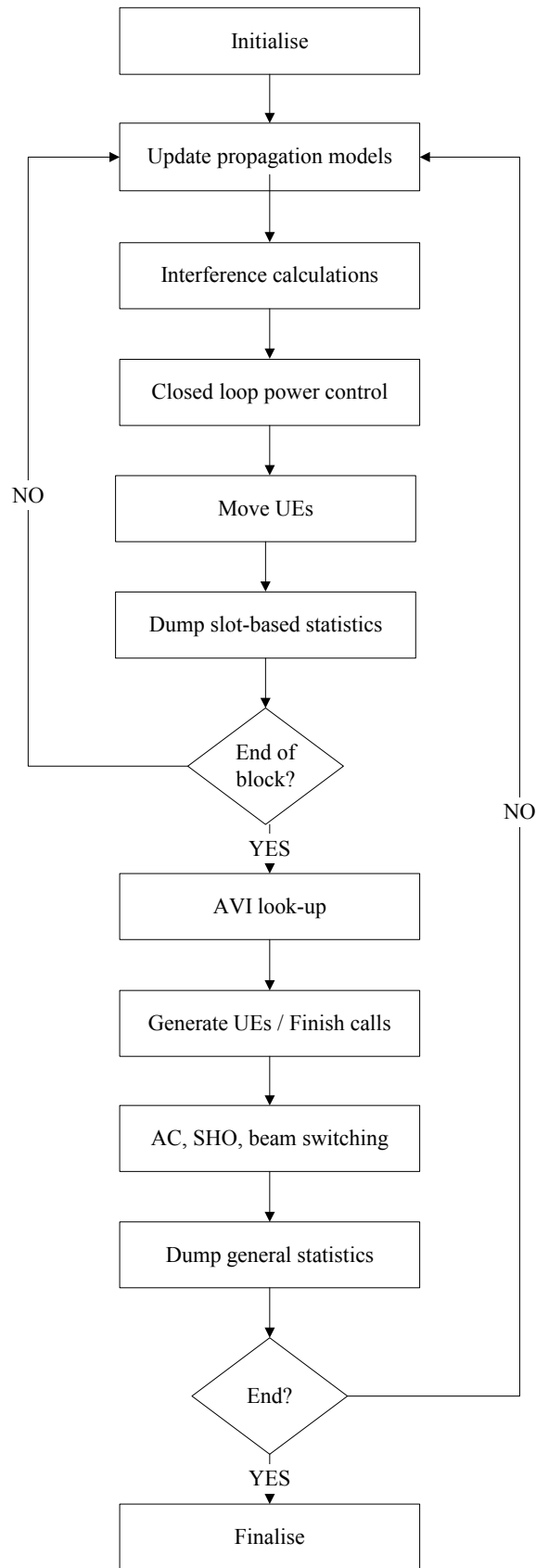
Figure 4.3: Simplified flow chart of the simulation tool.

When code blocking occurs, the situation is different, and here it is more interesting to analyse the case with partial deployment of AAs, since it illustrates the interesting soft capacity mechanisms that motivated the definition of the process to calculate the capacity gain reported in Section 4.3.6. Typically, code blocking is more likely to occur in cells with AAs and, as a consequence, these cells will generate less other cell interference towards the surrounding cells than in the reference case. As a result, the surrounding cells will have a better interference situation and, therefore, higher capacity will be reported for them. The fact that this extra capacity is due to the deployment of AAs in cells #0, #1 and #2 motivates the artificial capacity redistribution process described for the capacity gain calculation, which assumes that cells #3 to #11 have the same capacity as in the reference case and attributes all the extra capacity in the system to cells #0, #1 and #2.

For the sake of simplicity (shorter simulation time), only simulation results with AAs in cells number #0, #1 and #2 will therefore be presented in the following. Furthermore, it is important to stress that the obtained results are influenced by the underlying assumptions, which include the utilised AVI tables. The use of different AVI tables would have implied different power requirements per UE, which would have changed the absolute capacity figures and, therefore, the directionality of the interference and the reported channelisation code rates. However, the main trends, phenomena and conclusions are expected to remain the same if different AVI tables are used, although the specific reported figures are likely to differ from the ones presented here.

4.4.1 Optimal number of beams

Figure 4.4 shows the capacity gain versus the number of synthesized beams (N) for a four element AA, assuming a Vehicular A PDP, CS-64 traffic and AS=5°. Results with unlimited channelisation code resources and two scrambling code regions are presented. As can be seen, the configuration that maximizes the cell capacity corresponds to six beams. For a lower number of beams, the larger cross over depth between the beams results in a lower effective antenna gain. On the other hand, increasing the number of beams beyond six causes a larger pilot power overhead due to the S-CPICH per beam. The curves shown in Figure 4.4 illustrate the described trade-off between the two aforementioned mechanisms. Based on similar simulation results for different numbers of antenna elements ($M=6$ and $M=8$), it has been found that the optimum number of beams can be expressed as $N=M+2$. It is of paramount importance to stress that these results have been obtained assuming that the radio channels AS (5°) is smaller than the beamwidth for $M \in [4–8]$. For larger AS the optimum number of beams would become lower, due to a larger overlap between beams. Moreover, only even numbers of beams have been tested, since in this manner it is straightforward to divide the cell into two equally balanced scrambling code regions. In the sequel, all the simulations are run assuming the presented relationship between N and M.

4.4.2 Capacity gain versus the number of antenna elements

Figure 4.5 shows the capacity gain as a function of the number of antenna elements under different channelisation code constraints for Vehicular A and CS-64. In one of the presented cases, unlimited channelisation code resources per cell are assumed. The second case takes into account the channelisation code restrictions and assumes one scrambling code per cell with AAs. In the third case, two scrambling codes per cell with AAs are assumed, i.e. the cell is split into two code regions as shown in Figure 2.6 (on page 27), and channelisation code restrictions are considered.
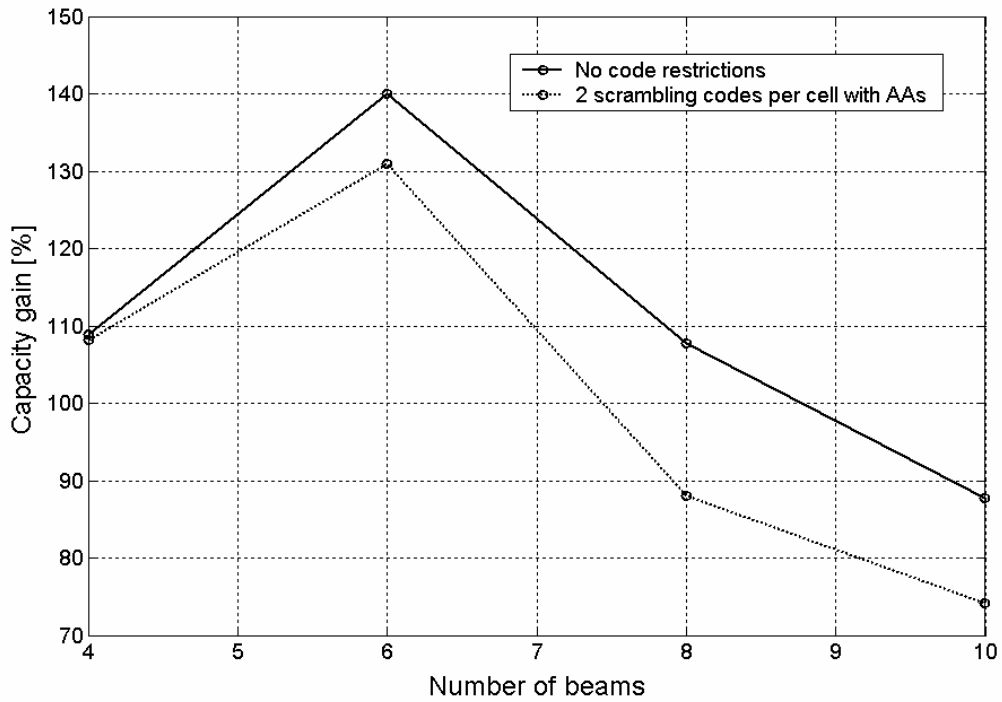
Figure 4.4: Capacity gain versus number of synthesized beams for ITU Vehicular A, CS-64, AS = 5º and *M* = 4.
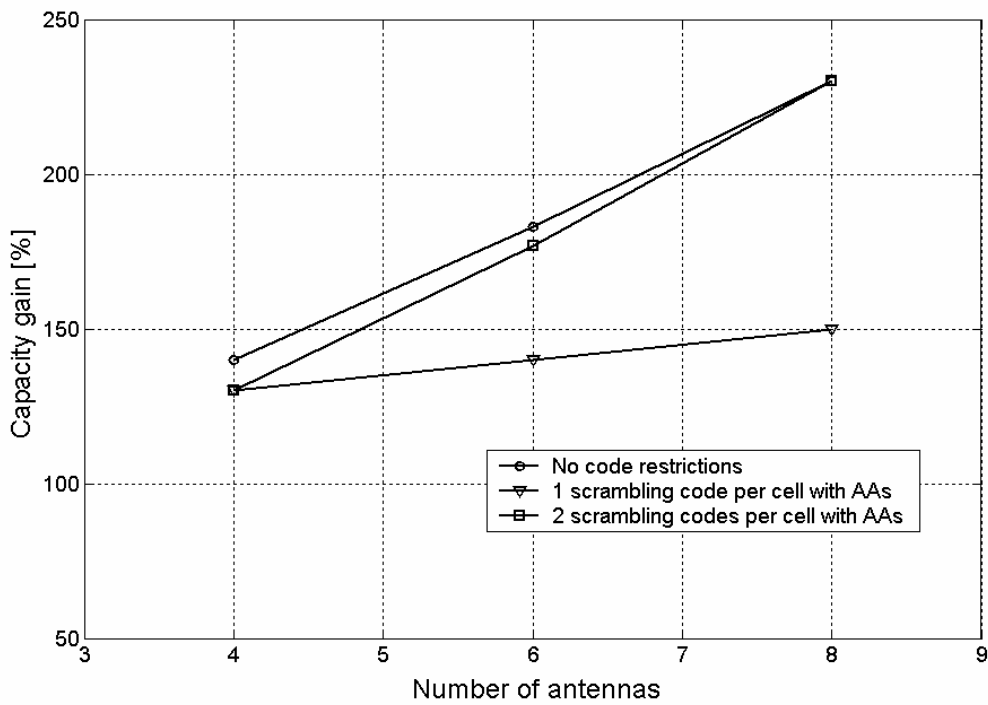

Figure 4.5: Capacity gain versus the number of antenna elements for ITU Vehicular A, CS-64 and AS = 5º.

It is observed that the capacity gain without channelisation code restrictions grows with the number of antenna elements, due to the narrower beams for increasing number of antenna elements. When only one scrambling code per cell is enabled, code blocking is experienced, which reduces the capacity gain. The code blocking is more dominant for a large number of antenna elements. However, when code blocking is experienced in cells with AAs, the amount of transmitted power in these cells remains below the target, which decreases the other cell interference in the surrounding cells. As a consequence of this, more capacity is allowed in the surrounding cells and the reported capacity gain still grows slightly with the number of antenna elements. In the case of four antenna elements, the code blocking rate reported in Table 4.3 for Vehicular A is relatively low (17%), so the aforementioned soft capacity mechanism allows the surrounding cells to compensate for the lost capacity in the cells with AAs. In fact, the capacity gain reduction compared with the case with no code restrictions is only 4%. However, for higher code blocking rates (e.g. for Pedestrian A, which has a code blocking rate of 30% with four antenna elements in the AA), the soft capacity mechanism is unable to compensate for the proportion of the blocked traffic due to channelisation code shortage. In this case, the capacity gain reduction compared with the case with no code restrictions is 21%. When two scrambling codes per cell with AAs are enabled, code blocking is no longer experienced. The lack of orthogonality between signals transmitted under two different scrambling codes results in a capacity gain degradation of 4% for Vehicular A and 8% for Pedestrian A as reported in Table 4.3. This penalty is larger for Pedestrian A because the relative orthogonality was already partly destroyed by radio channels with large time dispersion, such as Vehicular A. However, the observed penalty is much lower than the one that is experienced when two scrambling codes are introduced in an uncoordinated manner [90].

Table 4.3: The propagation environment's influence on the system performance for M=4 antennas, N=6 beams, AS = 5º and CS-64.

PDP	Code allocation	Capacity gain [%]	Capacity gain reduction compared with the case with no restrictions [%][11]	Code blocking rate [%]
Vehicular A	No code restrictions	140	0	0
	1 scrambling code per cell	130	4	17
	2 scrambling code per cells	130	4	0
Pedestrian A	No code restrictions	140	0	0
	1 scrambling code per cell	90	21	30
	2 scrambling code per cells	120	8	0

[11] Note that the capacity gain reduction is calculated expressing the capacity gain figures as linear multiplicative factors. Thus, going from a gain value of 140% (2.4) to 130% (2.3) involves a loss of (1-2.3/2.4)·100≈4%.

4.4.3 Code blocking as a function of the power delay profile

Assuming no code restrictions, the capacity gain equals 140% for both Vehicular A and Pedestrian A for *M*=4 antennas. The capacity gain reported in [13] equals 180% for the same number of antenna elements and environment. However, the results presented in [13] do not include the effect of code restrictions and the pilot overhead from having an S-CPICH per beam. With only one scrambling code per cell, the system becomes hard limited. In this situation, the code blocking rate for Vehicular A equals 17%, while it equals 30% for Pedestrian A. Despite the larger frequency diversity given by Vehicular A, the lower time dispersion in Pedestrian A provides more orthogonality between signals under the same scrambling code and hence allows for a higher absolute capacity per cell. With conventional sector antennas, the cell capacity with Pedestrian A is 19% larger than with Vehicular A. Since similar spatial filtering gains are experienced with both PDPs, the code blocking rate with Pedestrian A is therefore larger.

4.4.4 Code blocking as a function of the SHO settings

Table 4.4 shows the impact of the SHO settings on the code blocking rate for Pedestrian A and *M*=4 antennas. The SHO settings implicitly control the SHO overhead (SHOO) in the network and therefore also the average channelisation code consumption per UE.

$$SHOO \ [\%] = \left(\sum_{z=1}^{Z} np_z - 1 \right) \cdot 100 \ , \tag{4.13}$$

where Z is the maximum active set size for SHO and p_z is the probability of having a UE with z legs in the active set. Thus, when SHOO=30%, it means that each UE is consuming on average 1.3 channelisation codes in the network.

Table 4.4: The SHO settings' influence for Pedestrian A, *M*=4 antennas, *N*=6 beams, AS=5º and CS-64.

{*Wadd, Wdrop*} [dB]	Code allocation	Capacity gain [%]	Capacity gain reduction compared with the case with no restrictions [%][11]	Code blocking rate [%]
{1, 3} SHOO = 24%	No code restrictions	140	0	0
	1 scrambling code per cell	90	21	30
{3, 5} SHOO = 44%	No code restrictions	140	0	0
	1 scrambling code per cell	70	29	40

The settings {*Wadd, Wdrop*}={1,3} dB lead to a SHOO of 24%, while the settings {*Wadd, Wdrop*}={3,5} dB result in a SHOO of 44%. Increasing the SHOO from 24% to 44% results in an increase of the code blocking rate from 30% to 40%, conditioned on one scrambling code per cell and CS-64 traffic. Particularising the given expression of the code blocking rate to the case where {*Wadd, Wdrop*}={1,3} dB, the following can be written

$$Code\ blocking\ rate[\%]_{SHOO=24\%} = \left(1 - \frac{C_{Restricted}|_{SHOO=24\%}}{C_{Unrestricted}|_{SHOO=24\%}}\right) \cdot 100 = 30\% \qquad (4.14)$$

Thus,

$$\frac{C_{Restricted}|_{SHOO=24\%}}{C_{Unrestricted}|_{SHOO=24\%}} = 0.7 \qquad (4.15)$$

When setting {*Wadd, Wdrop*}={3,5} dB, the SHOO increases, which decreases the capacity that can be achieved under channelisation code restrictions, since the average code consumption per UE increases with the SHOO. As a very simple approximation, the following expression can be written

$$C_{Restricted}|_{SHOO=44\%} = \frac{1.24}{1.44} C_{Restricted}|_{SHOO=24\%} , \qquad (4.16)$$

assuming that the only thing that varies between the two SHO scenarios is the SHOO. Moreover, provided that the capacity of the system without channelisation code constraints is marginally affected when changing from one SHO configuration to the other, i.e. assuming that

$$C_{Unrestricted}|_{SHOO=44\%} = C_{Unrestricted}|_{SHOO=24\%} , \qquad (4.17)$$

it can be written than

$$Code\ blocking\ rate[\%]_{SHOO=44\%} =$$
$$\left(1 - \frac{1.24}{1.44} \frac{C_{Restricted}|_{SHOO=24\%}}{C_{Unrestricted}|_{SHOO=24\%}}\right) \cdot 100 = 40\%, \qquad (4.18)$$

which matches the simulation results perfectly. For both SHO settings, the code blocking problem is completely mitigated by splitting the cell into two scrambling code regions.

4.4.5 Capacity gain for different traffic types

The system performance for different types of traffic is presented in Table 4.5 for four antenna elements and Vehicular A. For CS-128, the capacity gain (expressed as a linear multiplicative factor) is decreased by 8% compared with CS-64. The UEs with CS-128 require higher transmitted power, which decreases the number of admitted UEs per cell, and consequently tends to yield a more directional spatial interference distribution. Recall that the maximum spatial interference suppression is obtained for the case with spatial white

interference[12]. This effect is automatically captured by the directional power based AC algorithm. On the other hand, no significant improvement in the capacity gain is observed for speech services compared with CS-64 (for a scenario without channelisation code restrictions), since the spatial interference distribution for these two services are comparable. One reason why both cases are comparable is that, despite the lower bit rate of the speech services, convolutional coding is used for speech services and higher E_b/N_0 values are required. For one scrambling code per cell, the code blocking rate for speech services equals 44%, while it only equals 17% for CS-64. The main reason for this deviation is the voice activity factor of 0.5 for speech services, while CS-64 is assumed to be transmitted with an activity factor of unity. Note that the reduced activity factor for speech services only decreases the average interference contribution from each UE, while the required channelisation code resources are assumed independent of the activity factor.

Table 4.5: The traffic types' influence on the system performance for Vehicular A, AS=5º, *M*=4 antennas, and *N*=6 beams.

Traffic type	Code allocation	Capacity gain [%]	Capacity gain reduction compared with the case with no restrictions [%][11]	Code blocking [%]
CS-64	No code restrictions	140	0	0
	1 scrambling code per cell	130	4	17
CS-128	No code restrictions	120	0	0
	1 scrambling code per cell	120	Negligible	9
Speech	No code restrictions	150	0	0
	1 scrambling code per cell	50	40	44

4.5 Code blocking and packet traffic

A simple first order extrapolation of the CS simulation results is presented in the following in order to illustrate how the code blocking rate is expected to evolve in a network

---

[12] This statement is considered to be valid under the following assumptions: (i) sufficiently large number of UEs, (ii) UEs uniformly distributed in the azimuth domain, (iii) same kind of traffic for all the UEs, (iv) same E_b/N_0 requirements for all the UEs, and (v) same shape for the radiation patterns of the beams pointed at the different azimuth directions.

with a mixture of CS and non-real time (NRT) packet traffic. In this analysis it is implicitly assumed that NRT traffic is carried by dedicated channels, and not by time shared packet channels such as the DL shared channel (DSCH) available in UMTS. The maximum number of CS UEs that can be admitted in a cell with no code restrictions is denoted by C_{CS}. The maximum number of UEs under a single scrambling code is denoted by C_{MAX}. Thus, the expression for the code blocking rate (expressed as a real number between zero and one for convenience) can be written as

$$B_{CODE} = \frac{C_{CS} - C_{MAX}}{C_{CS}} \quad for \quad C_{CS} > C_{MAX} \, , \tag{4.19}$$

when a certain proportion (f) of the resources is reserved for NRT traffic, the maximum number of UEs per cell under no channelisation code restrictions is denoted by C_{MIXED}. Notice that in general $C_{MIXED} > C_{CS}$, assuming that CS and NRT UEs operate at the same peak bit rate, with a significantly lower activity factor for NRT UEs (i.e., NRT traffic is assumed to be bursty). However, despite the burstiness of NRT UEs, they are still assumed to constantly occupy a channelisation code. Under these assumptions, the code blocking rate for mixed CS and NRT traffic can be written as

$$B_{MIXED} = \frac{C_{MIXED} - C_{MAX}}{C_{MIXED}} = 1 - (1 - B_{CODE})\frac{C_{CS}}{C_{MIXED}} \, , \tag{4.20}$$

Moreover, C_{MIXED} can be written as a function of C_{CS} under the following first order approximation; the average interference load contributed by a CS UE is the same as that of a NRT UEs, scaled with the NRT activity factor. Thus, when a certain proportion of the resources is reserved for NRT traffic, the equivalent number of UEs that ideally[13] can be admitted yields

$$C_{MIXED} = C_{CS}(1 - f) + C_{CS} f \frac{1}{\upsilon} \, , \tag{4.21}$$

where $\upsilon \in [0;1]$ is the NRT activity factor. Combining (4.19), (4.20) and (4.21) the code blocking rate for a mixed CS and NRT scenario can be expressed as

$$B_{MIXED} = 1 - (1 - B_{CODE})\frac{1}{1 + f\left(\frac{1}{\upsilon} - 1\right)} \, , \tag{4.22}$$

For four antenna elements, CS-64 traffic, Vehicular A, and {*Wadd, Wdrop*}={1,3} dB, the experienced code blocking rate is 17% (B_{CODE}=0.17) according to Table 4.3. Figure 4.6 shows the code blocking rate as a function of v for different values of f. It is observed that the code blocking rate increases with f and 1/v so more channelisation code sets are required for cells with a significant fraction of bursty NRT traffic. However, it should be emphasized that the results presented in Figure 4.6 are derived under simplified assumptions, so the curves only serve to show a general trend. The packet scheduler implementation and its ability to efficiently exploit the available transmit power and code resources will strongly influence the presented results.

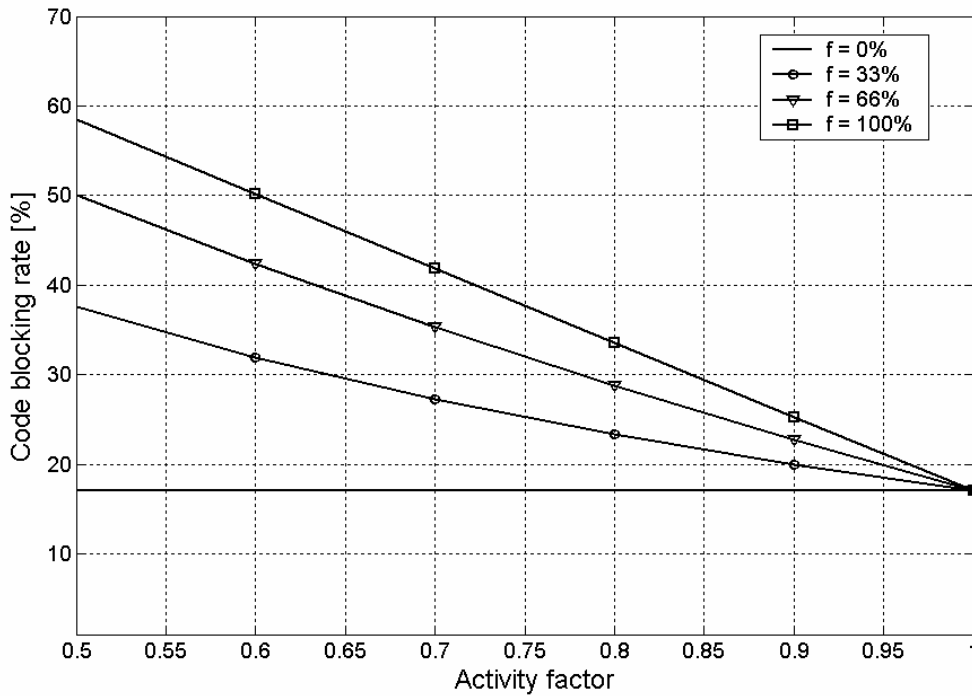[13] If channelisation code restrictions were not considered.

Figure 4.6: Code blocking rate versus the NRT activity factor for M = 4, CS-64, ITU Vehicular A, AS = 5º and {Wadd, Wdrop} = {1, 3} dB.

4.6 Concluding remarks

From dynamic simulation results with one scrambling code per cell, it is concluded that the capacity gain from AAs with CBF can make the system become channelisation code limited rather than interference limited. Notice that the results presented in this chapter have been obtained with a simulation tool that ignores the layer 3 signalling procedures and delays associated to all the beam switching and handover operations. Since the simulations have been conducted at low speeds (3 kmph), this is not considered to affect the presented system performance figures. However, at larger UE speeds this is expected to have an impact on the results. Therefore, the full modelling of the aforementioned layer 3 mechanisms is proposed for further study, in order to quantify the impact of the introduced delays on the system performance.

The utilised directional power based AC algorithm has been found to be able to automatically adapt the captured capacity gain to the spatial distribution of the interference. For example, when the bit rate of the CS connections is increased, the UEs require more transmit power at the Node-B, which decreases the number of UEs and makes the spatial distribution of the interference more directional. Under this scenario, less capacity gain from AAs is automatically experienced.

With no channelisation code restrictions, the capacity gain for CS connections at 64 kbps is 140% with four-element AAs and Vehicular A. With channelisation code restrictions, a code blocking rate of 17% is experienced when only one scrambling code is allocated per

cell. For Pedestrian A the same scenario yields a code blocking rate of 30%, because Pedestrian A allows better orthogonality among UEs under the same scrambling code and thus increases the absolute cell capacity. When the SHOO increases, the average channelisation code usage per UE grows, which results in larger code blocking rate.

A larger number of antenna elements at the AA increases the spatial filtering gain and, therefore, makes the channelisation code blocking problem more severe. In addition, when the connections have a low activity factor, the code blocking rate grows, since the average transmit power per UE is decreased, which increases the number of UEs that could be admitted in the system if there were no channelisation code restrictions. This effect has been experienced for speech traffic with DTX, which yields a code blocking rate of 44% for Vehicular A and four-element AAs.

In order to overcome this problem, a solution within the UMTS specifications is analysed, where the cell is split into spatially isolated scrambling code regions. With four-element AAs, there is a marginal penalty of 4-8% associated with this solution due to the lack of orthogonality between signals under different scrambling codes. Assuming an AA configuration with eight antenna elements, the capacity gain with real channelisation code limitations for Vehicular A and CS connections at 64 kbps equals 150% and 230% for one and two scrambling codes per cell, respectively. Therefore, the analysed solution turns out to be an effective method to overcome channelisation code limitations.

It is important to note here that the presented performance figures are strongly influenced by the utilised AVI tables. If different AVI tables (corresponding to different UE performance characteristics) were used, the reported figures would change. However, the presented trends and phenomena are expected to remain the same from a qualitative point of view. A similar comment applies to the partial use of the spatial channel model, which is described with more detail in Section 4.3.3. Even though the author does not expect it to have a significant effect on the conclusions and trends that have been identified, it is recommended for further study to conduct investigations in which the space-time model of the radio channel is fully integrated in the simulation set-up.

Based on simple first order approximations, the CS results are extrapolated to scenarios with a mixture of CS and NRT traffic in the network. The code blocking rate is shown to increase with the proportion of bursty NRT traffic in the network, which calls for more channelisation code resources. This is especially true for NRT traffic characterized by low activity factors, i.e. short bursty transmissions followed by relatively long periods of silence. It is therefore of paramount importance that cells with AAs support allocation of multiple scrambling codes in the beam domain in order to preserve the advantage of the spatial filtering gain offered by CBF. For a cell with a four-element AA, 2-3 scrambling codes should be enabled to minimize the code blocking rate to an acceptable level.

Nonetheless, the system performance with NRT traffic needs further attention, since the employed traffic models and the selected scheduling algorithms for cells with AAs are expected to impact the performance figures significantly. Therefore, the detailed simulation of such environment is proposed for further study in order to obtain more realistic and results for each specific situation.

Chapter 5

Downlink capacity gain with dual

antenna Rake receivers at the UE

5.1 Introduction

Implementation of advanced radio concepts at the user equipment (UE) is one of the potential techniques that can significantly increase the downlink (DL) capacity of terrestrial cellular systems. Previous link level studies have shown that large gains can be obtained by using antenna arrays (AAs) for DL signal reception. In interference limited GSM (Global System for Mobile communications) systems, the use of dual antenna receivers with interference rejection combining has been shown to suppress the multiple access interference by 5-10 dB, depending on the ratio between the dominant source of interference and the rest [99]. For the Universal Mobile Telecommunications System (UMTS), the link level improvement from the deployment of dual antenna Rake receivers with maximal ratio combining (MRC) (in the sequel referred to as 2Rake receivers) has been reported to range between 3 and 4.5 dB for a block error rate (BLER) target of 10%, depending on the frequency selectivity of the radio channel [63]. More advanced dual antenna receivers with linear minimum mean-square error chip level equalisers are described in [64], and their link level improvement over 2Rake in Vehicular A is reported to be up to 9 dB for UEs very close

to the serving Node-B [63]. However, their performance is more modest when the UE is far for the serving Node-B and other cell interference is not negligible.

However, little attention has been paid to the network level considerations related to the deployment of dual antenna receivers at the UE. Thus, the main objective here is to evaluate the DL cell capacity gain that can be achieved when 2Rake receivers are used at the UE under different environments and radio resource management (RRM) configurations. This study is focussed on DL power controlled dedicated channels (DCHs) with constant bit rate. The investigations are conducted in homogeneous networks and all the UEs have the same bit rate. Thus, the capacity gain can be defined on a cell basis, representing the increase of the number of UEs that can be served due to the use of 2Rake receivers at the UE.

Most of the results shown in this chapter are obtained by means of dynamic system level simulations. In addition, a theoretical study of the impact of the penetration rate of dual antenna Rake receivers on the achievable capacity gain is also conducted, and the outcome matches the simulation results. In this context, the penetration rate ($f \in [0; 1]$) is defined as the proportion of UEs implementing 2Rake receivers.

The chapter is organised as follows. The theoretical study of the capacity gain that is obtained when UEs with 2Rake receivers are deployed with a certain penetration rate is presented in Section 5.2. Section 5.3 describes the system model that is used for the simulations. Section 5.4 shows and discusses the simulations results. In the end, concluding remarks are given in Section 5.5.

5.2 Theoretical assessment of the capacity gain

This section presents a simple theoretical study in order to assess the capacity gain that is obtained when UEs with 2Rake receivers are deployed with a certain penetration rate. The following assumptions are assumed to be valid:

- All UEs have the same bit rate, and therefore the same processing gain (G).

- For the single antenna Rake receivers, the required energy-per-bit-to-noise ratio (E_b/N_0) at the input of the receiver equals ρ.

- The radio channels between all the UEs and their serving Node-Bs have the same time dispersion and, thus, the same orthogonality factor [53].

- There is a fraction $f \in [0; 1]$ of UEs implementing 2Rake receivers. Hence, f=1 means that all the UEs implement 2Rake receivers, while f=0 corresponds to the case where all the UEs have a single antenna Rake receiver. For this simple theoretical study, fraction and probability will be used interchangeably. Thus, if the fraction of UEs with 2Rake receivers is 0.3, the probability that a certain UE has a 2Rake is also 0.3.

- Perfect power control is assumed, which means that the transmit power towards each UE is adjusted so its E_b/N_0 requirement at the input of the receiver is exactly fulfilled.

- Soft handover (SHO) is not considered.

- All Node-Bs operate at full load, i.e. their average transmit power equals P_{Target}.

- UEs with 2Rake receivers require a lower E_b/N_0 at the input of the receiver. The reduction factor in the required E_b/N_0 is denoted by D. Thus, the required E_b/N_0 at the input of 2Rake receivers can be written as $\rho_{2Rake} = \rho/D$, with $D>1$.

- One scrambling code per cell is used. Thus, signals transmitted within the same cell are orthogonal, unless the time dispersion of the radio channel degrades the orthogonality.

Let us consider UE #i, which is equipped with a single antenna Rake receiver. Its E_b/N_0 can be approximated as

$$\rho = \frac{GP_i g_i}{P_N + P_{Target} g_i (1-\alpha) + P_{Other,i}},$$
(5.1)

where P_i is the signal power transmitted towards UE #i from its serving Node-B, P_N is the received thermal noise at the UE, and α is the orthogonality factor[14] [53]. The path gain between the serving Node-B and UE #i, including the corresponding antenna gain, is denoted by g_i, and $P_{Other,i}$ represents the wideband other cell interference received by UE #i. Rearranging (5.1),

$$P_i = \frac{\rho}{G} \left(\frac{P_N + P_{Other,i}}{g_i} + P_{Target}(1-\alpha) \right)$$
(5.2)

Let us now write an expression for the signal transmitted towards UE #i from its serving Node-B in the case where UE #i is equipped with a 2Rake receiver (P_i^{2Rake}). When writing this expression, it has been also assumed that the Node-Bs operate at full load. This means that, if some UEs deploy 2Rake receivers, a sufficient number of UEs is admitted in the system in order to have it fully loaded. Under these conditions, the values for P_{Target} and $P_{Other,i}$ remain as in (5.1). By combining (5.2) and the given definition about ρ_{2Rake}, it is possible to write

$$P_i^{2Rake} = \frac{P_i}{D},$$
(5.3)

where D is the already introduced factor that models the link level E_b/N_0 gain due to the 2Rake receiver. Since $D>1$, it is straightforward to conclude that $P_i > P_i^{2Rake}$. Thus, when UE #i has a single antenna Rake receiver and this receiver is replaced by a 2Rake receiver, the total transmit power from the Node-B is decreased, i.e. a certain amount of power ($P_i - P_i^{2Rake}$) is released, which is used for transmission towards new UEs in order to have the Node-Bs operating at full load. The possibility to admit these new UEs contributes to increase the system capacity. Taking into account the probability of having a 2Rake receiver implemented at a certain UE, the average amount of power that is released by UE #i due to the potential deployment of a 2Rake receiver (ΔP_i) can be expressed as

---

[14] When $\alpha=1$, it means that the orthogonality between signals transmitted under the same scrambling code is kept, while $0 \leq \alpha <1$ corresponds to the case where the orthogonality is partly or fully destroyed.

$$\Delta P_i = f\left(P_i - P_i^{2Rake}\right) \tag{5.4}$$

It has been assumed that, when UE #*i* deploys a 2Rake receiver, it releases a certain amount of transmit power at the Node-B, which can be used for serving new UEs. If UE #*i* has a 2Rake receiver, it is assumed that the extra UEs that can be served with the power released by UE #*i* are exposed to the same path loss and interference conditions as UE #*i*. Therefore, assuming that these new UEs also have a probability *f* of deploying a 2Rake receiver, the following expression can be written for the average power required by each one of these UEs

$$P_{ExtraUE,i} = fP_i^{2Rake} + (1-f)P_i \tag{5.5}$$

Therefore, it can be concluded that, on average, a given UE #*i* releases transmit power resources at the Node-B in order to serve the following number of UEs

$$N_{Extra,i} = \frac{\Delta P_i}{P_{ExtraUE,i}} = \frac{f(D-1)}{f + (1-f)D} = K \tag{5.6}$$

Thus, each UE allows on average the admission of *K* extra UEs in the same propagation conditions. Notice that *K* is independent of the actual path loss and interference of each specific UE, which allows a general expression of the capacity gain as a function of the penetration rate of dual antenna UEs

$$Capacity\ Gain\ [\%] = \frac{f(D-1)}{f + (1-f)D} \cdot 100 \tag{5.7}$$

Figure 5.1 shows the dependency between the capacity gain and *f* for different values of *D*. The selected values for *D* are 2 and 2.82, corresponding to the 3 dB and 4.5 dB link level gains mentioned in the introduction [63]. As it can be seen, the capacity gain does not grow linearly with the penetration rate. This non-linear behaviour becomes more patent for large values of *D*. For *f*=1, the capacity gain equals 100·(*D*-1). This means that for *D*=2, the reported gain at *f*=1 is 100%, i.e. the capacity is doubled.

5.3 System model

For this study, an upgraded version of the simulation tool employed in Chapter 4 was utilised in order to assess the capacity gain from UEs with 2Rake receivers. In this case, the author's contribution to the tool development comprised design and implementation of the support for Rake receivers with multiple antennas at the UE side.

5.3.1 Basic simulation methodology

An 18-cell network with three-sector sites like the one depicted in Figure 5.2 is simulated. In order to avoid the border effects, results are only taken from cells #6, #7, #8 and #14 (referred to as the set of monitored cells in the sequel). Output statistics of the rest of the cells are disregarded. The basic simulation methodology follows that of [92].
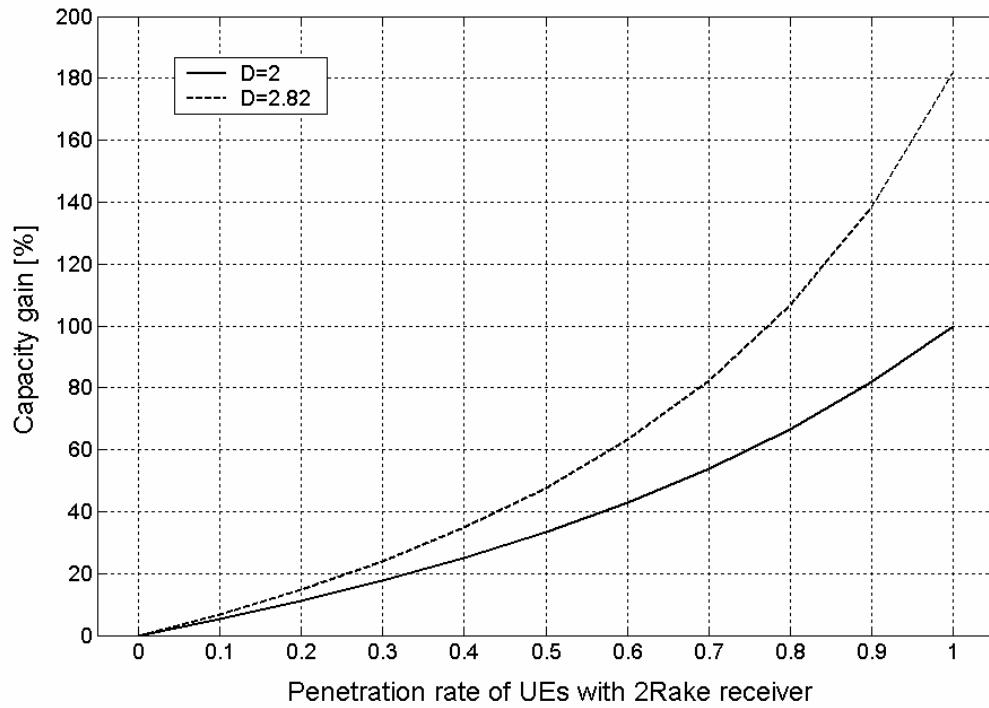
Figure 5.1: Theoretical capacity gain as a function of the penetration rate.
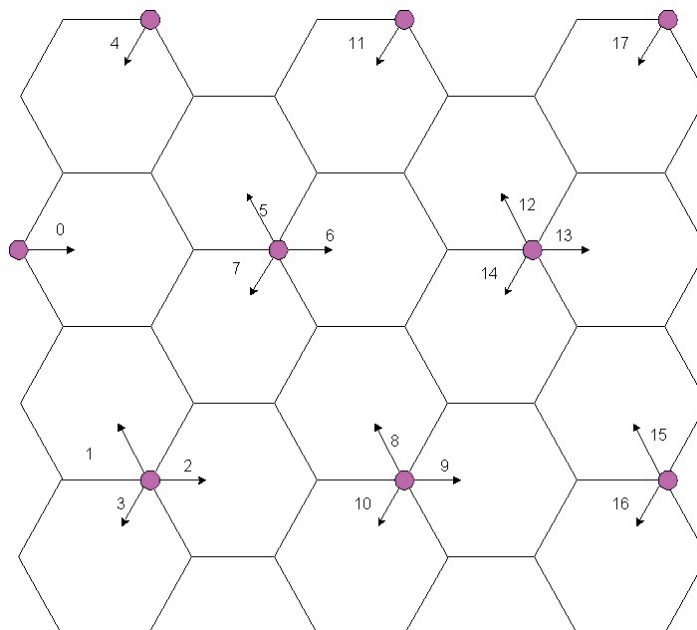

Figure 5.2: 18-cell network layout.

Each cell is covered by a sector antenna like the one described in Section 2.2.1.3, and only one scrambling code per cell is used. Walsh codes are used as channelisation codes, which are fully orthogonal if they are fully time synchronised and transmitted under the same scrambling code.

The deterministic path loss between each Node-B and each UE is calculated according to the single-slope model with an exponent of −3.5. Shadow fading is assumed to be lognormal distributed with an exponentially decaying spatial auto-correlation function in coherence with Gudmundsons model [94]. Multipath fading is modelled, where the power values of the individual paths are assumed to be independent Chi-square distributed. The considered multipath power delay profiles (PDPs) are Pedestrian A and Vehicular A [42].

For 2Rake receivers, two independent radio propagation channels are simulated between each Node-B and each dual antenna UE. Both radio channels have the same deterministic path loss and shadow fading. The average PDP is assumed equal and perfectly time aligned for both antennas, and the fast fading process affecting each propagation path is assumed to be independent from one antenna to the other (see Figure 5.3).
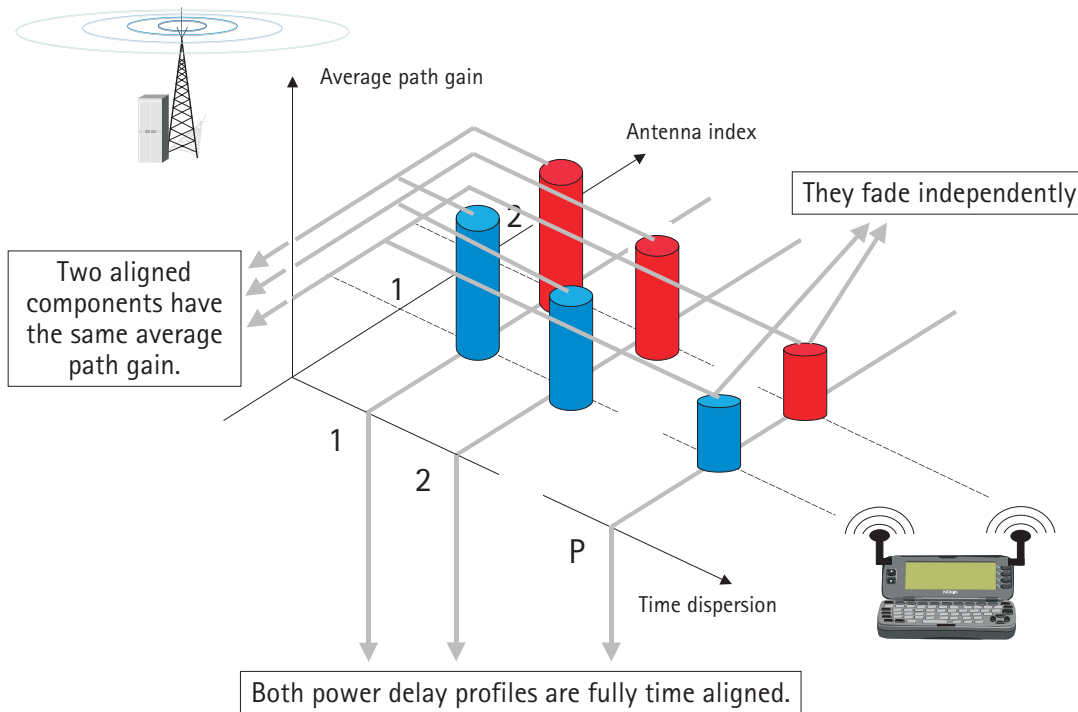
Figure 5.3: Two-dimensional multipath propagation environment.

5.3.2 Link level performance modelling

The simulator is operated at slot[15] level and the actual value interface (AVI) principle is used to model the link level performance of each Node-B−UE connection [93]. The explanations given here assume that a Rake receiver with MRC of a generic number of antenna elements is used. The E_b/N_0 is computed for each finger in every slot interval, followed by MRC of the signals from different Rake fingers at the different antennas of the

---

[15] Note that the slot duration is 0.667 ms.

UE. The effect of using orthogonal channelisation codes is included when modelling the E_b/N_0 at each finger, since the time-synchronised orthogonal own cell interference is subtracted from the interference term in the denominator. The E_b/N_0 at the output of the receiver is calculated as

$$\frac{E_b}{N_0} = \sum_{m=1}^{M} \sum_{n=1}^{N} \frac{G \cdot P_i g_L(s,i) g_{FF}^m(s,i,n)}{P_N + \sum_{b=1}^{B} \sum_{l=1}^{L} P_b^{Total} g_L(b,i) g_{FF}^m(b,i,l) - P_s^{Total} g_L(s,i) g_{FF}^m(s,i,n)} \tag{5.8}$$

where the notation given in Table 5.1 is used. Note that this expression assumes that the resulting E_b/N_0 value at the output of the Rake receiver can be computed as the sum of the E_b/N_0 values at the output of the different Rake fingers. Unlike in the analogue expressions given in Chapter 4, in this case this assumption is partly an approximation that assumes that the noise and interference components at the different Rake fingers are totally uncorrelated. As was already pointed out in Section 4.3.3, this is not totally true for the case in which the outputs of Rake fingers connected to the same antenna are combined (note that, as stated in Chapter 4, the effect of the partially correlated noise and interference is embedded in the AVI tables). However, when combining the outputs of Rake fingers connected to different antennas, it is fair to state that the noise components are totally uncorrelated. Regarding the interference, this statement is also true if the antennas are assumed to be totally uncorrelated, which is the case in this study.

Table 5.1: Notation for the E_b/N_0 calculation.

Symbol	Definition
M	Number of antennas at the UE
N	Number of Rake fingers connected to each antenna. Perfect MRC between them is assumed
L	Number of multipath components in the considered PDP
G	Processing gain
P_N	Power for the thermal noise at the UE
B	Number of cells in the network
P_i	Desired signal power transmitted towards UE #i
P_b^{Total}	Total wideband transmitted power at cell #b
$g_L(b, i)$	Path gain from the Node-B at cell #b to UE #i, including deterministic path loss, shadow fading and the corresponding antenna gain. Expressed in terms of power gain for convenience
$g_{FF}^m(b, i, l)$	Power gain of the fast fading multipath component #l of the link between the Node-B at cell #b and the mth receive antenna of UE #i
s	Cell in which the UE under evaluation is being served

The conversion from E_b/N_0 to BLER is based on results generated by link level simulations, which include the performance enhancements from coding and interleaving. From each block, the measured E_b/N_0 values for all the slots are geometrically averaged. This value is given as input to a mapping table that gives a block error probability (BEP). A random number (χ), which is uniformly distributed between zero and one is generated and compared with the obtained BEP. If χ<BEP, the block is labelled as erroneous. Otherwise, it is considered to be successfully decoded. Note that the same AVI table has been used for both single antenna Rake and 2Rake receivers[16], which means that completely ideal MRC of the signals coming from both antennas is assumed, which is an approximation. Moreover, channel estimation is assumed to be based on common pilots, which means that no degradation of the channel estimates for each one of the diversity branches has to be considered.

5.3.3 Offered traffic

UEs are uniformly distributed in the network and move with constant speed and direction. Circuit switched (CS) data calls over DCHs are simulated with a block length (interleaving period) of 10 ms (15 slots) and a Turbo encoder with a coding rate of 1/3 is used [1]. The simulated bit rate is 64 kbps, and the required spreading factor (SF) for this bit rate is 32. Thus, assuming that channelisation code resources corresponding to a code with SF 32 are reserved for common channels, a maximum of 31 UEs can be supported within one channelisation code set [31]. The call arrival process is modelled with a Poisson process, and the call length is assumed to be negative exponentially distributed with a mean length of 30 seconds.

5.3.4 Radio resource management

RRM algorithms, such as SHO, admission control (AC) closed loop power control (CLPC) and outer loop power control (OLPC) are simulated. In addition, a resource manager is implemented for each cell to keep track of the available channelisation code resources. If nothing is explicitly stated, the selected configuration for these algorithms is similar to the default settings used in Chapter 4 (see Table 4.2 on page 79). As already mentioned in Chapter 4 (Section 4.3.4, on page 74), this simulation tool does not explicitly include any layer 3 signalling mechanisms. This is estimated to have an effect on the system performance at medium-to-high UE speeds, due to the ignored layer 3 signalling delays. However, this is not the case at the low UE speed (3 kmph, according to Table 5.2) that is going to be used in this study.

In order to control the number of UEs in the system, a power based AC algorithm like the one described in Chapter 4 for sector antennas is used. According to that algorithm, a UE is admitted in the system if (i) the estimated total wideband average transmitted power at the Node-B after the admission is lower than the target level, and (ii) there are sufficient channelisation code resources.

In addition, simulations with and without SHO are conducted, in order to evaluate how the capacity gain from 2Rake receivers is affected by the diversity gain provided by SHO. For further explanations about SHO, the reader is referred to Section 4.3.4 of Chapter 4.

[16] For details about the manner in which these AVI tables were generated, the reader is referred to the information provided in Section 4.3.3.

For OLPC, two BLER targets (10% and 1%) are simulated, since the capacity gain from 2Rake receivers is expected to be higher for stricter quality requirements. See e.g. [49], which contains results showing that the link level gain from dual antenna receivers with MRC is larger when the system is operated at lower bit error rates. The parameters that have been considered for simulation are summarised in Table 5.2.

Table 5.2: Parameters for simulations.

Parameter		Value
Network set-up	Site-to-site distance	2 km
	Power allocated to the primary common pilot channel (P-CPICH)	1 W
	Coherence distance for shadow fading	50 m
	Standard deviation for shadow fading	8 dB
	Thermal noise power	-97.9 dBm
	PDP	Pedestrian A and Vehicular A
SHO	Max. active set size when SHO is active	3
	Candidate set size	8
	Wadd / Wdrop when SHO is active	2 / 4 dB, resulting in a SHO overhead of 30%
AC	P_{Target}	10W
Simulated traffic	Call arrival process	Poisson distributed
	Call duration	Negative exponentially distributed. Average duration = 30s.
	Connection type	Circuit switched
	Bit rate	64 kbps
	SF	32
	Coding	Turbo coding. Rate = 1/3
	Interleaving period	10 ms
	BLER target	10% and 1%
UE speed	3 kmph	
Simulation time	200 seconds	

5.4 Simulation results

Table 5.3 shows the capacity gain as a function of the penetration rate for both PDPs and a BLER target of 10%. The results in Table 5.3 assume simple hard handover, and restrictions in the number of available channelisation codes are not considered.

Table 5.3: Simulation results for a BLER target of 10%. No channelisation code restrictions are considered. SHO is disabled.

PDP	Penetration rate (*f*)	Capacity gain
Pedestrian A	0.5	46 %
	1	167 %
Vehicular A	0.5	41 %
	1	138 %

The results at both analysed penetration rates can be fitted with the theoretical curve derived in Section 5.2 (see Figure 5.4). In order to fit the analytical curves with the simulation results for *f*=1, the value of *D* is 2.67 (4.27 dB) for Pedestrian A and 2.38 (3.77dB) for Vehicular A. The reason why the capacity gain is larger in Pedestrian A is that Vehicular A offers more inherent frequency diversity, which prevents the 2Rake receivers from adding so much extra diversity gain. These are reasonable numbers for *D* if they are compared with the results presented in [63], which claims link level improvements from 2Rake of 4–4.5 dB for Pedestrian A, and of 3–3.5 dB for Vehicular A, both with a BLER target of 10%. Furthermore, the results shown in Table 5.3 are in line with the ones presented in [63] for similar settings and environment.

Table 5.4 shows capacity gain for *f*=1, different BLER targets and different SHO configurations. When generating these results, simulation campaigns with and without channelisation code restrictions have been conducted. For each cell, the code blocking rate is defined as

$$Code\ blocking\ rate[\%]=\left(1-\frac{C_{Restricted}}{C_{Unrestricted}}\right)\cdot100, \tag{5.9}$$

where $C_{Unrestricted}$ is the cell capacity that is achieved when no channelisation code restrictions are considered, and $C_{Restricted}$ is the cell capacity when the channelisation code restrictions are considered. Since a homogeneous network is run and the simulation time is sufficiently large, all the monitored cells have the same code blocking rate, and therefore no distinctions between cells within the set of monitored cells are done in this respect.

For the case without SHO, it can be clearly seen that the capacity gain without channelisation code restrictions is larger when the BLER target is lower, as already suggested by results presented in [49] regarding dual antenna receivers with MRC. For example, the capacity gain in Pedestrian A is 167% for a BLER target of 10%, and 294% for a BLER target

of 1%. As can be confirmed by these figures, the diversity gain from 2Rake grows improves when the BLER target is decreased.
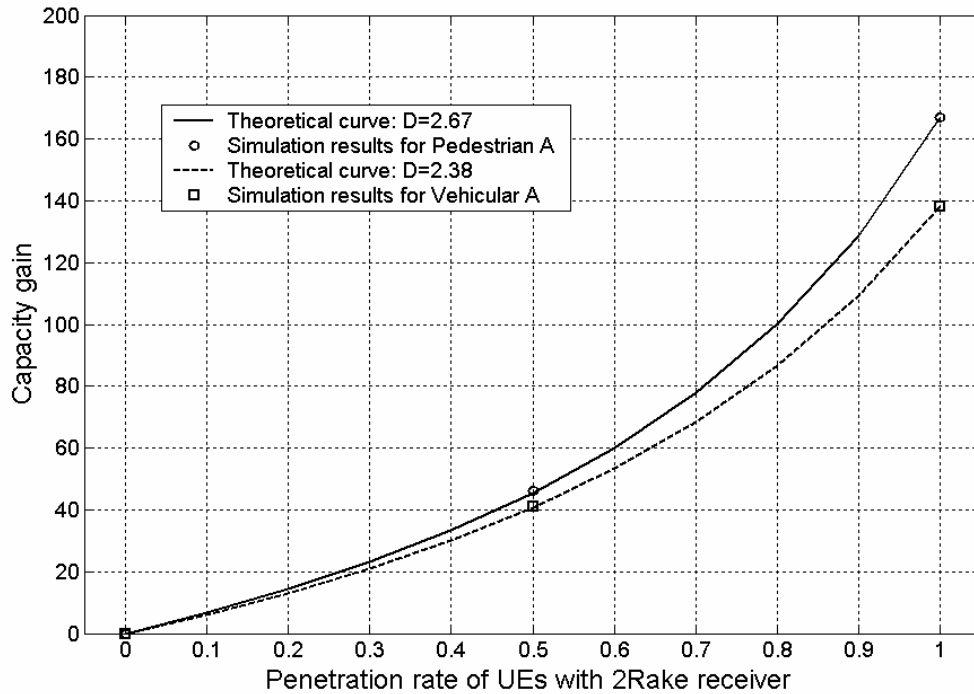
Figure 5.4: Theoretical capacity gain vs. simulation results at different penetration rates for a BLER target of 10%.

Table 5.4: Simulation results at 100% penetration rate (f=1).

PDP	SHO	BLER target	Capacity gain without code restrictions	Capacity gain with code restrictions	Code blocking rate [%]
Pedestrian A	OFF	10%	167%	72%	36
	OFF	1%	294%	268%	7
	ON	1%	229%	78%	46
Vehicular A	OFF	10%	138%	91%	20
	OFF	1%	183%	178%	2
	ON	1%	158%	111%	18

Let us analyse the influence of SHO on the capacity gain for a BLER target of 1%. When looking at the case where code restrictions are not considered, it can be seen that the

capacity gain from 2Rake receivers is lower when SHO is active, since SHO also provides diversity gain and the combination of several diversity mechanisms provides diminishing returns. For example, the capacity gain for Pedestrian A without SHO is 294%, while it is only 229% for a scenario with SHO.

A larger code blocking rate is experienced for higher BLER targets and radio channels with lower time dispersion. The reason is that, from an interference point of view, both mechanisms lead to higher capacity. This is due to two reasons: (i) a higher BLER target involves lower E_b/N_0 requirements and therefore allows more served UE with the same transmit power; and (ii) lower time dispersion preserves more orthogonality between UEs in the same cell, which increases the capacity. Since the code restrictions are fixed, code blocking has a more severe impact in scenarios facilitating larger absolute capacity. By analysing the two extreme cases without SHO, it can be seen that the code blocking rate for Pedestrian A with a BLER target of 10% is 36%, while it is 2% for Vehicular A and a BLER target of 1%. In general, the code blocking rate is higher with SHO, due to the higher average channelisation code consumption per UE. For example, the code blocking rate for Pedestrian A with a BLER target of 1% is 46% when SHO is active, compared with the code blocking rate of 7% that is experienced with hard handover.

Furthermore, it is important to stress that the presented results are influenced by the underlying assumptions, especially by the utilised AVI tables. The use of different AVI tables would have implied different power requirements per UE, which would have impacted the absolute system capacity and, therefore, the reported code blocking figures. Nonetheless, although different specific performance figures will be reported when different AVI tables are used, the main trends and conclusions described here are expected to remain valid.

5.5 Comments on the use of 2Rake receivers at the UE for packet traffic

Throughout this chapter, the study has been focused on CS connections on DCHs. The main conclusion is that, due to the deployment of 2Rake receivers at the UEs, the number of UEs that can be served is larger. However, those UEs with 2Rake do not experience any extra quality in the service they receive. Therefore, it is the network operator who obtains the gain in the case of CS traffic, since more UEs can be served with the same infrastructure.

In the case of packet switched traffic on DCHs, the situation is a bit different. Let us assume that the PS algorithm aims at delivering the same throughput to all the UEs. So, for each scheduling period, a set of a fixed number of UEs is selected and code multiplexed over the air interface. In this case, it is also assumed that each UE has an associated DCH with low bit rate, which is always active and acts as a reference for PS decisions regarding that particular UE. For the case where all the UEs have a single antenna Rake receiver, the PS algorithm finds the manner to distribute the power among all the UEs so that they all receive the same throughput. If now some of the UEs deploy 2Rake receivers, the PS detects that some of UEs (the ones implementing 2Rake receivers) need less transmit power on their associated DCH. Thus, when assigning the power resources in order to deliver the same throughput to all the UEs, the gain coming from the reduced transmit power towards the UEs with 2Rake receivers is distributed among all the UEs. In this way, all the UEs can be allocated some extra power, which therefore increases the throughput delivered to all of them.

In this case, the benefit from the 2Rake receivers implemented at some UEs is shared among all the scheduled UEs, which are allocated higher throughput.

If the PS algorithm were assigning the same average power resources to all the UEs and then selecting the delivered throughput towards each one of them according to their channel quality, the PS algorithm would realise that the UEs with 2Rake receivers need less transmit power on the associated DCHs. As a consequence, they would be estimated to have a better channel quality and would therefore be delivered larger throughput. In this case, the UEs with 2Rake receivers would obtain the benefit from the advanced receiver they deploy.

So far in the case of packet switched traffic on DCHs, it has been stated that the benefit from having some UEs with 2Rake receivers is enjoyed by the UEs. Depending on the scheduling strategy, it can happen that all the UEs in the network share this benefit. Moreover, it is also possible that the benefit is only enjoyed by the users having a dual antenna UE. However, these conclusions have been drawn under the assumption that the number of UEs that can be simultaneous served is kept constant. If this condition is relaxed, the network operator may choose to use the benefit from having UEs with 2Rake receivers in order to admit more UEs in the system. Obviously, in this case the network operator will obtain the gain.

5.6 Concluding remarks

The potential capacity gain from deploying 2Rake receivers at the UEs has been analysed by means of simple theoretical assessment and dynamic system simulations. The capacity gain grows in a non-linear way with the penetration rate of UEs with 2Rake receivers, which has been justified from a theoretical point of view.

Notice that the results presented in this chapter have been obtained with a simulation tool that ignores the layer 3 signalling procedures and delays associated to all the handover operations. Since the simulations have been conducted at low speeds (3 kmph), this is not considered to affect the presented system performance figures. However, at larger UE speeds this is expected to have an impact on the results. Furthermore, it must be also noted that the presented performance figures are strongly influenced by the utilised AVI tables. If different AVI tables (corresponding to different UE performance characteristics) were used, the reported figures would change, especially those concerning code blocking rates when introducing 2Rake receivers. However, the presented trends and phenomena are expected to remain the same from a qualitative point of view.

At 100% penetration rate (f=1), with a BLER target of 1% and without channelisation code restrictions, the capacity gain from 2Rake with hard handover is larger for Pedestrian A (294%) than for Vehicular A (183%), since Vehicular A provides frequency diversity that makes the increased diversity order due to 2Rake receivers provide diminishing incremental returns. When SHO is activated, the capacity gain decreases (229% in Pedestrian A, and 158% in Vehicular A), due to the diversity gain from SHO, which also makes the increase of the diversity order due to 2Rake receivers provide diminishing returns. In order to put into perspective the different scenarios regarding the capacity gain from 2Rake receivers, the following plot ranks them for the case where the BLER target is 1%.
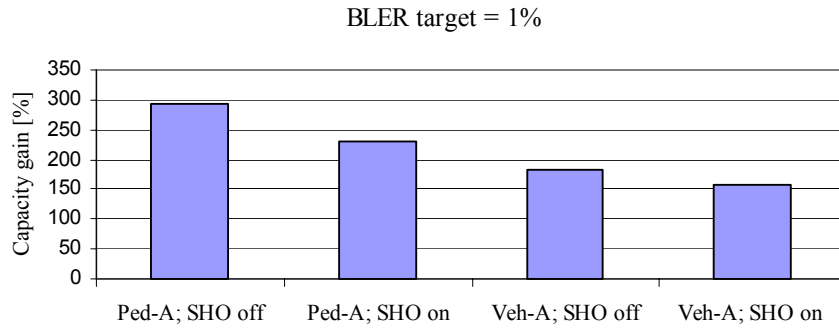
BLER target = 1%

Figure 5.5: Capacity gain from 2Rake receivers when *f*=1 and BLER target=1%. No channelisation code restrictions considered.

In this plot, it can be observed that, as more sources of diversity are present in the system (e.g. frequency diversity from Vehicular A or diversity gain from SHO) the capacity gain from 2Rake receivers (in the case with no channelisation code restrictions) becomes lower. This is a clear example of how the combination of several sources of diversity provides diminishing returns.

It has been also shown that the capacity gain for higher BLER targets tends to decrease. For example, in Pedestrian A, with a BLER target of 10% and hard handover, the capacity gain is 167%, compared with the gain of 294% that can be obtained when the BLER target is 1% and the rest of the conditions remain the same.

Unfortunately, code blocking appears when deploying 2Rake receivers at the UEs. This problem is more severe when the absolute cell capacity is larger, i.e. for Pedestrian A with large BLER targets. For example, in Pedestrian A, with a BLER target of 10% and hard handover, the code blocking rate is 36%. However, the code blocking rate drops to 7% when the BLER target is 1%. Moreover, though activation of SHO reduces the capacity gain, it causes an increase in the code blocking rate, due to the higher average code consumption per UE.

Unlike in the beamforming case described in Chapter 4, there is not a straightforward solution to overcome this problem. Note that this was possible in the CBF case due to the spatial filtering properties of AAs with CBF, which make it possible to spatially isolate regions with different scrambling codes. Even though the main message is that the system eventually becomes channelisation code blocked, the capacity gain figures for the case without channelisation code limitations are still considered to be useful. For example, a system that combines the use of CBF at the Node-B and 2Rake receivers at the UE will enjoy both the spatial filtering gain from CBF and the already described benefits from 2Rake receivers at the UE. The combination of both techniques makes the potential channelisation code shortage problem even more severe, but the possibility of the Node-B to allocate the scrambling codes on a beam basis opens for a solution to this problem. Probably, this solution requires the use of more scrambling codes than in the case of CBF at the Node-B with single antenna reception at the UE. As a consequence, the overall capacity gain is expected to be slightly below the multiplication of the capacity gains provided by both techniques separately, but the described capacity gain figures are still valid in order to estimate how much extra capacity can be added to the system in a situation in which the channelisation code blocking

problems can be avoided in a feasible manner. In Chapter 7, the evaluation of the combined use of CBF at the Node-B and 2Rake receivers at the UE is proposed as an item for further study, which is advised to be conducted by using specific AVI tables for 2Rake receivers, so that the assumption of ideal MRC between the two antennas can be suppressed.

Chapter 6

Network performance of HSDPA

with Tx/Rx diversity

6.1 Preliminaries

This chapter addresses the network performance of transmit and/or receive (Tx/Rx) diversity techniques for the High Speed Downlink Packet Access (HSDPA) concept of the Universal Mobile Telecommunications System (UMTS) [1] under different packet scheduling (PS) algorithms. Such evaluation is conducted primarily by means of dynamic system level simulations, although a simplified theoretical analysis is also shown in order to further validate the observed phenomena.

As mentioned in Chapter 2, only those antenna diversity techniques already standardised for the Release 5 of UMTS are taken into account for this study. At the Node-B, three transmission schemes are considered: (i) single antenna transmission, (ii) two branch open loop space time transmit diversity (STTD) [49], and (iii) two branch closed loop transmit diversity (CLTD) mode-1, as described in [37]. At the user equipment (UE), both single antenna reception and dual antenna Rake receivers (2Rake) using maximal ratio combining (MRC) [36] are studied. Finally, the combination of transmit diversity at the

Node-B and 2Rake at the UE is also studied, as a manner to enable multiple-input-multiple-output (MIMO) operation in UMTS.

Traditionally, the different Tx/Rx diversity techniques have mainly been analysed at link level [37], while only a few studies have considered the interaction with advanced PS algorithms at system level (see e.g. [100]). This study is focused on the analysis of Tx/Rx diversity techniques at system level, conditioned on three different PS algorithms: round robin (RR), fair throughput (FT) and proportional fair (PF) [101].

With RR, the UEs are served in a sequential order, without exploiting any a priori knowledge of the radio channel. Thus, this PS algorithm is often characterised as a blind PS algorithm that does not bring any multi-user diversity into the system.

Since the PS functionality is moved to the Node-B in HSDPA, fast quality based PS can be done, based on the channel quality indicator (CQI) reports sent by the UE [33]. This possibility is exploited by the PF algorithm, which benefits from the instantaneous knowledge of the radio channel of all the UEs. Hereby, PF provides a multi-user diversity gain that tends to limit the diversity gain that can be obtained from deploying antenna Tx/Rx diversity techniques. A theoretical study about the interaction between antenna diversity and multi-user diversity (obtained via fast quality based PS) is available in [102].

When FT is used, most resources are devoted to serving UEs under poor radio channel conditions, so all the UEs in the system are delivered the same throughput. As will be shown, these UEs are the ones for which the deployment of Tx/Rx antenna diversity techniques provides the largest throughput gain. Moreover, this PS algorithm does not bring any multi-user diversity gain and, therefore, the diversity gain that can be obtained from deploying antenna Tx/Rx diversity techniques is not limited in this respect.

The chapter is organised as follows. Section 6.2 shows a simple theoretical discussion about the interaction between multi-user and antenna diversity, together with the expected impact of the UE speed on the performance of fast quality based PS algorithms. The system model and simulation assumptions are described in Section 6.3. In Section 6.4, the simulation results are shown and discussed. Concluding remarks are given in Section 6.5.

6.2 Theoretical discussion

This section shows a simple theoretical discussion about the interaction between multi-user and antenna diversity, together with the expected impact of the UE speed on the performance of PS algorithms based on instantaneous knowledge of the radio channel. This discussion aims at highlighting the main mechanisms that govern the interaction between the analysed system parameters.

Let us assume a set of UEs, towards which there is an infinite amount of data to be transmitted. In the system under discussion, these UEs have to be served through a single time-shared channel, in which only one UE is served at a time. The PS algorithm serves the UE with the maximum instantaneous normalised channel quality. In other words, the PS algorithm aims at scheduling the UEs when they are experiencing constructive fading. For this simple discussion, the instantaneous channel quality for UE #i is defined by the instantaneous power value of the corresponding fast fading process:

$$g_i(t) = |h_i(t)|^2, \tag{6.1}$$

where $h_i(t)$ is the complex value of the fast fading process of UE #i for time instant t.

In order to characterise the system level performance, it is important to define the effective fast fading at the shared channel, which is defined in terms of power gain and is described as follows

$$g_{Eff}(t) = \max_{all\ i} \left\{ |g_i(t)|^2 \right\}, \tag{6.2}$$

where max{.} takes the maximum value among the arguments. In short, the effective fast fading at the shared channel for time instant t equals the power value of the fast fading for the scheduled UE at that time. Note that (6.2) implicitly assumes ideal instantaneous selection of the served UE.

The cumulative distribution function (CDF) of the effective fast fading at the shared channel in a single path propagation environment is depicted in Figure 6.1, where results for single antenna transmission and reception (denoted by 1Tx-1Rx) and STTD are shown. Note that, for this theoretical discussion, the power value of each fast fading process is assumed to be Chi-square distributed. In order to calculate this function, it has been assumed that all the UEs experience independent fading processes. Under this assumption, the following can be written:

$$P\big(g_{Eff}(t) \le g\big) = \prod_{all\ i} P\big(g_i(t) \le g\big) \quad \forall t, \tag{6.3}$$

where P(.) denotes probability. Also note that STTD has been modelled by assuming that the fast fading process of one UE (expressed in terms of power gain) equals the average of two independent fading processes like the one used for 1Tx-1Rx.

In this plot, it can be seen that each extra UE that is added to the system causes an increase in the diversity order, which can be noticed by a steeper CDF of the effective fast fading at the shared channel. At 1% outage, the value of g_{Eff} for one UE and 1Tx-1Rx equals -20 dB, while it is -0.1 dB for the case with 10 UEs. Therefore, a multi-user diversity gain of 19.9 dB is achieved when allowing 10 UEs in the system.

The diversity gain from STTD depends on the diversity that is already available in the system. When there is no multi-user diversity, i.e. when there is only one UE, the diversity gain at 1% outage from enabling STTD equals 8.5 dB. However, when there is multi-user diversity due to the presence of 10 UEs in the system, the gain from STTD is only 0.3 dB at 1% outage. This clearly indicates that STTD provides diminishing returns when there is another source of diversity in the system.
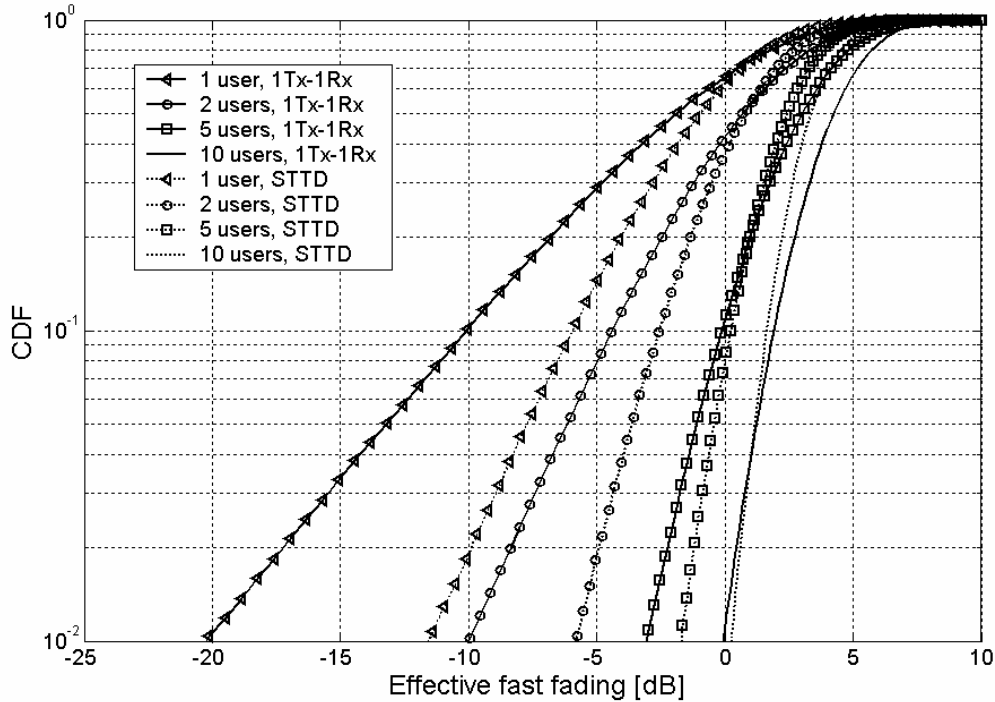
Figure 6.1: CDF of the effective fading process experienced at the shared channel for a single path propagation environment.

So far, all the attention has been devoted to deep fades. When there is multi-user diversity, the probability of a deep fade is decreased, since a deep fade is experienced at the shared channel only if all the selectable UEs are in a deep fade at the same time. In addition, the probability of having large signal quality is also decreased when enabling STTD, since large signal quality is typically experienced with STTD when both diversity branches are on top of a constructive fade at the same time. Therefore, the signal quality of a UE experiencing constructive fading is statistically worse when STTD is enabled. This can be seen in Figure 6.2, which shows the CDF of the effective fast fading for the single UE case. For the sake of better visibility, this plot is presented in linear scale and concentrates on the part of the dynamic range concerning constructive fading. As can be observed, when scheduling UEs only on the highest part of their fading dynamic range (the one corresponding to the region ranging from the 75% to the 100% percentile of the depicted CDF), STTD yields a loss.

When there are few UEs in the system, it is likely that the scheduled UE is in a point of its fast fading dynamic range in which STTD yields diversity gain. Thus, a capacity gain is expected in this case. However, when there are many UEs in the system, it is very likely that the scheduled UE is experiencing constructive fading. As stated before, the signal quality on top of a constructive fade is statistically lower when STTD is enabled. Thus, it is expected to have a loss when enabling STTD in a system in which PS based on the instantaneous normalised channel quality is conducted among a large number of UEs.
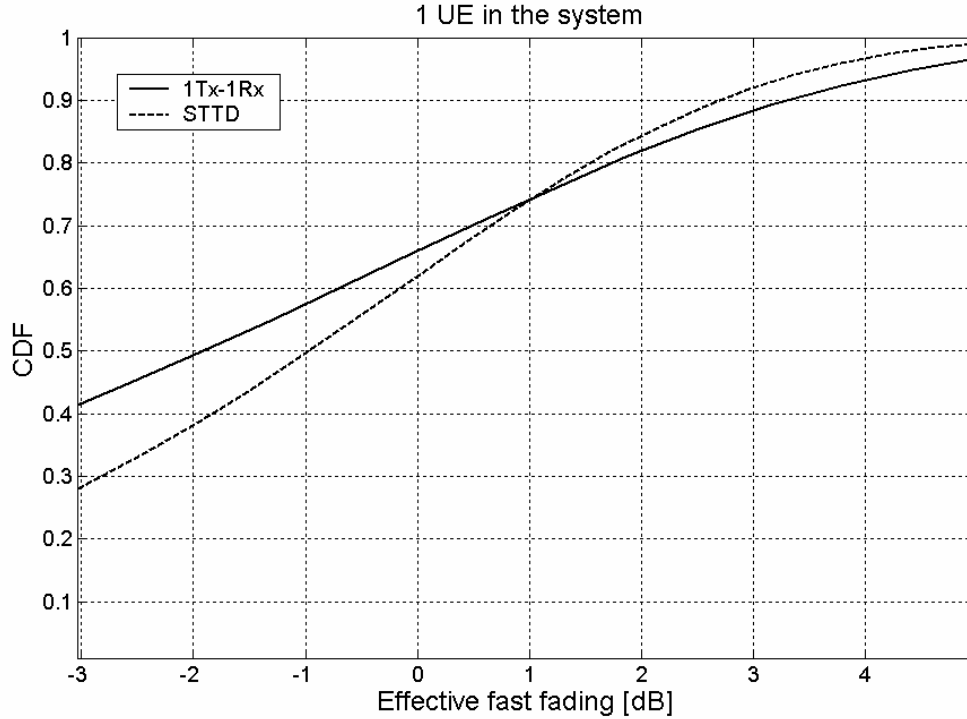
Figure 6.2: CDF of the effective fading process for a single UE in a single path propagation environment, focussing on the constructive fades.

In order to analyse this interaction from a system level perspective, the approach presented in [102] is followed, where the system capacity for the case of optimal link adaptation (LA) is expressed as

$$C = \int_0^\infty \int_0^\infty \log_2\left(1 + g_{Eff}G\right) \cdot f_G(G) \cdot f_{g_{Eff}}\left(g_{Eff}\right) dG \cdot dg_{Eff}\,, \tag{6.4}$$

where $f_X(X)$ denotes probability density function, and G is the so-called Geometry factor [103], which is defined as

$$G = \frac{E\{P_{Own}\}}{E\{P_{Other} + P_{Noise}\}}\,, \tag{6.5}$$

where P_{Own} denotes the own cell interference at the UE, P_{Other} is the other cell interference at the UE, and E{.} denotes expectation. As stated in [102], the SINR can be approximated as the product of the G factor and g_{Eff} in case of flat fading radio channel, constant interference power and 100% of the transmit power and channelisation codes allocated to HSDPA. For this theoretical discussion, these assumptions are assumed to hold. The G factor distribution shown in [104] is taken as an input for (6.4). As will be mentioned later, the adopted distribution matches well the one obtained from the system level simulator utilised in this study. Figure 6.3 shows the system capacity as a function of the number of UEs.
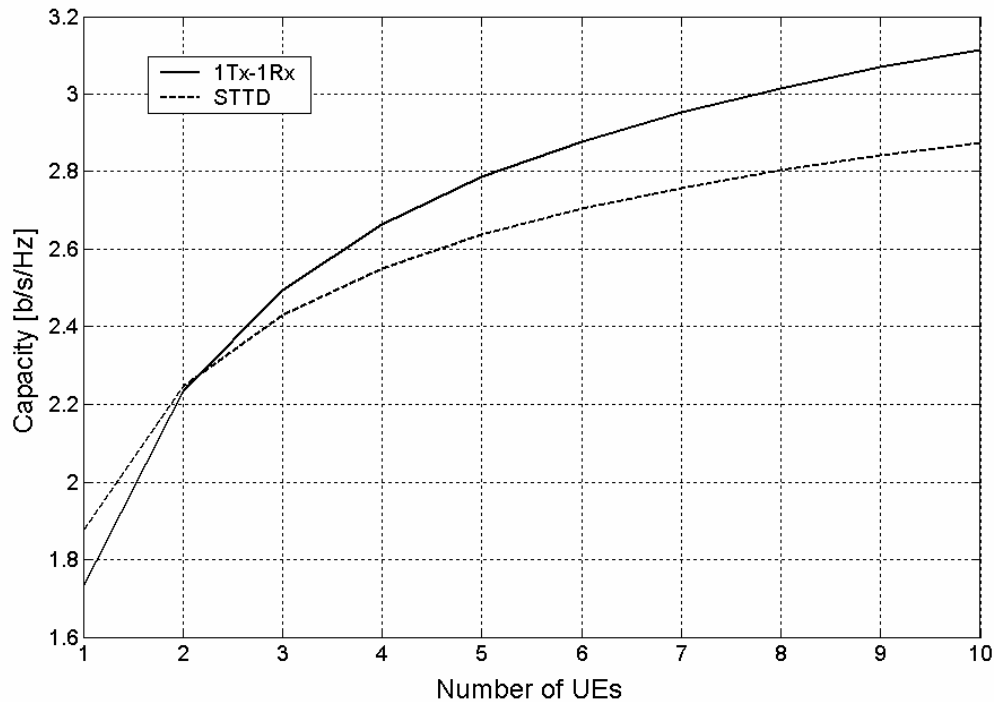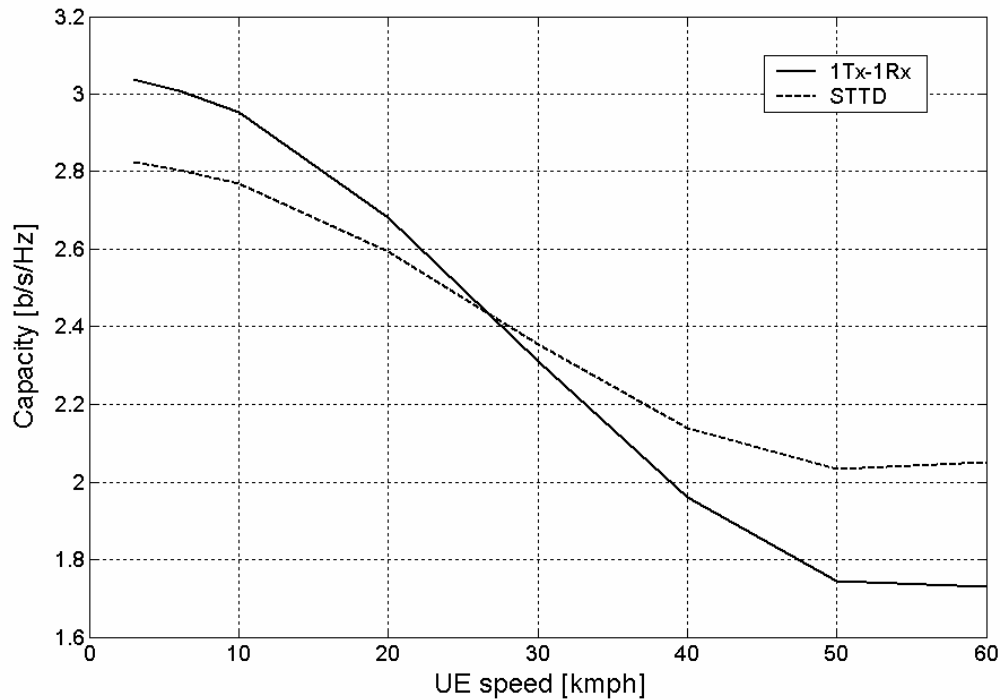
Figure 6.3: System capacity as a function of the number of UEs in a single path propagation environment.

As can be seen, STTD provides diversity gain for a number of UEs lower than three. From three UEs onwards, a system capacity loss from STTD is reported due to the fact that it is very likely that most of the scheduled UEs are experiencing constructive fading. As already stated, the signal quality when experiencing constructive fading is statistically lower when STTD is enabled.

These preliminary conclusions have been extracted assuming ideal instantaneous selection of the UE with the best instantaneous normalised channel quality. In practice, such operation is subject to delays. As a consequence, the conclusion of the analysis depends on the UE speed, since there are certain mechanisms that become more robust against delays (and thus against the UE speed) when STTD is enabled. Examples of such processes are the feedback procedures for the information required for LA and fast quality based PS. The interaction between UE speed, antenna diversity and fast quality based PS is analysed in this simple theoretical discussion. The influence of LA will be accounted for later by including the equivalent detailed model for the simulation campaigns.

Figure 6.4 concentrates on the case where there are 10 UEs in the system, among which the PS algorithm selects the one with the best normalised channel quality. Unlike in the previous plots, now the system applies a delay of 4 ms (two transmission time intervals −TTIs− in HSDPA), which elapses from the moment at which the selection of the best UE is done until the moment in which the result of such selection is applied.

Figure 6.4: System capacity as a function of the UE speed in a single path propagation environment.

As can be seen, at very low speeds, 1Tx-1Rx yields better performance, due to the reasons already mentioned throughout this section. However, as the UE speed increases, the performance of 1Tx-1Rx is degraded more than that of the STTD configuration. Thus, there is a UE speed value from which the STTD option becomes better. The reason is that, although STTD smoothens the constructive fades, thereby decreasing the system capacity when the there is a large number of UEs among which to choose, the reduction of the power gradient of the radio channel also makes the system less sensitive towards the delays in the scheduling decisions. Note that this simple theoretical discussion does not include other impairments, such as LA delays. In addition, though there is a delay in the selection of the scheduled UE, this selection is still done every slot (i.e. every 0.667 ms), while the lowest resolution for PS that can be achieved in HSDPA is three slots (one transmission time interval –TTI–). Furthermore, the expression in (6.4) is based on Shannon's capacity formula, which yields better capacity than the one that can be obtained in HSDPA. Therefore, though simulation results are expected to show the same trends, the actual UE speed at with both curves cross may differ significantly from the one presented here.

6.3 System model

At the moment in which the HSDPA studies had to be started, there were some restructuring tasks of the Nokia simulation platform ongoing. Under this changing environment, it was considered to be safer, and also educational, that the author developed a completely new software tool for the HSDPA studies. Since the tool did not support other Release 99 channels, this task was simpler and estimation was done that this was the optimal manner to achieve the largest set of results by the end of the Ph.D. study. The tool, which was

entirely developed by the author, includes some simplifications. One clear example is that only one cell is simulated with full detail, while the rest are just dummy sources of interference that provide the simulated cell with a realistic interference environment. However, it has to be pointed out that this simulation tool is far more complex and complete than the one developed in order to obtain the results in Chapter 3.

6.3.1 Basic simulation methodology

The basic simulation methodology follows that of [92], where a standard hexagonal grid with 3-sector sites is considered (see Figure 6.5). The simulator is operated at slot level, using the so-called actual value interface (AVI) to model the link performance of the connection between each UE and its serving Node-B [93].
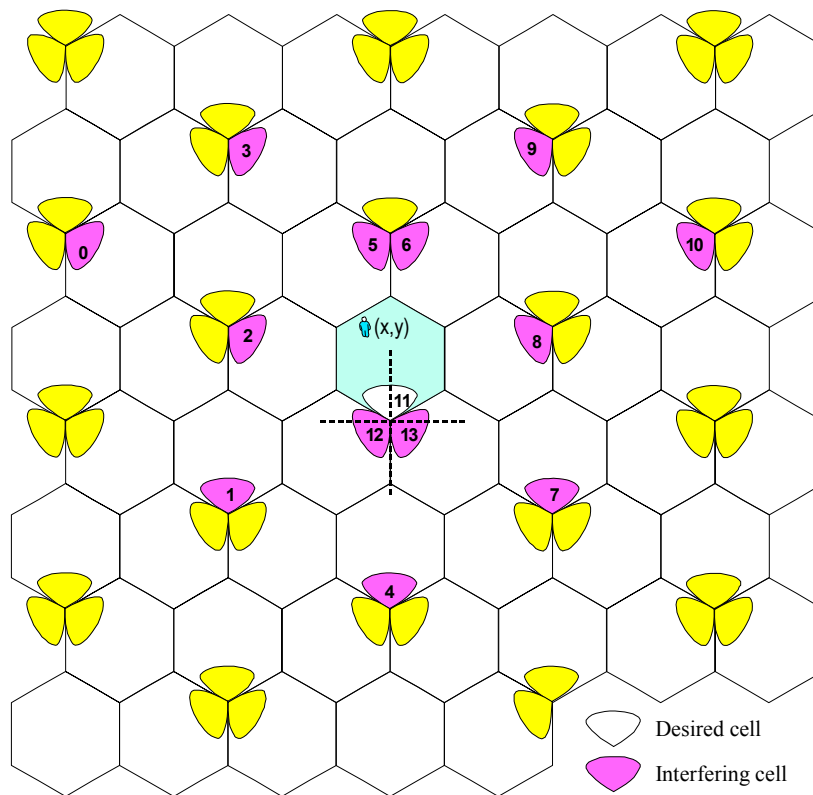
Figure 6.5: Simulated network layout.

The deterministic path loss between each Node-B and each UE is calculated according to the single-slope model with an exponent of –3.5. For each Node-B–UE link, as many independent flat fading processes as the number of taps in the power delay profile (PDP) are simulated. The power value of the flat fading processes is Chi-square distributed, and the complex amplitude of the radio channel at each tap is also computed, since it is required for the simulation of CLTD. Two modified PDPs are available for simulation: Pedestrian A and Vehicular A [42].

Shadow fading is assumed to be lognormal distributed. Given a certain Node-B, the shadow fading processes of the links between that Node-B and all the UEs in the system are uncorrelated. However, when two Node-Bs are located at the same site, their shadow fading

processes towards a given UE are fully correlated. All the cells are covered by sector antennas with the radiation pattern described in Chapter 2, on page 22.

Only the cell #11 is simulated in detail. The rest of them are equipped with dummy Node-Bs that transmit with constant power in order to provide cell #11 with realistic other cell interference. Though the surrounding Node-Bs transmit with constant power, their interference is not a constant contribution at the UE, since fast fading is simulated between each Node-B and each UE. Only UEs that would be served at cell #11 are simulated, i.e. UEs are generated in a way that the Node-B towards which they would experience the smallest path loss (averaged over fast fading) is the one serving cell #1.

Since only cell #11 is simulated in detail, handovers between this cell and the rest of the network must be avoided. In order to do so, the location of each UE is not varied along its whole packet call. However, this does not imply that the simulations are static, since the associated fast fading process of each UE is varied according to the UE speed that is given as input parameter. An intuitive model for this situation is the one in which the UE is constantly following in a circular trajectory at a certain speed. In this case, the radius of the described circular trajectory is very small and the centre is placed at the UE location. In other words, the UE is almost spinning around its permanent location. The speed at which the UE is moving along this circular trajectory is the UE speed specified as a parameter.

At the end of this section, a simplified flowchart of the simulation tool is depicted in order to provide further understanding of the adopted overall simulation strategy. See Figure 6.9, on page 125.

6.3.2 Model for the HSDPA concept

Fixed transmit power and a fixed number of channelisation codes (referred to as high speed physical downlink shared channel −HS-PDSCH− codes) are reserved for HS-PDSCH transmission. The SF of each HS-PDSCH code is 16. The remaining transmit power at the Node-B is assumed to be used by other channel types, and is also modelled as a constant source of transmit power. Therefore, all Node-Bs in the network transmit with identical constant power, which equals the maximum allowed value by the power amplifiers.

A single UE is served in each TTI. By means of a LA algorithm, the modulation and coding scheme (MCS) and the number of HS-PDSCH codes are selected as a function of the instantaneous channel quality experienced by the served UE. Selection of the optimum MCS is based on the CQI report from the UE [33]. For this study, the CQI report is modelled as the E_S/N_0 that is experienced at reception plus a lognormal distributed error to account for measurement inaccuracies. As will be shown, delays in the feedback of the CQI are included for this study. The criterion for selecting the MCS and the number of HS-PDSCH codes is that the data rate of the first transmission is maximised, while keeping its block error rate (BLER) below 30%. For simplicity, this study only considers the five MCSs listed in Table 6.1, although more options are allowed for the HSDPA concept. Possible LA algorithms for selection of optimum MCS are discussed in [105].

Table 6.1: Modulation and coding schemes.

Identifier	MCS #1	MCS #2	MCS #3	MCS #4	MCS #5
Modulation	QPSK	QPSK	16QAM	16QAM	16QAM
Effective code rate	1/4	1/2	3/4	1/2	3/4
Bit rate per HS-PDSCH code [kbps]	120	240	360	480	720

Hybrid Automated Request (H-ARQ) with Chase Combining is implemented in the simulator. Whenever a block (set of slots that are decoded all together; defined in this case as a set of three slots, which are transmitted over a TTI) is detected to be erroneous, a fast layer 1 retransmission process is started. After a certain delay (specified as a parameter), the block is retransmitted with the same number of HS-PDSCH codes and the same MCS. Then, the complex symbols of the received retransmission are soft combined with the ones of the faulty transmission. If successful decoding of the result is possible, the process is finished here. If not, another retransmission process is started, and the complex symbols of all the retransmissions are soft combined. In practice, there is a maximum number of retransmissions, after which the buffer containing the accumulated soft samples is flushed and the LA process is started all over again for the same data. The soft combining gain of retransmissions from using Chase Combining is modelled as described in [106].

Since 16QAM (quadrature amplitude modulation) is less spectral efficient than QPSK (quadrature phase shift keying), the LA algorithm tries to use the lower MCSs and adapt the number of HS-PDSCH codes to the instantaneous energy-per-symbol-to-noise ratio (E_S/N_0). However, for large E_S/N_0 values, the use of 16QAM starts to be needed in order to fully exploit the available channel quality.

Since there is a minimum delay between retransmissions, a stop and wait (SAW) procedure has been implemented in order to be able to continue the transmission towards a certain UE even though one of the blocks is waiting for a retransmission. The number of SAW channels is dimensioned according to the delay between retransmissions, so that the transmission towards the UE is not halted because of the delays in the retransmissions. Regardless of the selected PS algorithm, whenever there is a retransmission ready to be sent, it is given higher priority than the PS decision. As a consequence, the BLER target of the first transmission affects the potential multi-user diversity, since it impacts the probability of having a retransmission. Notice that when a retransmission overrules the PS decision, the multi-user diversity instantaneously disappears, since the UE to be scheduled is fixed. The danger of getting the system blocked by continuous retransmissions coming from an unfortunate LA operation is avoided by setting a maximum number of retransmissions.

6.3.3 Link level performance model

As already mentioned, the detection of the signals is modelled using the so-called actual value interface (AVI) principle [93]. With the AVI method, whenever a set of three slots completing a block has been received, the equivalent E_S/N_0 of the block is computed as the geometrical average of the E_S/N_0 values of all the slots in the block. Then, a lookup table (generated from extensive link level simulations, according to the HSDPA specifications [1])

maps the E_S/N_0 of the block to an equivalent block error probability (BEP). A uniform distributed number ($\chi \in [0;1]$) is generated and compared with the BEP. If $\chi <$ BEP, the block is labelled as erroneous. Otherwise, it is labelled good. Different AVI tables are used depending on the MCS that is utilised for transmission towards the UE, and a single set of AVI tables obtained for the 1Tx-1Rx case is used for all the considered antenna schemes. The latter is an approximation that neglects the following effects and phenomena:

- The channel estimation issues that appear when using transmit diversity.

- The non-ideal combining between the signals of different antennas that is experienced when using reception diversity. Hence, the fact that the same AVI tables are used for all cases implies the acceptance of the assumption that this combining operation can be performed in an ideal manner.

- The impact of the different degrees of signal quality fluctuation within one TTI that are experienced when antenna diversity is used. These differences are likely to affect the receiver performance. However, they have been neglected here due to the fact that specific AVI tables for these antenna schemes were not available.

Moreover, when applying this model to the reception of a block transmitted on several HS-PDSCHs, a lookup table generated for one single code is used, and the input value that is fed into this table equals the geometrically averaged E_S/N_0 divided into the number of used HS-PDSCH codes. The calculation process of the E_S/N_0 takes the effect from multipath propagation into account (including the so-called downlink orthogonality) and the potential gain from using Tx/Rx diversity techniques.

When generating the single-code AVI tables for a certain MCS, speed and PDP, the selected approach is, in general, similar to the one described in Section 4.3.3. However, the adopted procedure presents the following differences and particularities in comparison with the one in Section 4.3.3:

- In this case, the block length is fixed to three slots.

- Instead of measuring the BEP versus the geometrically averaged E_b/N_0 per block, the analysis is done based on the geometrically averaged E_S/N_0 per TTI.

- The MCS is not changed along one single link level simulation, i.e. LA is not activated.

- The interference model is more complete here, since own cell interference is explicitly included in the link level simulations. As a consequence, not only one single AVI table is generated for each MCS, speed and PDP. Instead, the number of AVI tables is multiplied with the number of considered G factors, which is used as described in Section 6.2. In this case, three different G factors were included: 3, 6, and 12 dB. For each look-up operation, the average G factor of the UE is measured, and the table generated for the nearest G factor is utilised.

- The utilised basic set of AVI tables corresponds to link level simulation campaigns in which retransmissions are not considered. When a retransmission occurs, the experienced soft combining gain is modelled as described in [106], which builds a model based on results that include retransmission and were obtained with the same link level simulator that was used to generate the AVI tables utilised here.

The expressions for the per-slot E_S/N_0 for UE #i are reported in the following, using the notation in Table 6.2. Note these expressions implicitly assume that a standard Rake receiver with maximal ratio Rake finger combining is used at the UE. Also note that uncorrelated antennas with equal branch power ratio at both the Node-B and the UE have been assumed.

Table 6.2: Notation for the relevant magnitudes in the interference calculation.

Symbol	Definition
N	Number of Rake fingers connected to each antenna. Perfect MRC between them is assumed
L	Number of multipath components in the considered PDP
SF	Spreading factor
P_N	Power for the thermal noise at the UE
B	Number of cells in the network
P_i	Desired signal power transmitted towards UE #i
P_b^{Total}	Total wideband transmitted power at cell #b
$g_L(b, i)$	Path gain from the Node-B at cell #b to UE #i, including deterministic path loss, shadow fading and the corresponding antenna gain. Expressed in terms of power gain for convenience
$g_{FF,t}^{r}(b, i, l)$	Power gain of the fast fading multipath component #l of the link between the tth transmit diversity branch of the Node-B at cell #b and the rth receive diversity branch of UE #i
$h_{FF,t}^{r}(b, i, l)$	Amplitude gain of the fast fading multipath component #l of the link between the tth transmit diversity branch of the Node-B at cell #b and the rth receive diversity branch of UE #i. It is a complex number
S	Cell in which the UE under evaluation is being served
w_k	Transmission weight for the kth transmit diversity branch in CLTD

1Tx-1Rx:

The E_S/N_0 for 1Tx-1Rx can be written as:

$$\frac{E_S}{N_0} = \sum_{n=1}^{N} \frac{SF \cdot P_i g_L(s,i) g_{FF,1}^1(s,i,n)}{P_N + \sum_{b=1}^{B}\sum_{l=1}^{L} P_b^{Total} g_L(b,i) g_{FF,1}^1(b,i,l) - P_s^{Total} g_L(s,i) g_{FF,1}^1(s,i,n)} \qquad (6.6)$$

Note that this expression assumes that the resulting E_S/N_0 value at the output of the

Rake receiver can be computed as the sum of the E_S/N_0 values at the output of the different Rake fingers. As described in Section 4.3.3, this is an approximation that assumes that the noise and interference components at the different Rake fingers are totally uncorrelated, which is not totally true but only an approximation (see Section 4.3.3 for more detailed explanations). In this case, the effect of the partially correlated noise and interference is also included in the HSDPA AVI tables.

Moreover, it must be also noticed that the effect of using orthogonal channelisation codes is included in (6.6), since the time-synchronised orthogonal own cell interference is subtracted from the interference term in the denominator. In this context, only one scrambling code per cell is assumed and, thus, all the interference coming from the serving Node-B is orthogonal when it is time-synchronised with the desired signal multipath component.

STTD:

$$\frac{E_S}{N_0} = \sum_{n=1}^{N} \frac{SF \cdot P_i \cdot \dfrac{g_L(s,i)}{2}\left(g_{FF,1}^1(s,i,n) + g_{FF,2}^1(s,i,n)\right)}{P_N + \displaystyle\sum_{b=1}^{B}\sum_{l=1}^{L} P_b^{Total} g_L(b,i)\frac{1}{2}\left(\begin{array}{c}g_{FF,1}^1(b,i,l)+... \\ ...g_{FF,2}^1(b,i,l)\end{array}\right) - P_s^{Total} g_L(s,i)\frac{1}{2}\left(\begin{array}{c}g_{FF,1}^1(s,i,n)+... \\ ...g_{FF,2}^1(s,i,n)\end{array}\right)} \quad (6.7)$$

For STTD, the expression for the E_S/N_0 is similar to that of 1Tx-1Rx. The only change is the way in which fast fading is modelled. With 1Tx-1Rx, the power gain of each fast fading multipath component is extracted from an independent flat fading process. When STTD is enabled, the power gain of each fast fading multipath component is calculated as the average of the powers of two independent flat fading processes (one per transmit diversity branch, as explicitly written in (6.7)). A similar approach is adopted in [37].

CLTD:

$$\frac{E_S}{N_0} = \sum_{n=1}^{N} \frac{SF \cdot P_i g_L(s,i) \cdot \left| w_1 f_{FF,1}^1(s,i,n) + w_2 f_{FF,2}^1(s,i,n) \right|^2}{P_N + \displaystyle\sum_{b=1}^{B}\sum_{l=1}^{L} P_b^{Total} g_L(b,i)\frac{1}{2}\left(\begin{array}{c}g_{FF,1}^1(b,i,l)+... \\ ...g_{FF,2}^1(b,i,l)\end{array}\right) - P_s^{Total} g_L(s,i)\frac{1}{2}\left(\begin{array}{c}g_{FF,1}^1(s,i,n)+... \\ g_{FF,2}^1(s,i,n)\end{array}\right)} \quad (6.8)$$

For CLTD, the denominator for the E_S/N_0 at each Rake finger remains the same as in STTD. If more than one cell were simulated in detail, the fast variations of the transmitter weights of the surrounding Node-Bs could be included. However, this is not the case, and it is assumed that each surrounding Node-B transmits uncorrelated signals with constant power from each one of the antennas. Thus, the interference power of signals coming from the two diversity antennas at each interfering Node-B is calculated by adding the power of the two diversity branches.

The numerator for the E_S/N_0 at each Rake finger contains the power of the corresponding desired signal multipath component. In order to calculate this, the complex amplitudes of the contributions from each one of the diversity branches are added, including the effect of the complex transmitter weights. Then, the power of the resulting complex signal is calculated.

2Rake:

$$\frac{E_S}{N_0} = \sum_{r=1}^{2} \sum_{n=1}^{N} \frac{SF \cdot P_i g_L(s,i) g_{FF}^r(s,i,n)}{P_N + \sum_{b=1}^{B} \sum_{l=1}^{L} P_b^{Total} g_L(b,i) g_{FF,1}^r(b,i,l) - P_s^{Total} g_L(s,i) g_{FF,1}^r(s,i,n)} \qquad (6.9)$$

The expression for 2Rake is based on the one for 1Tx-1Rx. The E_S/N_0 at each Rake finger connected to each antenna element is calculated as in (6.6). Then, in order to calculate the combined E_S/N_0, the E_S/N_0 values for the different fingers and antennas are summed. The same approach was used in Chapter 5, where it is stated that this expression implicitly assumes that the noise and interference at the output of different Rake fingers connected to the same antenna are uncorrelated, which is an approximation. However, this effect is later accounted for in the AVI tables. Moreover, this expression also assumes that the noise and interference at the output of different Rake fingers connected to different antennas is also uncorrelated. As also stated in Chapter 5, this statement is true for the thermal noise components, and also true for the interference if the antennas are uncorrelated, which is the case in this study.

CLTD+2Rake:

For CLTD at the Node-B and the 2Rake at the UE (CLTD+2Rake), the E_S/N_0 is modelled as:

$$\frac{E_S}{N_0} = \sum_{r=1}^{2} \sum_{n=1}^{N} \frac{SF \cdot P_i g_L(s,i) \cdot \left| w_1 f_{FF,1}^r(s,i,n) + w_2 f_{FF,2}^r(s,i,n) \right|^2}{\begin{array}{c} P_N + ... \\[4pt] \sum_{b=1}^{B} \sum_{l=1}^{L} P_b^{Total} g_L(b,i) \frac{1}{2} \left(\begin{array}{c} g_{FF,1}^r(b,i,l) + ... \\ ...g_{FF,2}^r(b,i,l) \end{array} \right) - P_s^{Total} g_L(s,i) \frac{1}{2} \left(\begin{array}{c} g_{FF,1}^r(s,i,n) + ... \\ g_{FF,2}^r(s,i,n) \end{array} \right) \end{array}} \qquad (6.10)$$

As can be seen, (6.10) combines the modelling issues that have been already commented when introducing the E_S/N_0 expressions for CLTD and 2Rake separately.

6.3.4 Packet scheduling

In this section, the three basic PS algorithms considered for this study are presented. These algorithms must be taken just as basic reference cases, which are useful to benchmark the performance of the different antenna configurations, and identify the different mechanisms that govern the interaction between antenna diversity and PS. For this study, it is assumed that the PS algorithm selects the UE to be served on a TTI basis. Note that one single UE is served in each TTI.

6.3.4.1 Round Robin

In RR, the UEs are served in sequential order, independent of the radio channel conditions for each UE. Hence, the scheduling is conducted blindly, which results in a relatively large variance in the average data rates among the UEs in the cell [107]. With this

algorithm, all the UEs have the same probability to be served, which does not mean that all of them obtain the same throughput, since each of them experiences different channel quality, i.e. UEs in good radio channel conditions are delivered more throughput.

6.3.4.2 Fair Throughput

The FT PS algorithm aims at delivering the same throughput to all the UEs in the cell. This can be done by serving the UE with the lowest delivered average throughput in the past. In this way, the system converges to a situation in which all the UEs are delivered the same throughput. With this PS algorithm, the fairness is obtained at the expense of serving UEs with a poor radio channel more often.

6.3.4.3 Proportional Fair

The PF PS algorithm selects the UE to be served in every TTI, according to a priority measure for each UE, which is expressed as [101]

$$A_i = \frac{R_i}{T_i} \tag{6.11}$$

for UE #i. In (6.11), R_i is the number of bits that UE #i can receive during the next TTI and T_i is the average throughput delivered to UE #i in the past, computed as the total number of bits successfully transmitted to that UE, divided by the time-period where there have been bits to transmit to that particular UE. Note that, in order to calculate R_i, the PS algorithm uses a priori information about the radio channel. The UE with the highest priority is served.

This algorithm aims at distributing the capacity among the UEs so the proportional fair equilibrium is reached. The proportional fair equilibrium is reached if an increase of X percent in throughput of any UE results in a total loss of more than X percent of the total throughput of the remaining UEs [108]. This approach provides an appealing throughput levelling mechanism by introducing a trade-off between cell throughput and fairness. Basically, after the initial convergence mechanisms have stabilised, this PS algorithm aims at scheduling UEs when they experiencing constructive fading, i.e., the selection metric is defined in such a way that the UE with maximum instantaneous normalised channel quality is selected. The aforementioned normalised instantaneous quality measure appears projected into the throughput dimension, in order to account for the non-linearity between E_S/N_0 and throughput caused by the use of higher order modulation schemes [109]. As a consequence, provided that all the UEs enjoy the same dynamic range, this PS algorithm provides a proportional fair distribution of resources among the UEs. In addition, the system throughput is enhanced by the fact that the UEs are served when they are experiencing constructive fading, which results in the so-called multi-user diversity gain [107].

6.3.5 Admission control

Whenever a HSDPA UE is generated, it can be admitted or blocked, depending on whether the maximum number of UEs that can be admitted in the service queue has been reached or not. Thus, the admission control criterion is very simple. Let N be the number of active UEs already being served in the cell. Then, a new UE can be admitted in the cell if

$$N < N_{MAX}, \qquad\qquad (6.12)$$

where N_{MAX} is set as a simulation parameter.

6.3.6 Measurement and feedback errors

The LA process, the reporting of CLTD weights and the operation of the proportional fair PS algorithm rely on measured information of the instantaneous radio channel experienced by the UEs. For LA and PS, this information is included in the CQI reports sent by the UEs, while in CLTD the UE estimates the optimum transmission weights and feeds them back to the Node-B.

The generation of the simplified CQI report, as introduced in Section 6.3.2, includes a lognormal distributed error to account for measurement imperfections at the UE. Similarly, the channel estimate for calculation of the optimum CLTD weight is also assumed to include a lognormal distributed channel estimation error. In this study, the standard deviation of the error for both CQI reports and channel estimation for derivation of the CLTD weight is assumed to equal 1dB, which is in line with the assumptions utilised in [109].

The CQI report is sent by the UE on the uplink high speed dedicated physical control channel (HS-DPCCH), while the CLTD weights are sent by the UE on the uplink dedicated physical control channel (DPCCH). Unfortunately, these uplink channels are not error free. For this study, the CQI reports are just added the aforementioned lognormal error, and no feedback error is considered. However, for the transmission of the CLTD weights (which also include a lognormal error in the channel estimates for calculation of the weights) the error probability of the uplink DPCCH is taken into account. For each slot, a random number between 0 and 1 is generated. If the number is below the error probability, the wrong set of CLTD weights is applied for downlink transmission. In this respect, it has to be pointed out that the UE is assumed to be able to conduct perfect antenna verification [33]. This means that, even though the wrong weights are applied, the UE is still able to estimate the radio channel for signal reception.

6.3.7 Feedback delays

Signalling delays for reporting of CLTD weights and CQI reports from the UEs are also included in the simulator. The delay figures given as parameters for the simulation campaigns must be interpreted in the following way:
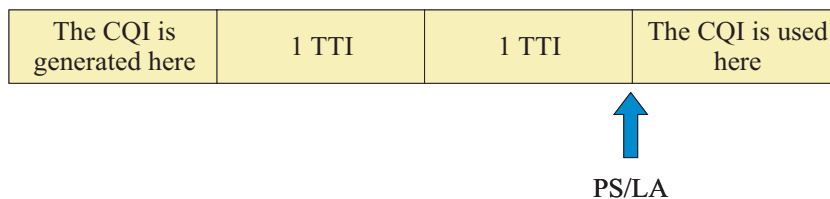
Figure 6.6: Example of CQI delay = 2 TTIs.
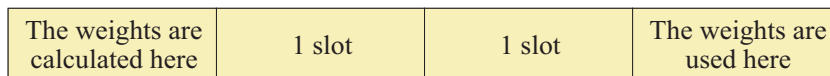
Figure 6.7: Example of CLTD delay = 2 slots.

6.3.8 Traffic modelling

A Poisson distributed call generation process is simulated. Whenever a new call is generated, the UE position is selected uniformly distributed within cell #11. Each call is assumed to consist of 100 kbits, which have to be transmitted to the UE. When the payload is successfully transmitted, the call is terminated.

The simulator offers the possibility to drop those UEs in very poor radio channel conditions. In this context, the dropping criterion is very simple: after the UE has been in the system for a period larger than T_{min}, the UE is dropped if the overall packet call throughput falls below a certain minimum R_{min}. By default, T_{min} and R_{min} are set to 10 seconds and 10kbps, respectively.

6.3.9 Default simulation parameters

The default simulation parameters are summarised in Table 6.3. At this point, it is convenient to show the CDF of the G factor that has been collected for the proposed set of parameters and simulation assumptions (see Figure 6.8). The presented distribution matches the one presented in [104] well.
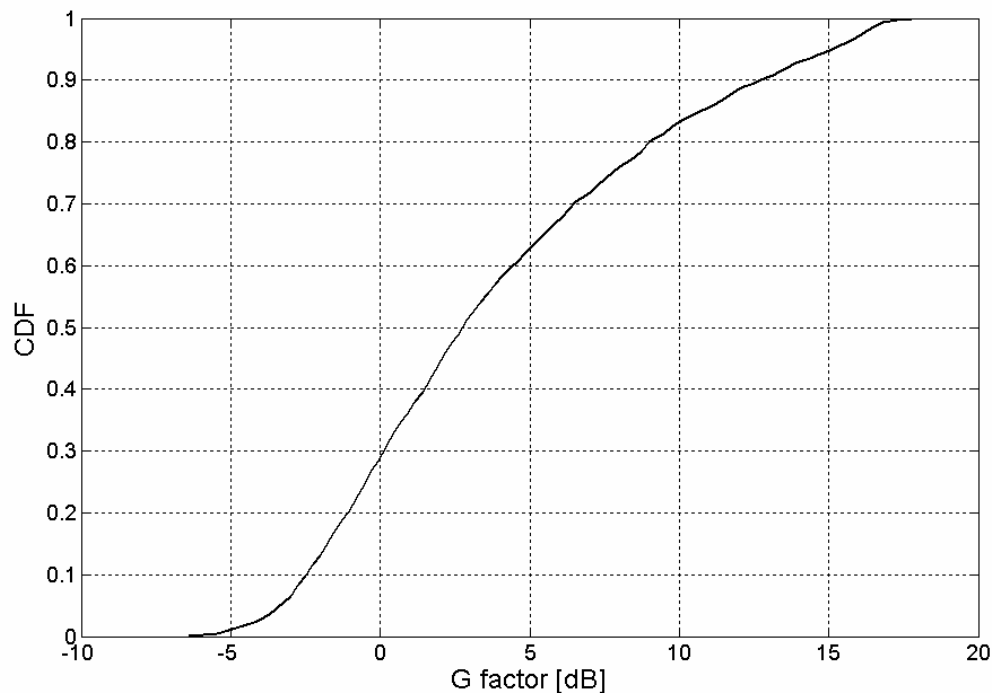

Figure 6.8: CDF of the G factor for the proposed set of parameters and simulation assumptions.

Table 6.3: Default simulation parameters.

Parameter	Value
Distance between sites	2000 m
Path loss exponent	3.5
PDP of the radio channel	Pedestrian A
Std of shadow fading	8 dB
UE speed	3 kmph
Max. transmit power at the Node-B	20 W
Power for HS-PDSCH transmission	9 W
Maximum number of HS-PDSCH codes	7
Max. number of active UEs in the cell[17]	32
Payload of each UE	100 kbits
Method for retransmissions	Chase combining
Delay for retransmissions	6 TTIs
Max number of retransmissions	6
Number of SAW channels	6
LA delay	2 TTIs
PS delay	2 TTIs
Delay for CLTD	2 slots
Error probability of the uplink feedback	4%
Antenna verification	Ideal

---

[17] Defined as the maximum number of UEs that can be queued in the Node-B so that the PS algorithm serves them according to the corresponding criteria. It corresponds to N_{MAX} in (6.12).
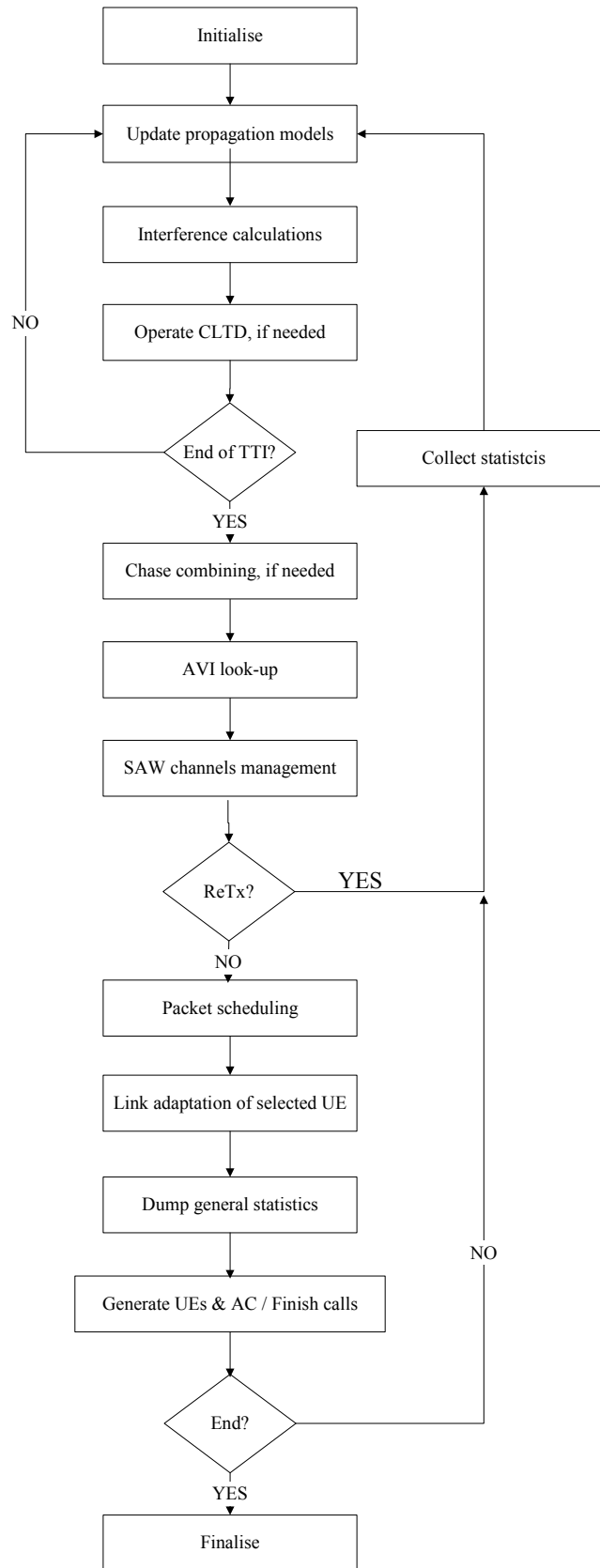
Figure 6.9: Simplified flow chart of the simulation tool.

6.4 Simulation results

This section begins by analysing the HSDPA cell capacity[18] for Pedestrian A at 3 kmph, under all the considered Tx/Rx diversity techniques and PS algorithms. These first simulations are run with a very large blocking probability (i.e. in an overload scenario), so that there are always 32 active UEs in the cell (see Table 6.3). In this way, it is easier to show how the PS algorithm delivers different throughput to UEs according to their G factor. In simulations with low blocking probability, such analysis is more complex, since the number of active UEs in the cell is time varying, which makes the individual UE throughput depend on the instantaneous number of active UEs in the cell, i.e. on the temporal load variations.

Afterwards, further analysis is conducted in order to assess the dependency of the HSDPA cell capacity gain on the maximum allowed number of active UEs in the cell, the UE speed and the multipath propagation environment.

In the end, after analysing the system performance and the impact of all the aforementioned effects in a situation with very high blocking probability, the basic case (Pedestrian A at 3 kmph) is selected for a more detailed analysis, in which the outage level (defined as the proportion of UEs that are dropped, blocked or obtain less than a certain throughput value) is included as an extra dimension.

6.4.1 Results for Pedestrian A and 3 kmph

The HSDPA cell capacity for an overload scenario is summarized in Table 6.4 for the different simulations cases.

Before discussing the results for different antenna configurations with more detail, it is convenient to show the relationship between the experienced average E_S/N_0 per TTI and the throughput that can be achieved if ideal LA is performed, constraint to the set of allowed MCSs and the maximum number of HS-PDSCH codes. Such curve is depicted in Figure 6.10 for Pedestrian A at 3 kmph and 7 HS-PDSCH codes. Shannon's capacity curve is also included as an upper bound for comparison[19]. Both curves follow the same logarithmic trend, and it can be seen how the achievable throughput saturates for E_S/N_0 values larger than 20 dB, due to the fact that, at this E_S/N_0, the maximum number of allowed HS-PDSCH codes are already used with the highest MCS, which does not allow higher throughput, even though larger E_S/N_0 values are experienced.

---

[18] In this context, HSDPA cell capacity refers to the throughput delivered with the resources (power and HS-PDSCH codes) allocated to HSDPA.

[19] Note that Shannon's equation is particularised for the case under study. Thus, the bandwidth is set to 5 MHz, and the wideband signal quality (before despreading) equals the E_S/N_0 divided into the spreading factor (16 in the case of HSDPA)

Table 6.4: Results for Pedestrian A @ 3 kmph.

Scheme	RR			PF			FT		
	HSDPA cell capacity [Mbps]	Gain over 1Tx-1Rx	Gain over RR	HSDPA cell capacity [Mbps]	Gain over 1Tx-1Rx	Gain over RR	HSDPA cell capacity [Mbps]	Gain over 1Tx-1Rx	Gain over RR
1Tx-1Rx	0.944	0%	0%	1.789	0%	90%	0.648	0%	-31%
STTD	1.063	13%	0%	1.662	-7%	56%	0.876	35%	-18%
CLTD	1.378	46%	0%	2.003	12%	45%	1.187	83%	-14%
2Rake	1.722	82%	0%	2.313	29%	34%	1.485	129%	-14%
CLTD+2 Rake	2.106	123%	0%	2.471	38%	17%	1.949	201%	-7%

As can be seen, the depicted curves are not linear, but logarithmic. This means that a certain E_S/N_0 gain is mapped into throughput gain in a more spectral efficient manner when the system is operated at low E_S/N_0 values. Let us show an example from the curve for Pedestrian A. When E_S/N_0=2 dB, a 3 dB E_S/N_0 gain is mapped into a throughput gain of 133%. However, when E_S/N_0=17 dB, the same E_S/N_0 gain yields a throughput gain of 50%. This is due to the fact that large E_S/N_0 values force the use of 16QAM, which is less spectral efficient compared with QPSK. This non-linearity between E_S/N_0 and throughput is of paramount importance when evaluating the gain from Tx/Rx diversity, since it is the reason why UEs in poor channel conditions (i.e. with low E_S/N_0 values) map the E_S/N_0 gain into a throughput gain in a more spectral efficient manner. At this point, it is important to emphasise that the presented results are influenced by the underlying assumptions, especially by the utilised AVI tables. The use of different AVI tables with the same propagation environment would have implied that the aforementioned non-linear relationships are exploited at different operation points, which will impact the use of the different MCSs and, therefore, will affect the spectral efficiency when mapping E_S/N_0 gain into throughput gain. Nonetheless, although different specific performance figures will be reported when different AVI tables are used, the main trends and conclusions described here are expected to remain unchanged.
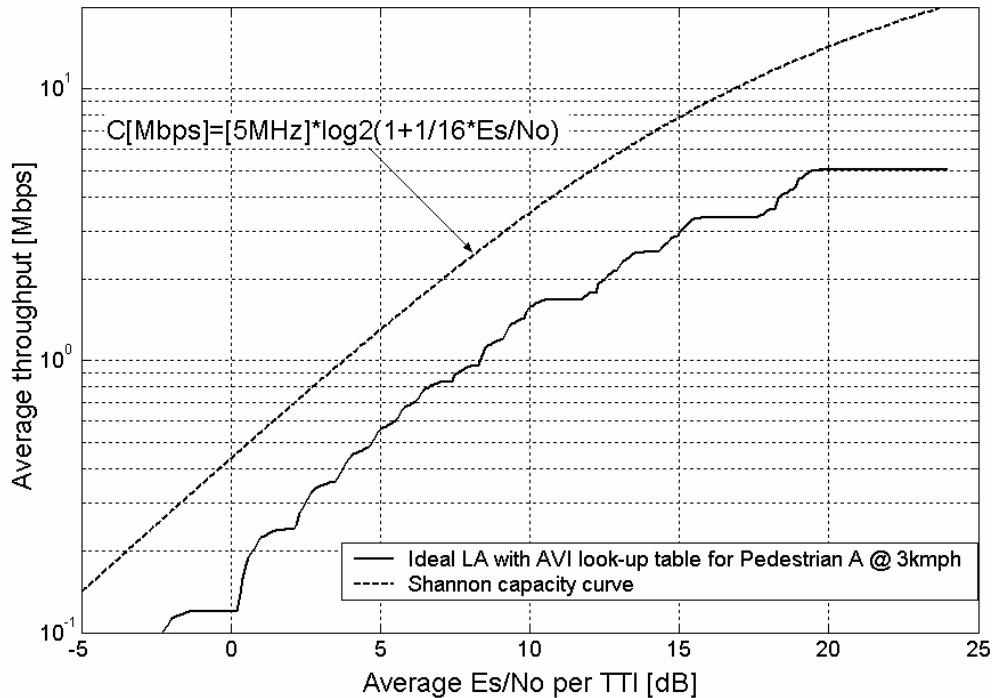
$$C[Mbps] = [5MHz]*log2(1+1/16*Es/No)$$

Figure legend: Ideal LA with AVI look-up table for Pedestrian A @ 3kmph; Shannon capacity curve.

Average throughput [Mbps] vs Average Es/No per TTI [dB]

Figure 6.10: Average Es/No per TTI vs. achievable throughput. Retransmission not considered.

6.4.1.1 Results for 1Tx-1Rx

As can be seen in Table 6.4, the PS algorithm yielding the highest HSDPA cell capacity for the 1Tx-1Rx case is PF, due to the fact that this PS algorithm takes advantage of fast information about the state of the radio channel. In fact, PF gives a HSDPA cell capacity gain of 90%, compared with RR. On the other hand, FT is the one providing the lowest HSDPA cell capacity, giving a loss of 31% compared with RR. The reason is that many resources are allocated to UEs under poor channel conditions in order to provide the same throughput to all the UEs in the cell.

This phenomenon is illustrated in Figure 6.11, which shows the average UE throughput as a function of the G factor. As it can be seen, FT provides the same average UE throughput for all the G factors (including the low ones), whereas RR does not assign so many resources to UEs with low G factors and, in return, delivers higher average throughput to the UEs with higher G factors. For UEs with very low G factors, PF still provides the same throughput as FT without seriously jeopardising the UE throughput for the rest of the G factors. This is possible because PF uses fast information about the state of the radio channel in order to schedule the UEs when they are experiencing constructive fading.

Figure 6.12 shows the CDF of the UE throughput for the three PS algorithms under study. As can be seen, FT delivers the same throughput to all the UEs, while RR and PF present relatively large variance in the throughput among the UEs in the cell. However, since PF uses information about the instantaneous state of the radio channel, the UEs are delivered higher throughput than with RR.
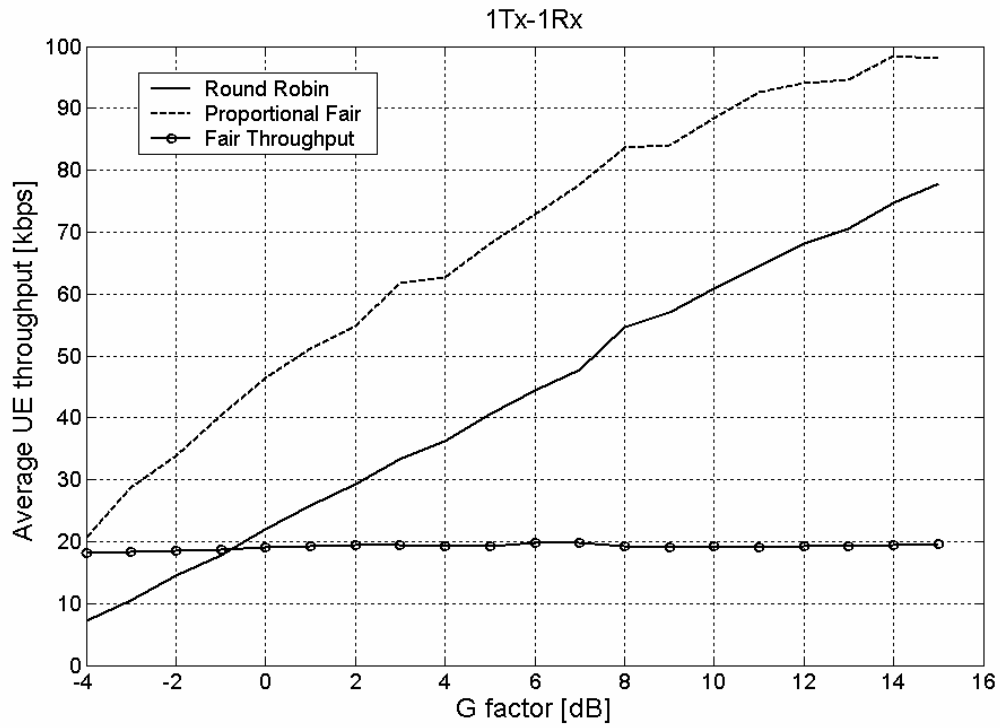
Figure 6.11: Average UE throughput vs. G factor. Pedestrian A @ 3kmph.
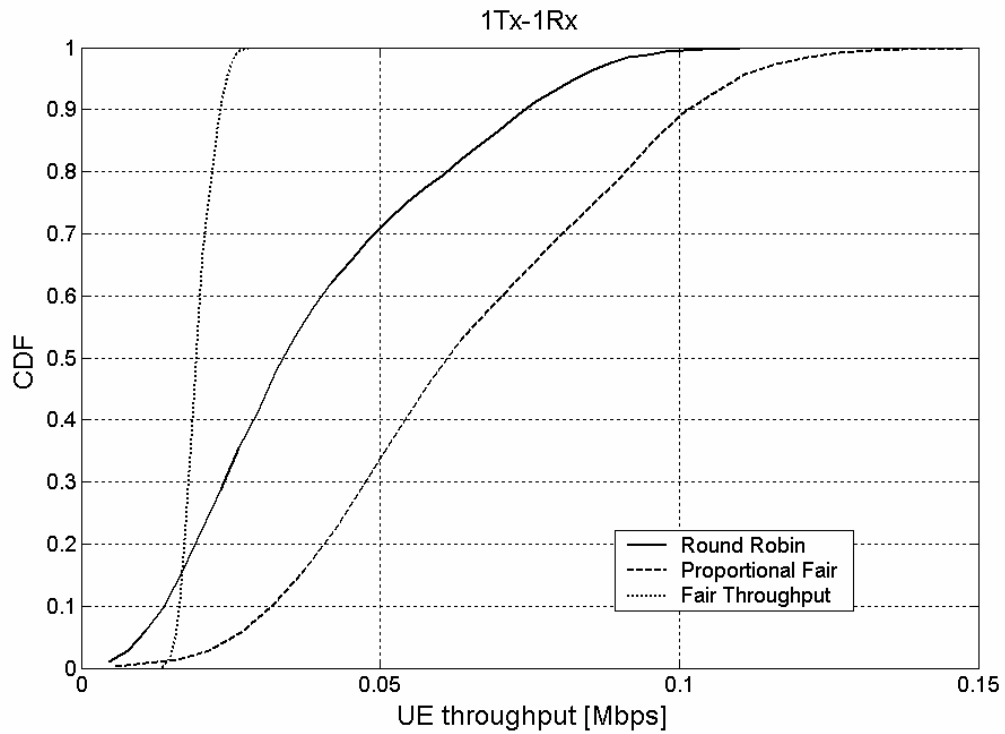

Figure 6.12: CDF of the UE throughput. Pedestrian A @ 3kmph.

In PF, due to the large experienced E_S/N_0 values, the probability of selecting higher MCSs is larger. On the other hand, FT focuses most resources on serving UEs under poor radio channel conditions. Thus, the probability of selecting higher MCSs in FT is lower. This is illustrated in Figure 6.13, which shows the MCS selection probability and a histogram of the number of used HS-PDSCH codes for 1Tx-1Rx with the three PS algorithms under study.

And last, before commenting on the results for the different Tx/Rx diversity techniques, a plot with the effective E_S/N_0 distribution at the shared channel with 1Tx-1Rx is presented in Figure 6.14. Similar to the definition of effective fast fading at the shared channel given in Section 6.2, the effective E_S/N_0 at the shared channel at time instant t is defined as

$$\left. \frac{E_S}{N_0}(t) \right|_{Eff} = \frac{E_S}{N_0}[k(t),t], \qquad (6.13)$$

where $E_S/N_0[i,t]$ is the E_S/N_0 of UE #i at time instant t, and $k(t)$ represents the UE that is scheduled at time instant t.
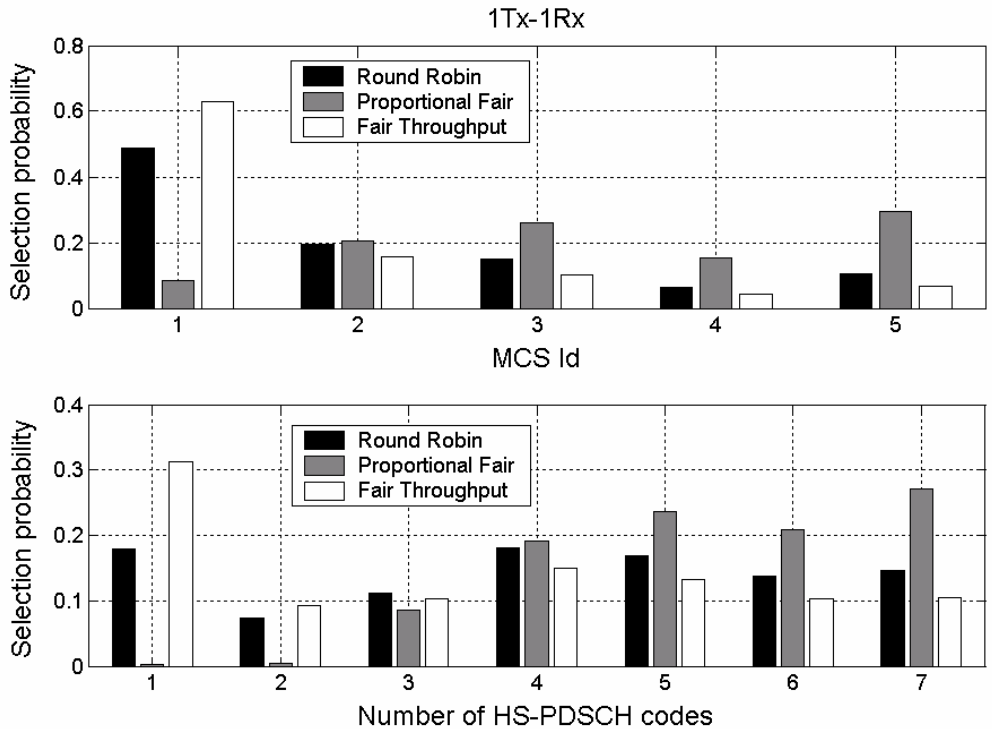
Figure 6.13: MCS selection probability and number of HS-PDSCH codes for 1Tx-1Rx. Pedestrian A @ 3kmph.

As can be seen in Figure 6.14, PF is the PS algorithm with the largest effective E_S/N_0 at the shared channel, since the UEs are scheduled when they are experiencing constructive fading. On the other hand, FT is the PS algorithm with the lowest effective E_S/N_0 at the shared channel, since UEs in poor channel conditions are served more often.
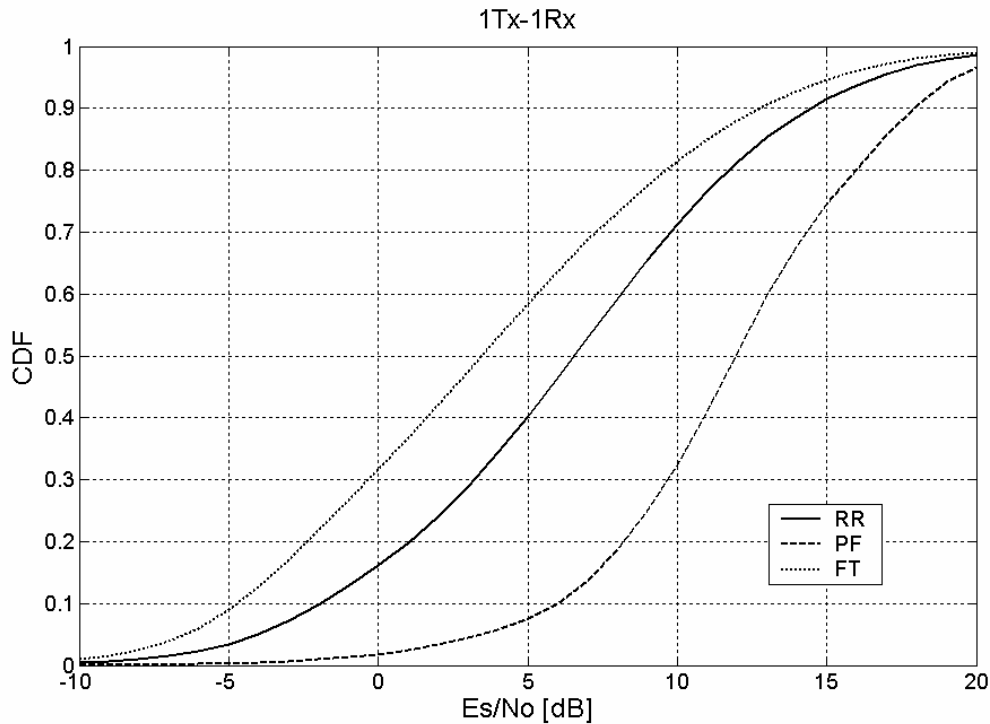
Figure 6.14: CDF of the effective E_S/N_0. Pedestrian A @ 3kmph.

6.4.1.2 Results for STTD

When STTD is combined with RR, a HSDPA cell capacity gain of 13% is experienced, while a loss of 7% can be observed for PF. In the case of FT, the achieved gain equals 35%.

The reason why STTD yields a loss in PF was already presented in Section 6.2, and this result is in line with the studies described in [100] and [102]. Other PS algorithms, such as RR and FT, serve UEs no matter what their channel quality is. Therefore, they also serve UEs when they are in the medium and lowest part of their fading dynamic range, where STTD provides a gain in terms of lower probability of having deep fades. This is not the case for PF, where the PS algorithm avoids transmission during deep fades.

In addition, the reason why STTD yields more capacity gain in FT than in RR is that FT concentrates more resources on serving UEs under poor channel conditions, typically far from their serving Node-B. These UEs operate at lower E_S/N_0 values (see Figure 6.14), which has been shown to facilitate more spectral efficient mapping of E_S/N_0 gain into throughput gain. This behaviour is due to the non-linear relationship between E_S/N_0 and throughput.

Notice however that, in spite of the HSDPA cell capacity loss that PF experiences when STTD is enabled, it is still the PS algorithm with the largest absolute HSDPA cell capacity. Compared with 1Tx-1Rx, the gain of going from RR to PF drops from 90% to 56% when STTD is used. Furthermore, when enabling STTD, the loss due to going from RR to FT drops from 31% to 18%.

6.4.1.3 Results for CLTD

The largest HSDPA cell capacity gain from CLTD is experienced for FT (83%), and the lowest one corresponds to PF (12%). The HSDPA cell capacity gain for RR is in between the two other figures (46%).

PF gives the lowest gain from CLTD due to two reasons: (i) it is the PS algorithm with the largest HSDPA cell capacity in the 1Tx-1Rx case, which means that the system is typically operated at larger E_S/N_0 values and therefore maps the E_S/N_0 gain into HSDPA cell capacity gain in a less spectral efficient manner; and (ii), the reduction of the power gradient of the radio channel provided by CLTD decreases the multi-user diversity gain from PF. Moreover, FT yields the largest HSDPA cell capacity gain due to the same reason that was presented for the STTD case.

In spite of the lower HSDPA cell capacity gain that PF experiences when CLTD is enabled, PF is still the PS algorithm with the largest absolute HSDPA cell capacity. Nevertheless, compared with the 1Tx-1Rx case, the gain of going from RR to PF drops from 90% to 45%, while the loss due to going from RR to FT drops from 31% to 14% when CLTD is used.

6.4.1.4 Results for 2Rake

The deployment of 2Rake receivers yields the highest HSDPA cell capacity gain in FT (129%), while it provides the lowest HSDPA cell capacity gain in PF (29%). The HSDPA cell capacity gain for RR is in between the two previous values (82%).

PF gives the lowest HSDPA cell capacity gain from 2Rake due to the same reasons that were presented for CLTD. Similarly, the reasons why FT experiences the highest HSDPA cell capacity gain from 2Rake are the same ones that were given for CLTD and STTD.

When comparing CLTD and 2Rake, it can be seen that the gain for 2Rake is larger. Though ideal CLTD should yield the same gain as 2Rake (in a flat fading channel), the simulated CLTD mode-1 scheme is subject to the practical impairments that were described in Chapter 2, which make it give a lower gain.

Again, in spite of the lower HSDPA cell capacity gain that PF experiences when 2Rake receivers are deployed, PF is still the PS algorithm with the largest absolute HSDPA cell capacity. Nevertheless, compared with the 1Tx-1Rx case, the HSDPA cell capacity gain of going from RR to PF drops from 90% to 34%, while the loss due to going from RR to FT drops from 31% to 14% when 2Rake receivers are used.

6.4.1.5 Results for CLTD+2Rake

The combination of CLTD and 2Rake involves the influence of all the mechanisms and phenomena that have been addressed when discussing each one of them on an individual basis. However, it is well-known that, when two sources of diversity are combined, the resulting gain is lower than just the combination of the two individual gains, i.e. they provide diminishing returns.

The deployment of CLTD+2Rake receivers yields the highest HSDPA cell capacity

gain in FT (201%), while it provides the lowest HSDPA cell capacity gain in PF (38%). The HSDPA cell capacity gain for RR is 123%.

In spite of the lower HSDPA cell capacity gain that PF experiences when CLTD+2Rake is selected, PF is still the PS algorithm with the largest absolute HSDPA cell capacity. Nevertheless, compared with the 1Tx-1Rx case, the gain of going from RR to PF drops from 90% to 17%, while the loss due to going from RR to FT drops from 31% to 7% when CLTD+2Rake is implemented.

Since CLTD+2Rake is the Tx/Rx diversity technique providing the largest HSDPA cell capacity gain, it is illustrative to plot the MCS selection probability and a histogram of the number of used HS-PDSCH codes for the three PS algorithms under study (see Figure 6.15). By comparing these results with the ones depicted in Figure 6.13 (in page 130), it can be observed how the selection probability of the highest MCSs and the number of used HS-PDSCH codes grows when Tx/Rx diversity techniques are deployed.
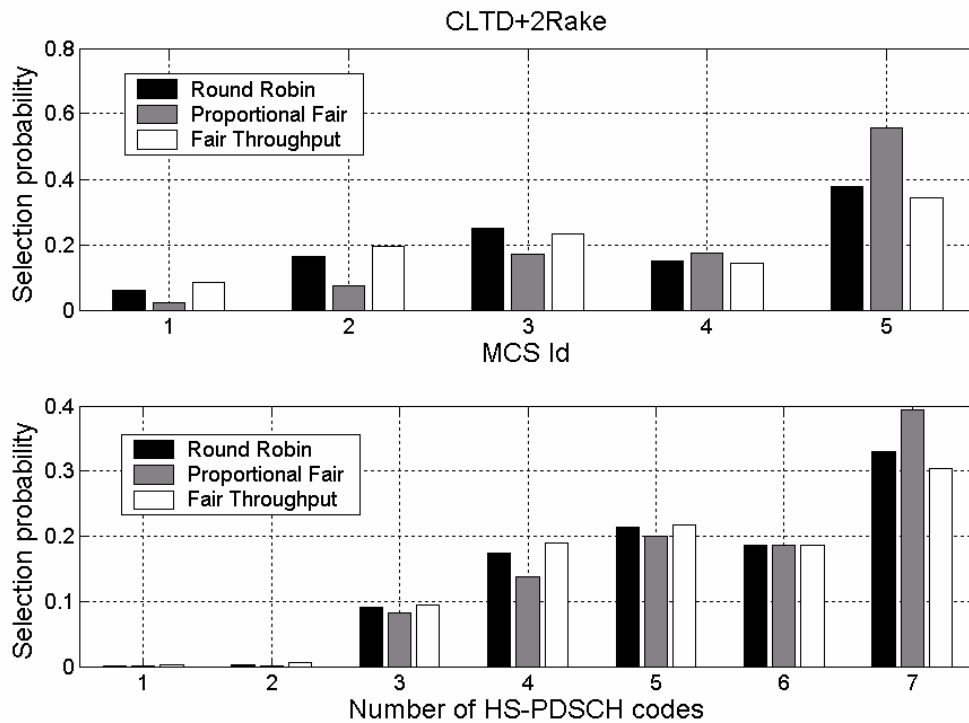

Figure 6.15: MCS selection probability and number of HS-PDSCH codes for CLTD+2Rake. Pedestrian A @ 3kmph.

6.4.2 Throughput gain per UE

The HSDPA cell capacity gain figures shown in the previous section give an indication of how the HSDPA cell capacity improves when Tx/Rx diversity techniques are deployed. However, these numbers do not provide a full picture about what happens in the system, since the HSDPA cell capacity gain does not affect all the regions in the cell in the same manner. In fact, the throughput gain is larger for those UEs at the cell edge, because these UEs typically

have lower E_S/N_0, which allows more spectral efficient mapping of E_S/N_0 gain into throughput gain.

Figure 6.16, Figure 6.17 and Figure 6.18 show the average UE throughput gain as a function of the G factor for all the PS algorithms under study. The reported figures are for Pedestrian A at 3 kmph. For example, CLTD+2Rake yields a HSDPA cell capacity gain of 123% for RR (see Table 6.4, in page 127), while the average UE throughput gain for UEs with G=-4 dB is 320%. As can be seen, for both RR and PF, the average UE throughput gain grows as the G factor diminishes. This is equivalent to a coverage gain, since UEs with low G-factor are typically located far from the serving Node-B.

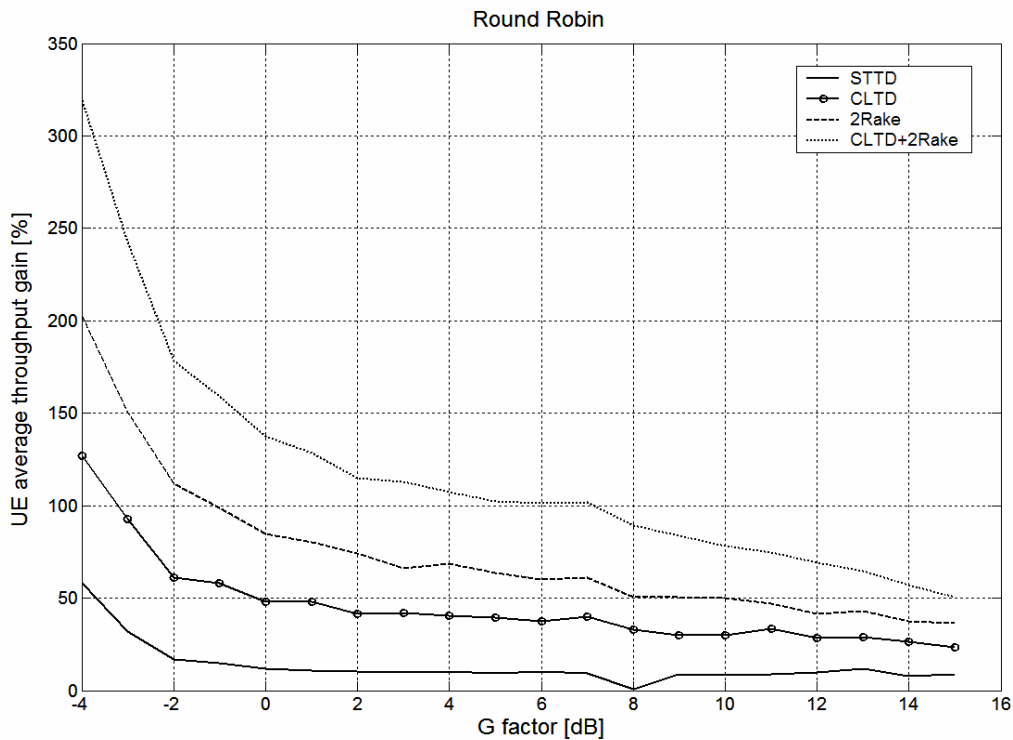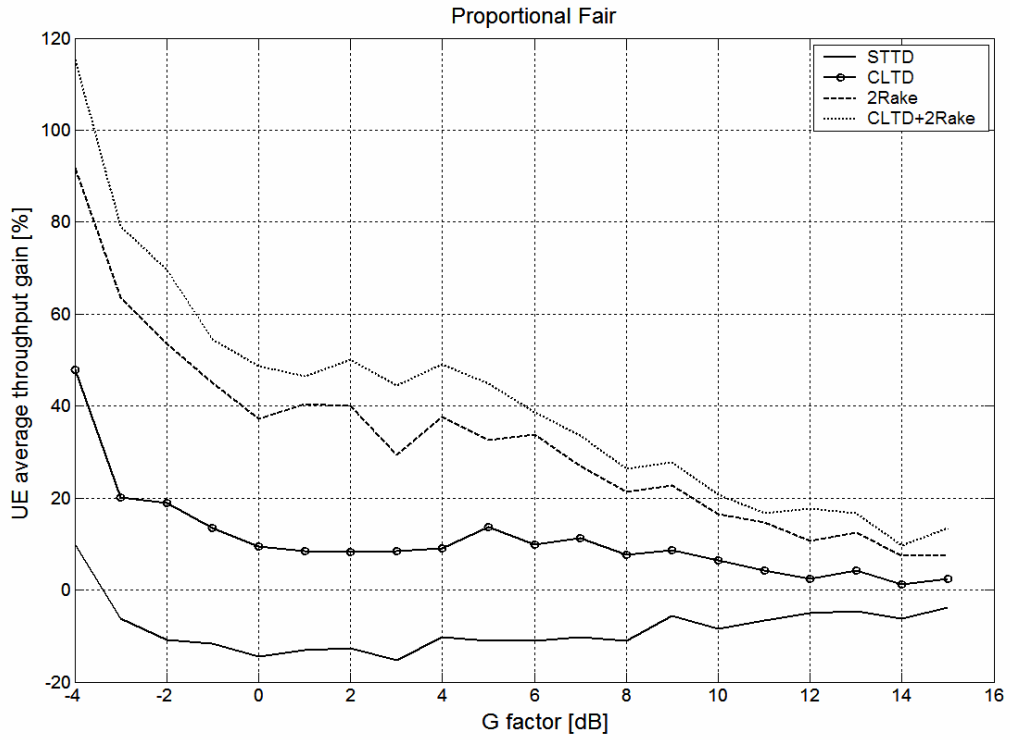**Figure 6.16: Average UE throughput vs. G factor for RR. Pedestrian A @ 3kmph.**

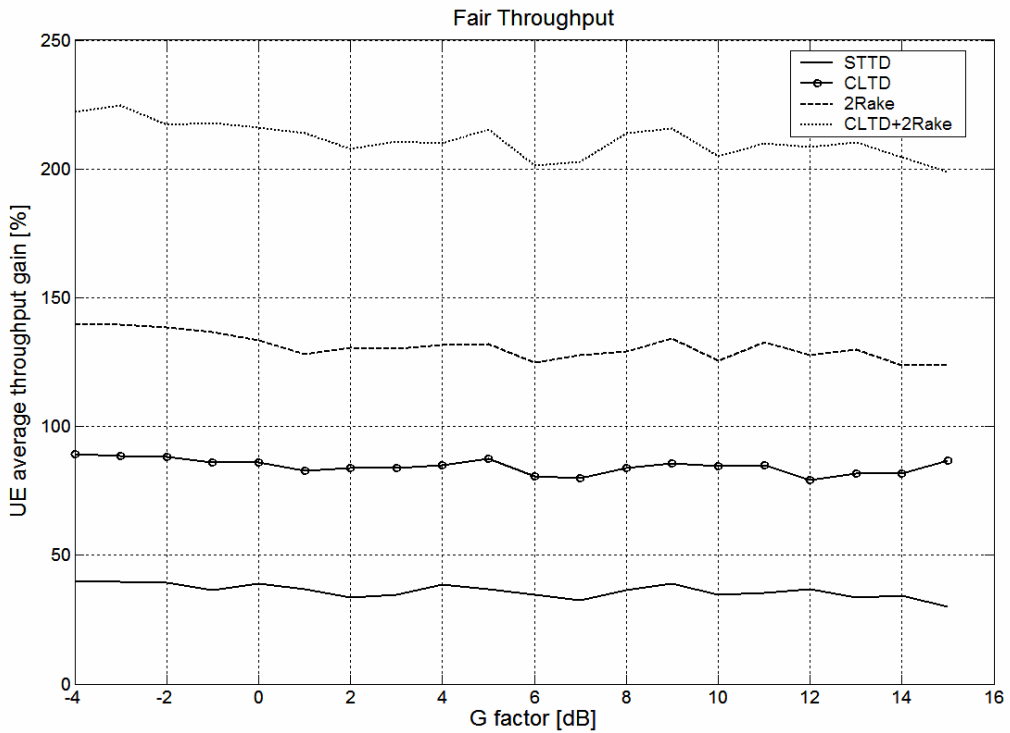**Figure 6.17: Average UE throughput vs. G factor for PF. Pedestrian A @ 3kmph.**

Figure 6.18: Average UE throughput vs. G factor for FT. Pedestrian A @ 3kmph.

Moreover, it can be noticed that the average UE throughput gain is lower for PF, compared with RR. Again, this is due to two reasons:

- In PF, the E_S/N_0 of the scheduled UEs is larger, which implies less efficient mapping of E_S/N_0 gain into throughput gain.

- The multi-user diversity provided by PF prevents the system from taking profit out of the increased diversity order due to Tx/Rx diversity. In fact, STTD yields a loss for almost all the values of the G factor. However, the rest of the Tx/Rx schemes do not give a loss because they do not only provide an increased diversity order, but also an average E_S/N_0 gain.

Furthermore, the same UE throughput gain is observed for all the G factors in the case of FT, which is in coherency with the working principle of this PS algorithm.

6.4.3 Impact of the maximum number of active UEs in the cell

All the simulation results presented so far have been obtained for N_{MAX}=32 (see Table 6.3, on page 124). For the conducted simulations in an overload scenario, this number is considered sufficiently high to provide enough multi-user diversity in the system. Under these circumstances, PF is always very likely to find a UE experiencing constructive fading, and therefore it can yield the significant HSDPA cell capacity gain figures that have been reported.

This section addresses the dependency of the multi-user diversity from PF upon N_{MAX}, with special emphasis on how the deployment of Tx/Rx diversity techniques affects this behaviour. Figure 6.19 shows the HSDPA cell capacity for PF as a function of N_{MAX}. As can be seen, the HSDPA cell capacity increases as N_{MAX} grows, due to the larger multi-user diversity. However, this growth is not indefinite, since the HSDPA cell capacity tends to saturate at some point. Throughout this section, it has been claimed that, for the utilised settings (N_{MAX}=32), STTD yields a loss when used with PF scheduling. In this plot, it can be seen that this statement is true from a N_{MAX} =5 onwards. When N_{MAX} is too low, PF does not have many UEs among which to choose. As a consequence, it cannot schedule UEs only on the top of constructive fades, since it is very often forced to serve UEs also in lower regions of their fading dynamic range. In such regions, STTD is not statistically worse than 1Tx1Rx and, thus, it can provide some gain. The observed trend for STTD is in line with the conclusions presented in Section 6.2.

Figure 6.20 shows the HSDPA cell capacity gain of PF over RR as a function of N_{MAX}. Notice that this gain diminishes when N_{MAX} decreases, due to the lower multi-user diversity. Moreover, as more advanced Tx/Rx diversity techniques are deployed, the gain from having PF becomes lower. Such conclusion has already been pointed out in this study. Furthermore, the information in this curve adds the fact that the gain from multi-user diversity saturates for a lower number of UEs when more advanced Tx/Rx diversity techniques are deployed.
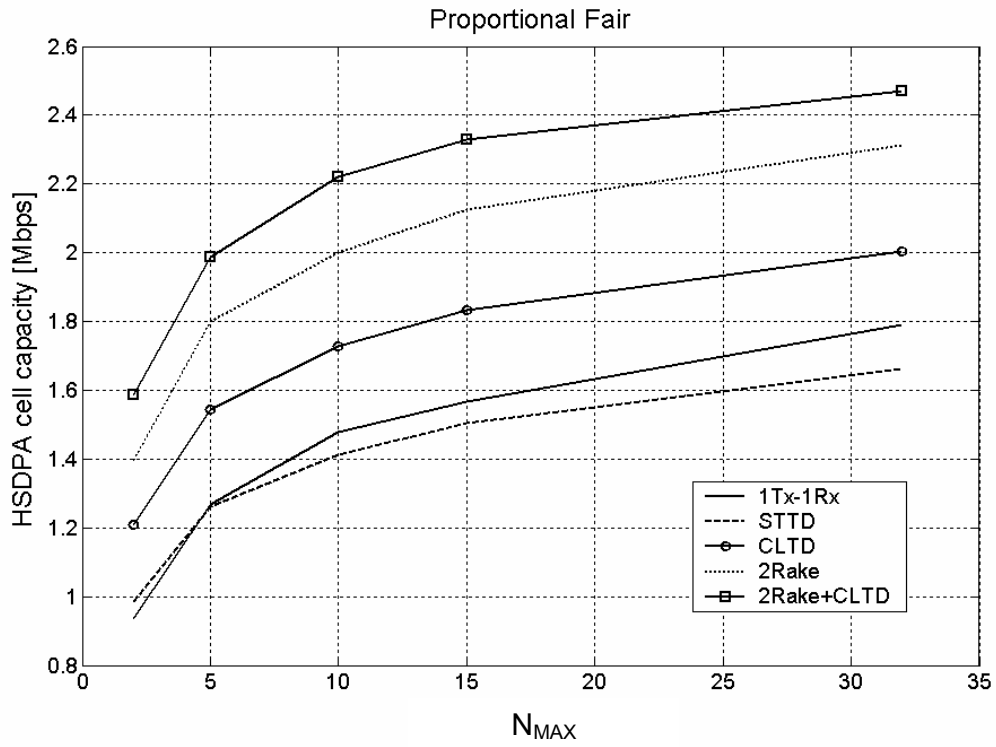
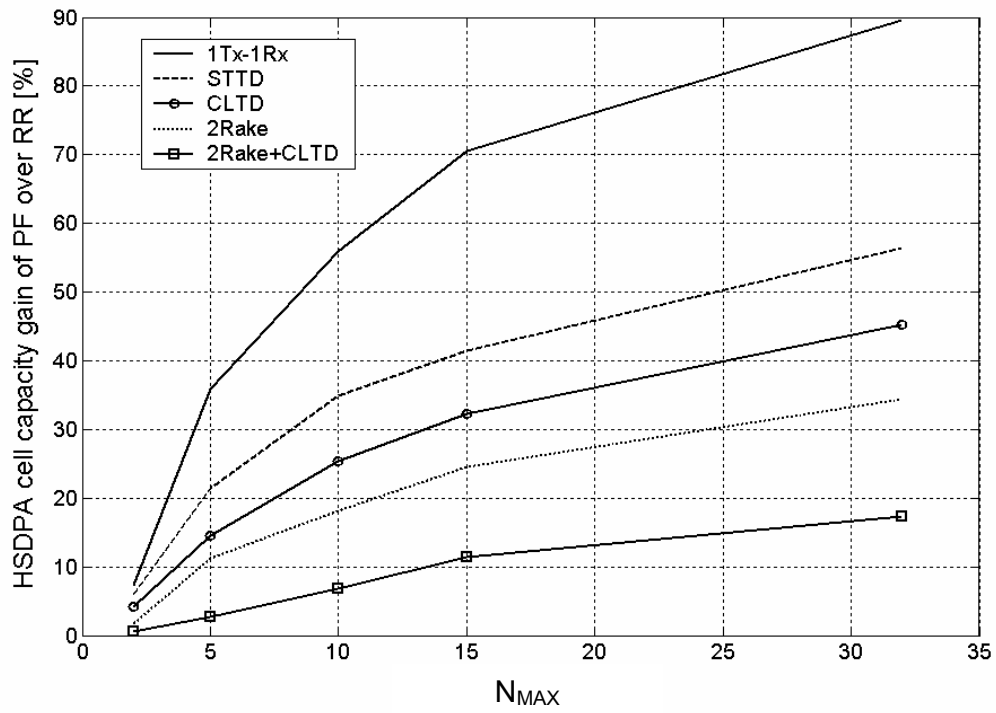**Figure 6.19: HSDPA cell capacity vs. N_{MAX} for PF and Pedestrian A @ 3kmph.**

Figure 6.20: Gain of PF over RR vs. N_{MAX} for Pedestrian A @ 3kmph.

6.4.4 Sensitivity analysis towards the UE speed

As already mentioned in this chapter, the operations of PF scheduling and LA are based on CQI reports, for whose application there is a certain processing and transmission delay. These delays, together with the ones affecting the application of the transmission weights in CLTD, make the HSDPA cell capacity sensitive to the UE speed. Figure 6.21 depicts the HSDPA cell capacity as a function of the UE speed for RR and Pedestrian A. As can be seen, the HSDPA cell capacity degrades when the UE speed increases. Note that, since this curve is depicted for RR, the only delays affecting the system in this case are the ones for LA and the transmission weights of CLTD.
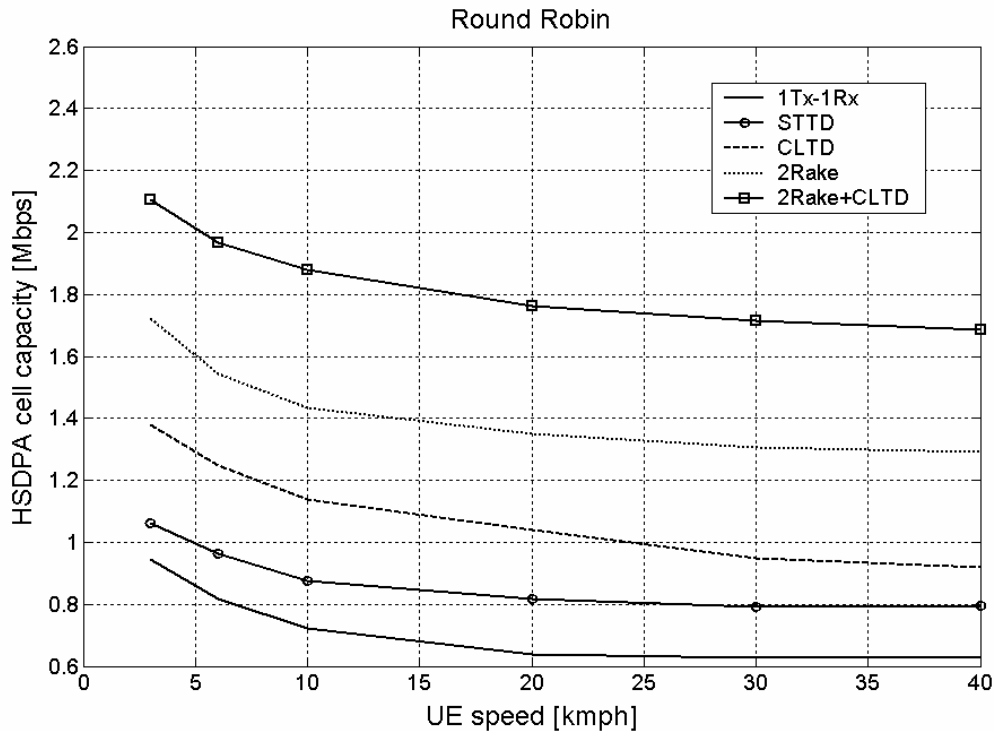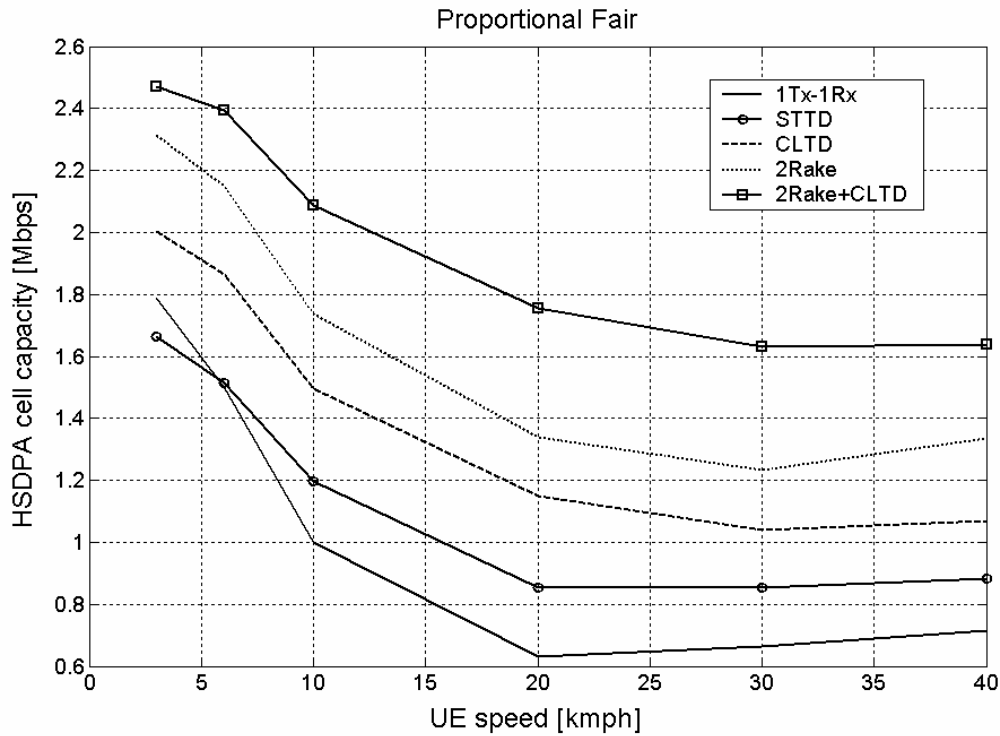

Figure 6.21: HSDPA cell capacity vs. UE speed for RR and Pedestrian A. N_{MAX} = 32.

Figure 6.22 shows the same information for PF, which is also heavily affected by the delays for PS. As can be seen, the degradation of the HSDPA cell capacity when the UE speed increases is larger for PF, since a CQI-delay dependent PS algorithm is introduced. In addition, the difference between the different Tx/Rx diversity techniques, in terms of how heavily they are affected by increasing the UE speed, is more exaggerated. For example, with RR, both 1Tx-1Rx and STTD experience a throughput reduction when the UE speed grows, but this reduction does not prevent STTD from always providing a gain over 1Tx-1Rx. However, for PF there is a change in the tendency when the UE speed grows: For low speeds, STTD yields a loss compared with 1Tx-1Rx. Nonetheless, for larger speeds, the stabilisation of the radio channel provided by STTD leads to a situation in which STTD offers a HSDPA cell capacity gain compared with 1Tx-1Rx. This is due to the fact that the lower power gradient of the radio channel makes the PS algorithm more robust towards the UE speed. Similar trends are observed in [102] and in Section 6.2 of this chapter.

Figure 6.22: HSDPA cell capacity vs. UE speed for PF and Pedestrian A. N_{MAX} = 32.

Table 6.5 summarises the degradation of the HSDPA cell capacity when going from 3 to 40 kmph. For both PF and RR, the antenna scheme experiencing the largest degradation for high UE speeds is 1Tx-1Rx, since it does not provide any mean to reduce the power gradient of the radio channel and, thus, suffers from larger variations in the experienced effective E_S/N_0 values. On the other hand, CLTD+2Rake is always the scheme with the lowest degradation, due to the fact that both CLTD and 2Rake contribute to reduce the power gradient of the radio channel. As a consequence, there are smaller effective E_S/N_0 variations and the net impact of the delays under study is less harmful. Another trend that can be observed is that PF is more sensitive than RR towards the UE speed, since it obtains its gain from scheduling the UEs with the best instantaneous normalised channel quality. When the delays become relatively significant (i.e. at high UE speeds), the capability of the system to track the instantaneous channel quality of the different UEs is seriously jeopardised. Note that that the reported HSDPA cell capacity reduction is dominated by the CQI signalling delay, since the feedback delay for CLTD is smaller. This is the main reason why the relative HSDPA cell capacity loss for CLTD does not significantly exceed the loss for the other antenna configurations with an equivalent diversity order.

6.4.5 Performance in frequency selective channels

Table 6.6 shows the HSDPA cell capacity with all the considered Tx/Rx diversity techniques and PS algorithms for Vehicular A at 3 kmph. For each PS algorithm, the same trends as in Pedestrian A are observed, i.e. CLTD+2Rake is the technique yielding the largest gain, followed by 2Rake, CLTD and STTD. With PF, STTD also gives a HSDPA cell capacity loss in Vehicular A. For comparison with the results in Pedestrian A, see Table 6.4 (page 127).

Table 6.5: HSDPA cell capacity reduction when going from 3 to 40 kmph. Pedestrian A.
$N_{MAX} = 32.$

Antenna scheme	Round Robin			Proportional Fair		
	HSDPA cell capacity @ 3 kmph	HSDPA cell capacity @ 40 kmph	HSDPA cell capacity reduction	HSDPA cell capacity @ 3 kmph	HSDPA cell capacity @ 40 kmph	HSDPA cell capacity reduction
1Tx-1Rx	0.94 Mbps	0.63 Mbps	34%	1.79 Mbps	0.72 Mbps	60%
STTD	1.06 Mbps	0.80 Mbps	25%	1.66 Mbps	0.88 Mbps	47%
CLTD	1.38 Mbps	0.92 Mbps	33%	2.00 Mbps	1.07 Mbps	47%
2Rake	1.72 Mbps	1.29 Mbps	25%	2.31 Mbps	1.34 Mbps	42%
CLTD+2Rake	2.11 Mbps	1.69 Mbps	20%	2.47 Mbps	1.64 Mbps	34%

Table 6.6: Results for Vehicular A @ 3 kmph. $N_{MAX} = 32.$

Scheme	RR			PF			FT		
	HSDPA cell capacity [Mbps]	Gain over 1Tx-1Rx	Gain over RR	HSDPA cell capacity [Mbps]	Gain over 1Tx-1Rx	Gain over RR	HSDPA cell capacity [Mbps]	Gain over 1Tx-1Rx	Gain over RR
1Tx-1Rx	0.712	0%	0%	1.079	0%	52%	0.635	0%	-11%
STTD	0.695	-2%	0%	0.918	-15%	32%	0.652	3%	-6%
CLTD	0.891	25%	0%	1.176	9%	32%	0.857	35%	-4%
2Rake	1.206	69%	0%	1.457	35%	21%	1.158	83%	-4%
CLTD+2 Rake	1.403	97%	0%	1.552	44%	11%	1.359	114%	-3%

With RR and FT, the achieved HSDPA cell capacity gains are lower in Vehicular A, since in this case the radio channel already provides frequency diversity, which prevents Tx/Rx diversity techniques from being able to bring so much diversity gain into the system. However, the gains of CLTD+2Rake and 2Rake in PF are larger for Vehicular A, which is an interesting finding. This is explained by the fact that the absolute HSDPA cell capacity in Vehicular A is lower, which implies that the system is operated at lower E_S/N_0 levels. As a consequence, the mapping of E_S/N_0 gain into throughout gain is more spectral efficient, which explains the observed results. This trend is not observed in the results with RR and FT, since these PS algorithms can benefit more from the Tx/Rx diversity techniques, and in this case the frequency diversity of the radio channel is of paramount importance. In the case of PF, the PS algorithm provides multi-user diversity and is not designed to operate in conjunction with other techniques that increase the diversity order of the system. For illustration, the MCS selection probability for both Vehicular A and Pedestrian A with PF is depicted in Figure 6.23. As can be seen, the probability of using lower MCSs is larger for Vehicular A, since the system is operated at lower E_S/N_0 levels.
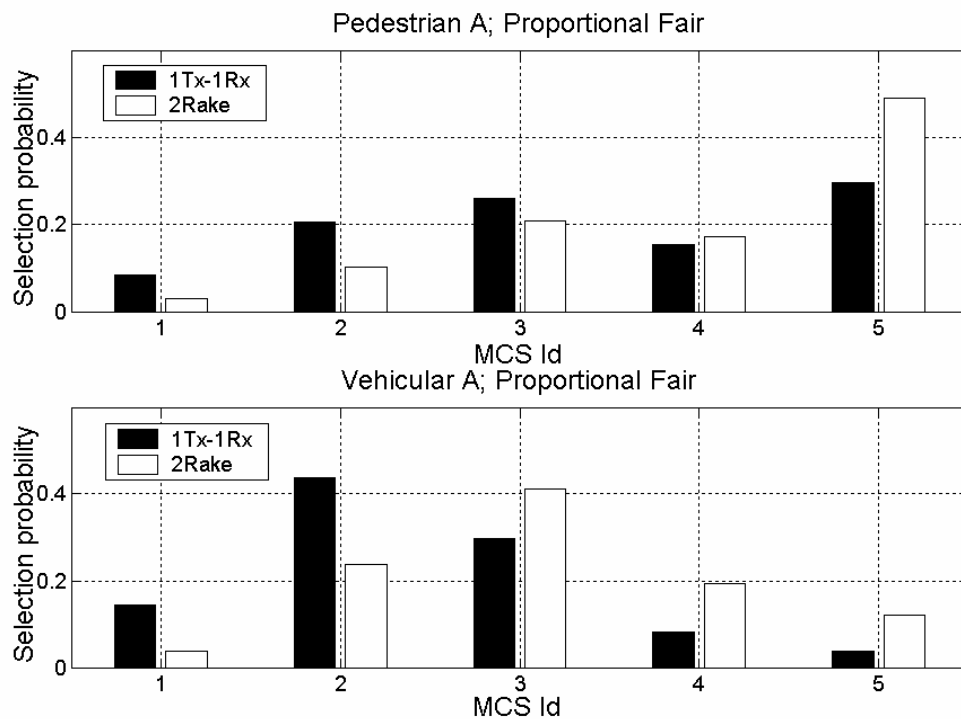
Figure 6.23: MCS selection probability of 1Tx-1Rx and 2Rake with PF scheduling for both Pedestrian A and Vehicular A. N_{MAX} = 32.

6.4.6 Evaluation under coverage constraints

Figure 6.24, Figure 6.25 and Figure 6.26 show the HSDPA cell capacity as a function of the outage in the system for the different PS algorithms and Tx/Rx diversity techniques. In this context, the outage in the system is defined as the proportion of UEs that are either blocked, dropped according to the criterion presented in Section 6.3.8, or admitted in the system but delivered a throughput that is lower than 64 kbps. This metric aims at providing a measure of the quality of service in the system, and the way in which it is defined must be

taken into account when analysing the presented simulation results. For these simulations, the selected environment is Pedestrian A at 3 kmph.

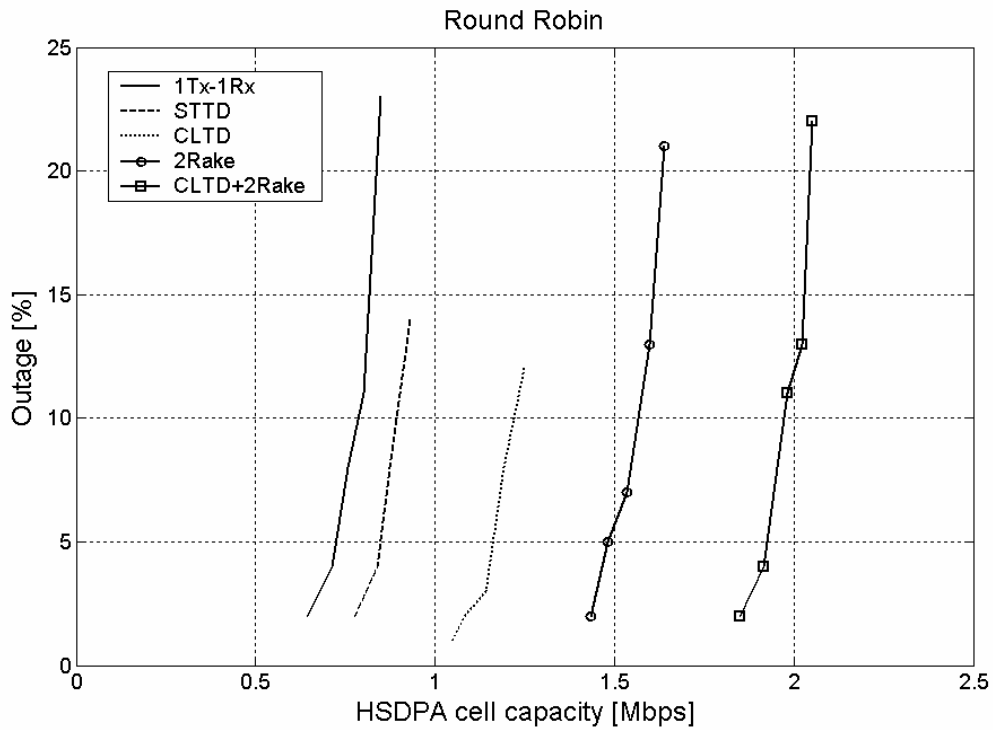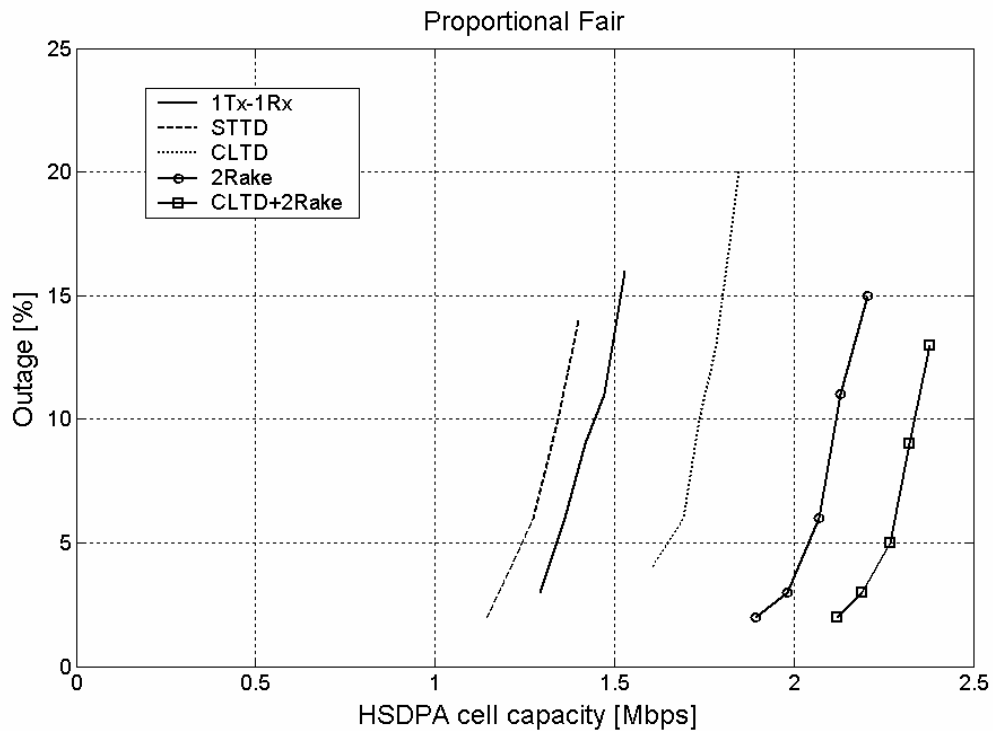**Figure 6.24: HSDPA cell capacity vs. outage for RR. Pedestrian A @ 3 kmph.**

Figure 6.25: HSDPA cell capacity vs. outage for PF. Pedestrian A @ 3 kmph.
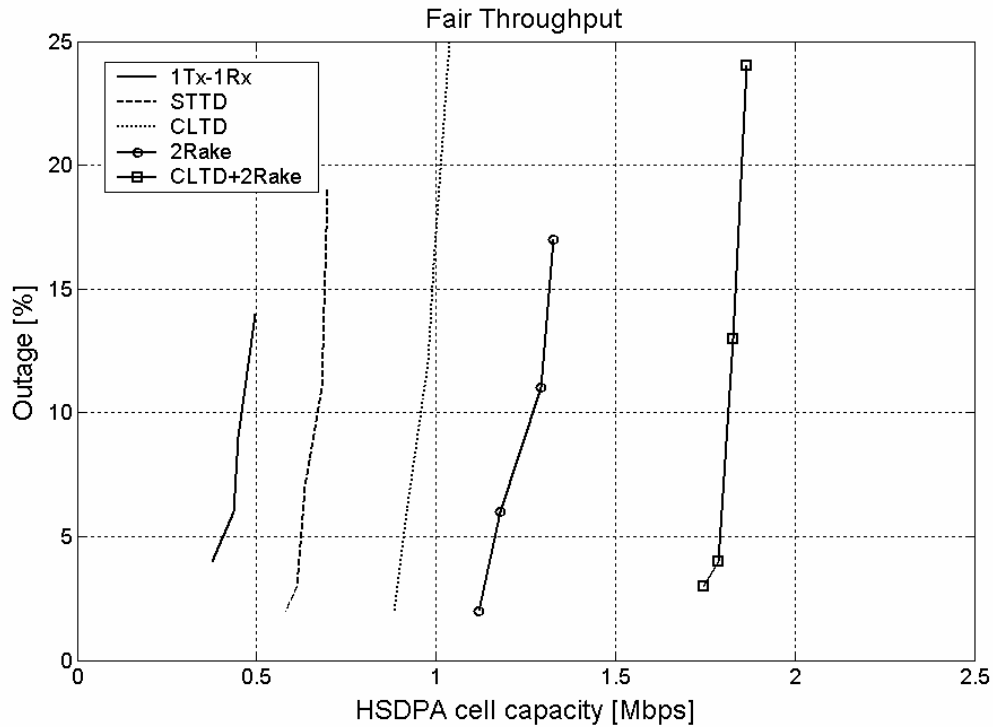
Figure 6.26: HSDPA cell capacity vs. outage for FT. Pedestrian A @ 3 kmph.

The HSDPA cell capacity gain results for the different PS algorithms and Tx/Rx diversity techniques at 10% outage are summarised in

Table 6.7, together with the figures that were presented for the overload scenario. As can be seen, the HSDPA cell capacity gain from Tx/Rx diversity is larger in the case with 10% outage than in the overload scenario.

In order to achieve the specified outage level, the offered load has to be decreased in such a way that there are some periods in which the number of active UEs in the cell is lower than N_{MAX}[20]. During these periods, there are less UEs among which to share the available resources and, as a consequence, the UEs get served more often and are delivered therefore higher throughput. As a result, there are UEs that are able to reach the minimum specified throughput just because of the existence of these periods with a low instantaneous number of active UEs. In an overload scenario, there would be too many UEs among which to share the resources and UEs in poor radio channel conditions would not receive the minimum specified throughput, thereby contributing to increase the outage. Thus, the scenario with 10% outage makes the system put more resources into serving UEs under poor radio conditions so that they do not fall in an outage situation. Since UEs under poor radio conditions are the ones obtaining the highest benefit from Tx/Rx diversity, the HSDPA cell capacity gain from deploying these techniques becomes larger for the scenario with 10% outage.

---

[20] Note that the number of active UEs in the cell is time-varying when the system is not in an overload scenario.

Table 6.7: HSDPA capacity gain at 10% outage. Pedestrian A @ 3 kmph. N_{MAX} = 32.

Scheme	HSDPA cell capacity gain for RR		HSDPA cell capacity gain for PF		HSDPA cell capacity gain for FT	
	Overload	10% outage	Overload	10% outage	Overload	10% outage
STTD	13%	14%	-7%	-8%	35%	46%
CLTD	46%	54%	12%	20%	83%	109%
2Rake	82%	99%	29%	46%	129%	176%
CLTD+2Rake	123%	149%	38%	61%	201%	293%

6.5 Concluding remarks

The HSDPA cell capacity gain due to the deployment of Tx/Rx diversity technique has been analysed under different PS algorithms. In general, it has been shown that there is a strong interaction between the performance of Tx/Rx diversity techniques and the selected PS algorithm.

RR, FT and PF have been compared for all the Tx/Rx diversity techniques and the outcome is that the deployment of these techniques is more beneficial (in terms of HSDPA cell capacity gain) for FT. This is mainly due to the fact that this PS algorithm focuses most of the resources on UEs at the cell edge, with have the poorest channel conditions and therefore allow more spectral efficient mapping of E_S/N_0 gain into throughput gain.

On the other hand, PF is the PS algorithm with the lowest HSDPA cell capacity gain from Tx/Rx diversity. Again, two main reasons have been identified for this behaviour: (ii) the working principle of PF makes it schedule UEs primarily when they are experiencing constructive fading, and in this case it is not very attractive to reduce the power gradient of the radio channel by increasing its diversity order, since the probability of having constructive fading peaks with large E_S/N_0 is reduced; and (ii), PF yields much higher HSDPA cell capacity in the 1Tx-1Rx case, which means that the system is operated at higher E_S/N_0 values, with the

subsequently lower spectral efficiency when mapping of E_S/N_0 gain into throughput gain. Nonetheless, it is important to stress that, although PF is the PS algorithm for which the deployment of Tx/Rx antenna diversity techniques brings the lowest HSDPA cell capacity gain, it is still the PS algorithm that shows the highest absolute HSDPA cell capacity figures for all the antenna configurations.

As an illustrative example of the different HSDPA cell capacity gains that can be obtained from Tx/Rx diversity with different PS algorithms, it can be highlighted that the HSDPA cell capacity gain from CLTD+2Rake in Pedestrian A at 3 kmph equals 201% for FT, while it is 123% and 38% for RR and PF, respectively.

The average UE throughput gain has been analysed as a function of the G factor, and the conclusion is that the UEs at the cell edge obtain much larger throughput gain that the ones in the vicinity of the serving Node-B. As a consequence, the benefits of Tx/Rx diversity techniques can be also interpreted as coverage gain. For example, in Pedestrian A at 3 kmph, CLTD+2Rake yields a HSDPA cell capacity gain of 123% for RR, while the average UE throughput gain for UEs with G=-4 dB is 320%.

A sensitivity analysis towards the UE speed has been conducted. For this matter, PF and RR have been compared, and the outcome is that PF is much more sensitive than RR to the UE speed. The reason for this is that RR does not require any fast information of the instantaneous state of the radio channel in order to conduct the scheduling, while this is not the case for PF. Another important finding is that the deployment of Tx/Rx diversity techniques makes the system more robust towards the UE speed, i.e., towards the negative impact of the delays, due to the fact the it reduces the power gradient of the radio channel. For example, in Pedestrian A at 3 kmph, STTD gives a loss of 7% compared with 1Tx-1Rx for PF, due to the degradation of the channel conditions on top of the constructive fades for STTD. However, as the UE speed grows, the extra robustness against speed provided by STTD makes PF perform better to such an extent that STTD starts giving a gain over 1Tx-1Rx. In fact, for Pedestrian A and PF, STTD starts providing a HSDPA cell capacity gain for UE speeds larger than 6 kmph. The trends presented here have been confirmed by the results of a simple theoretical study that analyses the gain from STTD when a fast quality based PS algorithm is used.

In the end, the HSDPA cell capacity has been shown as a function of the outage for all the considered PS algorithms and Tx/Rx diversity techniques. The outcome is that, although the main trends remain the same, the HSDPA cell capacity gain is larger when the system is operated at lower outage numbers, due to the fact that lower outage specially benefits those UEs with lower G factor, which are the ones obtaining the largest throughput gains from Tx/Rx diversity. For example, in Pedestrian A at 3 kmph and with 10% outage, the capacity gain from deploying CLTD+2Rake with RR, PF and FT is 149%, 61% and 293% respectively, while it is 123%, 38% and 201% in an overload scenario.

Of course, the presented performance figures are significantly influenced by the utilised AVI tables. The use of different AVI tables with the same propagation environment would imply that the aforementioned non-linear relationships are exploited at different operation points, which will impact the use of the different MCSs and, therefore, will affect the spectral efficiency when mapping E_S/N_0 gain into throughput gain. This is specially important here, since AVI tables generated for the 1Tx-1Rx case have been used for all the Tx/Rx antenna diversity schemes under consideration. Therefore, it is proposed as a natural follow-up of this work to repeat the analysis with AVI tables that are generated specifically for each considered antenna configuration. Nevertheless, although different specific performance figures will be

reported when different AVI tables are used, the main trends and conclusions described here are expected to still remain valid.

Moreover, another interesting follow-up for this work is to conduct the system evaluation putting more attention on higher layer protocols, e.g. TCP. Some of the mechanisms inherent to these protocols may constitute the reason why at a certain moment there are no data to transmit towards a certain UE. As a consequence, this UE cannot be scheduled even though its instantaneous channel conditions are the most appropriate, which will impact the available multi-user diversity in PF and therefore the available capacity gain when deploying Tx/Rx antenna diversity techniques.

Chapter 7

Conclusion

7.1 Preliminaries

The Ph.D. thesis provides an insight into the system level performance gain that can be achieved when advanced antenna concepts are deployed in cellular networks with wideband code division multiple access (WCDMA). The Universal Mobile Telecommunications System (UMTS) has been selected as a case study, and the assessment has been conducted primarily by means of system level simulations, although some theoretical studies have been also performed in order to illustrate and validate the trends that appear in the simulation results.

In general, the use of advanced antenna concepts has been found to yield significant gains in terms of system capacity, though they have also been proven to be beneficial in terms of e.g. coverage gain. Special emphasis has been put on capacity and radio resource management (RRM) considerations.

In this concluding chapter, a summary of the Ph.D. thesis is given. This summary is structured so that each section corresponds to a chapter of the Ph.D. thesis, in which the performance of a certain antenna array (AA) configuration is studied, starting by a short introductory overview of the advanced antenna concepts that have been studied within the framework of UMTS.

7.2 Adaptive antennas in UMTS

When the antenna elements of the AA are correlated and closely spaced, conventional beamforming (CBF) is a feasible technique that provides a capacity gain based on spatial filtering of the interference. In UMTS, CBF can be used at the Node-B for both signal transmission and reception. On the other hand, when the antenna elements are uncorrelated, the use of antenna diversity techniques has a larger potential.

In UMTS, transmit (Tx) diversity is only allowed at the Node-B, i.e. for downlink (DL) operation, and there are two possibilities: open loop Tx diversity (OLTD) and closed loop Tx diversity (CLTD). Both offer an increase in the diversity order. However, CLTD also provides an average signal-to-interference-plus-noise ratio (SINR) gain at the expense of the need for feedback information from the user equipment (UE), which makes the system more sensitive towards the UE speed.

Reception (Rx) diversity is allowed in UMTS for uplink (UL) and DL. When the branch power ratio between the antenna elements equals zero dB, Rx diversity with maximal ratio combining (MRC) yields an M-fold increase of the diversity order and an M-fold average SINR gain, where M is the number of antenna elements.

For HSDPA evaluation, only the Tx diversity techniques that are standardised for the Release 5 of UMTS are considered. In addition, the combination of these Tx diversity techniques with dual antenna Rake receivers with MRC at the UE is also analysed, as a manner to enable multiple-input-multiple-output (MIMO) operation.

7.3 Uplink capacity gain with beamforming AAs at the Node-B

UL power based admission control (AC) algorithms offer an attractive trade-off between capacity and coverage, while automatically taking advantage of the soft capacity gain offered by WCDMA. For CBF, generalisation of UL power based AC algorithms leads to the formulation of a directional power based AC algorithm, which adapts the captured capacity gain to the spatial distribution of the interference, while still maintaining the system stability.

Semi static system simulations for UL dedicated channels have shown that, with four-element AAs, the capacity gain ranges from 170% to 220%, depending on the spatial interference distribution. For a more directional spatial interference distribution, the captured capacity gain is lower. Moreover, the larger capacity gain facilitated by a higher number of antenna elements at the AAs is also automatically detected. For example, a capacity gain of 350% is captured with eight-element AAs and a directional spatial interference distribution like the one for which the four-element AAs give a capacity gain of 170%.

7.4 Downlink capacity gain with beamforming AAs at the Node-B

For DL, the capacity gain of CBF has been evaluated by means of dynamic system simulations for the configuration with a fixed grid of beams and a secondary common pilot channel (S-CPICH) per beam. Such evaluation has been conducted for power controlled dedicated channels (DCHs) and a directional power based AC algorithm has been used.

With no channelisation code restrictions, the capacity gain for circuit switched (CS) connections at 64 kbps is 140% with four-element AAs and Vehicular A. This gain is lower than the one for UL, primarily due to the S-CPICH pilot overhead. With channelisation code restrictions, a code blocking rate of 17% is experienced when one scrambling code per cell is enabled. For Pedestrian A the same scenario yields a code blocking rate of 30%, because Pedestrian A allows better orthogonality among UEs under the same scrambling code and therefore increases the absolute cell capacity. When the soft handover (SHO) overhead increases, the average channelisation code usage per UE grows, which results in a larger code blocking rate. Moreover, a larger number of antenna elements at the AA increases the spatial filtering gain and, therefore, makes the channelisation code blocking problem more severe. In addition, when the connections have a low activity factor, the code blocking rate grows, since the average transmit power per UE is decreased, which increases the number of UEs that could be admitted in the system if there were no channelisation code restrictions. This effect has been experienced for speech traffic with discontinuous transmission (DTX), which yields a code blocking rate of 44% for Vehicular A and four-element AAs.

In order to overcome the code blocking, a solution within the UMTS specifications is analysed, where the cell is split into spatially isolated scrambling code regions. With four-element AAs, there is a marginal penalty of 4-8% associated with this solution due to the lack of orthogonality between signals under different scrambling codes. Assuming an AA configuration with eight antenna elements, the capacity gain with real channelisation code restrictions for Vehicular A and CS connections at 64 kbps equals 150% and 230% for one and two scrambling codes per cell, respectively. It is therefore of paramount importance that Node-Bs with AAs support allocation of multiple scrambling codes in the beam domain in order to preserve the advantage of the spatial filtering gain offered by CBF. For a cell with a four-element AA, 2-3 scrambling codes should be enabled to minimize the code blocking rate to an acceptable level.

7.5 Downlink capacity gain with dual antenna Rake receivers at the UE

The capacity gain from using dual antenna Rake receivers with MRC (2Rake receivers) at the UE has been assessed by means of dynamic system simulations. The study is conducted for CS DL connections over power controlled DCHs. The dependency of the capacity gain on the penetration of UEs with 2Rake receivers is non-linear, which has been justified theoretically. At 100% penetration and without channelisation code restrictions, the capacity gain from 2Rake without SHO is larger for Pedestrian A (294% with a block error rate – BLER– target of 1%) than for Vehicular A (183%), since Vehicular A provides frequency

diversity. With SHO, the capacity gain decreases (229% in Pedestrian A and 158% in Vehicular A), due to the diversity gain from SHO. In addition, the capacity gain for higher BLER targets tends to decrease. For example, in Pedestrian A, with a BLER target of 10% and no SHO, the capacity gain is 167% (compared with the 294% capacity gain that is achieved in the same scenario with a BLER target of 1%).

Code blocking appears when deploying 2Rake receivers in a network with one scrambling code per cell. This problem is more severe when the absolute cell capacity is larger, i.e. for Pedestrian A with large BLER targets. For example, in Pedestrian A, with a BLER target of 10% and no SHO, the code blocking rate is 36%. However, the code blocking rate drops to 7% when the BLER target is 1%. Moreover, though activation of SHO decreases the capacity gain, it involves an increase in the code blocking rate, due to the higher average code usage per UE.

Enabling an extra scrambling code per cell when code blocking occurs is not a convenient solution in this case, due to the lack of orthogonality between signals transmitted with different scrambling codes [90]. This was possible in the case of AAs with CBF at the Node-B, since the spatial filtering properties of AAs makes it possible to split the cell into several spatially isolated scrambling code regions. Still, the results presented in this section regarding the achievable capacity gain when there are no channelisation code limitations are considered to be useful and insightful, since they allow estimation of the capacity gain that 2Rake receivers at the UE can provide when used in combination with another technique, e.g. CBF at the Node-B, that enables methods to overcome channelisation code limitations.

7.6 Network performance of HSDPA with Tx/Rx diversity

The benefit from deploying Tx/Rx diversity techniques in HSDPA has been analysed under three different packet scheduling (PS) algorithms: Round Robin (RR), Proportional Fair (PF) and Fair Throughput (FT). The evaluation has been conducted by means of dynamic system simulations, and the benefit from Tx/Rx diversity is measured in terms of HSDPA cell capacity gain and/or increased coverage. In general, it has been shown that there is a strong interaction between the performance of Tx/Rx diversity techniques and the selected PS algorithm.

FT is the PS algorithm with the largest gain from Tx/Rx diversity. This is due to the fact that it concentrates more resources on UEs under poor radio channel conditions, which have been shown to obtain the largest gain from Tx/Rx diversity.

On the other hand, PF is the PS algorithm with the lowest HSDPA cell capacity gain from Tx/Rx diversity. On reason is that UEs are scheduled primarily when they are experiencing constructive fading. In this case, it is not very attractive to reduce the power gradient of the radio channel by increasing its diversity order, since the probability of having constructive fading peaks with large signal strength is reduced. Another reason is that PF yields the highest HSDPA cell capacity in the 1Tx-1Rx case, which means that the system is operated at higher E_S/N_0 values, with the subsequently lower spectral efficiency when mapping of E_S/N_0 gain into throughput gain. As an example of the differences between the PS algorithms, the HSDPA cell capacity gain from CLTD+2Rake in Pedestrian A at 3 kmph equals 201% for FT, while it is 123%

and 38% for RR and PF, respectively. The reference HSDPA cell capacity figures for single antenna Tx and Rx are 648 kbps, 944 kbps and 1789 kbps for FT, RR and PF, respectively. Thus, even though PF is the PS algorithm with the lowest gain from Tx/Rx diversity, it is still the one with the largest HSDPA cell capacity. Note that the HSDPA cell capacity is defined as the throughput delivered with the resources (power and HS-PDSCH codes) allocated to HSDPA. The reported figures are obtained for the case where 45% of the Node-B maximum transmission power and 7 channelisation codes are allocated to HSDPA.

UEs at the cell edge obtain much larger throughput gain that the ones in the vicinity of the serving Node-B. Thus, the benefits of Tx/Rx diversity techniques can be also seen as a coverage gain. For example, in Pedestrian A at 3 kmph, CLTD+2Rake yields a HSDPA cell capacity gain of 123% for RR, while the average UE throughput gain for UEs with G=-4 dB is 320%.

PF is more sensitive than RR to the UE speed, since the fast variations of the radio channel have to be tracked in order to make the scheduling decisions. The deployment of Tx/Rx diversity techniques makes the system more robust towards the UE speed. For example, in Pedestrian A at 3 kmph, STTD gives a HSDPA cell capacity loss of 7% compared with 1Tx-1Rx for PF. However, as the UE speed grows, the extra robustness against speed provided by STTD reduces the performance degradation that PF experiences when the UE speed is increased. For UE speeds higher than 6 kmph STTD provides a HSDPA cell capacity gain over 1Tx-1Rx, which equals e.g. 36% at 20 kmph.

7.7 Future research

As a future study item in connection with Chapter 4 and Chapter 5, it would be interesting to investigate the influence of the delays introduced by layer 3 signalling mechanisms associated to handover and beam switching operations. The studies described in these chapters have been conducted for low UE speeds (3kmph), where it is assumed that these delays have no effect. However, at higher UE speeds, their impact on the system performance is expected to be more significant.

Still regarding the results included in Chapter 4, it would be also interesting to continue the study by simulating non-real time traffic with specific PS algorithms and traffic models in order to achieve a more realistic evaluation of how the code blocking problem affects the system performance when packet traffic is conveyed. This information is of paramount importance in order to dimension the number of scrambling codes that should be simultaneously supported at the Node-B. This suggestion also applies to the study described in Chapter 5. In this case, the code blocking evaluation is maybe not the most important aspect. Instead, the author considers it more interesting to measure how the gain from 2Rake receivers is exploited in the system, i.e. whether it is enjoyed by the network operator, the user owning a 2Rake UE or all the users in the system. The answer to this question is expected to depend on the applied scheduling policy.

Another potential follow-up of the work conducted in Chapter 4 is to fully integrate the space-time model of the radio channel in the simulation set-up in order to suppress the approximations that have been done in connection with the fast fading models. Moreover, studying the joint deployment of the schemes analysed in Chapter 4 and Chapter 5 would be also interesting in order to evaluate how many scrambling codes are necessary when CBF is conducted at the Node-B and 2Rake receivers are implemented at the UE. For such study, it

would be also convenient to utilise specific actual value interface (AVI) tables for UEs in SHO and/or implementing 2Rake receivers.

Regarding the HSDPA studies conducted in Chapter 6, a natural follow-up would be to extend the study to more advanced MIMO schemes. For this purpose, it would be convenient to elaborate specific AVI tables for each analysed antenna scheme. In fact, this could be also done for the antenna schemes already analysed in Chapter 6. In addition, the introduction of higher layer protocols, e.g. TCP, could limit the possibility to schedule a UE at a certain moment due to the lack of data to transmit in its allocated buffer at the Node-B. Since this effect would impact the available multi-user diversity with PF and, as a consequence, the achievable capacity gain from the deployment of advanced Tx/Rx antenna diversity techniques, its investigation is also recommended as a natural follow-up of this work.

References

[1]   H. Holma, A. Toskala (Editors). "WCDMA for UMTS. Radio access for third generation mobile communications", Second edition, John Wiley & Sons, Ltd, England, August 2002.

[2]   J. Laiho, A. Wacker, T. Novosad (editors), "Radio network planning and optimization for UMTS", *John Wiley & Sons, Ltd*, England, 2002.

[3]   S. Verdu, "Minimum probability of error for asynchronous Gaussian multiple-access channels", *IEEE Transactions on Information Theory*, Vol. 32, Issue 1, pp. 85-96, January 1986.

[4]   K.S. Schneider, "Optimum detection of code division multiplexed signals", *IEEE Trans. Aerospace Elect. Systems*, Vol. AES-15, pp. 181-185, January 1979.

[5]   Z. Xie, R.T. Short, C.K. Rushforth, "A family of suboptimum detectors for coherent multi-user communications", *IEEE Journal on Selected Areas in Communications*, Vol. 8, No. 4, pp. 683-690, May 1990.

[6]   P. Patel, J. Holtzman, "Analysis of a simple successive interference cancellation technique in a DS/CDMA system", *IEEE Journal on Selected Areas in Communications*, Vol. 12, No. 5, pp. 796-807, June 1994.

[7]   M.K. Varanasi, B. Aazhang, "Multistage detection in asynchronous code-division multiple-access communications", *IEEE Trans. on Communications,* Vol. 38, No. 4, pp. 5090-519, April 1990.

[8]   J. H. Winters, "Smart antennas for wireless systems", *IEEE Personal Communications*, pp. 23-27, February 1998.

[9]   K.I. Pedersen, P.E. Mogensen and J. Ramiro-Moreno, "Application and performance of downlink beamforming techniques in UMTS", *IEEE Communications Magazine*, Vol. 44, Issue 10, pp. 134-143, October 2003.

[10]   S. Andersson, B. Hagerman, H. Dam, U. Forssén, J. Karlsson, F. Kronestedt, S. Mazur, K. J. Molnar, "Adaptive antennas for GSM and TDMA systems"*, IEEE Personal Communications,* 6(3), pp.74–86, June 1999.

[11]   R. Stridh, M. Bengtsson, B. Ottersten*, "*System evaluation of optimal downlink beamforming in wireless communication"*, IEEE Proc. Vehicular Technology Conference*, Atlantic City,, pp. 343–347, October 2001.

[12]   A. F. Naguib, A. J. Paulraj, T. Kailath, "Capacity improvement with base station antenna arrays in cellular CDMA", *IEEE Trans. on Vehicular Technology*, Vol. 43, No. 3, pp. 691-698, August 1994.

[13]   A. Osseiran, M. Ericson, J. Barta, B. Goransson, B. Hagerman, "Downlink capacity comparison between different smart antenna concepts in a mixed service WCDMA system", *IEEE Proc. 54th Vehicular Technology Conference*, Vol. 3, pp. 1528-1532, September 2001.

[14]   J. H. Winters, "Optimum combining in digital mobile radio with cochannel interference", *IEEE Journal on Selected Areas in Communications*, Vol. 2, No. 4, pp. 528-539, July 1984.

[15]   K. I. Pedersen, P. E. Mogensen, "Evaluation of vector-RAKE receivers using different antenna arrays configurations and combining schemes", *International Journal on Wireless Information*

Networks, Vol. 6, No. 3, pp. 181-195, October 1999.

[16]   K. Hugl, J. Laurila, E. Bonek, "Downlink performance of adaptive antennas with null broadening", *IEEE Proc. Vehicular Technology Conference*, Houston, pp. 872-876, May 1999.

[17]   B. Van Veen, K.M. Buckley, "Beamforming: A versatile approach to spatial filtering", *IEEE ASSP Magazine*, pp. 4-24, April 1988.

[18]   Y. Guo, "Call admission control in multi-class traffic CDMA cellular system using multiuser antenna array receiver", *IEEE Proc. Vehicular Technology Conference*, Tokyo, pp. 365-369, May 2000.

[19]   Y. Hara, "Call admission control algorithm for CDMA systems with adaptive antennas", *IEEE Proc.52nd Vehicular Technology Conference*, Vol. 5, pp. 2518-2522, September 2000.

[20]   A. Yener, R.D. Yates, S. Ulukus, "Joint power control, multiuser detection and beamforming for CDMA systems", *IEEE Proc. Vehicular Technology Conference*, Houston, pp. 1032-1036, May 1999.

[21]   F. Rashid-Farrokhi, L. Tassiulas, K.J. Ray Liu, "Joint optimal power control and beamforming in wireless networks using antenna arrays", *IEEE Trans. on Communications*, Vol. 46, No. 10, pp. 1313-1324, October 1998.

[22]   C. Lee, R. Steele, "Closed-loop power control in CDMA systems", *IEE Proceedings on Communications*, Vol. 143, Issue 4, pp. 231-239, August 1996

[23]   T. Ojanperä, R. Prasad, H. Harada, "Qualitative comparison of some multiuser detector algorithms for wideband CDMA", *IEEE Proc. 48th Vehicular Technology Conference*, Vol. 1, pp. 46-50, May 1998.

[24]   3rd Generation Partnership Project (3GPP), www.3gpp.org.

[25]   3rd Generation Partnership Project, "Radio resource management strategies", TR. 25.922, Version 5.0.0, Available online at www.3gpp.org, March 2002.

[26]   A. Jalali, P. Mermelstein, "Power control and diversity for the downlink of CDMA systems", *Conference records on the 2nd International Conference on Universal Personal Communications*, Vol. 2, pp. 980-984, October 1993.

[27]   3rd Generation Partnership Project, "Physical channels and mapping of transport channels onto physical channels (FDD)", TS. 25.211, Version 4.6.0, Available online at www.3gpp.org, September 2002.

[28]   T. Ojanperä, R. Prasad, "Wideband CDMA for third generation mobile communications", *Artech House*, 1998.

[29]   A. Viterbi, "Principles of spread spectrum communications", Addison-Wesley, 1997.

[30]   F. Adachi, M. Sawahashi, K. Okawa, "Tree-structured generation of orthogonal spreading codes with different lengths for forward link of DS-CDMA mobile radio", *IEE Electronic Letters*, Vol. 33 No. 1, pp. 27–28, January 1997.

[31]   3rd Generation Partnership Project, " Spreading and modulation (FDD)", TS. 25.213, Version 5.2.0,

Available online at www.3gpp.org, September 2002.

[32] M. Hunukumbure, M. Beach, B. Allen, "Downlink orthogonality factor in UTRA FDD systems"*, IEE Electronic Letters*, Vol. 38, No. 4, pp. 196–197, February 2002.

[33] 3rd Generation Partnership Project, "Physical layer procedure", TS. 25.214, Version 5.4.0, Available online at www.3gpp.org, March 2003.

[34] 3rd Generation Partnership Project, "Multiplexing and channel coding (FDD)", TS. 25.212, Version 5.5.0, Available online at www.3gpp.org, June 2003.

[35] K. I. Pedersen, P. E. Mogensen, B. H. Fleury, " Spatial channel characteristics in outdoor environments and their impact on BS antenna system performance ", *IEEE Proc. 48th Vehicular Technilogy Conference* Vehicular Technology Conference, Vol. 2, pp. 719-724, May 1998.

[36] W. C. Jakes, "Microwave Mobile Communications", *IEEE Press*, 1974

[37] S. Parkvall, M. Karlsson, M. Samuelsson, L. Hedlund and B. Goransson, **"**Transmit diversity in WCDMA: link and system level results"**,** *IEEE Proc. 51st Vehicular Technology Conference*, Vol. 2, pp. 864-868, May 2000.

[38] 3rd Generation Partnership Project; Technical Specification Group Radio Access Network. TSG RAN WG1 #21-01-0879. "Increasing MIMO throughput with per-antenna rate control".

[39] G.J. Foschini, "Layered space-time architecture for wireless communication in a fading environment when using multi-element antennas", *Bell Labs Technical Journal*, Autumn, 1996.

[40] J. H. Winters, J. Salz, R. D. Gitlin, "The impact of antenna diversity on the capacity of wireless communication systems", *IEEE Transactions on Communications*, Vol. 42, Issue 234, pp. 1740-1751, February/March/April 1994.

[41] H. Holma, A. Tölli, "Simulated and measured performance of 4-branch uplink reception in WCDMA", *IEEE Proc. 53rd Vehicular Technology Conference*, Vol. 4, pp. 2640-2644, May 2001.

[42] European Telecommunications Standards Institute, "Selection procedures for the choice of radio transmission technologies for the UMTS", TR 101 112 (UMTS 30.03), Version 3.2.0, April 1998.

[43] O. Nørklit, P. C. F. Eggers, J. Bach Andersen, "Jitter diversity in multipath environments", *IEEE Proc. 45th Vehicular Technology Conference*, Vol. 2, pp. 853-857, July 1995.

[44] K. I. Pedersen, P. E. Mogensen, B. H. Fleury, "A stochastic model of the temporal and azimuthal dispersion seen at the base station in outdoor propagation environments", *IEEE Trans. on Vehicular Technology,* Vol. 49, No. 2, pp. 437-447, March 2000.

[45] J.B. Andersen, K.I. Pedersen, "Angle-of-arrival statistics for low resolution antennas", *IEEE Trans. on antennas and propagation*, Vol. 50, No. 3, pp. 391-395, March 2002.

[46] T.L. Fulghum, K.J. Molnar, A. Duel-Hallen, "The Jakes fading model for antenna arrays incorporating azimuth spread", *IEEE Trans. on Vehicular Technology*, Vol. 51, No. 5, pp. 968-977, September 2002.

[47] "Adaptive DCS antenna, the Tsunami project", *Technical Report*, *Celwave R.F.,* March 1996.

[48] A. F. Naguib, A. Paulraj, T. Kailath*,* "Capacity improvement of base-station antenna arrays cellular CDMA", *Conference Record of The Twenty-Seventh Asilomar Conference on Signals,*

Systems and Computers, Vol. 2, pp. 1437 -1441, November 1993

[49]   S.M. Alamouti. "A simple transmit diversity technique for wireless communications", *IEEE Journal on Selected Areas on Communications*, Vol. 16, No. 8, October 1998.

[50]   J. Hämäläinen, R. Wichman, "Closed-loop transmit diversity for FDD WCDMA systems", *Conference Record of the Thirty-Fourth Asilomar Conference on Signals, Systems and Computers*, Vol. 1, pp. 111-115, October 2000.

[51]   D. Gerlach, A. Paulraj, "Spectrum reuse using transmitting antenna arrays with feedback", *IEEE Proceedings of the International Conference on Acoustics, Speech, and Signal Processing*, Vol. 4, pp. 97-100, April 1994.

[52]   K .I. Pedersen, P. E. Mogensen, F. Frederiksen, "Joint directional properties of uplink and downlink channel in mobile communications", *IEE Electronic Letters*, Vol. 35, No. 16, pp. 1311-1312, August 1999.

[53]   K. I. Pedersen, P. E. Mogensen, "The downlink orthogonality factors influence on WCDMA system performance", *IEEE Proc. 56th Vehicular Technology Conference*, Vol. 4, pp. 2061-2065, September 2002.

[54]   T. Hedberg, S. Parkvall, "Evolving WCDMA", *Ericsson Review* nr. 2 2000, available at http://www.ericsson.com/about/publications/review/

[55]   T. Klingenbrunn. "Downlkink capacity enhancement of UTRA FDD networks", *Ph.D. Thesis*. Aalborg University, January 2001.

[56]   J. Hämäläinen, R. Wichman, "The effect of feedback delay to the closed-loop transmit diversity in FDD WCDMA". *IEEE Proceedings of the 12th IEEE International Symposium on Personal, Indoor and Mobile Radio Communications*, Vol. 1, pp. D27-D31, September 2001.

[57]   J. Hämäläinen, R. Wichman, "Feedback schemes for FDD WCDMA systems in multipath environments", *IEEE Proc. 53rd Vehicular Technology Conference*, Vol. 1, pp. 238-242, May 2001.

[58]   3rd Generation Partnership Project, "Tx diversity solution for multiple antennas", TR. 25.869, Version 1.0.0, Available online at www.3gpp.org, February 2002.

[59]   3rd Generation Partnership Project, "Improving HSDPA system throughput with selection transmit diversity", Technical Specification Group Radio Access Network. TSG RAN WG1 #22-01-1126.

[60]   G. Dolmans, L. Leyten, "Performance study of an adaptive dual antenna handset for indoor communications", *IEE Proceedings of Microwaves, Antennas and Propagation*, Vol. 146, No. 2, pp. 138-144, April 1999.

[61]   A. Kuchar, J.P. Rossi, E. Bonek, "Directional macro-cell channel characterization from urban measurements", *IEEE Transactions on Antennas and Propagation*, Vol. 48, No. 2, pp. 137-146, February 2000.

[62]   P. A. Ranta, M. Ventola, H. Berg, R. Wichman, M. Heikkilä, "On the evaluation of diversity reception in mobile terminals", *Proceedings of WPMC-01*, pp. 865-869, September 2001.

[63]   Mika Ventola, Esa Tuomaala, Pekka A. Ranta, "Performance of dual antenna diversity reception in WCDMA terminals", *IEEE Proc. 57th Vehicular Technology Conference*, Vol. 2, pp. 1035-1040, April 2003.

[64]   M. J. Heikkila, P. Komulainen, J.Lilleberg, "Interference suppression in CDMA downlink through adaptive channel equalization", *IEEE Proc. 50th Vehicular Technology Conference*, Vol. 2, pp. 978-982, September 1999.

[65]   C.E. Shannon, "Communication in the presence of noise", *Proceedings of the IRE and waves and electrons"*, pp. 10-21, January 1949.

[66]   A. Hottinen, O. Tirkkonen, R. Wichman, "Multi-antenna transceiver technique for 3G and beyond", John Wiley & Sons, Ltd, England, 2003.

[67]   J. Kuri, P. Mermelstein, "Call admission control on the uplink of a CDMA system based on total received power", *IEEE Proc. International Conference on Communications*, pp. 1431-1436, June 1999.

[68]   S. Kumar, S. Nanda, "High data-rate packet communications for cellular networks using CDMA: algorithms and performance", *IEEE Journal on Selected Areas in Communications*, Vol. 17, No. 3, pp. 472-492, March 1999.

[69]   Z. Dziong, L. Ming, P. Mermelstein, "Adaptive traffic admission for integrated services in CDMA wireless-access networks", *IEEE Journal on Selected Areas in Communications*, Vol. 14, No. 9, pp. 1737-1747, December 1996.

[70]   S. Hämäläinen, H. Holma, A. Toskala, "Capacity evaluation of a cellular CDMA uplink with multiuser detection", *IEEE Proc.4th International Symposium on Spread Spectrum Techniques and Applications*, Vol. 1, pp. 339-343, September 1996.

[71]   Y. Ishikawa, N. Umeda, "Capacity design and performance of call admission control in cellular CDMA systems", *IEEE Journal on Selected Areas in Communications,* Vol. 15, No. 8, pp. 1627-1635, October 1997.

[72]   B. Lavery, D. Everitt, "On the teletraffic characterization of cellular CDMA systems", *IEEE Proc. 43rd Vehicular Technology Conference*, pp. 416-419, May 1993.

[73]   Y. M. Jang, A. Jeehwan, "A connection admission control using transient outage probability in CDMA systems", *IEEE Proc. 52nd Vehicular Technology Conference*, Vol. 3, pp. 1412-1416, September 2000.

[74]   J. Choi, B. Saewoong, "Multiclass call admission control in QoS-sensitive CDMA networks", *IEEE Proc. International Conference on Communications*, Vol. 2, pp. 331-335, 2001.

[75]   K. Kim, Y. Han, C. Yim, K. Jeong, "A call admission algorithm with optimal power allocation for multiple class traffic in CDMA systems", *IEEE Proc. 52nd Vehicular Technology Conference*, Vol. 6, pp. 2666-2671, September 2000.

[76]   K. Kim, Y. Han, "A call admission control with thresholds for multi-rate traffic in CDMA systems", *IEEE Proc. 51st Vehicular Technology Conference*, Vol. 2, pp. 830-834, May 2000.

[77]   C. Y. Huang, R. D. Yates, "Call admission in power controlled CDMA systems", *IEEE Proc. 46th*

Vehicular Technology Conference, Vol. 3, pp. 1665-1669, May 1996.

[78]   J. Mueckenheim, U. Bernhard, H. Pampel, P. Gunreben, **"**Performance evaluation of connection admission control for W-CDMA networks using dynamic system simulations", *Proc. Symposium on Communications and Vehicular Technology*, pp. 174-177, 2000.

[79]   N. Dimitriou, R. Tafazolli*,* "Resource management issues for UMTS ", *IEE Proc. First International Conference on 3G Mobile Communication Technologies*, pp. 401-405, 2000.

[80]   I. Kim, B. Shin, D. Lee, "SIR-based call admission control by intercell interference prediction for DS-CDMA systems", *IEEE Communications Letters*, Vol. 4, Issue 1, pp- 29-31, January 2000.

[81]   Z. Liu, M. E. Zarki, "SIR-based call admission control for DS-CDMA cellular systems", IEEE Journal on Selected Areas in Communications, Vol. 12, Issue 4, pp. 638-644, May 1994.

[82]   H. Holma, J. Laakso, "Uplink admission control and soft capacity with MUD in CDMA", *IEEE Proc. 50th Vehicular Technology Conference*, Vol. 1, pp. 431-435, September 1999.

[83]   Y. Ma, J. J. Han, K. S. Trivedi, "Call admission control for reducing dropped calls in code division multiple access (CDMA) cellular systems", *IEEE Proc. INFOCOM 2000, Nineteenth Annual Joint Conference of the IEEE Computer and Communications Societies*, Vol. 3, pp. 1481 - 1490, March 2000

[84]   J. Outes, L. Nielsen, K. I. Pedersen, P. E. Mogensen, "Multi-cell admission control for UMTS", *IEEE Proc. 53rd Vehicular Technology Conference*, Vol. 2, pp. 987-991, May 2001.

[85]   J. Barta, M. Ericson, B. Goransson, B. Hagerman, "Interference distributions in mixed service WCDMA systems – Opportunities for advanced antenna systems", *IEEE Proc. 53rd Vehicular Technology Conference*, Vol. 1, pp. 263-267, May 2001.

[86]   M. Andersin, Z. Rosverg, J. Zander, "Soft and safe admission control in cellular networks", *IEEE/ACM Transactions on Networking*, Vol. 5, No. 2, April 1997.

[87]   K. I. Pedersen, P. E. Mogensen, "Directional power based admission control for WCDMA systems using beamforming antenna array systems", *IEEE Trans. on Vehicular Technology,* Vol. 51, No. 6, November 2002.

[88]   J. Knutsson, P. Butovitsch, M. Persson, R. D. Yates, "Downlink admission control strategies for CDMA systems in a Manhattan environment", *IEEE Proc. 48th Vehicular Technology Conference*, Vol. 2, pp. 1453-1457, May 1998.

[89]   S. Burley, "Downlink capacity estimation in a WCDMA cellular network", *IEEE Proceedings of the 12th IEEE International Symposium on Personal, Indoor and Mobile Radio Communications*, Vol. 1, pp. A26-A30, September 2001.

[90]   B. Göransson, B. Hagerman, S. Petersson, J. Sorelius, "Advanced antenna systems for WCDMA: link and system level results", *IEEE Proceedings of the 11th International Symposium on Personal, Indoor and Mobile Radio Communications*, Vol. 1, pp. 62-66, September 2000.

[91]   A. Osseiran, M. Ericson, "On downlink admission control with fixed multi-beam antennas for WCDMA system", *IEEE Proc. 57th Vehicular Technology Conference*, Vol. 2, pp. 1203-1207, April 2003.

[92]   S. Hämäläinen, H. Holma, K. Sipilä, "Advanced WCDMA radio network simulator", *IEEE Proc. of the IEEE Symposium on Personal, Indoor and Mobile Radio Communications*, pp. 509-604, September 1999.

[93]   S. Hämäläinen, P. Slanina, M. Hartman, A. Lappeteläinen, H. Holma, O. Salonaho, "A novel interface between link and system level simulations", *Proceedings of ACTS Summit 1997*, pp. 509-604, October 1997.

[94]   M.M. Zonoozi and P. Dassanayake, "Shadow fading in mobile radio channel", *Seventh IEEE International Symposium on Personal, Indoor and Mobile Radio Communications*, pp. 291-295, October 1996.

[95]   T. Buot, H. Zhu, H. Schreuder, S. Moon, B. Song, "Soft handover optimization for WCDMA". *Fourth International Symposium on Wireless Personal Multimedia Communications,* pp. 141-146, September 2001.

[96]   3rd Generation Partnership Project, "Radio Resource Protocol (RRC) specification", TS. 25.331, Version 5.2.0, Available online at www.3gpp.org, September 2002.

[97]   3rd Generation Partnership Project, "Beamforming enhancements", TR. 25.887, Version 1.3.0, Available online at www.3gpp.org, October 2002.

[98]   3rd Generation Partnership Project, "Interlayer procedures in connected mode", TS. 25.303, Version 5.1.0, Available online at www.3gpp.org, June 2002.

[99]   M. Escartin, P. A. Ranta, "Interference rejection with a small antenna array at the mobile scattering environment", *IEEE Proc. First Signal Processing Workshop on Signal Processing Advances in Wireless Communications,* pp. 165-168, April 1997.

[100]   A. G. Kogiantis, N. Joshi, O. Sunay, "On transmit diversity and scheduling in wireless packet data", *IEEE Proc. International Conference on Communications*, Vol. 8, pp. 2433 –2437, 2001.

[101]   J.M. Holtzman, "Asymptotic Analysis of Proportional Fair Algorithm", *IEEE Proc. PIMRC*, pp. F33-F37, September 2000.

[102]   L. T. Berger, L. Schumacher, J. Ramiro-Moreno, P. Ameigeiras, T. E. Kolding, P. E. Mogensen, "Interaction of transmit diversity and proportional fair scheduling", *IEEE Proc. 57th Vehicular Technology Conference*, Vol. 4, pp. 2423-2427, April 2003.

[103]   T. E. Kolding, F. Frederiksen, P. E. Mogensen, "Performance evaluation of modulation and coding schemes proposed for HSDPA in 3.5G UMTS networks", *Proceedings of WPMC-01,* pp. 307-312, September 2001.

[104]   H. Huang, S. Venkatesan, A. Kogiantis, N. Sharma, "Increasing the peak data rate of 3G downlink packet data systems using multiple antennas", *IEEE Proc. 57th Vehicular Technology Conference*, Vol. 1, pp. 311-315, April 2003.

[105]   K. Miyoshi, T. Uehara, M. Kasapidis, K. Hiramatsu, M. Uesugi, O. Kato, "Link adaptation methodfor HSDPA for W-CDMA", *Proceedings of WPMC-01*, pp. 455-460, September 2001.

[106]   F. Frederiksen, T.E. Kolding, "Performance and modeling of WCDMA /HSDPA transmission/H-ARQ schemes", *IEEE Proc. 56th Vehicular Technology Conference*, Vol. 1, pp. 472-476, May

2002.

[107] R. C. Elliott, W.A. Krzymien, "Scheduling algorithms for the cdma2000 packet data evolution", *IEEE Proc. 52nd Vehicular Technology Conference*, Vol. 1, pp. 304-310, September 2000.

[108] F. Kelly, "Charging and Rate Control for Elastic Traffic", *European Transactions on Telecommunications*, Vol. 8, pp. 33-37, 1997.

[109] T.E. Kolding, F. Frederiksen, P. E. Mogensen, "Performance aspects of WCDMA systems with High Speed Downlink Packet Access (HSDPA)", *IEEE Proc. 56th Vehicular Technology Conference*, pp. 477-481, September 2002.